

MODELLING AND OPTIMIZATION OF PYROLYSIS
OPERATING PARAMETERS FOR ENERGY GENERATION

By

ONOKWAI, ANTHONY OGOCHUKWU
MATRIC NO: 18PGBE000014

SUPERVISOR: ENGR. PROF. AJISEGIRI, E.S.A

CO-SUPERVISOR: ENGR. PROF. OKI, M

A FINAL REPORT

SUBMITTED TO THE

DEPARTMENT OF MECHANICAL ENGINEERING,
FACULTY OF ENGINEERING,
LANDMARK UNIVERSITY,
OMU-ARAN, KWARA STATE

IN PARTIAL FULFILMENT OF THE REQUIREMENTS FOR
THE AWARD OF PhD DEGREE
IN MECHANICAL ENGINEERING

OCTOBER, 2022

DECLARATION

I, Anthony Ogochukwu ONOKWAI, a Ph.D. student in the Department of Mechanical Engineering, Landmark University, Omu-Aran, hereby declare that this thesis entitled “Modelling and Optimization of Pyrolysis Operating Parameters for Energy Generation”, submitted by me is based on my original work. Any material(s) obtained from other sources or work done by any other persons or institutions have been duly acknowledged.

CERTIFICATION

This is to certify that this thesis has been read and approved as meeting the requirements of the Department of Mechanical Engineering, Landmark University, Omu-Aran, Nigeria, for the Award of Ph.D.

Engr. Prof. E. S. A. Ajisegiri
(Supervisor)

Date

Engr. Prof. M. Oki
(Co-Supervisor)

Date

Engr. Prof. J. O. Ojediran
(Head of Department)

Date

(External Examiner)

Date

ABSTRACT

The increasing call for clean and sustainable energy has been at the forefront of global efforts toward the drive for greener economies and sustainable developments amid other parameters. Problems are being faced in enhancing the quantity and quality of pyrolysis yields due to poor characterization of biomass and improper parameters mix during experimentation run. This study utilized response surface methodology (RSM) to model and optimize operating parameters for pyrolysis. Temperature, reaction time, heating rate, nitrogen, and particle size were chosen to maximize quantity, energy, and exergy efficiency of bio-oil, biochar, and non-condensable gases (NCG) of palm kernel shell (PKS), sugarcane bagasse (SCB), and shea butter wood (SBW) based on the outcome of experimental runs. A quadratic model was found fit for the optimization and elucidates the non-linear nature of the model response. The optimum bio-oil, biochar, and NCG are 47.5, 40.7, and 35.5 wt% for palm kernel shells; 48.4, 40.5, and 33.5 wt% for sugarcane bagasse; and 46.8, 42.5, and 34.2 wt% for shea butter wood respectively. Also, the optimum energy and exergy efficiency for bio-oil, biochar, and NCG are 53.3 and 48.2, 28.3 and 23.7, as well as 15 and 11.6% respectively. The probability value <0.05 , high Fischer-value (F-value) for bio-oil (303.95), biochar (877.64) and NCG (487.74) as well as coefficients of determination (R^2) of 0.98562, 0.9956 and 0.9921 for bio-oil, biochar and NCG respectively make the developed mathematical model suitable, reliable, responsive, and predicted the experimental data. The actual and predicted values for quantity, energy, and exergy efficiency of products of pyrolysis clearly showed that the experimental data are in good agreement with the predicted values. The Fourier Transform-Infrared Spectroscopy and Gas Chromatography-Mass Spectrometry (GC-MS) analysis of bio-oils and biochar depicted relatively high percentages of alcohol, oleic acid, aromatic and aliphatic hydrocarbons, phenol, aldehyde, and ketone. The Scanning Electron Microscope/Electron Dispersive X-Rays Spectroscopy (SEM/EDX) results for the biochar showed whitish deposits, cleaves, heterogeneous pores, cloudy and cloggy formations depicting inorganic materials, rapid volatile emission and efflorescence during pyrolysis processes at higher temperature. This study has successfully shown that modeling more than three pyrolysis operating parameters using a Response Surface Methodology (RSM) optimizes the pyrolysis yields as well as its energy and exergy efficiency. The biochar and bio-oil samples can be utilized as biofuel for industry applications and additives for waste management strategies, petrochemical industry, sorbent, and soil enhancers.

Word Count: 389

DEDICATION

This project is dedicated to God Almighty for His great support and journey mercies He gave me throughout this program. May His Holy Name be praised.

ACKNOWLEDGEMENTS

My deep appreciation goes to my supervisor, Engr. Prof. E. S. A. Ajisegiri and co-supervisor, Engr. Prof. M. Oki for their intellectual support, priceless encouragement, advice, guidance, mentorship, and indefatigable supervision that they generously carried out throughout this work. May Almighty God bless, protect and grant you and your lovely family long life, more wisdom, knowledge, and understanding.

The HOD, Department of Mechanical Engineering, Engr. Dr. R. A. Ibikunle, College and Departmental PG Coordinators, Engr. Dr. A. A. Adediran and Engr. Dr. O. Aderoba deserved a very resounding thank you for taking time to ensure the work followed the presentable format. I also owe deep and unreserved gratitude to all my Lecturers and Staff of the Department of Mechanical Engineering, Landmark University, that have contributed in one way or the other that made me achieve my ambition. May God reward and bless you.

Although it may not be convenient for me to mention the names of everyone that contributed immensely to bringing this project work into reality, I still owe some of them moral gratitude for their assistance, most especially my lovely wife, Mrs. Blessing, O. Onokwai-Atuyota, our God gave sons and daughter, Damian, Anslem, Jacinta and sisters. Also, to the following persons; Prof. C. Aremu, Engr. Prof. C. O. Osueke, Engr. Prof. J. O. Ojediran, Engr. Prof. O. S. I. Fayomi, Engr. Dr. A. O. Balogun, Engr. Dr. D. E. Ighravwe, Engr. D. Egbune, Engr. J. A. Oyebanji, Engr. E. Onokpite, Engr. Dr. P. P. Ikubanni, Engr. Dr. A. A. Adeleke, Engr. B. Ogunsemi, Engr. S. Okocha, pray that the Almighty God will continue to grant you all your heart desires. Amen.

TABLE OF CONTENTS

Title Page	i
Declaration	ii
Certification	iii
Abstract	iv
Dedication	v
Acknowledgment	vi
Table of Contents	vii
List of Table	xiii
List of Figures	xiv
List of Plate	xvi
Nomenclature	xvii
CHAPTER ONE: INTRODUCTION	1
1.1 Background of the Problem	1
1.2 Statement of the Research Problem	3
1.3 Justification of the Study	4
1.4 Aim and Objectives of the Study	5
1.5 Research Questions	6
1.6 Research Hypotheses	6
1.7 Scope of the Study	6
1.8 Significance of the Study	6

CHAPTER TWO: LITERATURE REVIEW	7
2.1 Conceptual Issues	7
2.2 Theoretical Review	11
2.2.1 Biomass	11
2.2.2 Types of biomass component	11
2.2.3 Biomass conversion process	13
2.2.4 Biochemical conversion	13
2.2.5 Thermochemical conversion	14
2.2.5.1 Thermochemical conversion; gasification	14
2.2.5.2 Thermochemical conversion; combustion	17
2.2.5.3 Thermochemical conversion; liquefaction	17
2.2.5.4 Thermochemical conversion; pyrolysis	18
2.2.6 Basic principles of pyrolysis	21
2.2.7 Type of pyrolysis	22
2.2.7.1 Fast pyrolysis`	22
2.2.7.2 Flash pyrolysis	24
2.2.7.3 Intermediate pyrolysis	24
2.2.7.4 Slow pyrolysis	25
2.2.8 Products of Pyrolysis	25
2.2.8.1 Pyrolysis liquid product	25
2.2.8.2 Pyrolysis solid product	26
2.2.8.3 Gas	26
2.2.9 Pyrolysis Reactor	26

2.2.9.1 Fixed bed reactor	26
2.2.9.2 Fluidized bed reactor	27
2.2.9.3 Circulating fluid bed (CFB) reactor	27
2.2.9.4 Vacuum pyrolysis reactor	27
2.2.9.5 Rotating cone reactor	27
2.2.9.6 Auger reactor	28
2.2.9.7 Plasma reactor	29
2.2.9.8 Microwave reactor	29
2.2.9.9 Solar reactor	29
2.3 Empirical Review	31
2.3.1 Biomass characterization	31
2.3.2 Influence of operating parameter on pyrolysis yields	33
2.3.3 Energy and exergy analysis of pyrolysis process	35
2.3.4 Modelling and optimization of thermochemical conversion process	38
2.3.5 Response surface methodology (RSM)	40
2.4 Gap Identified in the Literature	41
CHAPTER THREE: MATERIALS AND METHODS	43
3.1 Source of Materials	43
3.2 Pretreatment of Raw Biomass	46
3.3 Physicochemical Analysis	49
3.3.1 Proximate analysis of oven-dried powdered biomass	49
3.3.2 Ultimate Analysis of oven-dried powdered biomass	49
3.4 Structural Composition Analysis Oven-dried Powdered Biomass	50

3.5	Heating Value Analysis of Oven-dried Powdered Biomass	50
3.6	Thermogravimetric Analyses (TGA) of Sun-dried Powdered Biomass	51
3.7	Evaluation of Ignitability Index (I _i)	53
3.8	Research Design	55
3.9	Pyrolysis Experimental Setup	61
3.10	Experimental Procedure	65
3.11	Energy and Exergy Analysis	67
3.11.1	Energy analysis	67
3.11.2	Exergy analysis	74
3.12	Fourier Transfer Infrared Spectroscopy (FT-IR) Analysis	82
3.13	Gas Chromatography-Mass Spectrometry (GC-MS) Analysis	83
3.14	Scanning Electron Microscopy (SEM)/Energy dispersion X-ray Spectroscopy (EDS) Analysis	83
3.15	Research Instrument	84
	CHAPTER FOUR: RESULTS AND DISCUSSION OF FINDINGS	83
4.1	Proximate Analysis	86
4.2	Ultimate Analysis	89
4.3	Structural Composition Analysis	91
4.4	Heating Value Analysis	93
4.5	Thermogravimetry analysis (TGA)	95
4.6	Ignitability Index (I _i)	98
4.7	Statistical Design Format for Bio-oil, Biochar, and NCG yields	100
4.8	Statistical Model Development	105

4.8.1	Statistical models for bio-oil yield	105
4.8.2	Statistical models for biochar yield	107
4.8.3	Statistical models for NCG yield	108
4.9	Influence of Individual Parameters on the Products of Pyrolysis	110
4.9.1	Influence of temperature on the products of pyrolysis	110
4.9.2	Influence of particle size on the products of pyrolysis	113
4.9.3	Influence of heating rate on the products of pyrolysis	115
4.9.4	Influence of reaction rate on the products of pyrolysis	119
4.9.5	Influence of nitrogen flow rate on the products of pyrolysis	119
4.10	Influence of Two Most Significant Parameters on the Products of Pyrolysis	121
4.11	Optimized Value of Pyrolysis Operating Parameters for Bio-Oil, Biochar and NCG Yields	127
4.12	Design of Experiment (DOE) for Energy, Exergy Efficiency and Exergy Destruction of Bio-oil, Biochar, and NCG yields	141
4.13	Statistical Modelling for Energy Efficiency of Products of Pyrolysis	146
4.14	Statistical Modelling for Exergy Efficiency of Products of Pyrolysis	147
4.15	Influence of Operating Parameters on Energy and Exergy Efficiency of Products of Pyrolysis	148
4.16	Optimization of operating parameters on energy and exergy efficiency of products of pyrolysis	156
4.17	Physicochemical Properties of the Bio-oil Samples	161

4.18	Fourier Transform Infrared (FTIR) Spectroscopy Analysis for Bio-oil Yields	164
4.19	Fourier Transform Infrared (FTIR) Spectroscopy Spectrum Analysis for Biochar Yields	173
4.20	Gas Chromatography and Mass (GC-MS) Spectrometry Analysis for Bio-oil Yields	186
4.21	SEM Analysis for Biochar Yields	194
4.22	SEM/EDX Analysis for Biochar Yields	198
	CHAPTER FIVE: SUMMARY, CONCLSION AND RECOMMENDATIONS	204
5.1	Summary	204
5.2	Conclusion	204
5.3	Recommendations	208
5.4	Contribution to Knowledge	209
	REFERENCES	210
	APPENDICES	237

LIST OF TABLES

2.1	Merits and Demerits of Types of Reactors	29
3.1	Design of Experiment (DOE) using Central Composite Design	60
3.2	Specific Enthalpy, Entropy and Higher Heating Value of Selected Compounds of the Pyrolysis Gas Constituents	73
3.3	Coefficients for Constant Pressure Specific Heat of NCG	78
3.4	Standard Chemical Exergy of Selected NCG	80
4.1	Proximate Analysis of Biomass (Oven-Dried Basis)	88
4.2	Ultimate Analysis of Biomass (Oven-Dried Basis)	90
4.3	Structural Analysis of Biomass (Oven-Dried Basis)	92
4.4	HHV and LHV of Biomass (Oven-Dried Basis)	94
4.5	Experimental Design Matrix and the Corresponding Pyrolysis Yields from Palm Kernel Shell	102
4.6	Experimental Design Matrix and the Corresponding Pyrolysis Yields from Sugarcane Bagasse	103
4.7	Experimental Design Matrix and the Corresponding Pyrolysis Yields from Shell Butter Wood	104
4.8	Summary of Optimization of Operating Parameters	134
4.9	Optimum values of pyrolysis products obtained from this study and previous works	138
4.10	Statistical Analysis of optimum values of pyrolysis products obtained from this study and previous works	139

4.11	Experimental Design Matrix and the Corresponding Energy and Exergy Efficiency from Palm Kernel Shell	143
4.12	Experimental Design Matrix and the Corresponding Energy and Exergy Efficiency from Sugarcane Bagasse	144
4.13	Experimental Design Matrix and the Corresponding Energy and Exergy Efficiency from Shell Butter Wood	145
4.14	Summary of Optimization of Energy and Exergy Eff. of Products of Pyrolysis	160
4.15	Physico-chemical Properties of Bio-oil	163
4.16	Functional Group Composition from Pyrolysis of Bio-oil from PKS	166
4.17	Functional Group Composition from Pyrolysis of Bio-oil from SCB	169
4.18	Functional Group Composition from Pyrolysis of Bio-oil from SBW	172
4.19	Functional Group Composition from Pyrolysis of Biochar from PKS	176
4.20	Functional Group Composition from Pyrolysis of Biochar from SCB	180
4.21	Functional Group Composition from Pyrolysis of Biochar from SBW	184
4.22	Chemical Composition of Bio-oil from PKS	191
4.23	Chemical Composition of Bio-oil from SCB	192
4.24	Chemical Composition of Bio-oil from SBW	193
4.25	Products of Pyrolysis and their Applications	202

LIST OF FIGURES

2.1	Biomass Conversion Process	8
2.2	Biomass Components	12
2.3	Basic Principle of a Gasifier	16
2.4	Schematic Diagram for Pyrolysis Process	20
3.1	Pretreatment and Characterization of Biomass Processes	54
3.2	Flowchart for the Modelling and Optimization	59
3.3	Pyrolysis Set-Up Exploded	63
3.4	Pyrolysis plant reactor	64
3.5	Flowchart for experimental runs	66
3.6	Pyrolysis system	68
3.7	Energy Generated from Electric Heating Element	69
4.1	TGA of Weight Loss at a Heating Rate of 10 ⁰ C/min	97
4.2	Ignitability Index	99
4.3	Influence of Temperature on Products of Pyrolysis	112
4.4	Influence of Particle Size on Products of Pyrolysis	114
4.5	Influence of Heating Rate on Products of Pyrolysis	116
4.6	Influence of Reaction Time on Products of Pyrolysis	118
4.7	Influence of Nitrogen Flowrate on Products of Pyrolysis	120
4.8	Surface Plots of Bio-oil	123
4.9	Surface Plots of Biochar	125
4.10	Surface Plots of NCG	127

4.11	Response Optimization for Bio-oil	130
4.12	Response Optimization for Biochar	131
4.13	Response Optimization for NCG	132
4.14	Actual and Predicted Bio-oil, Biochar and NCG	136
4.15	Energy Efficiency of Individual Gases	151
4.16	Influence of Two Most Important Parameters on Energy Efficiency of Pyrolysis Yields	153
4.17	Influence of Two Most Important Parameters on Exergy Efficiency of Pyrolysis Yields	155
4.18	Optimization of the Energy and Exergy Efficiency of Bio-oil Yields	157
4.19	Optimization of the Energy and Exergy Efficiency of Biochar Yields	158
4.20	Optimization of the Energy and Exergy Efficiency of NCG Yields	159
4.21	FT-IR Spectrum of Bio-oil Yield from PKS	165
4.22	FT-IR Spectrum of Bio-oil Yield from SCB	168
4.23	FT-IR Spectrum of Bio-oil Yield from SBW	171
4.24	FT-IR Spectrum of Biochar Yield from PKS	175
4.25	FT-IR Spectrum of Biochar Yield from SCB	179
4.26	FT-IR Spectrum of Biochar Yield from SBW	183
4.27	GC-MC of Bio-oil Compounds Produced from PKS	188
4.28	GC-MC of Bio-oil Compounds Produced from SCB	190
4.29	GC-MC of Bio-oil Compounds Produced from SBW	191
4.30	SEM Analysis of Palm Kernel Shell	195
4.31	SEM Analysis of Sugarcane Bagasse	196

4.32	SEM Analysis of Shell Butter Wood	197
4.33	SEM/EDX Analysis of Palm Kernel Shell	199
4.34	SEM/EDX Analysis of Sugarcane Bagasse	120
4.35	SEM/EDX Analysis of Shell Butter Wood	201

LIST OF PLATES

3.1	Pictorial representation of methodology	44
3.2	Raw biomass prior to pretreatment	45
3.3	Grinding and Oven Drying of Biomass Samples	47
3.4	Treated Powdered Biomass for Characterization	48
3.5	Weighing of the Sample and Placing of the Samples in a Carbonite Muffle Furnace for Proximate Analysis	52
3.6	Pyrolysis Plant Experimental Set-up	62
3.7	FT-IR, GC-MS and SEM/EDS Machines	84

NOMENCLATURE

BBD = Box-Behnken design

BFR-CCS = Biomass-Fuelled power plant energy

C = Carbon

CCD = Central composite design

CFB = Circulating fluid bed

CV = Coefficient of variance

DOE = Design of experiment

$En_{Ch}^{Biomass}$ = Chemical energy of biomass

$En_{Ph}^{Biomass}$ = Physical energy of biomass

En_{Ph}^{NCG} = Physical energy of non-condensable gases

$En_{Total}^{Biomass}$ = Total energy of biomass

En_{Ch}^{NCG} = Chemical energy of non-condensable gases

$En_{Biomass}$ = Energy of biomass

$En_{electric}$ = Energy of heating element

$En_{electric}$ = Energy of heating element

En^{Ki} = Kinetic energy

En^{Po} = Potential energy

ER = Equivalent ratio

$Ex_{Ch}^{Biomass}$ = Chemical exergy of biomass

$Ex_{Ph}^{Biomass}$ = Physical exergy of biomass

$Ex_{Total}^{Biomass}$ = Total exergy of biomass

$EX_{Biomass}$ = Exergy of biomass

$EX_{irreversibilities}$ = Energy loss during pyrolysis process

FC = Fixed carbon

FTIR = Fourier Transform Infra-Red Spectroscopy

GCMS = Gas Chromatograph-Mass-Spectrometry

H = Heating rate

H = Hydrogen

HHV = Higher heating value
HTC = Hydrothermal carbonization
 I_i = Ignitability index
LHV = Lower heating value
 M_{Biochar} = Mass of biochar
MC = Moisture contents
N = Actual experimental runs
N = Nitrogen
n = Number of independent parameters
 N_2 = Nitrogen flowrate
 n_c = Repeated number of identical runs
NCG = Non-condensable gases
P = Particle sizes
PKS = Palm kernel shell
 PR_{peak} = Maximum power rating
p-value = Probability value
R = Gas constant
R = Reaction time
 R^2 = Coefficient of determination
RSM = Response surface methodology
SBW = Shea butter wood
SCB = Sugarcane bagasse
SEM/EDX = Scanning Electron Microscopy/Energy Dispersive X-ray
T = Temperature
TGA = Thermogravimetry analysis
 T_{heating} = Heating element temperature
 T_p = Pyrolysis temperature
VM = Volatile matter
 $x_i x_j$ = Coded independent parameters
y = Response
 y_c = Biochar yield

y_N = Non-condensable gases yield

y_o = Bio-oil yield

$\Psi_{\text{biochar}}, \Psi_{\text{bio-oil}}, \Psi_{\text{NCG}}$ = Exergy Efficiency of Biochar, Biooil and NCG

$\beta_{\text{biochar}}, \beta_{\text{bio-oil}}, \beta_{\text{NCG}}$ = Correlation parameter for Biochar, Bio-oil and NCG

β_{biomass} = Correlation parameter for raw biomass

CHAPTER ONE

INTRODUCTION

1.1 Background to the Study

Energy plays a vital role in most human activities; it is the premise of industrial civilization and the bedrock of industrial revolution. Without energy, the modernization of our life and cities would not have been actualized. Previously, the demand for energy sources was minimal due to the fact that it was primarily utilized for cooking, heating and transportation. But, as time went by, coupled with tremendous growth in population and technological advancement caused the need for more energy demand (Alfa *et al.*, 2021; Owamah *et al.*, 2022). This high energy demand necessitated the quest by man for a different source of energy and some have a negative effect. For instance, fossil fuels constitute the primary energy resource used to power human technological advancement, since the industrial revolution (Suriapparao and Tejasvi, 2022). However, there were consequences, as studies have shown that the high volume of pollutants through fossil fuels emissions sequel to its usage is harmful to public health and the environment (Okonkwo *et al.*, 2018; Ojediran *et al.*, 2020; Ibikunle *et al.*, 2022; Akogun *et al.*, 2022).

Renewable energy is considered an attractive and reliable energy source that is abundantly available in all parts of the world (Ahmed *et al.*, 2018; Oyebanji *et al.*, 2022). The exploit of renewable energy has continued to be on the rise in contrast with other forms of energy sources available on earth due to their devastative impacts, one such is hydrocarbons (fossil fuel) which is one of the most commonly consumed energy which daily poses negative impacts on the environment and human beings at large. Thus, discussions on global warming, pollution, climate change, depleting ozone, and others have taken the front burners in recent times (Chukwuneke *et al.*, 2019; Balogun *et al.*, 2019).

Kan *et al.* (2016) observed that the most researched source of renewable energy has remained biomass because it presently contributes about 13% of the world's energy supply, its composition includes 38-50% of cellulose, 23–32% of hemicellulose, 15–25% of lignin and

different segments (i.e., inorganic species and extractives) with a total percentage of 5–13% in biomass (Goodman, 2020; Aguiar *et al.*, 2021). The pros of the use of biomass as a source of fuel is numerous which includes; vast availability; fuel yield optimization; various energy forms that can be harnessed, cheap in terms of raw materials cost, etc. The production of transport fuel, electricity, and even heat has been achievable with most of these technologies (anaerobic digestion, pyrolysis, combustion, gasification, and hydrolysis) through the use of biomass materials (Kuhe and Aliyu, 2015; Lee *et al.*, 2017; Balogun *et al.*, 2019; Sharma *et al.*, 2022).

The degradation of biomass into bio-oil, biochar, syn-gas, involves complete thermochemical conversion procedures, such as pyrolysis, liquefaction, gasification, torrefaction, and carbonization (Chowdhury *et al.*, 2017; Wang *et al.*, 2018). Adeleke *et al.* (2020) reported that the quality and quantity of pyrolysis yields can be affected negatively by a poor determination of the physicochemical, thermal, and structural composition of the biomass prior to its pyrolysis. Balogun *et al.* (2021) emphasized the need to investigate the thermal degradation and decomposition behaviour of biomass before selecting them for thermochemical conversion to enhanced their yields, while Nwosu *et al.* (2015) reported a variation of similar lignocellulose biomass due to geographical location, intrinsic component of the biomass, soil type, and climatic conditions where the biomass samples are sourced and cultivated.

The ability to decompose biomass via the pyrolysis process into bio-oil, biochar, and non-condensable gases makes it more efficient for industrial, commercial, and domestic applications. Therefore, optimization of pyrolysis operating parameters such as temperature, reaction time, heating rate, nitrogen flow rate, and particle size by maximizing the quantity and quality of products of pyrolysis have been a great concern to many researchers (Hossain *et al.*, 2017; Kumar *et al.*, 2019; Laouge *et al.*, 2020; Suriapparao and Tejasvi, 2022). To obtain a higher efficiency in biomass conversion, a higher temperature is needed. Hence the decomposition of biomass relies on the quantity of heat supplied during the pyrolysis process. Various researches have confirmed the role of temperature within the range of 450-550°C was sufficient for bio-oil yield, although could vary depending on biomass and other process parameters (Guedes *et al.*, 2018). Biswas *et al.* (2020) opined that the possibility of obtaining maximum bio-oil yield in pyrolysis depends on the type and size of the biomass sample, while Bartoli *et al.* (2016) and Gautam and Chaurasia *et al.* (2020) observed that secondary reaction could occur if the reaction time is

prolonged enough thus resulting in repolymerization, recondensation, thermal cracking, and carbonization processes which might contribute to lower bio-oil yields.

This study focuses on the thermochemical decomposition of biomass via pyrolysis process to produce bio-oil, biochar, and non-condensable gases (NCG) in the absence of oxygen. Pyrolysis has become one of the crucial processes practiced in different parts of the world which aids and makes agricultural practices more modern (Wanga *et al.*, 2019; Varma and Mondal, 2017; Laouge *et al.*, 2020). It varies across bio-based feeds and fundamentally hydro-carbons in the conversion to useful products. Till today, challenges are being faced in the maximum utilization of products from biomasses in terms of energy and other related uses (Daioglou *et al.*, 2016; Singh *et al.*, 2020). This poses the need for more research in this area as great potential can be achieved.

In this study, an intermediate pyrolysis process was utilized to convert various biomass species such as palm oil shells, sugarcane bagasse, shea butter wood to bio-oil, biochar, and NCG using a fixed bed reactor system. During the thermochemical conversion process, variations of independent pyrolysis typical parameters namely; temperature, particle sizes, heating rate, and residence time were utilized to investigate their effects on the quantity of pyrolysis products. Modelling and optimization were carried out by considering the various independent parameters used during experimental runs to improve products quality and quantity. Also, ways and manners to increase the efficiency of the pyrolysis plant during operation would be investigated via energy and exergy analysis.

1.2 Statement of the Problem

Renewable and clean energy remains a better option in ameliorating the elevated concern about global warming, climate change, and the decline of fossil fuel reserves (Alatzas *et al.*, 2019). Energy from fossil fuels constitutes environmental pollution, ozone depletion, and consequential global warming. Furthermore, energy from fossil and other sources are not enough to solve our social, commercial and technological requirements. Hence, there is a need for cost-effective, renewable, sustainable and alternative energy sources that will complement conventional energy sources (Gupta *et al.*, 2020)

For many years, a lot of works had been carried out on the various processes of converting biomass into biofuels as sources of energy generation. Nevertheless, problems are being faced in enhancing the quantity and quality of pyrolysis yields due to the poor characterization of biomass prior to its pyrolysis (Balogun *et al.*, 2019; Oyebanji *et al.*, 2021). Also, the determination of heating value which serves as a basis for the design and operation of a thermochemical conversion process takes time due to the inaccessibility of combustion calorimeter, researchers generally used an elemental analyzer to obtain the ultimate, and other equipment for proximate or structural composition analyses discretely (Xing *et al.*, 2019; Gianluca *et al.*, 2020; Ibikunle *et al.*, 2021).

During the production of bio-oil, biochar, and NCG; challenges are being faced with attaining the right operational conditions for maximum production. Most times, the production does not follow a linear relationship and thus rigorous experimentation and modelling are required in quantifying the typical operating parameters such as particles sizes in an inert gas environment, temperature, reaction time, heating rates and nitrogen flow rate (Guedes *et al.*, 2018; Kumar *et al.*, 2021). These challenges are centered on combining parameters optimally and creating a model that best describes the experimental work for future purposes (Suriapparao and Tejasvi, 2022).

Furthermore, challenges facing optimization of the desired pyrolysis product quality and quantity have been a major concern for many researchers by taking into consideration, the reduction of costs and environmental parameters during the production process (Hossain *et al.*, 2017; Laougé *et al.*, 2020). Also, thermodynamic inefficiencies lead to an energy imbalance in the pyrolysis process leading to energy loss in the during the process and products of pyrolysis (Wang *et al.*, 2016; Etika *et al.*, 2019; Ramesh and Murugavelh, 2020; Zhang *et al.*, 2020).

1.3 Justification of the study

This study will help in ameliorating the consequential effects of energy from fossil fuels and in addition, will generate clean energy (Yosoon *et al.*, 2017). The results of characterization from this study will aid in the selection of the right biomass that will enhance the quality and quantity of yields from pyrolysis during thermochemical processes (Gautam and Chaurasia, 2020).

The developed model and optimization in this study will spot out areas that might need improvements in the existing pyrolysis process, development of new processes, and optimization

of the performance of future pyrolysis plants (Myers and Montgomery 2000; Hossain *et al.*, 2017; Lee *et al.*, 2017). It will further suggest if more parameters are to be considered for the effective and efficient production of pyrolysis yields. The determination of the components that will lead to inefficiency and wasteful processes within the thermodynamic systems via exergy analysis will also help minimize irreversibilities in the system, enhance adequate utilization of resources, and performance monitoring of future pyrolysis operation processes (Ramesh and Murugavelh, 2020; Esfandi *et al.*, 2020).

Finally, the Bio-oil and biochar obtained after the thermochemical conversion process via pyrolysis can be utilized as fuel for automobile vehicle, furnace and boilers as well as agricultural and pharmaceutical industries (Chukwunke *et al.*, 2019; Varma and Mondal *et al.*, 2017; Adekiya *et al.*, 2020; Oyebanji *et al.*, 2022).

1.4 Aim and objectives of the study

The aim of this study is to model and optimize the pyrolysis' operating parameters for renewable energy generation.

Therefore, the specific objectives of this study are to:

- i. determine the physico-chemical, structural composition, and thermal properties of biomass prior to its pyrolysis;
- ii. model and optimize the pyrolysis' operating parameters using response surface methodology (RSM) to enhance pyrolysis yields;
- iii. carry out energy and exergy analysis of the pyrolysis process in order to evaluate the useful energy, detect energy losses and enhance the efficiency of the system; and
- iv. investigate the product quality of the bio-oil and biochar yields using Fourier Transform-Infrared (FT-IR) Spectroscopy, Gas Chromatography-Mass (GC-MS) Spectrometry, Scanning Electron Microscope (SEM)/Electron dispersive X-Rays (EDX) Spectroscopy.

1.5 Research Questions

The following research questions was considered in this study:

- i. What are the effects of pyrolysis' operating parameters on the quality and quantity of biochar, bio-oil, and non-condensable gases produced?
- ii. How can irreversibility in the pyrolysis plant be reduced?

1.6 Research Hypotheses

- i. Pyrolysis operating parameters do not influence the yield of pyrolysis products.
- ii. Entropy does not influence the efficiency of bio-oil, biochar, and NCG yields.

1.7 Scope and Limitation of the Study

Modelling and optimization of pyrolysis operating parameters such as temperature, heating rate, reaction time, nitrogen flow rate, and particle size using response surface methodology would be performed and the influence of the operating parameters on the energy and exergy efficiency of the products of pyrolysis would be investigated via energy and exergy analysis. Finally, the quality of the bio-oil and biochar yields would be investigated using Fourier transform Infra-Red (FT-IR) Spectroscopy, Chromatography-Mass (GC-MS) Spectrometer, Scanning Electron Microscope/ Energy Dispersive X-Ray Analysis (SEM/EDX) techniques. Inability to get Elemental Analyzer, GM-MS, FTIR, and SEM/EDX machines due to their high cost. These setbacks were overcome with time.

1.8 Significance of the study

The desired products being biofuels have several benefits apart from the research achievement and economic concerns. The pyrolysis yields help in addressing the United Nations sustainable development goals of SDG 7 (affordable and clean energy), and SDG 13 (climate action) which are expected to be achieved by 2030 in every country around the world (SDR, 2020; SDG, 2020).

CHAPTER TWO

REVIEW OF RELATED LITERATURE

2.1 Conceptual Issues

Biomass can be used in its natural state to provide heat when combusted and then converted to energy for power generation. However, it cannot be used as liquid fuel like oil and gas in its natural state. It has to be converted to a resource that has similar biocharacteristics to oil and gas. Currently, biomass as a renewable energy source is eco-friendly and its demand is increasing drastically because it is sustainable when compared to conventional energy sources such as coal, oil and natural gas (Ojediran *et al.*, 2020; Gautam and Chaurasia, 2020). The rapid population growth of the world, coupled with increasing demand for energy per capita and the consequences of global warming, birthed an alternative energy source that is long-lasting (Bardazzi and Pazienza, 2020). The importance of biomass cannot be overemphasized because of its ability to be transformed to bio-fuel and activated carbon through physical, biological, and thermal processes (Jahirul *et al.*, 2012). Biomass can be generally stated as the putting together of a composite mix of biological materials, for example, proteins, lignin, fats and carbohydrates in the form of starch, hemicellulose and cellulose. It is vital to recognize that the physical and chemical features of biomass are different in a distinct manner with respect to the original of the biomass, for example, lignin and carbohydrates are the major constituents of biological materials which originate from crops or plants, it also depends on the type of plant (Laouge *et al.*, 2020). Also, some biomass are obtained as products of waste from plants, residue from forest vegetation, waste from demolition and construction, waste generated by communities, human and cattle excretions etc. The use of fuels obtained from biological materials in liquid form is an essential substitute in order to avoid the effects of direct burning of biological materials in solid form, which can cause air, pollution and attended health challenges (Heidari *et al.*, 2019; Fahmy *et al.*, 2020; Ding *et al.*, 2020).

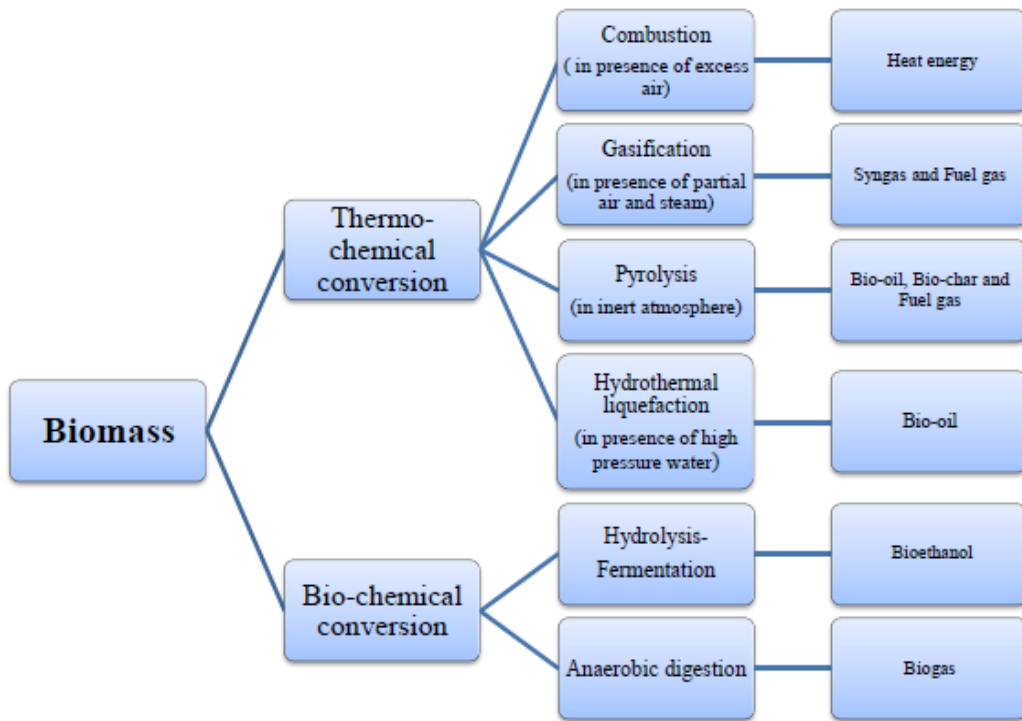


Figure 2.1: Biomass Conversion Process (Sharma, 2015)

The production of gas from coal began in the mid-1600s, particularly in 1665, in England (IBM Micromedex, 2019). The coal was heated in an airtight furnace i.e., coke oven to produce coke and then coal gas as a by-product. Towards the end of the eighteenth century, more gasification processes based on the conversion of coke to carbon monoxide and hydrocarbon evolved, providing gas in larger quantities (Thengane *et al.*, 2018). In the 1850s, ‘town gas’ which was gotten from the gasification of coal became widely used for lighting in London (Heidari *et al.*, 2019). Over time, the use of industrial gas went beyond lighting and cooking. It became useful for heating and the production of methanol, ammonia, fertilizers etc. (Guedes *et al.*, 2018). Recently, it is been utilized for the generation of electricity and liquid transport fuel production (Paykani *et al.*, 2022).

At the same time, more evolution and developments occurred in piping and steam drum technology. This led to the invention of gastight equipment that had more compact installations and could operate at pressures above 2 bar (Hejazi *et al.*, 2016). In the 1920s when the cryogenic separation of air into nitrogen and oxygen went into commercialization, continuous gasification became possible and the invention like the Lurgi moving bed pressurized gasification process etc. occurred (Hossain *et al.*, 2017). Producer gas (often used to refer to the product gotten from gasification) was first used to power a combustion engine in 1881 (Isitan *et al.*, 2019). During World War II, the supply of liquid fuel became difficult. This resulted in the search for an alternative source of fuel and eventually aroused interest in gasification. There were more than a million small units of gasifiers that ran on wood and charcoal readily available in the 1940s (Jafri *et al.*, 2018). However, when liquid fuel became available again, the interest in gasification declined. But research work continued in countries like South Africa, Brazil, Indonesia, the Philippines and China (Liu *et al.*, 2020).

Also, in 1973 and 1980, the oil crisis created new interest in biomass and coal gasification. Looking at history, it can be seen that there has been an intermittent interest in biomass gasification for developed countries. But it has not been the same for developing countries (Junna *et al.*, 2017). Developing countries have shown a growing interest in the gasification and pyrolysis of agricultural wastes especially for the supply of energy to remote places. But due to the growing volume of organic waste and the deterioration in the climate, developed countries are beginning to see gasification as a resourceful process for the conversion of organic waste to other energy forms including transport fuels (Aliyu *et al.*, 2021).

The process of thermochemical conversion is highly established and it's a technology that was originally developed for the processing of chemical and petroleum products, therefore the application of agricultural biomass in this procedure makes it challenging as a result of complex issues such as oxygen, moisture, sulfur, nitrogen and other metal contents (Evangelou *et al.*, 2012). Since biofuels are derived from biomass, the process of conversion: chemical, physical-biological or a blend of these processes are key to their kind and features, e.g., biodiesel, biogas and ethanol can be produced employing microbial or enzymatic fermentation without or with the use of physical and chemical pretreatment stages (Cantrell, 2012). Nevertheless, conversion of biomass into bio-oil, biochar, NCG, etc. involves completely thermochemical conversion procedures, such as pyrolysis, liquefaction, gasification, torrefaction, and carbonization (Wang *et al.*, 2017; Hassan *et al.*, 2017; Laouge *et al.*, 2020). Scientific research and development in thermochemical conversion of biomass hold a vital part in solving practical and sustainable energy as a result of the current energy crisis in Nigeria (Muller-Hagedorn and Bockhorn, 2007; Dideolu *et al.*, 2018).

Thermochemical conversion is one of the most effective ways of converting biomass to biofuels (Zhang and Zhang, 2019). It deals with the decomposition of biomass under controlled heating or oxidation at a high temperature above 150°C to produce biofuels such as solid, liquid and gaseous fuels etc. In all these energy transformation processes, pyrolysis has given rise to more liquid fuel and biochar production that has its benefits in the environmental and oil and gas sector for air, water and gas purification. Its usage also extends to agricultural, medical, industrial sectors in powering equipment like boilers, turbines, compressors, heat exchangers and internal combustion engines (EIA, 2017; Kumar *et al.*, 2019). Pyrolysis study is also important in solid biomass and wastes processes. However, the production is costly and challenging. How relevant recent research focuses on overcoming these technical and economic limitations in order to contend with fossil fuel (Choi *et al.*, 2015; Mohammed *et al.*, 2017; Oyebanji *et al.*, 2021).

Pyrolysis is the process in which biomass undergoes decomposition to biofuels, bio-oil and biochar in the absence of oxygen (Ramesh and Murugavelh, 2021). It also deals with devolatilization by removing volatile from coal (Wan *et al.*, 2015). The pyrolysis process can be carried out at a temperature which ranges between 300-700°C. This makes the process to be better than other biomass decomposition processes such as gasification (>700°C) and combustion (>900°C).

2.2 Theoretical Review

2.2.1 Biomass

Renewable energy such as biomass is huge and limitless in existence, its annual production rate is high and it is geographically widespread throughout the world. According to Guedes *et al.* (2018), biomass is a product of the plant, produced through photosynthesis using sunlight for the conversion of water and carbon dioxide into organic matter. Examples of biomass are energy crops (miscanllus, switchgrass), food crops and crop residue during processing (corn cobs, sugar cane, rice husk, wheat straw, bagasse), horticulture (yard waste), wood or forest residues (dead trees, branches and tree stumps), animal farming (manure, rich in nitrogen and phosphorous sewage plant), municipal solid waste (paper, grass clippings, food scraps, clothes, furniture, product packaging) etc. (Goyal *et al.*, 2008; Adeniyi and Ighalo, 2020).

2.2.2 Types of biomass component

It is imperative to understand the feedstock material composition in the production of fuels and chemicals from biomass (Jafri *et al.*, 2018). Biomass chemical composition in herbaceous or lignocellulosic can be biocharacterized by the following five main components: cellulose, hemicellulose, lignin, ash and extractives. Cellulose, a polysacbiocharide of glucose monomers is the most abundant biopolymer on earth. It has some linkages holding it together, these linkages enable cellulose to have hydrolysis resistance.

Hemi-cellulose biomass is an amorphous heteropolymer which makes it more prone to hydrolysis than crystalline cellulose. It is the second main component of biomass and comprising various types of carbohydrates such as mannose, glucose and xylose (Jafri *et al.*, 2018). The combination of cellulose, hemicellulose and lignin make up 90% of lignocellulosic biomass and 80% of herbaceous biomass. Lignin is the third major biomass component. It has an intricate aromatic alcohols array and it's intertwined with the cellulose and hemicellulose fraction of the biomass structure. The lignin provides rigidity to lignocellulosic materials due to its interwoven nature, such as trees as reported by Chowdhury *et al.* (2017). Biomass minor components which include extractives/volatiles (water and ethanol soluble) and ash makes up a smaller portion of the biomass composition (Obuka *et al.*, 2019) as seen in Figure 2.2.

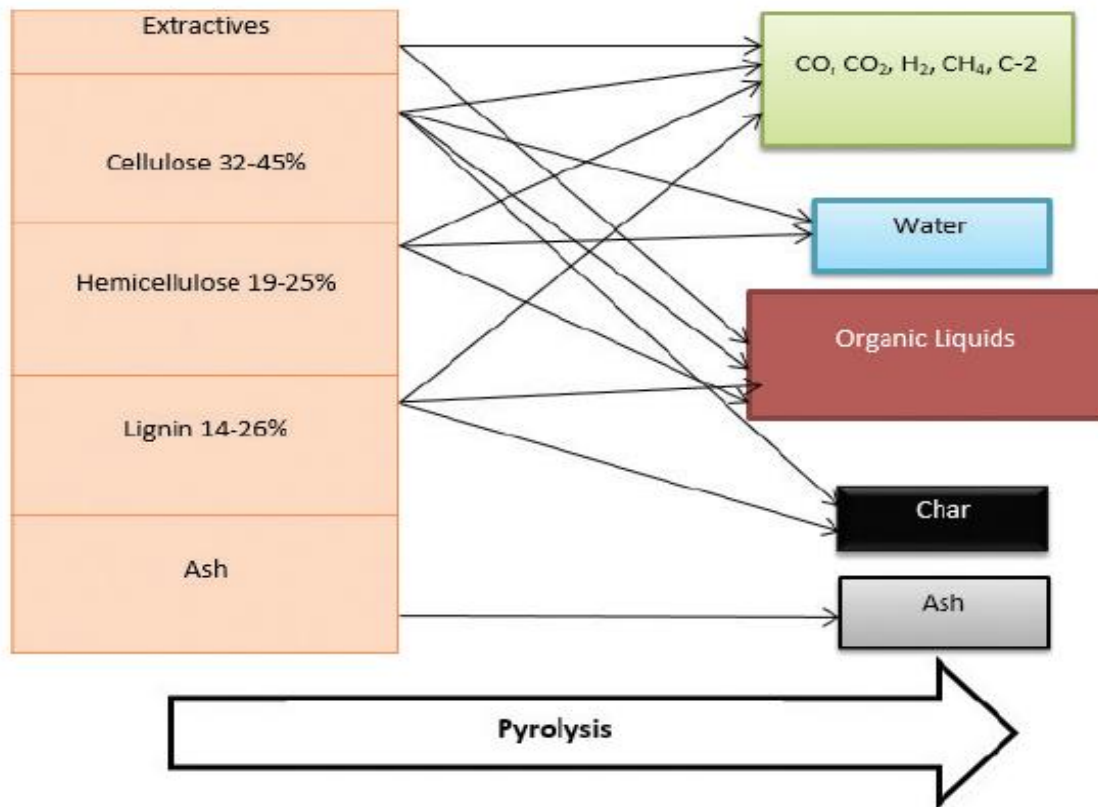


Figure 2.2: Biomass Component (Chowdhury *et al.*, 2019)

2.2.3 Biomass conversion process

In the decomposition of biomass species to chemicals and fuel, the physical properties of the biomass such as the particle size and moisture content are important parameters (Shaheed *et al.*, 2019). Small amount particle sizes are usually required during the thermochemical method of biomass conversion, unlike biological conversion that requires a large range of particle sizes (Maliutina *et al.*, 2017; Yang *et al.*, 2019; Fahmy *et al.*, 2020), while the final size is dependent on the processing system utilized. Some other physical properties aside particle size and moisture content include; bulk density which affects the cost of handling and transportation positively when the density is low, and elastic properties/microstructure which influence the compressibility and interaction of inter particles when the biomass is introduced into the reactor via the hopper opening as well as their compressibility, elastic properties, and microstructure (Yosoon *et al.*, 2017).

In the work of Xiong *et al* (2016), it was established that the increase in ash content affects biomass conversion negatively due to its reduction in the efficacy of the dilute acid pretreatment for biological processes while having an increased biochar yields and fouling in the various thermochemical processes (Akinola and Fapetu, 2015; Bonfim *et al.*, 2021). However, these ash contents could be removed through leaching and air classification (Ogunsola *et al.*, 2018; Onarheim *et al.*, 2020).

2.2.4 Biochemical conversion

Biomass conversion to ethanol involves the use of bacterial, microorganisms and enzymatic hydrolysis to break down biomass into gaseous or liquid fuels. Anaerobic digestion is a sequence of decomposition of organic materials such as solid waste, food waste, animal manure, industrial waste, poultry litter and sewage *etcetera* in chemical reactions through the metabolic pathways of naturally occurring microorganisms in an environment free of oxygen to produce biogas and biofertilizer. During biological conversion, the biomass can be converted to liquid fuels such as biodiesel, biogas, cellulosic ethanol etc., which serves as a substitute to petroleum-based fuels (Fontes, 2009; Daoglou *et al.*, 2016; Dahunsi *et al.*, 2019; Daniela *et al.*, 2020).

2.2.5 Thermochemical conversion

The conversion of biomass into bio-oil, biochar, syn-gas, and so on involves thermochemical conversion procedures, such as pyrolysis, liquefaction, gasification, torrefaction, and carbonization (Liu *et al.*, 2020). Scientific research and development in thermochemical conversion of biomass hold a vital part in solving practical and sustainable energy as a result of the current crisis in energy consumption (Adeleke *et al.*, 2020). Thermochemical conversion is one of the most effective ways of converting biomass to biofuels. It deals with the decomposition of biomass under controlled heating or oxidation at a high temperature above 150°C to produce biofuels such as solid, liquid, gaseous fuels, etc. (Salina *et al.*, 2020). These products generated can be converted directly to energy or chemicals such as bio-diesel, methane gas or carbon (IV) oxide etc.

There are various thermal technologies in harnessing stored biomass energy and are grouped according to the production of their principal energy carrier during the conversion process. Depending on the admission of oxygen into the thermochemical conversion process (usually as air), these carriers include heat, gas, liquid and/or solid products (Abnisa *et al.*, 2011; Materazzi and Lettieri, 2017).

2.2.5.1 Thermochemical conversion; gasification

Gasification is heat or thermal treatment of biomass at a high temperature of greater than 600.1°C using a measured quantity of gas agents like H₂O, O₂, CO₂ and air, producing a high proportion of the product mixed with a gas consisting of hydrogen, carbon monoxide, carbon dioxide, ammonia and nitrogen branded as syngas or gases obtained from synthesis, which is combustible gases and small quantities of a solid product also called biochar and ash (Kumar *et al.*, 2020a; Aliyu *et al.*, 2021). There are some kinds of catalytic agents required in this procedure, The study is, anhydrous carbonate mineral, nickel-based superalloy and alkaline earth metals (Stegen and Kaparajua, 2020). This process has generally stood on principles of incomplete oxidation/incomplete combustion, which produces an unclean, high temperature and reduced energy gas which piped straight into the appropriate equipment (dryers, boilers). Adding to its limited uses and repeatedly complex ecological challenges, this technology is not an efficient basis of functional energy. Total appropriation of this process to biological material involves

various successive and corresponding outcomes, which are energy absorbing and must be made stable by incomplete burning gas (Aghbashloa *et al.*, 2019).

Furthermore, in recent times biomass gasification has received so much attention. Biological material is changed to simpler yields, carbon dioxide and hydrogen gas, in an enhanced quality of oxygen and water which forms steam at high heat application of at least 800.1⁰C. The end yields are synthetic gas and ash, its quantity may vary depending on the source of the biological material. Synthetic gas has several uses some of which include fuels and raw material to chemical industries. Therefore, this process has a tremendous technique of separating biological form of energy of nitrogen, phosphorus, sulphur, chlorine, and other metal impurity of various kinds of biological materials devoid of additional cure (Kuhe and Aliyu, 2015; Kumar *et al.*, 2020b).

The transformation of wastes into useful gas and fuel is carried out in reacting equipment known as gasifier, their categorization is based on their interaction with solid wastes, catalytic and adsorbing agents and measure of the use of gas agents. Types of gasifiers are; entrained flow, fluidized bed and moving or fixed bed gasifiers as shown in Figure 2.3.

Some issues mitigating against the improved development of this process are high investment cost, optimistic power productivity, dehydrating of biological materials and crushing, the contribution of oxygen, repairs and cleaning of the reactors and practicability of the economy. Also, the produced gas is expensive to store or transport, therefore, demands instant use of the fuel (Varma and Mondal., 2017; Shi *et al.*, 2019).

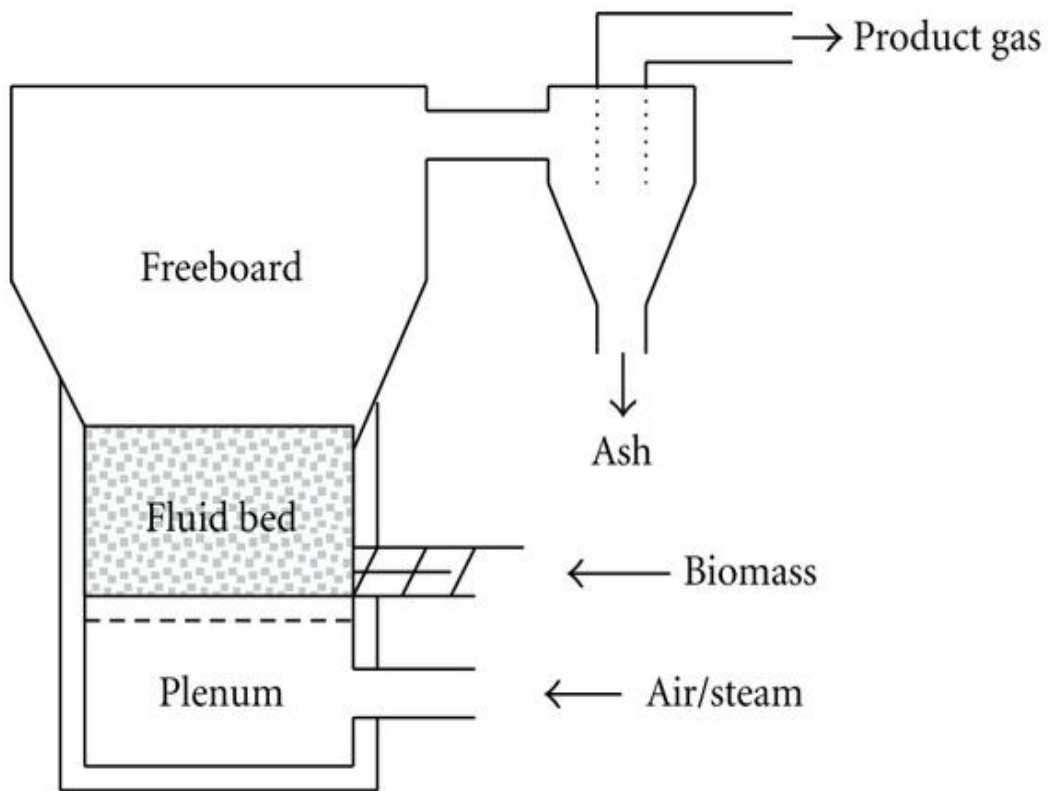


Figure 2.3: Basic Principle of a Gasifier (Liu *et al.*, 2019)

2.2.5.2 Thermochemical conversion; combustion

Biomass combustion widely practiced in developing countries to provide heat and energy for industrial and agricultural purposes (Romuli *et al.*, 2019; Ibikunle *et al.*, 2019). Non-renewable fossil fuels such as oil, coal, and natural gas are mainly utilized as a primary energy resource in developed countries which could be depleted in the next 40-50 years (Isabel *et al.*, 2017). Thermal conversion of organic matter with an oxidant (normally oxygen) by combustion method to produce primarily carbon dioxide and water incomplete oxidation.

Conventional combustion technologies are used to raise steam through biomass combustion, the steam can be used to produce electricity through the expansion of the steam in a conventional turbo-alternator. Several combustion technology variants have been developed. Grate type boilers are one of the technologies used for biomass conversion. The advantage of grate boilers includes relatively low investment costs, low operating costs and good operation (Oyejobi *et al.*, 2020).

2.2.5.3 Thermochemical conversion; liquefaction

Liquefaction is a thermochemical conversion process that can occur directly or indirectly. In direct liquefaction, the biomass species undergoes hydrothermal liquefaction or rapid pyrolysis to generate oils, liquid tars and condensable gases e.g., bio-oil, while indirect liquefaction deals with the utilization of catalysts to decompose biomass and convert it to NCG e.g., H₂, CO₂, CO, CH₄, C₂H₆, and condensable gaseous pyrolysis products e.g., liquid fuels (Khonde *et al.*, 2016).

Liquefaction is a thermo-chemical process requiring a catalyst under high temperature and pressure in order to change solid biological material to the desired product of liquefied fuels or other biological chemicals. In this process, large molecule materials are broken down into smaller compounds in the presence or without the use of a catalytic agent in the substrate or by the application of a solvent that generates many forms of compounds, generally known as biological oil or biological crude. The achieved products have tiny molecules which are not stable and can readily react and undergo another polymerization into products of oily biocharacteristics with a varying range of molar mass dispersal. Also, in this procedure, water as a solvent disintegrates the tiny molecules further to micro compounds by the removal of water, hydrogen

and carbon. Once these micro compounds are produced, The study are reorganized through polymerization, condensation and cyclization into a fresh compound (Chowdhury *et al.*, 2017).

This process should not be confused with pyrolysis when compared, because both processes vary in operational data, in the need of a catalyst, and their end products. The products of this process are primarily liquefied and have little quantity of gas constituents at pressure and heat variations between 4900-21000 kPa, and 250.1-351°C respectively, using some salts of alkali metals as a catalytic agent. The liquefaction process sometimes needs additional reactants like hydrogen and carbon monoxide to speed up the complete operation.

This process does not sufficiently describe the main function of the catalytic agent. Some long-standing researchers offered procedures for sodium carbonate and potassium carbonate for liquefying biological material. These agents hydrolyze the large molecules (lignin, hemicelluloses, cellulose) into smaller molecules, a reaction is done to further it break down into more tiny molecules by the removal of water, hydrogen, oxygen, and carbon (Kumar *et al.*, 2020b). This process can produce fuels in liquid form which can be compared to products of petroleum including some valuable by-products; hence, new developments in this process have shown that the process may not be fruitful at a marketable level (Khonde *et al.* 2016; Obuka *et al.*, 2019). Some aspects controlling the marketing of this process could be the low productivity of bio-oil which is between 20.2–55.1% and has inferior oil quality in comparison to modern options like pyrolysis, because of its type of liquid product, stringent operating data, which are increased heat and pressure reactions, and need of a catalytic agent e.g., Carbon monoxide C₃H₇OH, C₄H₉OH and glycerin.

2.2.5.4 Thermochemical conversion; pyrolysis

Thermal degradation of biomass via pyrolysis method has gained more popularity because it is an efficient, low operational cost, reduced feedstock transportation from point of production to consumption destination, and capable of producing liquid, solid and gaseous fuel in the absence of oxygen unlike torrefaction to yield mainly solid fuel (Xueyong *et al.*, 2017; Gautam and Chaurasia, 2020). The term “Pyrolysis”, can be defined as the thermal treatment or decomposition of biomass or organic matters in the absence of oxygen, to produce solid, liquid and gaseous

products (Morgano *et al.*, 2018; Liu *et al.*, 2020). The resources for biomass include wood and their wastes, agricultural produce, their wastes and byproducts, urban solid wastes, excretion from livestock, wastes obtained after treatment of food items and aquatic life. The main biological constituents of these biological wastes are categorized into lignin, celluloses, and hemicelluloses. Pyrolysis is the application of high temperature or thermal degradation of biological wastes known as biomass without air (oxygen), or it can also be defined as a thermo-chemical process in which these biological substances are decayed in the presence of heat under a non-reactive environment, these process stages are: fragmentation, the formation of product and dehydration, these products are fuel gas products, charcoal, and bio-oil. The process of heat degradation of cellulose ensures the following reaction: a slow decomposition, and ash formation on heating at lower temperatures; and a rapid decomposition at increased temperatures (Eke *et al.*, 2019; Soka *et al.*, 2020).

According to Jaffar *et al.* (2020), pyrolysis product includes; gases, bio-biochar, and bio-oil. The major purpose of pyrolysis is to produce liquids for fuel or chemical production. During pyrolysis processing, breakdown of large compound hydrocarbon molecules of biomass into comparatively smaller and simpler molecules occurs, such as; gas, liquid, and biochar as shown in Figure. 2.4.

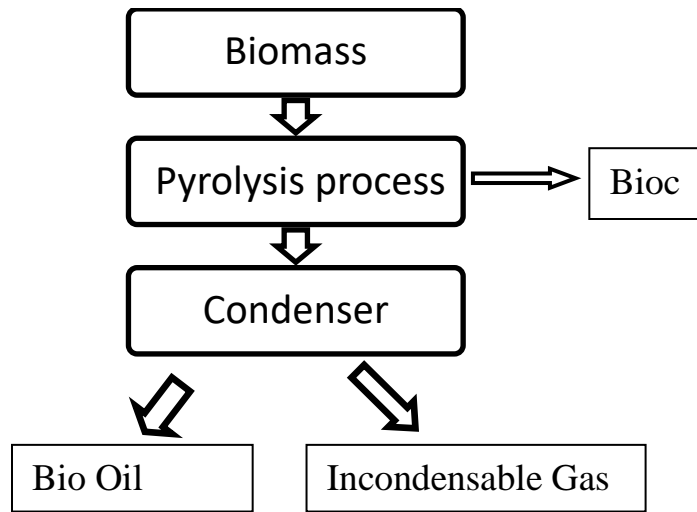


Figure 2.4: Schematic diagram for Pyrolysis Process (Guedes *et al*, 2018)

2.2.6 Basic principles of pyrolysis

Pyrolysis process involves the use of heat to break down lignocellulosic biomass which takes place under an inert atmosphere where the flow of nitrogen or argon is normally required devoid of oxygen. There are various complex procedures involved in the chemical reaction of pyrolysis, producing gases (methane, hydrogen, CO and CO₂) biochar and bio-oil (Isitan *et al.*, 2019; Kazawadi *et al.*, 2021). Pyrolysis is known as an antecedent of gasification or combustion processes that do not require agents like oxygen and steam (Gautam and Chaurasia, 2020). It has similarity to processes like cracking, devolatilization, carbonization, torrefaction, dry distillation, destructive distillation, and thermolysis, but having no comparison with gasification (Imam and Capareda, 2012; Ferreira *et al.*, 2020).

Pyrolysis is known as an antecedent of gasification or combustion processes that do not require agents like oxygen and steam (Gautam and Chaurasia, 2020). It has similarity to processes like cracking, devolatilization, carbonization, torrefaction, dry distillation, destructive distillation, and thermolysis, but having no comparison with gasification (Imam and Capareda, 2012; Ferreira *et al.*, 2020). During the process, decomposition of the substrate of biomass commences at about 349-549°C and can continue to 699-799°C in the absence of air or oxygen (Bridgwater, 2012; Varma and Mondal, 2017; Chukwunke *et al.*, 2019; Hu *et al.*, 2020), compared to 800 – 1000°C for gasification and combustion which is above 900-1500°C (Yueshi *et al.*, 2014; Arni *et al.*, 2018). Incomplete pyrolysis processes are known as torrefaction, whereby, the biomass undergoes thermal pretreatment in the absence of oxygen at a temperature range of 200-300°C to produce carbon (Balogun *et al.*, 2018; Zhang *et al.*, 2018; Abdenacer and Djalal, 2020), while carbonization is extreme pyrolysis or slow pyrolysis process whereby carbon is mostly left behind as its residue when the biomass is heated at a temperature range 200-300°C (Narzari *et al.*, 2017; Guedes *et al.*, 2018). The constituents of biomass are hemicellulose, lignin, cellulose, pectin etc., these large molecules of biological material begin to break down into small molecules which are mainly composed of a long polymeric chain of cellulose, lignin, hemicellulose, pectin and others (Jaffar *et al.*, 2020). The larger molecules of organic materials start to decompose to yield smaller molecules, which leaves the pyrolysis process as gases, condensable vapours and biochar. The fraction of product obtained from the process is based on some parameters which are, pressure, temperature, time, rate of heating, kinds of precursors,

configuration and design of the reactor, and moisture content of biomass which should be less than or equal to 10.1% (Kumar *et al.*, 2020c).

For higher moisture content in biomass, there's also a high probability of end products becoming liquids than when biomass contains a low quantity of moisture which produces a large quantity of dust instead of oil. At temperatures less than 449°C and slower heating rate, biochar is produced, for higher temperatures of more than 799°C and high heating rate gaseous product and ash are produced while bio-oil is produced by the addition of intermediate temperatures and moderately high heating rate. At the first process of pyrolysis, at a temperature range of 249 – 300°C, hot smoke is released at ten times faster than the later stage (Shi *et al.*, 2019; Sekar *et al.*, 2022). Biocharcoal is produced from wood as biomass, it produces a tiny quantity of smoke, before now, it was used in the extraction of iron during the melting of its ore which had a lot of challenges giving rise to the development of extracting energy from biomass by this process of pyrolysis, gasification and combustion (Magdziarza *et al.*, 2020). The process of combustion involves the burning of biological material in the presence of oxygen to generate heat, however, the proficiency of this exercise is not suitable. The process of gasification is conducted in the presence of an atmosphere of oxygen to produce gaseous products like fuels, while pyrolysis which leads the stage can be taken as a part of gasification and combustion which will yield gaseous fuels (Magdziarza *et al.*, 2020; Numes *et al.*, 2022).

2.2.7 Type of pyrolysis

2.2.7.1 Fast pyrolysis

Fast pyrolysis is a direct thermochemical technique. During this process, the feed material or biomass is heated at an increased temperature range of 400-600°C at a faster heating rate of 10-200 °C/s, with a short solid residence time of 0.5-10 sec and with fine particle size less than 1mm feedstock without oxygen (Paenpong and Pattiya, 2016; Pattiya, 2018; Zhong *et al.*, 2022). With reference to the original mass of the feed material, this process can generate between the ranges of 61-74.9% of biofuels in liquid form, biochar deposits of biomass of 15.5 – 24.9%. Oyebanji *et al.* (2018), reported that fast pyrolysis favours high production of bio-oil at a yield of about 70% with a high presence of complex organic compounds such as aromatic hydrocarbons,

ether, alcohol, organic acid, sugars, phenols, etc., which can be utilized for chemical production. More so, it has the potential of generating about 10.5 – 20.5% gas, these depend on the original feedstock utilized (Pattiya, 2018).

Some merits of this procedure are:

- It is possible and economical to scale up this process.
- The feed stock for this process is easily obtainable as it can use wastes from forests, manufacturing and urban communities.
- Logistics surrounding transportation and storage of the liquid products (fuel) is easily obtainable.
- Products from this process can be further transformed into other usable products.

The demerit of this process is that it cannot retain vapour for a long time, but if the obtained vapour and aerosol are cooled down immediately after the process, this can provide for increased yield of the bio-oil. Some applied uses of this process are electricity generation for industries, provision of fuel in the form of liquid biofuel for industrial turbines, boilers, and engines (Obuka *et al.*, 2019). Fast pyrolysis is divided into two namely; Garret pyrolysis and Georgia Tech bed process,

- **Garret pyrolysis**

Before now coal has been the raw material for pyrolysis this is known as pyrolysis of coal but recently the use of biological materials also called biomass as a raw material is a novel in the process of pyrolysis. The main objective of this procedure is the production of biological fuel. In this process, the waste biological material is allowed to mix with biochar at high temperature and recycle gas which is also at a high temperature. It is then followed up by the pyrolysis process which is also at a high temperature and a short holding time within the range of 801-802°C and 9.8 – 10.1 seconds respectively (Foong *et al.*, 2020). The products are then collected and separated (liquid and biochar).

- **Georgia Tech entrained bed process**

During this procedure, the raw material/feed or the biomass is properly grinded and sifted to obtain a grain size of about 0.9 mm, moisture is then removed to about 9.9% before being used as a feedstock to the reactor where the process of pyrolysis occurs in the presence of an inert gas

e.g., nitrogen. The temperature of the process is about 501°C and a product yield of approximately 50.1% and 30.1% gaseous matter is anticipated (Foong *et al.*, 2020).

2.2.7.2 Flash pyrolysis

Solid, liquid and gas can be obtained from the flash pyrolysis process as products. During this process, the production of bio-oil can be enhanced to an average of 75.1%. This is done by quickly removing the volatility of the product in the presence of a non-reactive environment, with a rapid heating rate above 1000°C and high reaction temperatures within the range of 900-1300°C. The process has low gas retention or residence time of less than 0.5sec. The major demerit of the process is that it has reduced the balance of heat energy. This is as a result of biochar who acts as a catalyst, the product (oil), turns out to be thick and it retains some solid matter. Also, the high heating and heat transfer rates can only be attained when the biomass particle sizes are very small around (60-140 mesh size). Another classification of this process is ultra-rapid pyrolysis, with a very low retention time of 0.49 seconds and a very high rate of heating, this procedure is utilized basically for the manufacture of bio-oil and biochar (Palumbo *et al.*, 2019; Tokmurzin *et al.*, 2022).

2.2.7.3 Intermediate pyrolysis

Intermediate pyrolysis among the pyrolysis methods has been mentioned to ensure high bio-oil and moderate biochar and NCG yields. It is the most suitable route to optimize co-pyrolysis yields by fully utilizing all the pyrolysis product yields and improving the bio-oil yield when compared to fast pyrolysis. It also tends to treat high moisture content present in the biomass. Hence, making the biochar yield attain activated carbon due to comprehensive interaction with steam (Yang *et al.*, 2017; Yang *et al.*, 2018; Kazawadi *et al.*, 2021). Intermediate pyrolysis is a direct thermochemical technique, in which the feed material is heated at an increased temperature range 450-650°C at a heating rate of 10-100 °C/min, with a residence time of 5-30min and with fine particle size less than 2mm feedstock without oxygen (Bertero and Sedran, 2015; Morgano *et al.*, 2018).

2.2.7.4 Slow pyrolysis

The main purpose of this process is the production of biocharcoal which can be obtained by the addition of a reduced temperature range of 150-300°C and a rate of heating less than 10°C/min. Vapour in this procedure has a long residence time of about 5.1 – 30.2 mins with a particle size range of 1-2 mm. Organic substances at a gaseous state will keep reacting with themselves to produce a little quantity of liquid and biochar. Bio-oil has low quality in this process (Arni, 2018; Mortari *et al.*, 2021). The main cause of the reduction in the generation of bio-oil during this process is the long residence time which causes a continuous breakdown. Low heat transfer and longer retention times in the process causes a need to increase the addition of energy (Halder *et al.*, 2019). In addition, slow pyrolysis can be categorized into conventional and carbonization pyrolysis with increased retention time and a very low rate of heating.

2.2.8 Products of pyrolysis

Pyrolysis solely involves the breaking down of large complex molecules into several smaller molecules. In view of these its product can be classified into three principal types:

- Liquid products
- Solid products
- Gas products

2.2.8.1 Pyrolysis liquid product

The pyrolysis' liquid products are known as; bio-oil, tar or bio-crude, which is a black tarry fluid that holds up approximately 20% moisture content. It consists of homologous phenolic compounds. The bio-oil product of liquid biomass is a mixture of complex hydrocarbons having large oxygen and water contents. Bio-oil could be further categorized into five broad categories considering compounds formed in it (Aziz *et al.*, 2018; Gautam and Chaurasia, 2020)

2.2.8.2 Pyrolysis solid product

Biochar is the solid form yield of pyrolysis. Biochar contains primarily carbon approximately 85%, but could also contain some percentage of oxygen, hydrogen and some

inorganic ash if it is present in the parent biomass. Biochar heating value ranges from 25 MJ/kg to 32 MJ/kg dry basis, as a result of these it is considered to be substantially higher than that of the parent biomass or its liquid product (Jafri *et al.*, 2017). Considering biomass being carbon-neutral, the combustion of biochar could also be accepted to be more environmentally friendly than coal (Lee *et al.*, 2017).

2.2.8.3 Gas

Gases (condensable vapour) and non-condensable (primary gas) are produced in the decomposition of biomass. Biomass containing heavier molecules, undergoes condensation upon cooling, adding to the liquid yield of pyrolysis. The NCG mixture, however, is made up of lower-molecular-weight gases which include; carbon dioxide, carbon monoxide, methane, ethane, and ethylene. These gases do not undergo condensation on cooling (Mohammed *et al.*, 2017).

2.2.9 Pyrolysis reactor

Reactor importance in any pyrolysis processes cannot be underestimated. Biomass reactors are aimed to satisfy specific conditions such as; heating temperature, vapour product residence time and required pressure for a high bio-oil yield. The following are types of biomass reactors:

2.2.9.1 Fixed bed reactor

It is a simple method that produces bio-oils that are largely homogeneous in size and have a low fines content (Qian *et al.*, 2019; Inayat *et al.*, 2022). It consists of the gas cooling compartment and the cleaning system that uses dry filters, wet scrubbers, and cyclones to filter out debris. The solid sample is permitted to move through a vertical shaft during the reaction where it comes into contact with an ascending counter-current gas stream product. Important components of these reactors, such as a feeding unit (fuel), a device for removing the ash, and the gas escape unit, are made of steel, firebricks, or concrete (Aziz *et al.*, 2018).

2.2.9.2 Fluidized bed reactor

The solid phase and the liquid phase coexist in a fluidized bed reactor, which is renowned for its simple design and operation technology. The technology is accomplished by forcing pressurized fluid via the solid substance. A fluid bed reactor is appropriate for intermediate and fast pyrolysis (Treedet and Suntivarkorn, 2018; Cao *et al.*, 2018).

2.2.9.3 Circulating fluid bed (CFB) reactor

Circulating fluid bed (CFB) is reactor type suitable for high throughputs, as a reality of this is used at petroleum and petrochemical industries in demand for high throughputs. The Heat transfer method involved in CFB involves recirculation of heat from heated sand in the chat combustion chamber. CFB reactor has some similarities with bubbling and twin fluid bed gasifier, the system gives good performance and high liquid yield. This can be achieved in a variety of ways, but the major difference includes that the biochar residence time can be said to be almost the same as for the vapour residue time. More also the gas and biochar are more affected as a result of higher gas velocities which can result in higher biochar contents in the collected bio-oil (Treedet and Suntivarkorn, 2018).

2.2.9.4 Vacuum pyrolysis reactor

The vacuum pyrolysis reactor is a slow pyrolysis reactor due to the relatively low heat transfer rate. Vacuum pyrolysis reactor utilizes the vacuum system technology to produce bio-oil in a range of 35-50 wt% (Dusso *et al.*, 2022). The vacuum is a lower pressure region compared to the atmospheric pressure located inside the reactor. The boiling point of substances obtained within the reactor is less compared to that reached atmospheric pressure. In lieu, carbon conversion in this pyrolysis type is far more easily reached. The technology has a short residence time during chemical processes due to its low operating pressure more also it had larger biomass particle size processing ability but requires special solids feeds and discharging devices in order to have an effective seal all the time (Carrasco *et al.*, 2017; Abomohra *et al.*, 2021).

2.2.9.5 Rotating cone reactor

A rotating cone reactor is a type of thermochemical technology which converts biomass into usable fuel in the presence of inert gas. This method utilizes the mechanical mixing of

biomass and sand as against the mixing of the biomass in hot sand driven by an inert gas. Major parts of this reactor are; a sand circulating system having a riser, a fluid bed biochar combustor. Biochar is combusted to generate the required heat for the pyrolysis process by reheating the inert sand that is already re-circulated in the reactor. Though the setbacks of the design of this reactor is its complexity. Also, its oil remains the only product of this technology while the high bio-oil yield high makes it highly considerable, and gases were flared (Gonzalez-Quirog *et al.*, 2017).

2.2.9.6 Auger reactor

Auger reactor is an environmentally friendly technology that uses a screw to transfer the biomass through a heated cylindrical tube depleted of oxygen (Campuzano *et al.*, 2019). During this process, the thermochemical conversion of the feedstock takes place while devolatilized and gasified at a temperature range of 400°C to 800°C. These led to the production of biochar and condensation of gases into bio-oil (Ding *et al.*, 2019; Jalalifar *et al.*, 2020).

2.2.9.7 Plasma reactor

A plasma reactor is a thermal conversion process that uses plasma (charged particles) for biomass (organic matter) conversion into fuel (synthetic gas). According to Tang and Huang (2005) and Serov *et al.* (2019), plasma reactors comprise a cylindrical quartz tube, fitted with two electrodes made of copper or tungsten for ionization of gases. The thermal conversion takes place as a result of a very high-temperature ionization of the gases to produce syngas and slag. The thermochemical dissociation of the organic matter is known as plasmolysis. Products of this thermochemical conversion are syngas and slag. The syngas obtained is pure calorific mainly carbon monoxide and hydrogen. Some of the advantages of this method include; safe means of destroying chemical and wastes, prevention of hazardous waste from reaching the landfills, recovery of ashes and particulates and production of syngas. Some of the disadvantages include; high capital cost, need for regular maintenance, high operational cost, low energy production and high energy consumption (Serov *et al.*, 2019).

2.2.9.8 Microwave reactor

In this technology, there is high energy transfer due to molecules and atoms interaction using the microwave. This a new technology of pyrolysis which can be used effectively on an industrial basis (Ethaib *et al.*, 2020; Ge *et al.*, 2021). The whole pyrolysis and drying processes are carried out in a microwave oven chamber operating on an electricity source. In the time past, this reactor has shown to be very effective in the recovery of chemical from biomass.

2.2.9.9 Solar reactor

In this technology, solar energy is stored as chemical energy. The mechanism consists of a quartz tube having an external opaque wall, exposed to high solar radiation capable of high temperature (>700°C) generation in the reactor (Sobek *et al.*, 2019). Having these technology help to reduce pollution and it's never tampered with during the heating process. The reactor start-up and shut downtime are also very fast.

Table 2.1: Merits and Demerits of Types of Reactors

Reactor type	Merit	Demerit	References
Fixed bed	<ol style="list-style-type: none"> 1. The design is simple 2. Dependable results 3. Independent biomass size 4. Easy mode of operational procedures 5. High heat transfer rate 6. Effective temperature control 	<ol style="list-style-type: none"> 1. High carbon conservation 2. Long solid residence time 3. Low ash formed 	Chowdhury <i>et al.</i> (2017); Aziz <i>et al.</i> (2018)
Bubbling fluidized bed	<ol style="list-style-type: none"> 1. Simple in design 2. Easy mode of operational procedures 3. The temperature can be regulated easily 4. High heat transfer rate 	<ol style="list-style-type: none"> 1. Mainly utilized for large-scale application and small biomass sizes 2. Operating costs is high 	Laouge <i>et al.</i> (2019); Cao <i>et al.</i> (2018)

Vacuum	<ol style="list-style-type: none"> 1. Pure bio-oil 2. Processes large particles 3. Requires no inert gas 4. Low temperature 5. Condense liquid product 	<ol style="list-style-type: none"> 1. Slow operating process 2. Requires high solid residence time 3. Mainly utilized for large-scale application 4. Poor heat and mass transfer rate 5. More water generated 	Menendez <i>et al.</i> (2004); Carrasco <i>et al.</i> (2017)
Auger compact	<ol style="list-style-type: none"> 1. Inert gas not required 2. High heat transfer 	<ol style="list-style-type: none"> 1. Lower process temperature 2. Moving parts in a hot zone 3. Low Heat transfer rate 	Campuzano <i>et al.</i> (2019); Jalalifar <i>et al.</i> (2020)
Plasma	<ol style="list-style-type: none"> 1. Higher energy density 3. Higher rate of heat transfer 3. Easy process control 4. Higher consumption of electrical power 	<ol style="list-style-type: none"> 1. Operating costs is high 2. Requires small biomass sizes 	Serov <i>et al.</i> (2017)
Microwave	<ol style="list-style-type: none"> 1. Heat transfer rate is high 2. Effective temperature control 3. Compact structure 4. Higher heating rate 5. Large-size biomass temperature distribution 	<ol style="list-style-type: none"> 1. Involves high temperature 2. Electrical power consumption is high 3. Higher cost of operation 	Ethaib <i>et al.</i> (2021); Ge <i>et al.</i> (2021)
Solar	<ol style="list-style-type: none"> 1. Dependent on renewable energy 2. A high Heating rate is obtained 	<ol style="list-style-type: none"> 1. High temperature 2. Dependent on weather 	Sobek <i>et al.</i> (2019)

Rotating cone	1. Hot sand and biomass substrate is circulated by centrifugal force 2. Requires no carrier gas	1. Difficult to operate and required small biomass sizes 2. Difficult large-scale application	Gonzalex-Quirog <i>et al.</i> (2017)
----------------------	--	--	--------------------------------------

2.3 Empirical Review

2.3.1 Biomass characterization

Augustine *et al.* (2015) evaluated the structural composition of woody and non-woody biomass. Gravimetric, spectroscopic, and chromatography were employed. Results showed that cellulose and hemicellulose contents greatly influenced the emission of volatile matter.

Ayeni *et al.* (2015) studied the structural modification of siam weed via alkaline oxidative periodic treatment [NaOH-H₂O₂- with Ca (OH)₂-H₂O₂], as well as the enzymatic conversion of siam weed into bioenergy. Also, pretreatment of the siam weed was performed to obtain the optimum targets at 70°C for 3 hr. Results showed that the raw cellulose content of 44.29% increased to 47.18% while the lignin of 24.2% dropped to 21.09%. Finally, the pretreatment led to disruption in the biomass.

In the work of Aladin *et al.* (2017), an empirical study on the importance of selecting approximate material and design conducted. The result showed that the utilization of a suitable reactor for the pyrolysis process helps to minimize cost and enhance the quality of bio-oil production. The study was limited to the effect of reactor types on biomass fuel products.

Ogunsola *et al.* (2018) performed an empirical study on the analysis of wood fuel (Fuel properties and characterization) of different selected wood wastes (Saw Dust) such as Afara, Arere, Iroko, Ayin and Obeche wood. The fuel rating of the selected wood is 1.75 (Obeche), 2.6 (Ayin), 3.13 (Masonia), 3.25 (Iroko), 3.25 (Afara) and 2.0 (Arere). It was observed that Iroko and Afara wood had the worst fuel properties while obeche had the best fuelwood properties. The work was limited to the fuel rating of several biomass materials, but no mention of any optimization of the process.

Echeverria *et al.* (2018) evaluated the macro structural effect of a corncob. The chemical composition showed that the cellulose, hemicellulose, and lignin contents were 40.95, 38.94, and 16.54 wt%, respectively. An upgrade of cellulose content (64.12 wt%) was observed after

pretreatment. Also, the hemicellulose and lignin contents decreased to 19.76 and 10.16 wt%. The study also recorded high amount of glucose of 40.90 g L⁻¹

Baruah *et al.* (2018) investigated products formed in oil shale pyrolysis and used TGA coupled with TGA-FTIR to establish the decomposition zones. Their work applied TGA-FTIR in the shale oil characterization at optimum conduction and observed that the shale oil showed an abundance of high energy density aliphatic compounds.

Romuli *et al.* (2019), worked on “Thermo-Gravimetric Analysis” (TGA) utilizing a fixed-bed quartz reactor to obtain a suitable degradation model and investigate the effect of operating conditions on product distribution. In their work, it was observed that at a temperature range of 250.15 to 450.15°C, thermal decomposition occurred which could be described by the three-parallel reactions model. The study noted that yields of gas, liquid and biochar influenced by the temperature and hold time within the fixed-bed quartz reactor.

Asibor *et al.* (2019) investigated the physicochemical and thermal properties of Obeche, Albizia, Bombax, Apa, Acacia, Okwen, Ohian, Ukpe, Otu, Ekhimi, and Ohain. The results observed that the samples' heating value ranged between 87.51 – 90.94%, ash content ranged between 0.2 – 2.76%, and moisture content ranged from 8.62 – 10.53%. The ultimate results showed the average carbon, hydrogen, oxygen, nitrogen, and sulphur contents for the samples are 52.03, 5.41, 42.31, 0.23, and 0.023 wt% respectively. This work concluded that the physical and chemical properties of the biomass samples were within the desired ranges. Also, the experimental calorific values of the samples range from $0.8666 \leq x \leq 0.929$. Finally, Apa was found to be the most suitable among the sample for energy generation while obeche was noted to be the least suited.

Mansor *et al.* (2019) studied pineapple biomass characterization to determine the quantity of lignocellulose content and its effect on heating value. Their result shows that the biomass leave recorded cellulose (30 wt%), hemicellulose (37 wt%), and lignin (22 wt%) when compared to stem and root due non-wooden nature of the leave. The findings also indicated that pineapple biomass has more hemicellulose and cellulose content and possesses different thermal stability when compared to stem and root due to their varying chemical structure.

Umar *et al.* (2020) investigated palm kernel shell for potential syngas production by exploring the proximate, elemental and higher heating value. The elemental components and structural composition were determined using X-ray fluorescence and scanning electron

microscopy (FESEM) techniques. Results showed that palm kernel shell recorded carbon of 48.4%, hydrogen of 5.85%, and oxygen of 45% for the ultimate analysis, while the proximate analysis recorded a volatile matter, fixed carbon, ash and moisture contents of 73.4, 29.4, 6.0 and 5.8 wt% respectively. Also, the calorific value was 18.84 MJ/kg.

2.3.2 Influence of pyrolysis parameters

Bridgwater *et al.* (1999) carried out a detailed comparison of the various types of reactors used for the pyrolysis process by putting into consideration, the cost, merit, and demerit of each reactor and their criterion for design and material selection. The study opined that the ablative reactor generally is very difficult to design and scaled up due to its complexity and multiple moving parts when compared to another reactor. Also, Kostas *et al.* (2020) deduced that the reactor is mainly utilized when the biomass particle sizes are large and the volume of gas carriers is low during the production of condensable and non-condensable gases. Modelling and optimization of the operating parameters were not carried out. The study only compared various reactors for optimum biomass yield production.

Ruiz *et al.* (2013) designed and fabricated a fixed bed reactor for the decomposition of biomass to biofuel using the pyrolysis process. The reactor consists mainly of a fixed bed reactor, liquid collectors and liquid fuel. During the test, the temperature of the reactor bed, feed particle size and running time was altered and a higher heating value of devdaru seeds of 24.22 MJ/kg was obtained. In this work, design and fabrication were fine, operating parameters were altered as stated but only liquid yields were noted during the pyrolysis process.

Olagbende *et al.* (2016) carried out a modification of a fixed bed reactor for the pyrolytic decomposition of royal Poinciana (*Delonix Regia*) pods, seed and husk to biofuel and biochar. The samples were heated at various temperatures ranged 300-500°C at 50°C interval, each lasting for about 7hours. It was deduced that the yield of bio-oil from seed was higher than that of the husk and pods. Also, biochar and biofuel were generated in a significant amount. The study proposed that other parameters such as residence time and heating rates should be investigated.

A fixed-bed batch type pyrolysis reactor for the production of oil was designed and fabricated by Aziz *et al.* (2016). The operation temperatures ranged from 430 to 500°C. Results showed that biochar, pyrolytic gas and pyrolytic oil yields were 38.3, 12.7 and 49% respectively.

This report only used a fixed bed reactor type within a temperature range in their investigation. No optimization of the process was also mentioned.

An investigation of the effects of the pyrolysis residence time and temperature on various biochar yields were carried out by Junna *et al.* (2017), it was observed that an increase in residence time at about 8 hours at 300°C reduce the yield of biochar generated while the residence time had little effects on the biochar yield at 600°C, instead, it led to a change in the surface and internal structure of the biochar.

Carrasco *et al.* (2017), studied “the techno-economic for producing liquid fuels from forest residues” for their work, laboratory experiment was performed via pyrolysis process to obtain product yields and composition. Aspen Plus process simulation for a feed rate of 2000 dry metric tons per day was utilized to determine the energy requirements and equipment sizes estimation. The research was restricted to forest residues and results showed that the forest residue yielded 24% biochar by weight. Similarly, bio-fuel yields were 16% by mass and 40% by energy. From their results, it was observed that the material stream could be used to produce hydrogen sufficiently for the hydrotreatment without requiring external natural gas. Their work demonstrated that the oil yields from forest residues, in comparison to other pyrolysis oil yield through catalytic hydrocracking and then gasification of pyrolysis biochar to generate syngas. Limitations include a type of biomass investigated which is forest residues, pyrolysis method was not stated while hydro treating was involved. But from their result, it was deduced that the simulation of the process revealed a high chance of obtaining sufficient bio-oil.

The thermochemical conversion of carbonaceous biomass species such as sawdust, empty fruit bunch, and giant miscanthu into bio-oil and biochar using a pilot-scale circulating fluidized bed reactor was carried out by Yong *et al.* (2018). The study proposed that additional units for metal and biochar removal should be provided during pyrolysis plant design so that the required amount of bio-energy could be collected during the operation process. The result showed that heating value, moisture; and ash contents influenced the yield of bio-oil. Also, during the fast pyrolysis process, the optimum bio-oil yield was recorded when the biomass was heated at 500°C.

Piloto-Rodríguez *et al.* (2020) investigated the parametric study of flash pyrolysis of *Jatropha* oil cake using nitrogen (N₂) in an electrically heated fluidized bed reactor. From their result, the pyrolysis oil had a calorific value of 19.66 MJ/kg and could be upgraded to a higher quality bio-fuel or serve as a source of low-grade fuel directly. In this work, a parametric study

was carried out in an electrical operate fixed bed reactor. No optimization of the parameters was mentioned and nitrogen and reaction temperatures were only investigated during the pyrolysis process.

Gautam and Chaurasia (2020) investigated the effects of kinetic parameters such as temperature, residence time of volatile, and reactor length on the yield pyrolysis products using neem bark, bamboo, rice husk, rice straw. Results showed that maximum clean syngas was generated for neem bark (52.61 vol%), while the optimum yield of bio-oil of 46.93% was generated for bamboo at 450°C.

Magdziarz *et al.* (2020) adopted a hydrothermal carbonization (HTC) process to investigate the effect of temperature, residence time, and physiochemical properties on the yield of the pyrolysis products such as biochar and liquid fuel using energy crop (*sida hermaphrodita*), wood biomass (pine) and agricultural waste. The HTC was carried out in the reactor at a temperature of 220°C at 4 hours residence time. Consequently, Py-GC-MS apparatus was used to investigate the pyrolysis process of the hydrobiochars. After the biomass had been pyrolyzed at 400, 500, and 600°C, it was deduced that rapid temperature heating, short residence time as well as the physiochemical components of the biomass influenced the yield of bio-oil and biochar with short residence time. The study was unable to convert the heat loss from the reactor to another form of energy e.g., electricity.

2.3.3 Energy and exergy analysis of pyrolysis process

A chemical thermodynamic model was developed by Yueshi *et al.* (2014) to predict the product composition of a biomass gasification system. Preheated air and steam were used during the process while the ratio of steam to mass as well as temperature was also analyzed. It was observed that the chemical energy output of the produced syngas was at its peak level when the S/B ratio was 1.83. However, it was stated that continuous increase in S/B ratios above the recommended limit greatly affect the energy and exergy efficiencies negatively while a rapid increase in preheating temperature enhanced the chemical energy of the energy and exergy efficiencies as well the syngas produced (Moshi *et al.*, 2020). Finally, peak values of 81.5 and 76.2% were obtained for the energy and exergy efficiencies respectively. Modelling was mentioned, exergy and energy analysis was carried out, but no optimization, conversion of fuel into power was mentioned.

Peters *et al.* (2015a) carried an exergetic analysis of biofuel generation using a fast pyrolysis process and hydro-upgrading. The results showed that stream reforming reactor greatly reduces the efficiencies in the process. The research was unable to point out the component that led to instability in energy and exergy efficiencies. The study only considered the effect of temperature and residence time. In the work of Nyazika *et al.* (2019), the effects of heating rate, residual time, structural parameter, and temperature on physical and chemical modelling of biomass were investigated and their results showed that the models were able to reproduce the experimental results. Optimization of the operating parameters was not performed in this research.

Peters *et al.* (2015a), in their work, presented an assessment of bio-refinery process exergetic performance. Their analysis was based on catalytic hydro upgrading of bio-oil using fast pyrolysis and then upgraded to synthetic fuels in a catalytic hydrotreating process. Commercial software was used to simulate the biorefinery process and then analyzed using exergetic analysis. From their work the following analysis was carried out; definition of exergy balances for each component of the plant and the calculations of the exergetic efficiencies and exergy destruction rates at the component, section, and plant level, identified the thermodynamic inefficiencies, and reveals the process improvements. From their results, 60.1% was the exergetic efficiency obtained for the overall biofuel process while 77.7% exergetic efficiency was obtained for the biorefinery upgrading process. The study concluded that the steam reforming process contributed the highest overall exergy destruction taking place within the biorefinery as a result of the steam-reforming reactor and the associated heat exchangers. Their work didn't carry out modelling and optimization of the system, a simulator was used to analyze the energy and exergy. The heat exchanger was mentioned in their work and the efficiency of the bioenergy was reported.

In the study of Rupesh *et al.* (2016), gasification was explained as a thermo-chemical reaction for converting biomass into fuel gases in a reactor while noting that the efficiency of conversion depends on the effective working of the gasifier. The study used energy and exergy analysis to analyze various performances of different biomasses during gasification in a quasi-equilibrium model. The feasibility of different biomass materials as a feedstock gasifier was compared. It was also inferred that low ash and increase moisture contents led to an appreciable increase in the energy and exergy efficiencies. Their work didn't consider optimization and

modeling of the system used, exergy and energy analysis was carried out by considering the only temperature.

Gonzalez *et al.* (2019) investigated biomass thermochemical conversion into energy by carrying out energetic and exergetic analysis for syngas production from biomass gasification along with its potential use for heat and power generation was carried out using air as the gasifying agent. From the results, cold-gas and hot-gas efficiencies of 74.5 and 84.6% were stated achievable by considering an ER ratio of 0.34, it was also noted that energy loss represented about 15.3% of the total energy input to the gasifier. In this work, the air was used as the gasifying agent. In the thermochemical conversion, no modelling optimization of the process was mentioned. Energy and exergy analysis carried out in their study only investigated the effect of temperature on the energy and exergy efficiencies.

Yan *et al.* (2019) researched biomass-fueled power plant energy, exergy, and economic analyses, with carbon capture and sequestration. The study firstly validated the sequestration (BFP-CCS) models before building the integrated model of BFP-CCS. Next was a characterization of the BFP-CCS and analysis of the energy, exergy and economics, and the optimum operating condition of BFP-CCS. The study obliged that steam turbines and solid oxide fuel cells are the biggest contributors to the energy and exergy losses in any BFP-CCS. No modelling and optimization of the process were carried out.

Singh *et al.* (2020) carried out work on pigeon pea stalk and eucalyptus Torrefaction in a tubular quartz reactor in the presence of nitrogen at a constant residue time and heating rate of about 200 °C. The study observed that under a moderate torrefaction (250 °C), the two biomass (feedstocks) in review recorded solid yield of 63-64% with by-products obtained in the range of 19-29% (liquid) and NCG at 8-18%. The study noted that from their analysis, the energy and exergy value of the solid product decreased while there was an increment in the NCG and liquid when the temperature increases. It was further noted that CO has a major effect on energy and exergy and solid recorded the highest Energy and exergy followed by liquid and then NCG. Exergy efficiency of a solid product derived was at the Range of 52 - 54% in moderate torrefaction condition. Finally, the study noted that recuperation of energy from by-products (liquid and NCG) could increase the energy recovery in solid by 8-9%. The only temperature was altered during the pyrolysis process while other operating parameters were kept constant. Also, no modelling and optimization were carried out, exergy and energy analysis were reported.

2.3.4 Modelling and optimization of thermochemical conversion process

In the works of Sharma *et al.* (2015), a comprehensive particle scale model for biomass pyrolysis process using the phenomenological approach was developed. Particle shrinkage and drying were considered and results showed that the rate of biomass decomposition to end products increased as moisture content increase. The optimization of the process parameters on the yield of bio-oil was not carried out.

Panneerselvam and Sai (2016) formulated a computational fluid dynamic model of biomass fast pyrolysis in a fluidized bed to investigate the effect of biomass particle type, density and size, and temperature. The research was limited to kinetic models. It was observed that this effect has a great impact on the generation of biochar and biofuels.

Hejazi *et al.* (2016) developed a reactor and particle model to predict the drying and biochar and biofuel yield from the pyrolysis of biomass. Results showed that a decrease in particle size and increase in reactor enhanced the time take to complete the conversion and heat-up process of the biomass. The energy and exergy efficiency of the power plant developed were not investigated.

Xiong *et al.* (2016) carried out a multi-scale computational fluid dynamic model to predict the effect of bubbling bed hydrodynamic in a reactor. It was observed that the production of mean tar increases as the fluidization velocity increased. Also, the yield of mean tar increases with a decrease in the size of the sand particle. The research carried out hydrodynamic model in the reactor.

Crespo *et al.* (2017) performed optimization of production bio-oil from *Acacia mangium* wild wood. The effects on temperature, particle size, and heating rate on the bio-oil yield were investigated using a two-level parametrial design while response surface methodology was utilized to obtain the optimum conditions for the generation of bio-oil. The study did not consider residence time which affects the yield of pyrolysis products. Also, the quality of the bio-oil yield was not tested. Results showed that the optimal values for temperature, heating rate, and particle size were 499.5°C, 120°C/min, and 0.46 mm respectively. Also, results obtained from gas chromatography-mass spectrometry (GC-MS) showed that the percentage of phenol produced was higher when compared to other components.

Pattiya *et al.* (2018) reported higher bio-oil yield in an increased gas flow from 1 L/min to 1.5 L/min. The study further noted no significant increase in the liquid yield from 1.5 L/min

to 3 L/min. The optimum bio-oil yield was achieved at a temperature and residence time of 550°C and 0.5 sec respectively.

Hameed *et al.* (2019) review biomass pyrolysis models such as kinetic, network, and mechanistic models. The study concluded that further work should be done on energy and exergy analysis as well as multiscale models such as phenomenological and hydrodynamic model by considering reactions of all biomass components and potential interactions.

Saleh *et al.* (2019), intending to optimize gasification systems, used municipal waste for air gasification and experimentally investigated it using a fluidized-bed reactor. Equivalence ratio (ER) and temperature parameters were considered, energy and exergy analyses were performed. Results obtained revealed that the produced gas energy and exergy contents increased sharply then declined when the temperature exceeded 650°C. The research was restricted to the gasification of biomass. Also, only equivalent ratio and temperature parameters were investigated.

Moshi *et al.* (2020) worked on a biomass gasification system, a model was developed to predict the product composition with the aid of highly preheated air and steam. In their work, it was stated that industrial-scale gasifiers constituted a huge financial investment hence the need to develop a model. The study developed a five-step equilibrium model using ASPEN PLUS software for the gasifier. It was found that the model could predict accurately the performance of the system by a close comparison of the simulation and experimental results. A thermodynamic analysis was carried out based on the achieved model while relying on the first and second laws to obtain various S/B ratios and preheating temperatures of the gasifying agent. From their results, S/B ratio was obtained as 1.83 highest syngas was produced. The study also noted that higher S/B ratios had energy and exergy efficiencies negative effect, nothing that the produced syngas chemical energy and the two efficiencies increases by preheating temperatures. 81.5 and 76.2%, respectively represented the peak values for the energy and exergy efficiencies. Relying on the peak values calculated. The study suggested a thermodynamically and practically possible operating region was determined for industrial applications. The study was based on biomass decomposition via the gasification process only.

2.32.5 Response surface methodology (RSM)

Some researchers proposed the utilization of response surface methodology (RSM) to optimize the operating parameters of the various systems (Absina *et al.*, 2011; Hossain *et al.*, 2019; Laougé *et al.*, 2020). RSM combines statistical and numerical optimization techniques to create empirical equations and ascertain how given conditions affect targeted responses. It was initially created for the improvement of industrial processes with several input parameters. The input parameters are the independent parameters, whereas the performance measures are regarded as response (Mohammed *et al.*, 2017).

Kiliç *et al.* (2014) implemented RSM to study *Euphorbia rigida* fast pyrolysis optimization conditions. The maximum bio-oil yield of 35.3 wt% was obtained at corresponding optimum parameters of temperature (600°C), heating rate (200°C min⁻¹), and nitrogen flow rate (100 mL min⁻¹).

Kumar *et al.* (2019) employed RSM using centre composite design (CCD) to optimize kinetic parameters of pyrolysis of *Saccharun munja*. Results showed that optimum bio-oil yield (46 wt%) was recorded at a temperature of 525°C and time of 60 min.

In the work of Hossain *et al.* (2019), RSM method was used to optimize the operating parameters such as N₂ flow rate, temperature, and microwave power to optimize the yield of biochar and hydrogen gas yields during the pyrolysis process. The software proposed three optimized operating parameters for enhanced the yield of H₂, biochar, and the combination of H₂ and biochar. Statistical tests conducted using ANOVA showed that RSM method is very reliable for the optimization of biomass pyrolysis process' parameters. The research only investigated biochar yield from the pyrolysis products. Also, residence time and heating rate were kept constant throughout the process.

Kadlimatti *et al.* (2019) optimized pyrolysis operating parameters such as temperature, residence time and nitrogen flow rate from fast pyrolysis food waste using RSM. An optimum bio-oil yield (30.24 %) was recorded at a temperature, residence time and nitrogen flowrate of 400°C, 30 min and 50 mL/min respectively.

Laougé *et al.* (2020) utilized RSM with central composite design to model and optimize pyrolysis operating conditions to enhance the performance of pyrolysis of palm oil shells. Results showed that optimum bio-oil generated was 46.4 wt% when the temperature, particle size,

reaction time, and nitrogen flowrate was 500°C, 2 mm, 60 min and 2 ml/min respectively. Their work carried out modelling and optimization of the system, no report on energy and exergy and generated bio-oil yields was reported.

2.4 Gaps Identified in the Literature

Recognizing the dearth of information regarding modelling and optimization of pyrolysis operating process, the best of available knowledge in literature revealed paucity or no information on the utilization of more than four operating parameters. However, the best available model to optimize pyrolysis for enhanced yields are experimental runs carried out using fast pyrolysis process which were limited to a temperature range of 350-600°C.

This study therefore focuses on the modelling and optimization of the intermediate pyrolysis process putting into consideration five operating parameters such as temperature, heating rate, residence time, and particle sizes to avoid error that might occur due to insufficient consideration of pertinent parameters. Also, the experimental runs will be carried out using a temperature range of 320-720°C.

In exergy and energy analysis, most researchers only investigated the influence of two pyrolysis operating parameters on the energy and exergy efficiency of bio-oil, biochar and NCG, while in this study five parameters would be investigated. Also, the parameters that are responsible for energy loss within the system would be detected.

The response surface methodology (RSM) based on central composite design (CCD) would be utilized to manipulate these operating parameters. The optimized value of these parameters will be determined to ensure quality and improve the quantity of pyrolysis products to minimize waste and production costs. This essentially requires accurate modelling to enhance the effect on the pyrolysis process. Reaction temperature, heating rate, particle sizes, and residence time play a vital role in the production process showing often a linear relationship with the production but at some desired set-point.

The modelling and optimization of the biomass pyrolysis process are crucial for developing new processes, optimize the performance of the processes, enhance the design and formulate new products (Myers and Montgomery, 2000; Guedes *et al.*, 2018; Ferreira *et al.*,

2020). Also, the functional group and chemical composition of the bio-oil and biochar would be determined using FT-IR and GC-MS techniques, while the morphology, image resolution and phases of the would be investigated Scanning Electron Microscope (SEM)/ Electron dispersive X-Rays Spectroscopy (EDX).

CHAPTER THREE

MATERIALS AND METHODS

The graphical representation of methodology shown in Figure 3.1, is the summary of the processes utilized in achieving the objectives of this research.

3.1 Source of Materials

Lignocellulose biomass samples, namely shea butter wood, baobab wood, melina wood, obeche wood, bamboo, palm kernel shell, rice husk, coconut shell, corn cobs, siam weed, moringe oleifera, lemon grass and mexican sunflower were sourced from the sawmill, palm oil mill, and local farms in Omu-Aran, Kwara State, Nigeria (Latitude $8^{\circ}08'18.85''N$ and Longitude $5^{\circ}06'9.36''E$), while the sugarcane bagasse and the sugarcane straw were obtained from Ajasse Ipo, Kwara State, Nigeria ($8^{\circ}13'60''N$ Latitude and $4^{\circ}49'0''E$ Longitude). Plate 3.1 depicts the raw biomass samples prior to pretreatment.

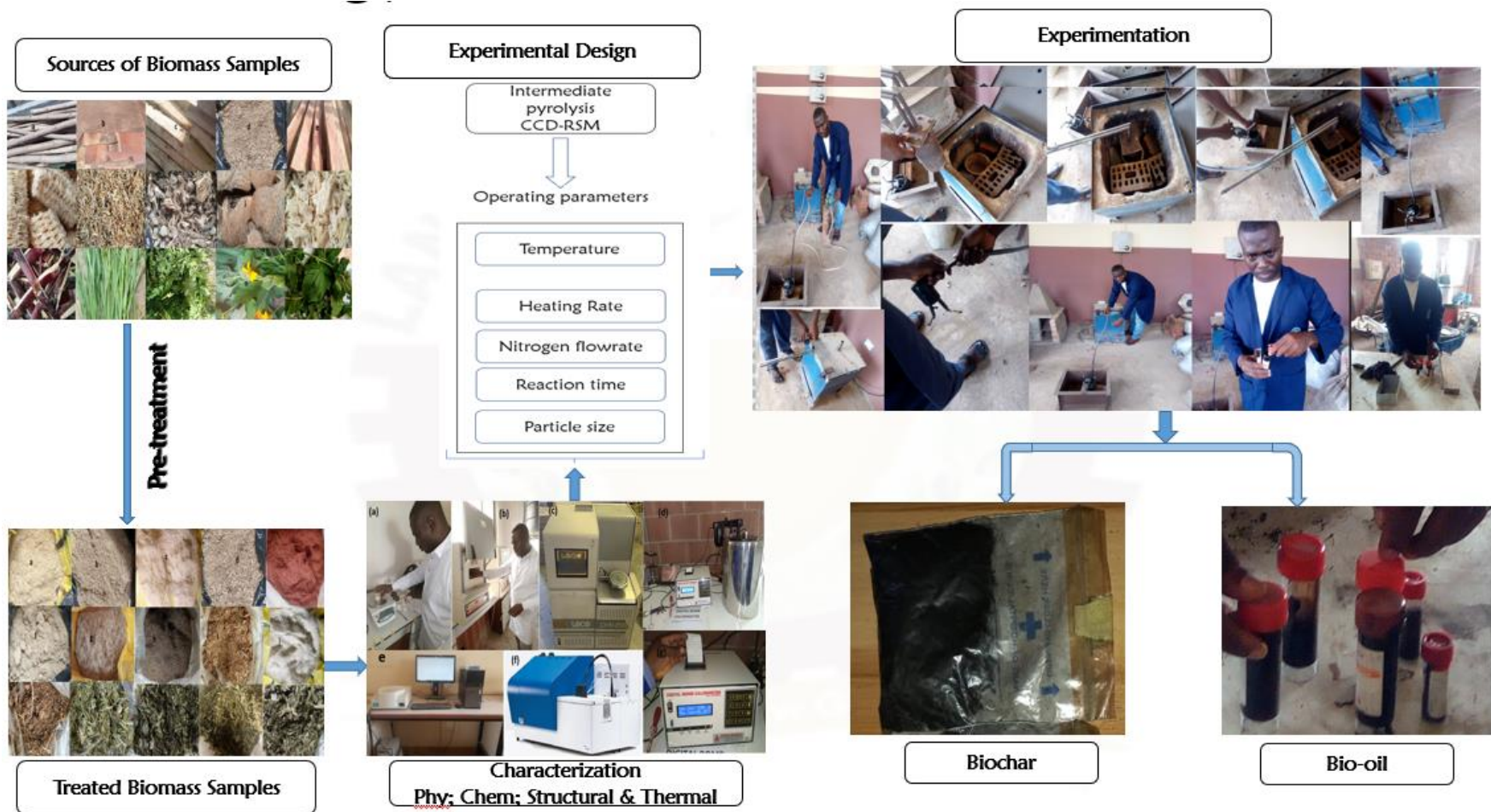


Plate 3.1: The pictorial representation of methodology



Plate 3.2: Raw biomass prior to pretreatment (a) Bamboo (b) Baobab wood (c) Meliana wood (d) Obeche wood (e) Shea butter wood (f) Corn cob (g) Rice husk (h) Palm kernel shell (i) Coconut shell (j) Sugarcane bagasse (k) Sugarcane straw (l) Lemon grass (m) Moringa oleifera (n) Mexican sunflower (o) Siam weed

3.2 Pretreatment of Raw Biomass

The biomass samples were sorted and rinsed with distilled water to remove contaminants such as stones and other foreign objects and sun-dried for five days (5 h/day) to remove surface and residual water impurities to enhance grindability (Adeleke *et al.*, 2021). The sun-dried biomass samples were milled with a ball milling machine and sieved to various particle sizes with a diameter (d_p) of 0.1-0.2 mm, 0.2-0.4 mm, 0.4-0.6 mm, 0.6-0.8 mm, and 0.8-1.0 mm in Geotechnics laboratory, Civil Engineering Department, Landmark University, Omu-Aran, Kwara State to enhance densification (Kshirsagar and Kalamkar, 2020). Thereafter, the biomass samples were oven-dried by placing them in a muffle furnace at $105 \pm 2^\circ\text{C}$ for 7 hours in the Microbiology Laboratory, Landmark University, Omu-Aran for the samples to be dried. This method was adopted, because previous studies reported that the biomass samples under investigation do not have volatile compound at standard temperature and pressure. Hence, leading to an increase in surface area, heating value, and average molecular weight of the bio-oil and biochar yields (Wang *et al.*, 2008; Adegoke *et al.*, 2014; Acevedo *et al.*, 2019; Quan *et al.*, 2019). Finally, the oven-dried biomass samples were stored in a zip-lock polyethylene bags at ambient temperature for characterization and pyrolysis experiment. Plate 3.2 shows the pretreatment process, while Plate 3.3 presents the biomass samples after pretreatment.



Plate 3.3: (a) Grinding (b) Oven drying of biomass samples in Civil Engineering Laboratory of Landmark University, Omu-Aran



Plate 3.4: Treated Powdered biomass for characterization (a) Bamboo (b) Baobab wood (c) Meliana wood (d) Obeche wood (e) Shea butter wood (f) Corn cob (g) Rice husk (h) Palm kernel shell (i) Coconut shell (j) Sugarcane bagasse (k) Sugarcane straw (l) Lemon grass (m) Moringa oleifera (n) Mexican sunflower (o) Siam weed

3.3 Physicochemical Analysis

3.3.1 Proximate analysis of oven-dried powdered biomass

Carbolite muffle furnace (Model: CWF1223-230SN+and02-3216P1) in the Biochemistry Laboratory, Landmark University, Omu-Aran (Plate 3.4a-b) was used to determine the proximate analysis such as moisture content (MC), fixed carbon (FC), volatile matter (VM) and ash content. According to ASTM E 1358 – 97 standards, the moisture content was determined, whereby, 0.5 g of the oven-dried biomass samples were transferred into an empty crucible. The mass of the crucible plus biomass was weighed and recorded. The samples were heated in a muffle furnace at 105°C for 2h. The Volatile matter (VM) was determined using the ASTM E872-82 by weighing an empty crucible and then placing 1 g of each biomass in a muffle furnace, maintained at 900°C for 8 min all through. Finally, the weight was measured and recorded. Deploring ASTM standard ASTM D1102-84, the biomass ash content was evaluated using a muffle furnace. 1 g of biomass sample was measured into a silica crucible and later transferred into a muffle furnace, maintained at 105°C for an hour. The crucible was transferred into the desiccator to cool down to room temperature. After that, the crucible was transferred into a muffle furnace charged at 585°C for 3 hours. The FC was determined by difference using equation 3.1 as suggested by (ASTM E 1358 – 97, 2006; ASTM D1102-84, 2007; ASTM E872-82, 2006)

$$FC = 100 - (MC\% + VM\% + Ash\%) \quad 3.1$$

3.3.2 Ultimate analysis of oven-dried powdered biomass

The carbon (C), hydrogen (H), and nitrogen (N) contents were determined using LECO CHN 2000 Elemental Analyzer (Plate 3.4c) based on ASTM D5373-21 standard. Whereby 0.5 g of the sample was measured into a crucible charged into a GenLab oven maintained at 105°C for 1 h and encapsulated in a thin foil to fit into the LECO CHN 2000 Elemental Analyzer. After that, the sample was transferred into the purge chamber of the furnace, maintained at 1300°C for 7 min. While the sulphur content (S) was determined using ASTM D4239-11 by placing 2 g of the biomass in a flame photometer and maintaining it at a temperature greater than 1000°C, after that, the sulphur detector detected the sulphur present (3.4f). Finally, the oxygen component was determined by difference as shown in equation 3.2 as proposed by (ASTM D5373-21, 2016; ASTM D4239-11, 2011)

$$Oxygen = 100 - (C\% + H\% + N\% + S\%) \quad 3.2$$

3.4 Structural Composition Analysis Oven-Dried Powdered Biomass

The extractive content in the biomass was determined by first adding 100 mL of acetone used as a solvent for extraction into a 2 g of oven-dried raw biomass (A) placed into a cellulose thimble. The boiling and rising of the mixture were carried out at 70°C for about 20 min. The sample was dried in a Genlab oven for 2 hour and maintained at a temperature range of 105-110°C until a constant weight was attained (B). The number of extractives was determined using Eqn. (3.3) as proposed by (Mansor *et al.*, 2019). The hemicellulose content was obtained by adding 150 mL of 500 mol/m³ sodium hydroxide (NaOH) into an extractive free (B) biomass sample. The mixture was boiled with distilled water at a temperature of 80°C for 3.5 hours. After that, the sample was filtered via vacuum filtration and then washed with deionized water until neutral pH was attained, freeing the sample from Na⁺. The sample was finally oven-dried to a constant weight (C) at 105-110°C. The amount of hemicellulose content was determined using Eqn. (3.4) as proposed by Adeleke *et al.* (2020). The lignin content was determined by adding 3mL of 72% sulphuric acid (H₂SO₄) into an extractive free (B) biomass sample. The sample was kept at atmospheric temperature for 6 h, then stirred very well at 30 min intervals to ensure complete hydrolysis, then boiled at a temperature of 100°C for 1 hour. After that, the sample was filtered via vacuum using a filtering crucible and then washed with deionized water until there was no more detection of SO⁴⁺ via titration process with 10% of BaCl solution. The sample was finally oven-dried to a constant weight (D) at 105-110°C. The final weight is recorded as lignin content. The cellulose content is obtained by difference, assuming that the biomass sample consists of extractives, hemicellulose, lignin, and cellulose only

$$\text{Amount of Extractive (g)} = A - B \quad (3.3)$$

$$\text{Amount of Hemicellulose (g)} = B - C \quad (3.4)$$

3.5 Heating Value Analysis of Oven-Dried Powdered Biomass

The higher heating value (HHV) was obtained using the ASTM D2015-00 standard. About 2 g of pellet biomass sample was measured into a crucible and then placed in a high-pressure oxygen atmosphere metallic cylinder (bomb) at a current temperature (25°C) under a pressure of 20 bars. The bomb was immersed in the adiabatic equipment filled with water and the sample ignited electrically. The results were then displayed on the Mohan Brothers bomb calorimeter

(Plate 3.4g). The LHV was calculated from HHV using eqn. (3.5) as proposed by (ASTM D2015-00, 2000; Merdun and Laouge, 2020).

$$\text{LHV (MJ/kg)} = \text{HHV} - (0.218 \times \text{H}) \quad (3.5)$$

Where, H = weight % of hydrogen obtained via ultimate analysis

3.6 Thermogravimetric Analyses (TGA) of Oven-dried Powdered Biomass

After performing the proximate, ultimate, structural composition, and heating value analysis, TGA analysis was performed only on the seven best samples out of fifteen lignocellulose biomass samples, based on their high energy potential. The thermal degradation and decomposition behaviour of the selected biomass samples were investigated using a Perkin Elmer TGA 4000 analyzer (Plate 3.4e). About 3 mg of each biomass was loaded into the crucible. The samples were heated in the TGA analyzer from 30 to 850°C at a steady heating rate of 10°C/min under an inert environment of a continuous nitrogen flow rate of 80ml/min (Merdun and Laouge, 2020).

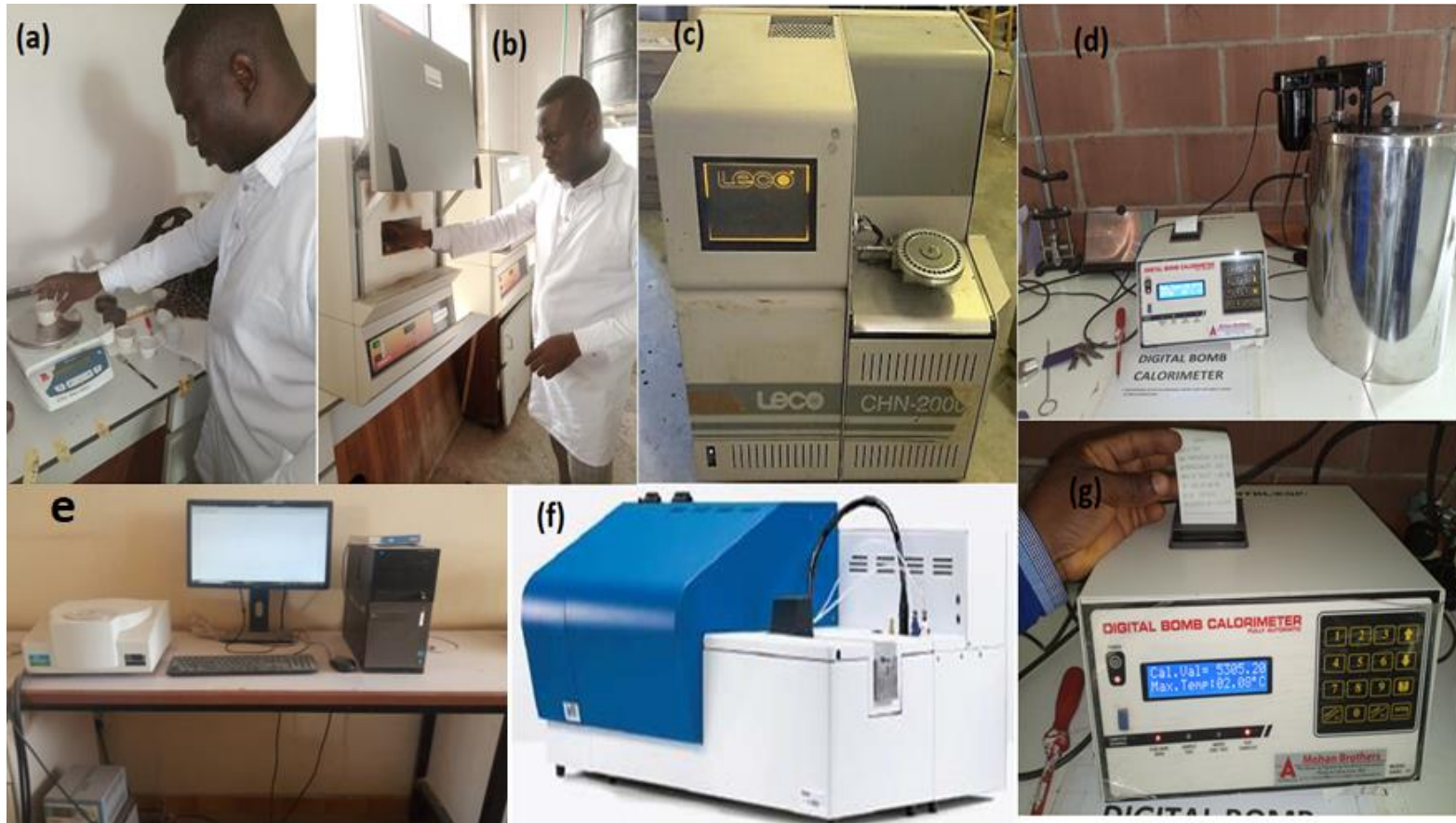


Plate 3.5: **(a)** Weighing of the sample **(b)** Placing of the samples in a carbolite muffle furnace for proximate analysis **(c)** PerkinElmer LECO CHN 2000 Elemental Analyzer for carbon, hydrogen, and nitrogen analysis **(d)** Mohan Brothers bomb calorimeter **(e)** Perkin Elmer, USA TGA 4000 analyzer **(f)** 2TS 6000 for total Sulphur analysis (flame photometer) **(g)** Display and printing of the HHV results using a bomb calorimeter

3.7 Evaluation of Ignitability index (I_I)

The pretreatment of the biomass processes and its characterization schematically is presented in Figure 3.1. The ignitability index of the oven-dried biomass samples were determined using Eqn. (3.6) respectively, as reported by Adeleke *et al.* (2020).

$$I_I = \frac{(HHV - 81FC)}{(VM + MC)} \quad (3.6)$$

Where, HHV = Higher heating value; FC = Fixed carbon; VM = volatile matter; MC = Moisture contents, I_I = Ignitability index

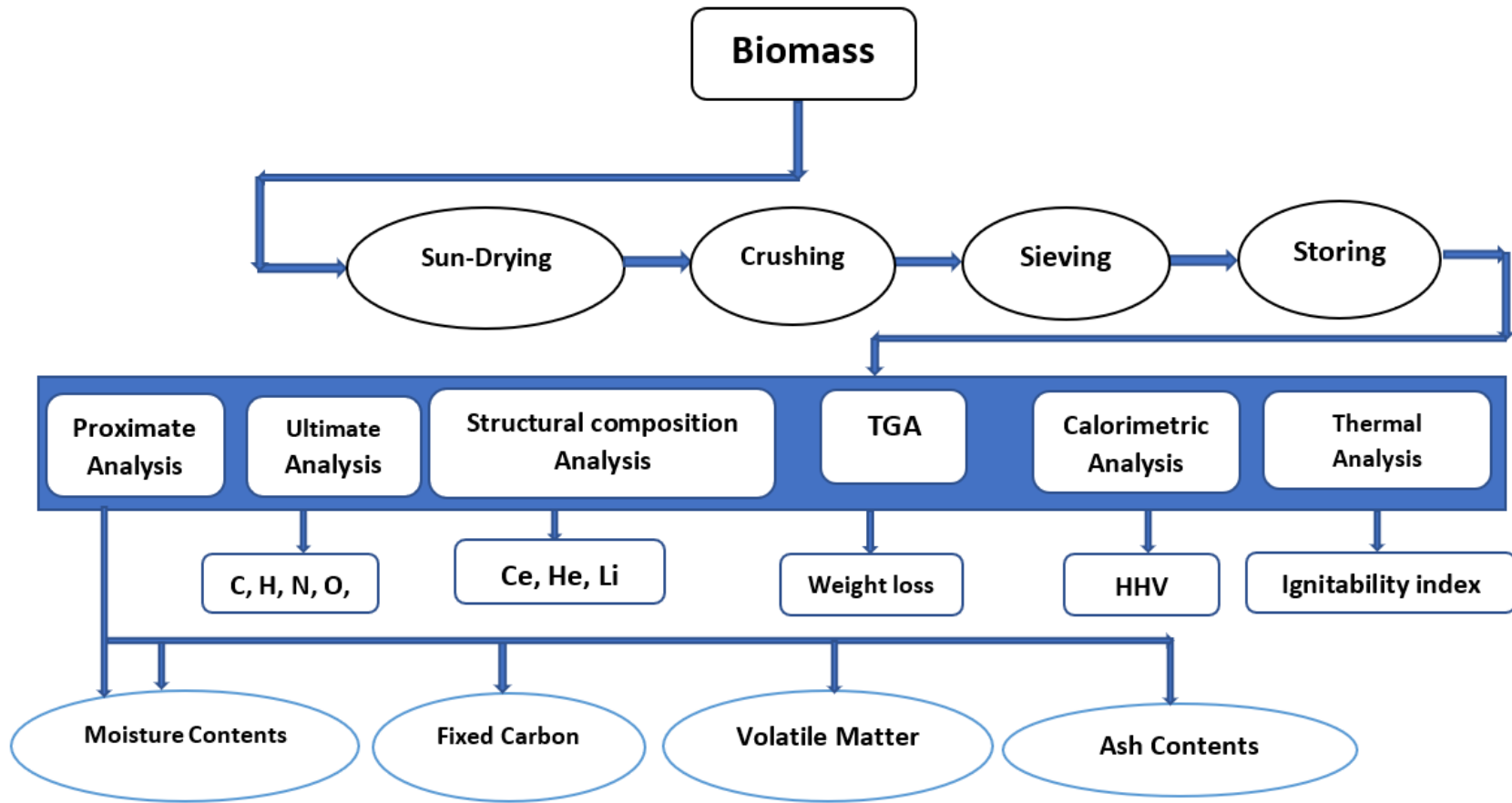


Figure 3.1: Pretreatment and Characterization of Biomass Processes

3.8 Research Design

The method adopted was based on the outcome of the experimental design. The first phase of the experiment commenced with a design matrix layout for the explanatory parameters and the scalar response(s) by adapting design of experiment (DOE) framework (Lee *et al.*, 2017; Laougé *et al.*, 2020). The type of experimental design used was central composite design. Though methods such as Central Composite design (CCD) and Box-Behnken Design (BBD) are utilized to perform RSM, CCD was adopted in this study because it is a widely used statistical method for fitting second-order model and optimization independent parameters of pyrolysis yields as well as energy and exergy efficiency of the yield of biochar, bio-oil and non-condensable gases (Singh *et al.*, 2020). CCD is also more reliable, save time and raw materials, determine the regression model equations operating conditions from the appropriate experiments, investigates the interactions between independent parameters affecting the pyrolysis process, and is efficient when the effects of several operating conditions on the final output are considered by suggesting the minimum number of test runs (Tsai *et al.*, 2006; Abnisa *et al.*, 2011; Laougé *et al.*, 2020). This study comprises of 5 independent parameters with 3 major responses (with sub-responses), so instead of performing multiple analyses, the RSM reduces the time for analysis due to increased computational ability (by reducing numerical data into coded parameters in its black box and recalculating it back to numerical) and majorly by grouping analysis together for multi-objective functions (Lee *et al.*, 2017). Depending on statistical judgments like P-value and F-values, RSM aids in explaining whether to stick to *FRACTIONAL FACTORIAL DESIGN* → for 1st-degree polynomial relationships or *CENTRAL COMPOSITE DESIGN* → for 2nd-degree polynomial relationships for all independent parameters and responses (Dhanavath *et al.*, 2019). Interestingly, RSM also aids interaction between independent parameters and responses which can be maximized, minimized, or set at a specific target (Hossain *et al.*, 2017). Since the interactions are only in the 2nd order, the *CENTRAL COMPOSITE DESIGN* (CCD) does a good job (Kumar *et al.*, 2019).

The experiments were conducted with six responses in CCD (biochar, bio-oil, NCG, energy and exergy efficiencies of bio-oil, biochar and NCG) using five independent parameters (temperature, N₂ flow rate, reaction time, heating rate, and particle and each

considered at five levels namely; $-1, +1, 0, -\alpha$ and $+\alpha$ (Alipanahpour *et al.*, 2017; Lee *et al.*, 2019). The alpha value depends on a number of parameters in the parameterial part of the design and was determined using Eqn. (3.7).

$$\alpha = [2^n]^{1/4} \tag{3.7}$$

$$\alpha = [2^5]^{1/4} = 2.3 \text{ approximately } 2.0$$

Where n is the number of independent parameters (Abnisa *et al.*, 2011; Savasari *et al.*, 2015). The value of alpha is presented at -2 and +2. The modeling and optimization of the operating parameters involved three steps, the first step was utilized to determine a mathematical relationship between the response and independent parameters using Eqn. (3.8) (Absina *et al.*, 2011; Laougé *et al.*, 2020; Samuel *et al.*, 2021).

$$y = f(X_1, X_2, X_3, \dots, X_n) \tag{3.8}$$

Where y is the response, f is the unknown function of response, $X_1, X_2, X_3, \dots, X_n$ is known as independent parameters and n is the number of independent parameters. It was assumed that the independent parameters are quantitative and not qualitative as well as controllable by experiments as proposed by Laougé *et al.* (2020) and Hossain *et al.* (2017).

The second step would be utilized to estimate the coefficients (e.g., constant, linear, quadratic, and interactive) in a mathematical model using a second-order model (quadratic equation) as shown in Eqn. (3.9). The criterion for selecting the second-order model was based on the significance of the model relative to alpha (P-value) constraint and coefficient of determination (R^2). Finally, predicting the responses and checking for the adequacy of the model by obtaining its significance and lack-of-fit which is a degree of the failure of the model in representing data in an experimental domain (Hossain *et al.*, 2017; Laouge *et al.*, 2020). The performance of the model was ascertained by analyzing its results with ANOVA to determine the significance of the model (P-value) and R^2 . Also, the response plots linking the input and output parameters such as one parameter, the main interaction parameters, contour and surface plot, desirability plot are generated and as well as the optimized value of the independent parameters such as temperature, particle sizes, heating

rate, reaction time and nitrogen flowrate and energy and exergy efficiency of the biochar, bio-oil, and NCG are determined from the desirability analysis as shown in Figure 3.2

$$y = \beta_0 + \sum_{i=1}^k \beta_i x_i + \sum_{i=1}^k \beta_{ii} x_i^2 + \sum_{i=1}^k \sum_{j>1}^k \beta_{ij} x_i x_j + \varepsilon_i \quad \text{Eqn. (3.9)} \quad (\text{Myers and Montgomery, 2000;}$$

Lee *et al.*, 2019; Onokwai *et al.*, 2022)

Where, x_i and x_j are coded independent parameters such as reaction temperature, particle sizes, heating rate, and residence time.

The interactions of the x_i and x_j are automatically computed by the design expert version 7.0.3 software (Stat-Ease) via a backend algorithm based on hierarchical order of preference. y is pyrolysis yields known as dependent parameters (responses) as reported by Savasari *et al.* (2015), Lee *et al.* (2017), and Laougé *et al.* (2020). Where β_0 is the constant coefficient, β_i , β_{jj} and β_{ij} are the coefficients for linear, quadratic, and interaction effects, k is the number of independent parameters, ε_i is the random error in the experiment.

The experiments were carried out using predefined independent parameters such as reaction temperature, particle sizes, heating rates, and residence time. These parameters were selected due to their influences on the yield of bio-oil, biochar, and condensable gases such as CO, CO₂, H₂ and CH₄ from pyrolysis plants as reported by Gautam and Chaurasia. (2017); Varma and Mondal *et al.* (2017); Lee *et al.* (2017); Guedes *et al.* (2018); Laougé *et al.* (2020). Fifty (50) experimental runs were conducted to support the data obtained from the RSM using centre composite design (CCD) as shown in Eqn. (3.11) as used by (Lee *et al.*, 2017; Kumar *et al.*, 2019; Laougé *et al.*, 2020; Kshirsagar, and Kalamkar, 2020).

$$N = 2^k + 2n + n_c = 2^5 + 2(5) + 8 = 50 \quad (3.10)$$

Where, N is the actual experimental runs, $n_c = 8$ and it is the repeated number of identical runs at the centre points of the centre composite design. This value (8) of n_c is chosen in order to better estimate the experimental error for the quadratic effect as reported by Kumar *et al.* (2019); Kshirsagar and Kalamkar (2020); Youcai and Tao (2021). k is the number of independent parameters such as temperature, particle sizes, reaction time, nitrogen flow

rate, and heating rate; n is the number of levels e.g., temperature (320, 420, 520, 620, and 720°C). The temperature ranging from 320 to 720°C was chosen because what is obtainable in all the literature at my disposal revealed that optimum biochar, bio-oil, and NCG yields were attained at a temperature of 350-400, 400-600, and 600-700°C, respectively (Lee *et al.*, 2017; Mohammed *et al.*, 2017; Varmal and Mondal *et al.*, 2018; Kumar *et al.*, 2019; Chukwunneke *et al.*, 2019; Oyebanji *et al.*, 2021). The number includes the standard 2^k parameterial with its origin at the center, so that a quadratic number of independent parameters can be generated as reported by Abnisa (2011); Kumar *et al.* (2019); and Laougé *et al.* (2020)

The results of design of experiment (DOE) based on central composite design (CCD) are shown in Table 3.1. Column (3-7) shows the real level of the parameters (independent parameters) such as temperature (T), particle sizes (Ps), heating rate (HR), reaction time (R), and nitrogen flowrate (N₂), column (8-12) show the coded parameters, while column (8-16) depicts the responses (dependent parameters) such as biochar (Y_c), bio-oil (Y_o) and non-condensable gases (Y_n) as well as energy and exergy efficiency of bio-oi, biochar, and NCG. The flow chat for the modelling and optimization of the operating parameters are shown in Figure 3.3, while the variability between the experimental and predicted data was determined using coefficient of variation (Eqn. 3.11).

$$\text{Coefficient of variation (CV\%)} = \frac{\text{Standard deviation (s)}}{\text{mean}(\bar{x})} \times 100 \quad (3.11)$$

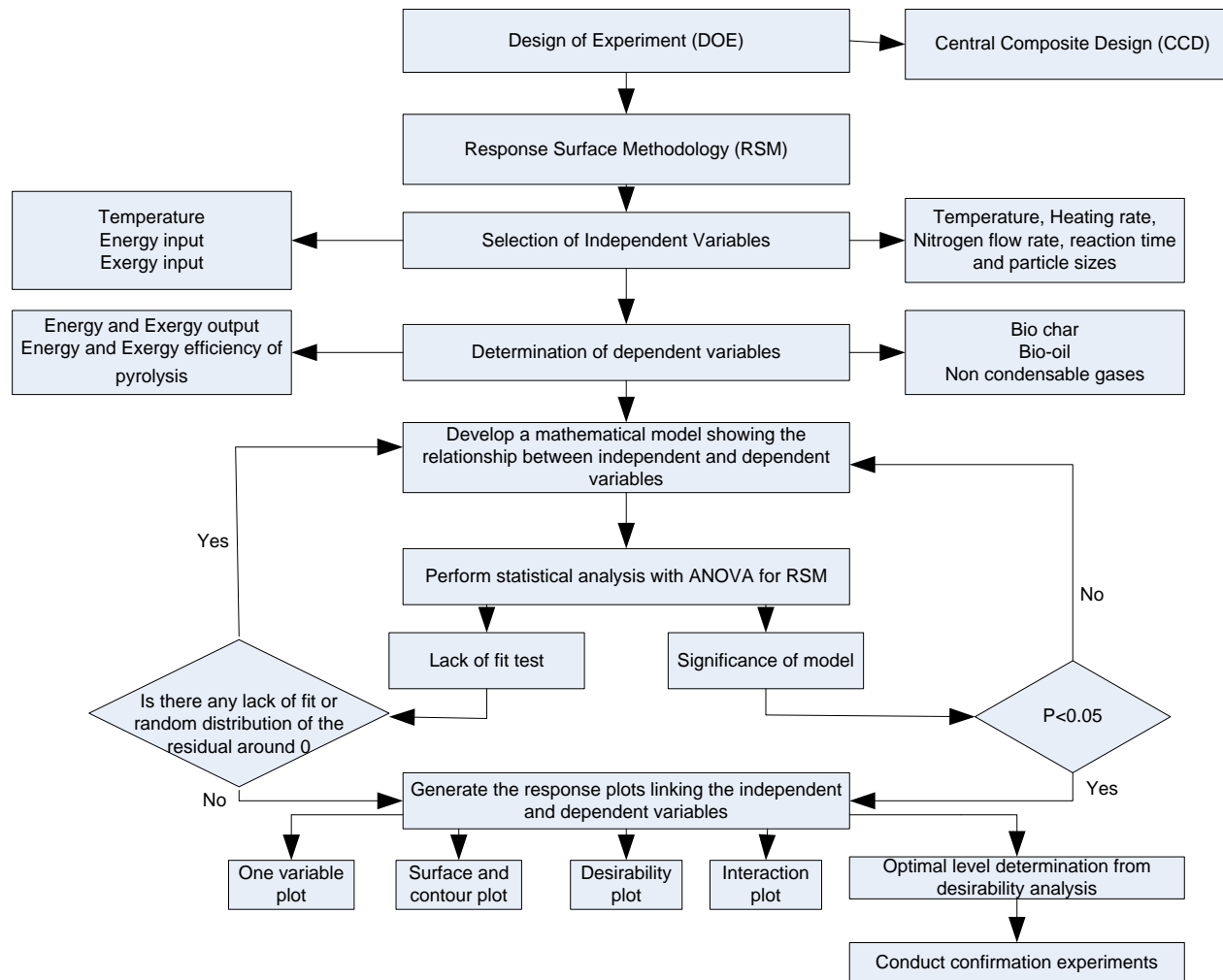


Figure 3.2: Flowchart Bio-oil and biochar for the modeling and optimization

Table 3.1 Design of Experiment (DOE) using central composite design (CCD)

Std	Run	Independent Parameters										Responses									
		T(°C)	R(min)	HR(°C/min)	N ₂ (L/min)	Ps(mm)	T(°C)	R(min)	HR(°C/min)	N ₂ (L/min)	Ps(mm)	Y _o (w%)	Y _c (w%)	Y _n (w%)	En _o (w%)	En _c (w%)	En _n (w%)	Ex _o (w%)	Ex _c (w%)	Ex _n (w%)	
36	1	520	10	17.5	125	0.5	0	0	0	0											
48	2	520	15	17.5	125	0.5	0	0	0	2											
35	3	520	20	17.5	125	0.5	1	-1	1	-1											
16	4	720	25	27.5	225	0.1	1	-1	-1	1											
17	5	320	5	7.5	25	0.9	0	0	0	0											
47	6	520	15	17.5	125	0.5	-1	1	1	-1											
37	7	520	15	12.5	125	0.5	-1	-1	1	1											
18	8	720	5	7.5	25	0.9	0	0	0	0											
22	9	720	5	27.5	25	0.9	1	-1	1	-1											
23	10	320	25	27.5	25	0.9	0	0	0	0											
7	11	320	25	27.5	25	0.1	1	-1	-1	-1											
34	12	420	15	17.5	125	0.5	0	0	0	0											
43	13	520	15	17.5	125	0.5	1	-1	-1	-1											
1	14	320	5	7.5	25	0.1	1	1	1	1											
3	15	320	25	7.5	25	0.1	1	1	-1	1											
39	16	520	15	17.5	75	0.5	1	1	-1	-1											
32	17	720	25	27.5	225	0.9	0	-2	0	0											
12	18	720	25	7.5	225	0.1	2	0	0	0											
5	19	320	5	27.5	25	0.1	-1	-1	-1	-1											
31	20	320	25	27.5	225	0.9	-1	1	1	-1											
44	21	520	15	17.5	125	0.5	0	0	-2	0											
21	22	320	5	27.5	25	0.9	-1	1	-1	-1											
30	23	720	5	27.5	225	0.9	1	1	1	-1											
19	24	320	25	7.5	25	0.9	0	0	0	0											
42	25	520	15	17.5	125	0.3	1	-1	-1	1											
14	26	720	5	27.5	225	0.1	0	0	0	-2											
25	27	320	5	7.5	225	0.9	-1	-1	1	-1											
41	28	520	15	17.5	125	0.7	-1	1	-1	-1											
38	29	520	15	22.5	125	0.5	-1	1	1	1											
6	30	720	5	27.5	25	0.1	-1	-1	-1	1											
20	31	720	25	7.5	25	0.9	-1	-1	-1	-1											
46	32	520	15	17.5	125	0.5	-1	-1	1	1											
9	33	320	5	7.5	225	0.1	0	2	0	0											
50	34	520	15	17.5	125	0.5	0	0	2	0											
8	35	720	25	27.5	25	0.1	0	0	0	0											
11	36	320	25	7.5	225	0.1	1	1	1	-1											
33	37	620	15	17.5	125	0.5	-1	1	-1	1											
4	38	720	25	7.5	25	0.1	1	-1	1	1											
49	39	520	15	17.5	125	0.5	-1	-1	1	-1											
10	40	720	5	7.5	225	0.1	1	-1	1	1											
40	41	520	15	17.5	225	0.5	-1	1	-1	1											
2	42	720	5	7.5	25	0.1	1	1	-1	1											
13	43	320	5	27.5	225	0.1	0	0	0	0											
29	44	320	5	27.5	225	0.9	-1	-1	-1	-1											
27	45	320	25	7.5	225	0.9	-2	0	0	0											
28	46	720	25	7.5	225	0.9	1	1	1	1											
26	47	720	5	7.5	225	0.9	-1	1	1	1											
24	48	720	25	27.5	25	0.9	0	0	0	0											
45	49	520	15	17.5	125	0.5	0	0	0	0											
15	50	320	25	27.5	225	0.1	1	1	-1	-1											

3.9 Pyrolysis Experimental Setup

The pyrolysis set-up comprised of a cylindrically insulated reactor, gas collector, condenser, ice bath, PID temperature controller, inert gas flow system, and electric heater of 4 kW capacities (Plate 3.6). An experimental run was performed using a fixed-bed reactor (Figures. 3.4) by varying the temperature, reaction time, heating rate and particle size, and nitrogen flow rate to maintain an inert environment in the reactor.

- **Description of the Reactor**

The reactor (Figure 3.4), which is one of the major components of the pyrolysis plant was made of stainless steel of grade AISI 316 because it can withstand the operating temperature of 300-750°C, high resistance to corrosion resistance, low maintenance cost, and affordable (Heidari *et al.*, 2019). The maximum capacity of the reactor is 1000 g, maximum power rating of the furnace is 1kW-hr operating at 1000°C, a height of 2140 mm and diameter of 1700 mm similar to the work of (Aziz *et al.*, 2018; Adnisa *et al.*, 2011). The inert atmosphere in the reactor during the pyrolysis process was maintained using nitrogen gas in accordance with the procedure stated by Heidari *et al.* (2019). The gas pressure from the cylinder was controlled and regulated using a multi-stage nitrogen gas pressure regulated of model MUREX-10 with a variable control valve of capacity 6-40 l/min (Hossain, 2020; Uddin *et al.*, 2012). Hot gases flow via the inner tube and condense as water circulates within the tube. The reactor temperature was measured using a k-type thermocouple with a range between 100 – 850°C which was inserted into the reactor (Pourkarimi *et al.* 2019).



Plate 3.6: Pyrolysis plant experimental set-up

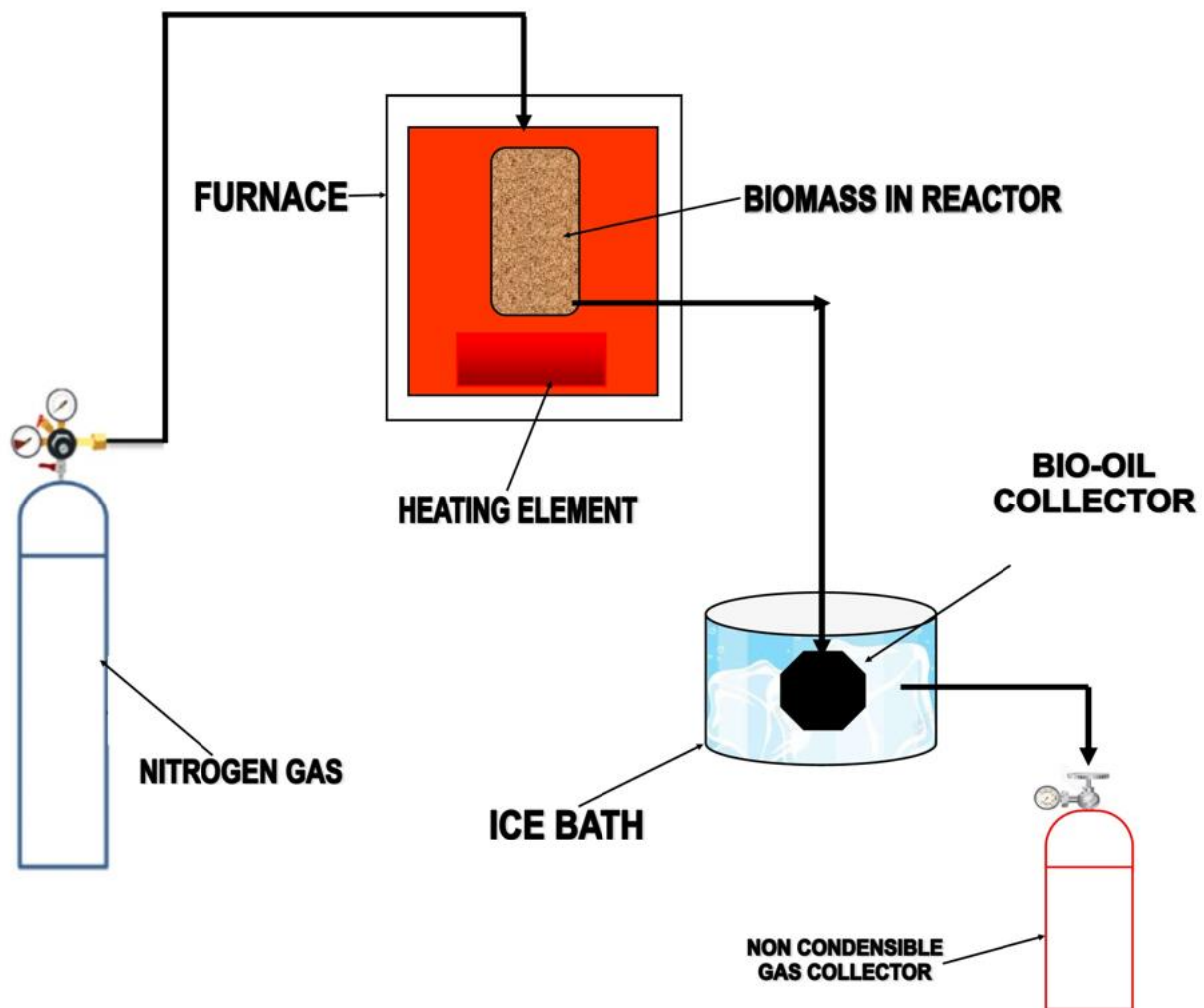


Figure 3.3: Pyrolysis setup exploded in 2D

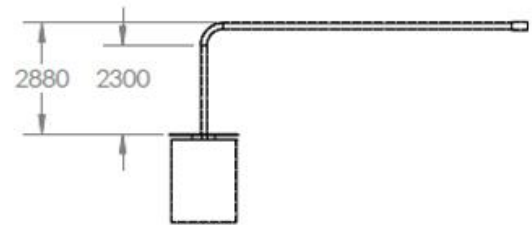
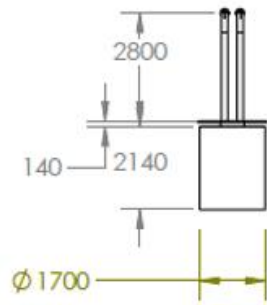
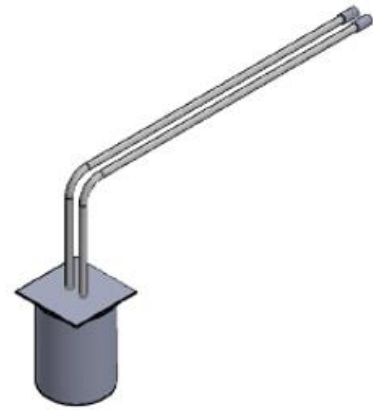
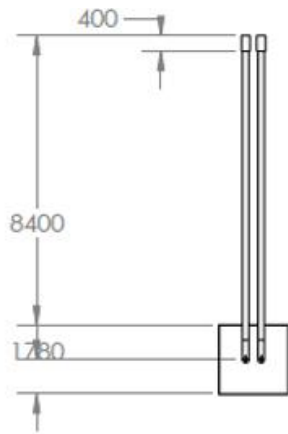


Figure 3.4: Pyrolysis Plant Reactor

3.10 Experimental Procedure

An experimental run was performed using three lignocellulose biomass samples such as palm kernel shell (PKS), sugarcane bagasse (SCB), and shea butter wood (SBW) due to their high energy potential obtained after the characterization of the biomass samples. The biomass samples were fed into the reactor, covered, and properly fastened for a run at a pre-set furnace temperature range of 320, 420, 520, 620, and 720 °C nitrogen flow rate of 25, 75, 125, 175, 225 mL/min, a heating rate of 7.5, 12.5, 17.5, 22.5, 27.5 °C/min with various particle sizes with a diameter (d_p) of 0.1-0.2, 0.2-0.4, 0.4-0.6, 0.6-0.8, and 0.8-1.0 mm for a residence time of 5, 10, 15, 20, 25 min at 5 runs each for each pyrolysis process. The bio-water mixture which was automatically separated into bio-oil and water were generated by passing the gas through a condenser. The weight of product yield was determined (bio-oil and bio-biochar) by obtaining the mass balance (bio-gas) (Gupta *et al.*, 2020). The flowchart for the experimental runs is shown in Figure 3.5

After the fixed bed reactor has been heated to the desired temperature, the biomass species of various sizes weigh 100 g was feed into the fixed bed 304 stainless steel tubular reactor chamber via a 10L feed hopper (Carrasco *et al.*, 2017; Lin *et al.*, 2019) at approximately holding time of about 15min as reported by Gautam and Chaurasia (2020); Aziz *et al.* (2018); Olagbende *et al.* (2016); and Uddin, *et al.* (2012). The reactor was equipped with an inert (nitrogen gas) supply. The vertical furnace was heated via electric heating element and the temperature was measured using a k-type thermocouple that was fixed inside the reactor.

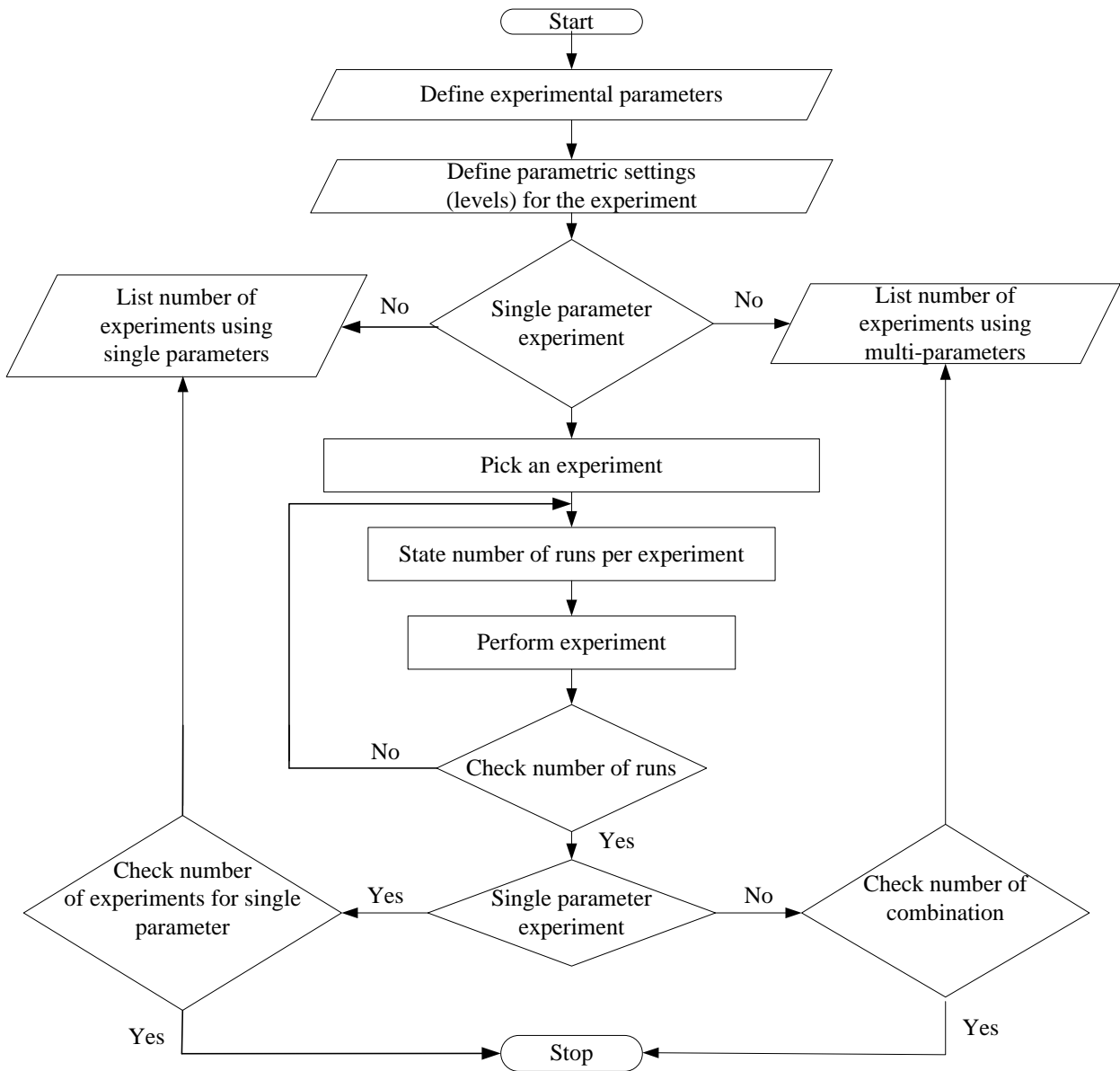


Figure 3.5: Flowchart for experimental runs

3.11 Energy and Exergy Analysis

The influence of pyrolysis operating parameters on total energy and exergy output as well as energy and exergy efficiency of the pyrolysis products was investigated in order to enhance the efficiency of the pyrolysis yield (Wang *et al.*, 2016). The energy analysis was based on the first law of thermodynamics, while the concept exergy analysis was based on the second law of thermodynamics. Exergy does not obey the principle of conservation of energy due to irreversibility in the system (Peters *et al.*, 2015b). It is the maximum available energy or the quality of energy in terms of work that is obtainable when a pyrolysis process is in thermal equilibrium with its surroundings. Exergy analysis enables useful parts of energy to be identified and to determine the thermodynamic inefficiencies that the pyrolysis process would be able to detect. The pyrolysis process was done as the three (3) products are channeled into three (3) bomb calorimeters. This was done to reduce experimental error and quickly ascertain the exergies of the 3 components. Once the energies were attained, the exergies were also calculated (Peters *et al.*, 2015b; Wang *et al.*, 2020).

3.11.1 Energy analysis

The energy and exergy analysis of the pyrolysis plant was analyzed according to Wang *et al.* (2016); Yan *et al.* (2019); Singh *et al.* (2020). The summation of energy from the electric heating furnace and raw biomass is referred to as input energy, while the output energy is the summation of energy generated from the biochar, bio-oil, and non-condensable gases obtained after the pyrolysis process. Other energies such as heat loss, heat retained and electric energy generated as photons are negligible because they are infinitesimally small during the pyrolysis process as reported by Wang *et al.* (2016); Singh *et al.* (2020) as shown in Figure 3.6.

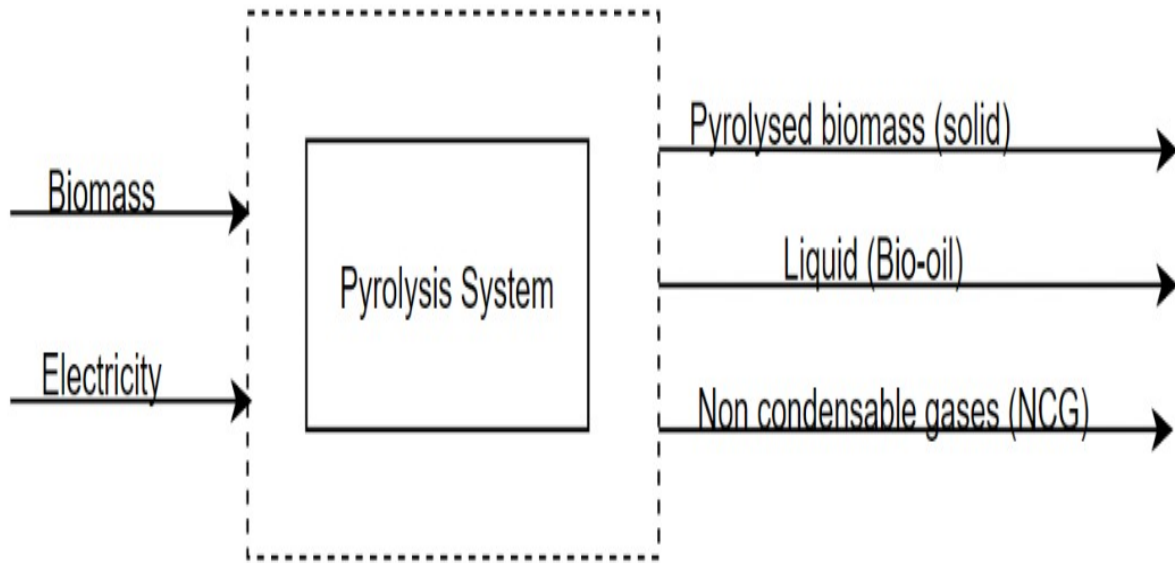


Figure 3.6: Pyrolysis System

❖ **Total energy input**

• **The energy of electric heating furnace**

During pyrolysis process, the total energy consumption in kJ for 1kg raw biomass (Figure 3.7) in the fixed bed reactor can be determined using Eqn. (3.12)

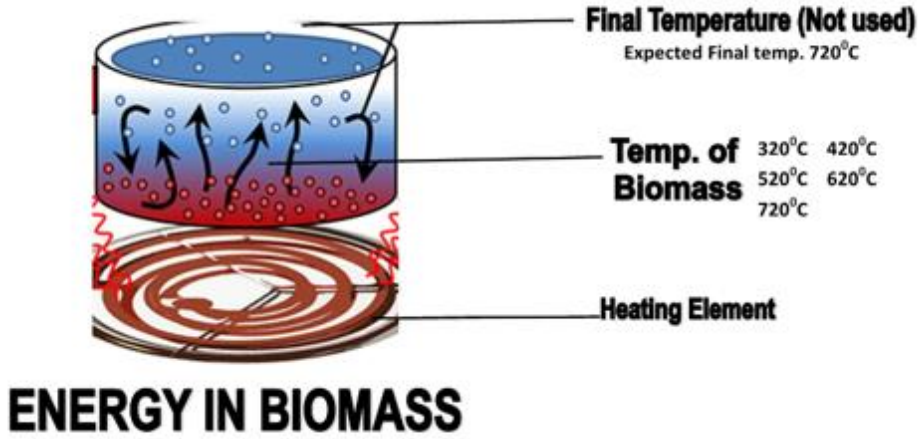


Figure 3.7: Energy generated from the electric heating element (Singh *et al.*, 2020)

$$En_{Electric} = PR_{peak} \times 3600 \times \frac{T_{pyrolysis}}{1000^{\circ}C} \times t_{heating} \times \frac{1}{M_{biomass}} \quad (3.12)$$

Where, $En_{Electric}$ is total electric energy consumption in kJ/kg raw biomass, PR_{peak} (1kW-hour) is the maximum power rating of an electric furnace at 1000°C, $T_{pyrolysis}$ is the pyrolysis temperature ranged (320, 420, 520, 620, 720°C), $t_{heating}$ is the total duration in hours when heating is on.

$En_{Electric}$ is taken as the energy of the energy consumption in kJ to 1kg raw biomass and it is assumed that there is no heat/power loss from the electric heating furnace, that power is converted into energy per mass of the biomass. So power is multiplied by the temperature of the pyrolysis process per mass multiple by the time taken to perform the experimental runs. The 1000°C is released per 1000°C of the element (Singh *et al.*, 2020).

- **The energy of raw biomass**

-

The potential and kinetic energy of raw biomass are negligible during pyrolysis process. Also, the physical energy of raw biomass during pyrolysis is very small when compared to chemical energy at a lower temperature range (below 50°C) as reported by Parvez *et al.* (2016); Wang *et al.* (2016); Singh *et al.* (2020); Zhang *et al.* (2020) and therefore, the total energy of raw biomass is equal to the chemical energy as shown in Eqn. (3.13).

$$En_{biomass} = En_{ch}^{biomass} = M_{biomass} \times HHV_{biomass} \quad (3.13)$$

Prior to experimentation, the fresh biomass samples were pretreated via cleaning, drying, crushing, sieving and sorting and then store in a sterilized stainless container. The biomass samples were characterized to determine their physicochemical properties and the best third biomass with negligible impurities were utilized for experimental runs. Hence, there is a negligible impact of impurities. Also, the reason impurities are avoided by taking into consideration the equipment and biomass is to ensure that the experiment best fits theoretical models like energy and entropy as reported by Singh *et al.* (2020).

- **Energy of biochar**

Just as considered in the energy of biomass during the pyrolysis process, the same effect of negligible energies (potential, kinetic, and physical) was also considered due to the lower temperature range of 200-350°C. Hence, the total energy of biochar which is equal to the chemical energy is determined using Eqns. (3.14a) - (3.14b) as reported by Singh *et al.* (2020) and Tang *et al.* (2019).

$$En_{total}^{biochar} = En_{biochar}^{ch} \quad (3.14a)$$

$$En_{total}^{biochar} = m_{biochar} \times HHV_{biochar} \quad (3.14b)$$

Where $En_{biochar}^{ch}$ is the chemical energy of biochar, $En_{total}^{biochar}$ is the total energy of biochar, and $HHV_{biochar}$ is the higher heating value of biochar in MJ/kg which can be determined via bomb calorimeter and the potentiality of the biochar of being a fuel from the elemental analysis of its component.

- **The energy of bio-oil products**

Just as presented for the energy of biochar, the kinetic and potential are negligible during pyrolysis process. Also, the physical energy of bio-oil is very small in comparison with the chemical energy of bio-oil because the temperature is in the lower range (less than 500°C).

Therefore, the total energy of bio-oil is equal the chemical energy which can be calculated using Eqn. (3.15a-3.15b) as reported by Peters *et al.* (2015b); Ramesh and Murugavelh (2020), and Singh *et al.* (2020).

$$En_{total}^{biochar} = En_{bio-oil}^{ch} \quad (3.15a)$$

$$En_{total}^{bio-oil} = m_{bio-oil} \times HHV_{bio-oil} \quad (3.15b)$$

Where $En_{bio-oil}^{ch}$ is the chemical energy of bio-oil, $HHV_{bio-oil}$ is the higher heating value of bio-oil in MJ/kg which can be determined via bomb calorimeter and the potentiality of the bio-oil of being a fuel from the elemental analysis of its component.

- **The energy of NCG**

The total energy obtained from the NCG equals the sum of individual energy values as shown in Eqn. (3.16)

$$En_{Total}^{NCG} = En^{ph} + En^{ki} + En^{po} + En^{ch} \quad (\text{Tang } et al., 2019; \text{Wang } et al., 2016) \quad (3.16)$$

Where En_{Total}^{NCG} is the total energy, En^{ph} is the physical energy of NCG, En^{ki} is the kinetic energy of NCG, En^{po} is the potential energy of NCG, En^{ch} is the chemical energy of NCG.

The potential and kinetic energy of NCG is negligible since both values are very small during pyrolysis process. The physical energy of NCG is considered because their values are not negligible due to their high-temperature range of 500 -720°C during the pyrolysis process, unlike the physical energy of raw biomass, biochar, and bio-oil which is negligible due to their very low values as a result of their lower temperatures range (<500°C) during the pyrolysis process (Singh *et al.*, 2020). Also, apart from the chemical energy, the gases perform work physically by the number of moles, n, gas constant, R, and the temperature (T) utilized to decompose the biomass (Peters *et al.*, 2015a; Wang *et al.* 2016). Once the gas has a potential energy of n, R, and T in the ideal state, it can have a certain volume depending on the pressure it moves (Singh *et al.*, 2020). Hence Eqn. (3.16) will become;

$$En_{total}^{NCG} = En_{NCG}^{ch} + En_{NCG}^{ph} \quad (\text{Khan } et al., 2020; \text{Singh } et al., 2020) \quad (3.17)$$

Chemical energy of NCG is given by

$$En_{NCG}^{ch} = \sum n_i HHV \quad (\text{Wang } et al., 2016; \text{Ramesh and Murugavelh, 2020}) \quad (3.18a)$$

Where En_{NCG}^{ch} is the chemical energy of NCG during pyrolysis process, HHV is the higher heating value of the constituent gas, kJ/kmol, n_i is the mole number of flue gas

Physical energy of NCG is given by

$$En_{NCG}^{ph} = \sum n_i h_i \quad (\text{Tang } et al., 2019; \text{Singh } et al., 2020) \quad (3.18b)$$

Where En_{NCG}^{ph} is the physical energy of bio-oil, h_i is the specific enthalpy value, kJ/kmol, n_i is the mole number of flue gas

Specific enthalpy (h_o) and higher heating value (HHV) of selected individual NCG components (NCG) were obtained under a standard condition of some gases shown in Table. 3.2.

Table 3.2: Specific enthalpy (h_o), entropy (s_o), and higher heating value (HHV) of selected compounds of the pyrolysis gas constituents

Gas	h_o (kJ/kmol)	s_o (kJ/kmolK)	HHV (kJ/kmol)
CO ₂	9364	213.685	-
H ₂	8468	130.574	285,840
CH ₄	-	186.16	890,360
CO	8669	187.543	282,990

(Singh *et al.*, 2020; Khan *et al.*, 2020)

The enthalpy change of formation of methane (CH₄) was not captioned in Table 3.2 because CH₄ cannot be measured directly which makes the enthalpy of methane hard and expensive to attain (Peters *et al.*, 2015b). Also, the HHV value of CO₂ cannot be included in the energy budget because it is not a fuel, it is already in a saturated state and cannot combust. The energy efficiencies of the pyrolysis products were determined from Eqn. (3.19a) -(3.19d) as reported by Wang *et al.* (2020) and Zhang *et al.* (2020).

$$\text{Energy efficiency (\%)} = \frac{\text{Useful energy output}}{\text{Total Energy input}} \times 100 \quad (3.19a)$$

$$\eta_{\text{biochar}} = \frac{En_{\text{total}}^{\text{biochar}}}{En_{\text{biomass}} + En_{\text{electric}}} \times 100\% \quad (3.19b)$$

$$\eta_{\text{bio-oil}} = \frac{En_{\text{total}}^{\text{bio-oil}}}{En_{\text{biomass}} + En_{\text{electric}}} \times 100\% \quad (3.19c)$$

$$\eta_{\text{NCG}} = \frac{En_{\text{total}}^{\text{NCG}}}{En_{\text{biomass}} + En_{\text{electric}}} \times 100\% \quad (3.19d)$$

Where, η_{biochar} , $\eta_{\text{bio-oil}}$, η_{NCG} , are energy efficiencies of pyrolysis of biochar, bio-oil, and NCG during pyrolysis process respectively.

$En_{\text{total}}^{\text{biochar}}$, $En_{\text{total}}^{\text{bio-oil}}$ and $En_{\text{total}}^{\text{NCG}}$ are total energy of biochar, bio-oil, and NCG during pyrolysis process respectively.

3.11.2 Exergy analysis

Prior to the determination of energy balance, four (4) assumptions were considered as reported by Singh *et al.* (2020)

- i. The pyrolysis reaction was performed in a laboratory scaled plant within a control-volume unit.
- ii. Input exergy is from raw biomass and electric heating furnace.
- iii. Output exergy is from product biochar, bio-oil, and NCG during the pyrolysis process.
- iv. The internal exergy loss (irreversibility) is from the lost part.

The energy balance will be calculated using Eqn. (3.20)

$$Ex_{\text{electric}} + Ex_{\text{biomass}} = Ex_{\text{total}}^{\text{NCG}} + Ex_{\text{total}}^{\text{bio-oil}} + Ex_{\text{total}}^{\text{biochar}} + Ex_{\text{irreversibility}} \quad (3.20)$$

Where, $Ex_{electric,T}$ is the total exergy value of electrical power consumption of the furnace and is equivalent to electrical energy as given in Eqn. (3.21) (Ramesh and Murugavelh, 2021), $Ex_{biomass}$ is the total exergy value of raw biomass, Ex_{total}^{NCG} , $Ex_{total}^{bio-oil}$ and $Ex_{total}^{biochar}$ are the exergy of NCG, bio-oil, and biochar respectively during pyrolysis process, $Ex_{irreversibility}$ is the energy loss during pyrolysis process.

- **Exergy of raw biomass**

The physical, kinetic, and potential exergy is negligible since their values are very small in comparison to chemical exergy as explained in the energy of raw biomass.

$$Ex_{biomass} = Ex^{ch} = \beta_{biomass} M_{biomass} LHV_{biomass} \quad (\text{Zhang } et al., 2020) \quad (3.21a)$$

Where $M_{biomass}$ is the mass of biomass, $\beta_{biomass}$ is the correlation parameter for raw biomass, and can be calculated via Eqn. (3.21b) postulated by Gourmelon *et al.* (2015) and Wang *et al.* (2016).

$LHV_{biomass}$ is lower heating value in kJ/kg for raw biomass and can be determined using Eqns. (2.21c) respectively as used by Singh *et al.* (2020). The $LHV_{biomass}$ accounts for exergy and not $HHV_{biomass}$. $HHV_{biomass}$ is the heating value for the total energy while $LHV_{biomass}$ is the useful heating value as postulated by Abnisa *et al.* (2011) and Wang *et al.* (2016).

$$\beta_{biomass} = \frac{1.0412 + 0.216 \frac{H}{C} - 0.2499 \frac{O}{C} \left(1 + 0.7884 \frac{H}{C} \right) + 0.0450 \frac{N}{C}}{1 - 0.3035 \frac{O}{C}} \quad (3.21b)$$

$$LHV_{biomass} = HHV_{biomass} - (0.218 - H) \quad (3.21c)$$

Where H, C, O, and N are the hydrogen, carbon, oxygen, and nitrogen contents in wt%, The physicochemical properties were determined during the characterization of the biomass via ultimate and proximate analysis. The characterization was carried out prior to experimentation as explained during the biomass characterization process (ultimate and proximate analysis).

$HHV_{biomass}$ is higher heating value of raw biomass in kJ/kg. LHV is only used to correlate to exergy using a correction parameter, $\beta_{biochar}$.

Exergy of Non-condensable gases (NCG)

The total exergy value of the Ex_{Total}^{NCG} equals the sum of all kinds of exergy values associated with the NCG at a given condition and can be determined as shown in Eqn. (3.22a) as suggested by Etika *et al.* (2019) and Snoussi *et al.* (2020)

$$Ex_{Total}^{NCG} = Ex_{NCG}^{ph} + Ex_{NCG}^{ch} + Ex_{NCG}^{po} + Ex_{NCG}^{ki} \quad (3.22a)$$

Where Ex_{NCG}^{ph} , Ex_{NCG}^{ch} , Ex_{NCG}^{po} and Ex_{NCG}^{ki} are physical, chemical, potential, and kinetic exergy of non-condensable gases during pyrolysis process respectively. If the kinetic energy and potential exergy of NCG are negligible during pyrolysis process as discussed during the energy of NCG, the equation will become

$$Ex_{Total}^{NCG} = Ex_{NCG}^{ph} + Ex_{NCG}^{ch} \quad (\text{Singh } et al., 2020) \quad (3.22b)$$

The physical exergy of NCG can be obtained using Eqn. (3.22c)

$$Ex_{NCG}^{ph} = n_i (h - h_0) - T_0 (s - s_0) \quad (\text{Wang } et al., 2020; \text{Singh } et al., 2020) \quad (3.22c)$$

Where n is the mole flow rate (Number of moles = Mass of the substance / Molar weight) of NCG, s_0 and h_0 are specific entropy and enthalpy of gas (NCG) under ambient condition s and h are the specific entropy and enthalpy of gas under operating condition.

The change of specific enthalpy ($h - h_0$) and change in specific entropy ($s - s_0$) are denoted as

$$(h - h_0) = \int_{T_0}^T C_p dT \quad (\text{Al-Weshahi } et al., 2013; \text{Singh } et al., 2020) \quad (3.23a)$$

$$(s - s_0) = \int_{T_0}^T \frac{C_p}{T} dT - R \ln \frac{P}{P_0} \quad (\text{Wang } et al., 2016) \quad (3.23b)$$

The empirical formula was utilized to calculate the specific enthalpy C_p for the NCG components as shown in Eqn. (3.24a)- (3.24b).

$$C_p = a + bT + cT^2 + dT^3 \quad (\text{Peters } et al., 2015a; \text{Tang } et al., 2019) \quad (3.24a)$$

Where, R is the general gas constant; C_p is the specific heat capacity at a constant pressure of NCG, while a, b, c, and d are the constant coefficients (independent of temperature) which are shown in Table 3.3.

Table 3.3: Coefficients for constant pressure specific heat of NCG

NCG	H ₂	CO	CO ₂	CH ₄
A	29.11	28.16	22.26	19.89
b*10 ²	-0.192	0.168	5.981	5.024
c*10 ⁵	0.4	0.533	-3.501	1.269
d*10 ⁹	-0.87	-2.222	7.469	-11.01
Temperature range, (°C)	0-1500	0-1500	0-1500	0-1500

(Wang *et al.*, 2016; Singh *et al.*, 2020)

The chemical exergy of NCG (Ex^{ch}) can be obtained using Eqn. (3.24b) as suggested by (Wang *et al.*, 2016)

$$Ex_{NCG}^{ch} = n \sum x_i (ex_i^{ch} + RT_0 \ln \gamma_i x_i) \quad (3.24b)$$

Where, x_i is the mole fraction of the i-th component (individual gases) in the NCG; γ_i , the activity coefficient of individual gases in the NCG, is unity for ideal mixture; ex_i^{ch} is the specific chemical exergy of i-th component (individual gases) under a standard condition in NCG, as shown in Tables 3.4

Table 3.4: Standard chemical exergy of selected NCG at 25°C, 0.1MPa

Gas	H ₂	CO	CO ₂	CH ₄	C ₂ H ₄
Ex_{std}^{ch}	236,100	275,100	19,870	831,650	1,317,680

(kJ/kmol)

(Singh *et al.*, 2020; Wang *et al.*, 2016)

- **Exergy of biochar products**

The kinetic, potential, and physical exergy of the biochar during pyrolysis process are negligible because the values are very small in comparison to the chemical exergy of biochar as postulated by Peters *et al.* (2015b) and Singh *et al.* (2020).

The total exergy which is equal to the chemical exergy can be determined using Eqn. (3.25a-d)

$$Ex_{total}^{biochar} = Ex_{biochar}^{ch} \quad (\text{Peters } et al., 2015a) \quad (3.25a)$$

The chemical exergy of pyrolyzed biomass can be calculated using Eqn. (19)

$$Ex_{biochar}^{ch} = \beta_{biochar} M_{biochar} LHV_{biochar} \quad (\text{Singh } et al., 2020) \quad (3.25b)$$

Where $Ex_{biochar}^{ch}$ is the chemical exergy of biochar products, $\beta_{biochar}$ is the correlation parameter for a bio-oil product, $M_{biochar}$ is the mass of biochar and $LHV_{biochar}$ is lower heating value in MJ/kg for biochar products generated during the pyrolysis process, which can be determined using Eqns. (3.22c) and (3.22d) respectively

$$\beta_{biochar} = 1.0437 + 0.1896 \frac{H}{C} + 0.0617 \frac{O}{C} + 0.0428 \frac{N}{C} \quad (\text{Zhang } et al., 2020) \quad (3.25c)$$

$$LHV_{biomass} = HHV_{biomass} - (0.218 - H) \quad (\text{Abnisa } et al., 2011; \text{Khan } et al., 2020) \quad (3.25d)$$

Where, C is carbon, H is hydrogen, O is oxygen, N is nitrogen content of pyrolyzed biomass (biochar) in wt.% and W is moisture content of pyrolyzed biomass (biochar) in w%.

- **Exergy of bio-oil products**

As stated earlier during the exergy analysis of biochar products, the kinetic, potential, and physical exergy is negligible, therefore, the total exergy of bio-oil products is equal to the chemical exergy of liquid products. The chemical exergy of the bio-oil products can be calculated using Eqn. (3.26) according to Singh *et al.* (2020)

$$Ex_{bio-oil}^{ch} = \beta_{bio-oil} M_{bio-oil} LHV_{bio-oil} \quad (3.26)$$

Where $Ex_{bio-oil}^{ch}$ is the chemical exergy of bio-oil, $\beta_{bio-oil}$ is correlation parameter for a bio-oil product, $M_{bio-oil}$ is the mass of bio-oil and $LHV_{bio-oil}$ is lower heating value in kJ/kg for bio-oil product generated during the pyrolysis process, which can be determined using Eqns. (3.27a) and (3.27b) respectively according to Wang *et al.* (2016); Gourmelon *et al.* (2016)

$$\beta_{bio-oil} = 1.0401 + 0.1728 \frac{H}{C} + 0.0432 \frac{O}{C} + 0.2169 \frac{S}{C} \left(1 - 2.0628 \frac{H}{C} \right) \quad (3.27b)$$

$$LHV_{bio-oil} = HHV_{bio-oil} - M_w \times h_f \quad (3.27c)$$

Where h_f is the latent heat of vaporization (2260 kJ/kg) and M_w is mass of moisture content (wt%) in a bio-oil product which can be obtained via Karl Fischer titrimetric method?

The exergy efficiencies of non-condensable gases, biochar, and bio-oil are the ratio of the exergy value to the total exergy value input into the pyrolysis as suggested by Parvez *et al.* (2016); Singh *et al.* (2020), and Zhang *et al.* (2020) as shown in Eqns. 3.28a-3.28c

$$\psi_{NCG} = \frac{Ex_{total}^{NCG}}{Ex_{biomas} + Ex_{electric}} \times 100\% \quad (3.28a)$$

$$\psi_{biochar} = \frac{Ex_{total}^{biochar}}{Ex_{biomas} + Ex_{electric}} \times 100\% \quad (3.28b)$$

$$\psi_{bio-oil} = \frac{Ex_{total}^{bio-oil}}{Ex_{biomas} + Ex_{electric}} \times 100\% \quad (3.28c)$$

$$\psi_{loss} = 100\% - (\psi_{NCG} + \psi_{biochar} + \psi_{bio-oil}) \quad (3.29)$$

Where, Ex_{total}^{NCG} , $Ex_{total}^{biochar}$ and $Ex_{total}^{bio-oil}$ are exergy of NCG, biochar, and bio-oil respectively;

ψ_{NCG} , $\psi_{biochar}$ and $\psi_{bio-oil}$ are exergy efficiencies of non-condensable gases, biochar, and bio-oil, respectively; $\psi_{loss,T}$ represents the loss exergy efficiency.

3.12 Fourier Transfer Infrared (FT-IR) Spectroscopy Analysis

The FTIR analysis was determined using Agilent technology Cary 630 FTIR model (Plate 3.5a) installed at the central Laboratory, Ahmadu Bello University, Zaria. 12 mg of the biochar samples were closed and pressed to the pellet placed on top of a crystal, while the bio-oil samples were open and allowed to smear on top of the crystal. After that, the samples were identified for coding by checking a blue line from red and green regions. Finally, the peaks of the samples were determined by dragging the samples to obtain a wavelength as well as transmittance or absorbance (Gautam and Chaurasia, 2020).

3.13 Gas Chromatography Mass Spectrometry (GC-MS)

The sample was analyzed using Agilent Technologies 7890A GC and 5977B MSD (Plate 3.5b), while the GC-MS system's experimental settings were as follows: Hp 5-MS standard non-polar capillary column, 30 M in length, 0.25 mm ID, and 0.25 μm film thickness. The flow rate of the mobile phase (carrier gas: He) was fixed at 1.0 ml/min. The temperature program (oven temperature) for the gas chromatography portion was 40°C elevated to 250 °C at 5 °C/min, and the injection volume was 1 μl . The samples that had been dissolved in methanol were totally scanned at a range of 40-650 m/z, and the findings were compared by using Nist Mass Spectral Library search program as proposed by Laouge *et al.* (2020) and Mohammed *et al.* (2017).

3.14 Scanning Electron Microscopy (SEM)/Energy Dispersion X-ray (EDX) Spectroscopy Analysis

Scanning electron microscopy (SEM) was used to determine the quality, image resolution, and morphology of the biochar yield. A variety of signals on the biochar surface was generated by scanning the biochar surface with a finely focused high-energy electrons beam. Afterward, electron bombardment resulted in the emission of low-energy secondary electrons, the backscattering of high-energy primary electrons, and the emission of element-specific X-radiation. The elemental analysis of SEM surfaces was determined using EDX as shown in Figure 3.8. The EDX detectors split the characteristics X-rays of various elements present in the biochar samples into an energy spectrum to determine the abundance of specific elements via EDX software as postulated by Lee *et al.* (2017).

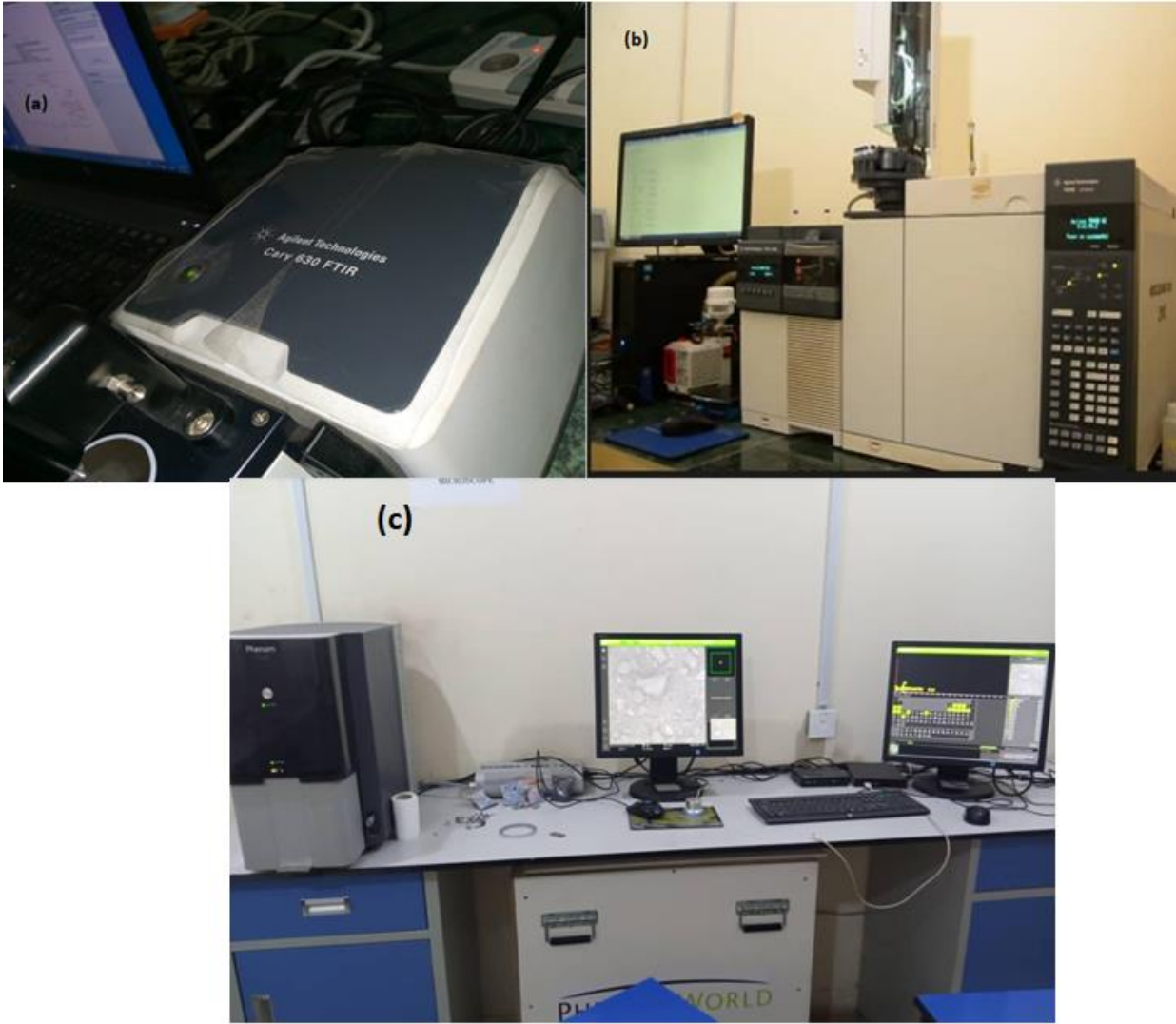


Plate 3.7: (a) FTIR machine (b) GC-CM machine (c) SEM/EDX Machine

3.15 Research Instruments/Tools

The list of equipment utilized in this study and their uses are shown in Table 3.5

Table 3.5: Research Instruments/ Tools

S/N	Tools	Functions
1	Ansys software	Determined the functionality of the plant with different specifications.
2	Design-Expert	Software package by Stat-ease Inc. that is mostly utilized to perform the design of experiment.
3	k-type thermocouple	Measured the temperatures inside the reactor
4	Perkin Elmer STA 600	Employed to obtain proximate analysis such as, moisture content, volatile matters, ash, pH, fixed carbon, corrosive, etc.
5	Elemental Analyzer	Employed to obtain ultimate analysis such as carbon, hydrogen, oxygen, nitrogen, Sulphur.
6	Chromatography-Mass Spectrometer	Identified the chemical compounds in the bio-oil samples
7	FTIR Machine	Determined the functional groups in the bio-oil and biochar samples
8	Scanning Electron Microscope (SEM) and Surface Area Analysis (BET)	Examined the morphology (structure), phases, and high-resolution image of biochar surface.

CHAPTER FOUR

RESULTS AND DISCUSSIONS OF FINDINGS

4.1 Proximate Analysis

The average values of the proximate analysis of the oven-dried lignocellulose biomass samples are presented in Table 4.1. The percentage of the MC ranged from 0.12 to 0.49 wt%, the VM ranged from 34.73 to 88.82 wt%, the FC varied between 9.08 to 44.70 wt%, and ash contents varied between 0.9 to 20.00 wt%. The values obtained for bamboo, rice husk and sugarcane bagasse (Table 4.1) are in close agreement with the findings of Gautam and Chaurasia (2020). The value of FC (9.08 wt%) and Ash (2.51 wt%) presented for obeche wood (Table 1) in this study is in close agreement with the findings of Ogunsola *et al.* (2018) who reported FC and Ash as 10.23 and 11.89 wt% respectively. The VM (84.80 wt%) obtained for meliana wood (Table 4.1) in this study is moderately higher than the 81.42 wt% reported by (Adeleke *et al.*, 2020) for woody biomass. The proximate analysis obtained from corncob (Table 4.1) shows that the VM (79.87 wt%) is approximately equal to 77.14 wt%, as reported by (Kartal and Ozveren, 2021). Likewise, the value FC (15.39 wt%) in this study is within the same range reported by Quan *et al.* (2018) whose value is 14.37 wt%. The results presented for siam weed are similar to the values reported by Ayeni *et al.* (2018) whose VM, FC, and Ash contents are 71.2, 18.4, and 4.67 wt% respectively. Similarly, the values of VM (34.73 wt%) and FC (44.70 wt%) followed the same trend as the findings of Bello *et al.* (2017) who reported 36.45 and 42.76 wt% for VM and FC respectively.

The MC in all the lignocellulose biomass (Table 4.1) are less than 0.5% due to excessive drying of the biomass in an oven at a temperature of 105°C for 1h before characterization. These results are similar to those reported by others (Ayeni *et al.*, 2018; Gautam and Chaurasia, 2020) who reported approximately zero percent for the MC on an oven-dried basis. The low MC were recorded to make them suitable for the pyrolysis process since less energy would be needed to vaporize the biomass in the reactor and enhance the thermal energy generated and conversion efficiency during the process. Obeche wood (88.04 wt%) has the highest VM, closely followed

by sugarcane bagasse (84.82%) and shea butter wood (82.92 wt%). At the same time, moringa oleifera (35.64 wt%) and rice husk (64.80 wt%) possess the lowest volatile matter. The high VM of obeche wood, sugarcane bagasse, and shea butter wood would increase the heating value, devolatilization reactivity, ignitability, and burn gases in the reactor, thereby leading to a high bio-oil and non-condensable gases yields (Kpalo *et al.*, 2021). Moringa oleifera (19.24 wt%), lemon grass (9.98 wt%) and sugarcane straw (9.60 wt%) have the highest ash content, making them unsuitable for pyrolysis. An increase in the percentage of ash content would reduce the amount of bio-oil yield due to catalytic cracking of the bio-oil into NCG and low biochar yield. Also, the low ash contents in shea butter wood, sugarcane bagasse and palm kernel shell help reduce harmful substance (e.g., slag) which may lead to fouling, corrosion, etc. during the pyrolysis process, thereby minimizing extensive maintenance of the pyrolysis plant (Nagarajan and Prakash, 2021). Hence, making them favourable for the pyrolysis process. The high FC present in siam weed, palm kernel shell and lemon grass would enhance the time to yield biochar and bio-oil due to the high energy released. The variations in the results, when compared with previous studies, are due to geographical location, the intrinsic composition of the biomass, soil type where the biomass is sourced and cultivated (Acevedo *et al.*, 2019).

Table 4.1: Proximate Analysis of Oven-Dried Biomass

SAMPLE	MC (wt%)	VM (wt%)	FC (wt%)	Ash (wt%)
Woody/Forestry				
Bamboo	0.41 ± 0.04	80.40 ± 0.90	15.04 ± 0.12	3.52 ± 0.02
Baobab wood	0.33 ± 0.04	83.16 ± 0.90	15.14 ± 0.42	1.15 ± 0.02
Melina wood	0.35 ± 0.05	82.80 ± 1.25	14.79 ± 0.08	2.06 ± 0.01
Obeche wood	0.37 ± 0.07	88.04 ± 1.20	9.08 ± 0.42	2.51 ± 0.01
Shea butter wood	0.29 ± 0.03	82.92 ± 1.17	15.89 ± 0.45	0.90 ± 0.01
Agro-wastes				
Corn cob	0.44 ± 0.06	79.87 ± 0.90	16.19 ± 0.43	3.50 ± 0.02
Rice husk	0.49 ± 0.05	64.80 ± 1.15	16.44 ± 0.11	20.00 ± 0.01
Palm kernel shell	0.30 ± 0.02	73.70 ± 0.50	22.50 ± 0.25	3.50 ± 0.01
Fruits				
Coconut shell	0.40 ± 0.02	77.66 ± 1.25	20.10 ± 0.89	1.85 ± 0.02
Sugarcane bagasse	0.28 ± 0.03	84.82 ± 1.05	13.60 ± 0.23	1.30 ± 0.02
Sugarcane straw	0.48 ± 0.05	77.25 ± 1.18	13.31 ± 0.64	9.60 ± 0.06
Grass/Leaves				
Lemon grass	0.46 ± 0.07	66.87 ± 0.90	23.95 ± 0.97	9.98 ± 0.05
Moringa oleifera	0.42 ± 0.03	35.64 ± 0.92	44.70 ± 0.14	19.24 ± 0.02
Mexican sunflower	0.39 ± 0.02	77.96 ± 1.03	13.13 ± 0.33	8.47 ± 0.02
Siam weed	0.12 ± 0.08	78.48 ± 1.11	20.10 ± 0.10	1.30 ± 0.02

****MC-Moisture contents; Volatile matter; FC-Fixed carbon; HHV: Higher heating value;**

LHV: Lower heating value

4.2 Ultimate Analysis

Table 4.2 shows the average values of the ultimate analysis of lignocellulose biomass, whose carbon contents ranged from 40.35 to 50.00 wt%; hydrogen contents ranged from 5.02 to 6.45 wt%. The nitrogen contents varied between 0.15 to 1.75 wt%, the oxygen contents from 43.13 to 51.68 wt% and the sulphur contents varied between 0.04 to 0.43 wt%. The biomass carbon, hydrogen, nitrogen, oxygen, and sulphur contents of each biomass sample are presented in Table 4.2. Comparing this study with various research, the results present for meliana wood and shea butter wood fall within the range of values for hardwood reported by Vassilev (2010) who reported (C:49.6 wt%, H: 6.1 wt%, N: 0.1% wt, O: 44.1 wt% and S: 0.06 wt%) and (C: 52.3 wt%, H: 6.1 wt%, N: 0.3 wt%, O: 41.2 wt% and S: 0.10 wt%), while the carbon contents (45.11 wt%) of bamboo obtained in this study closely agreed with 45.9-46.3 and 48.76 wt% reported by Posom and Sirisomboom (2017) and Gautam and Chaurasia (2020) respectively. The value obtained from corncobs (Table 4.2) is very close to the values reported by Quan *et al.* (2018) whose carbon, hydrogen, nitrogen, oxygen and sulphur contents are 47.18, 6.03, 0.22 46.34 and 0.23 wt% respectively. Similarly, the value obtained for rice husk (Table 2) compared very well with the values of Efomah and Gbabo (2015), Gautam and Chaurasia (2020), Fauzan *et al.* (2018) and Vassilev *et al.* (2010) whose values are (C: 45.20 wt%, H: 5.80 wt%, N: 1.02 wt%, O: 47.60 wt%, S: 0.21 wt%), (C: 35.92 wt%, H: 5.05 wt%, N: 0.26 wt%, O: 58.77 wt%), (C: 40.87 wt%, H: 5.59 wt%, N: 0.45 wt%, O: 53.09 wt%, S: 0.03 wt%) and (C: 49.3 wt%, H: 6.1 wt%, N: 0.8 wt%, O: 43.70 wt%, S: 0.08 wt%).

Shea butter wood, palm kernel shell, Sugarcane bagasse and baobab wood have the highest carbon and low oxygen, nitrogen, and sulphur contents, making them more useable for the pyrolysis process. Their low sulphur and nitrogen contents make them more suitable for pyrolysis due to their low tendency to emit harmful gases that lead to the formation of NO_x and SO_x into the atmosphere when burnt (Nagarajan and Prakash, 2021). Hence, The study can produce environmentally friendly fuel due to their low emission of SO_x and NO_x gases that plants can utilize during photosynthesis.

Table 4.2: Ultimate Analysis of Oven-Dried Biomass

SAMPLE	C (wt%)	H (wt%)	N (wt%)	O (wt%)	S (wt%)
Woody/Forestry					
Bamboo wood	45.11 ± 0.36	5.91 ± 0.03	0.28 ± 0.01	48.51 ± 0.28	0.19 ± 0.001
Baobab wood	49.61 ± 0.17	5.61 ± 0.02	1.05 ± 0.01	43.13 ± 0.11	0.60 ± 0.06
Melina wood	47.44 ± 0.16	5.65 ± 0.02	0.21 ± 0.01	46.70 ± 0.16	0.11 ± 0.01
Obeche wood	47.69 ± 0.23	5.70 ± 0.01	0.57 ± 0.01	46.00 ± 0.12	0.04 ± 0.003
Shea butter wood	50.00 ± 0.82	6.00 ± 0.03	0.20 ± 0.02	43.79 ± 0.24	0.01 ± 0.001
Agro-wastes					
Corn cob	47.90 ± 0.91	6.10 ± 0.02	0.51 ± 0.01	45.30 ± 0.23	0.19 ± 0.01
Rice husk	40.35 ± 0.19	5.25 ± 0.03	0.31 ± 0.02	54.08 ± 0.15	0.01 ± 0.001
Palm kernel shell	48.90 ± 1.12	5.38 ± 0.02	0.22 ± 0.01	45.03 ± 0.15	0.02 ± 0.001
Coconut shell	48.59 ± 0.30	5.99 ± 0.03	0.20 ± 0.01	45.21 ± 0.27	0.01 ± 0.006
Fruit residues					
Sugarcane bagasse	47.31 ± 0.20	6.45 ± 0.06	0.15 ± 0.01	45.99 ± 0.19	0.10 ± 0.01
Sugarcane straw	44.09 ± 0.46	5.94 ± 0.01	0.50 ± 0.01	49.10 ± 0.17	0.27 ± 0.01
Grass/Leaves					
Lemon grass	41.12 ± 0.15	5.29 ± 0.03	1.75 ± 0.01	51.68 ± 0.19	0.06 ± 0.001
Mexican Sunflower	45.34 ± 0.16	5.32 ± 0.03	2.49 ± 0.02	46.83 ± 0.12	0.02 ± 0.003
Moringe oleifera	45.42 ± 0.24	5.02 ± 0.04	2.95 ± 0.01	44.97 ± 0.12	0.43 ± 0.05
Siam weed	45.63 ± 0.16	5.76 ± 0.01	1.24 ± 0.01	46.27 ± 0.41	0.10 ± 0.01

****C: Carbon; H: Hydrogen; N: Nitrogen; O: Oxygen; S: Sulphur**

4.3 Structural composition analysis

The average structural composition analysis (Table. 4.3) shows that the biomass species' cellulose, hemicellulose, and lignin contents ranged from 12.95 to 45.80 wt%, 11.72 to 36.72 wt% and 7.12 to 45.41 wt%, respectively. The results presented for woody/forestry biomass samples (Table 3) fall within the range of values for hardwood reported by (Roger *et al.*, 2021), whose values are (Ce: 45.4 wt%, He: 26.0 wt%, Li: 23 wt%). The cellulose (Ce) contents obtained from sugarcane bagasse (Table 3) agreed well with the report of (Nwosu and Muzakir, 2015). Similarly, the hemicellulose and lignin contents correlated very well. The cellulose contents for moringa oleifera (Table 3) is moderately lower than 13.7 wt% reported from Mishra and Sinha (2020). The values for sugarcane bagasse (Table 4.3) agreed well with the findings of Varma and Mondal (2017) who reported 47.6, 39 and 11.2 wt% for cellulose, hemicellulose and lignin contents respectively.

All the biomass samples considered exhibit higher cellulose and hemicellulose over lignin composition, except siam weed, coconut shell and palm kernel shell, whose lignin contents are slightly higher than their cellulose and hemicellulose contents. This implies that the biomass is suitable for the pyrolysis process because increased cellulose and hemicellulose contents increase the pyrolysis rate. Hence, it degrades mostly volatile products, e.g., bio-oil and NCG yields. At the same time, the palm kernel shell is more suitable for biochar yields since an increase in lignin contents reduces the pyrolysis rate, which retard the decomposition of volatile products. Hence, it favours the yield of biochar production.

Table 4.3: Structural Composition Analysis of Oven-Dried Biomass

SAMPLE	Cellulose %	Hemicellulose %	Lignin %
Woody/Forest			
Bamboo wood	40.96 ± 0.92	25.83 +0.52	21.96 +0.24
Baobab wood	44.35 ± 0.17	27.75 + 0.51	22.35 +0.31
Melina wood	42.61 ± 0.97	29.63 + 0.45	26.30+ 0.32
Obeche wood	44.14 ± 0.18	26.86 + 0.25	24.78 +0.24
Shea butter wood	45.80 ± 0.14	30.43 + 0.23	23.42+0.32
Agro-waste			
Corn cob	41.62 ± 0.14	34.01 +0.41	17.45 +0.48
Rice husk	36.31 ± 0.83	20.20 + 0.17	19.50 +0.45
Palm kernel shell	28.92 ± 0.14	25.01 + 0.10	45.41 +0.40
Fruits			
Coconut shell	35.06+0.12	25.55 +0.24	37.86 +0.24
Sugarcane bagasse	43.99 + 0.93	29.49 + 0.12	27.80 +0.45
Sugarcane straw	40.81+ 0.15	29.97 + 0.35	20.42 +0.23
Grass/Leaves			
Lemon grass	40.14 + 0.16	25.78 + 0.14	20.65 +0.42
Mexican sunflower	47.71+0.15	36.72 + 0.42	15.54 +0.36
Moringe oleifera	12.95 + 0.12	11.72 +0.65	7.12 +0.13
Siam weed	27.82+0.10	26.21 + 0.11	29.64 + 0.34

****Ce-Cellulose; He-Hemicellulose; Li-Lignin**

4.4 Heating Value Analysis

The higher heating value (HHV) and lower heating value (LHV) varied from biomass to biomass because their fuel characteristics differed (Table 4.4). The highest HHV and LHV recorded were 21.80 and 20.49 MJ/kg for shea butter wood, while corncob has the lowest HHV and LHV at about 16.97 and 15.60 MJ/kg.

Results obtained from Palm kernel shell (Table 4.4) show that the HHV closely agreed with the report the 18.84 MJ/kg reported Umar *et al.* (2020) but moderately lower than 20.71 MJ/kg reported by Torsosa-Masia *et al.* (2007). In the case of sugarcane bagasse, the HHV is slightly higher than 17.70, 17.70 and 17.32 MJ/kg reported by Channiwala *et al.* (2002), Munir *et al.* (2000) and Suarez *et al.* (2000), respectively. Similarly, the HHV and LHV reported for bamboo, obeche wood, and shea butter wood in this study, as shown in Table 4.4, are in consonant with what Chukwunke *et al.* (2019) and Oyebanji *et al.* (2022) reported for Mahogany wood (HHV: 21.26MJ/kg and LHV: 20.27MJ/kg). Lophira alota wood (HHV: 21.20MJ/kg and LHV: 18.08MJ/kg), respectively. Results obtained from lemon grass is fairly higher than 17.7MJ/kg reported by Gravalos *et al.* (2016) for plant leaves/weeds. The increase in the HHV and LHV of shea butter wood, obeche wood and palm kernel shell were attributed to their high fixed carbon (FC) and carbon contents which is the primary source of heat (Kpala *et al.*, 2021; Umar and Sulaiman *et al.*, 2021; Sawadogo *et al.*, 2018), while the decrease in HHV and LHV recorded for corncobs resulted from their high ash and moisture contents (Akinola and Fapetu, 2015; Oladejo *et al.*, 2020).

Furthermore, shea butter wood, baobab wood and siam weed are more suitable for the pyrolysis process as its low ash. Moisture contents and high fixed carbon and carbon contents would enhance their hydrocarbon contents, increasing their heating value and rapid decomposition of the biomass in the reactor.

Table 4.4: HHV and LHV of Oven-dried Biomass

SAMPLE	HHV(MJ/kg)	LHV(MJ/kg)
Woody/Forestry		
Bamboo wood	19.80 ± 0.37	18.51 ± 0.73
Baobab wood	21.40 ± 0.47	20.18 ± 0.24
Melina wood	20.50 ± 0.47	19.21 ± 0.34
Obeche wood	20.10 ± 0.76	18.85 ± 0.16
Shea butter wood	21.80 ± 0.69	20.49 ± 0.44
Agro-wastes		
Corn cob	18.11 ± 0.24	16.78 ± 0.14
Rice husk	16.63 ± 0.79	15.49 ± 0.45
Palm kernel shell	19.98 ± 0.44	18.70 ± 0.25
Coconut shell	19.97 ± 0.52	18.63 ± 0.34
Fruit residues		
Sugarcane bagasse	18.60 ± 0.57	17.31 ± 0.52
Sugarcane straw	17.01 ± 0.08	15.58 ± 0.05
Grass/Leaves		
Lemon grass	17.23 ± 0.35	16.08 ± 0.25
Mexican Sunflower	17.45 ± 0.83	16.30 ± 0.45
Moringe oleifera	16.97 ± 0.24	15.60 ± 0.66
Siam weed	20.60 ± 0.14	19.54 ± 0.26

HHV: Higher heating value; LHV: Lower heating value

4.5 Thermogravimetry analysis (TGA)

Figure 4.1 depicts the thermogravimetry analysis (TGA) profile from the thermal reaction of bamboo, corncobs, sugarcane bagasse, obeche wood, palm kernel shell, and shea butter wood and lemon grass under an inert environment (nitrogen flow rate, 1 ml/min) at a steady heating rate of 10⁰C/min in the temperature range of 30 to 850°C. The TGA curve (Figure 4.1) helps determine the purity, thermal stability, drying, thermal degradation, weight loss, and structural composition of the biomass when subjected to heating at different temperatures. This is necessary because cellulosic, hemicellulosic, and lignin contents in the biomass exhibit various decomposition behaviour (Özsina and Pütün, 2019; Gajeraa *et al.*, 2020). TGA, also known as pyrolytic decomposition of biomass, undergoes three phases over a broad temperature range preheating phase (moisture evaporation), volatile devolatilization, and carbonization (Balogun *et al.*, 2017; Ozyuguran and Yaman, 2018; Mishra and Mohanty, 2018; Menares *et al.*, 2020; Rasool and Kumar, 2020)

In the first stage, known as the preheating stage (moisture evaporation phase), passive pyrolysis of the biomass occurred at about 42-110°C, resulting in drying and decomposition of a low quantity of volatile components due to the emission of free water and chemically bonded water known as the water of constitution (Merdun and Laouge, 2020), which was extended up to a temperature of 180°C. Approximately 5.2 wt% weight loss was recorded, similar to what Halder *et al.*, (2019) and Umar *et al.*, (2021) reported for lignocellulose biomass. The fluctuations of the TG curve were due to the biomass utilized to carry out the experimental runs, which had been oven-dried and possessed low MC (Akinola and Fapetu, 2015). During the second stage, known as the volatile devolatilization stage (180-580°C), thermal degradation of hemicelulosic and cellulosic polymers coincided, leading to the formation of an excessive number of small-molecule gas and liquids phase components with a relatively large molecular weight (Dwivedi *et al.*, 2019). A greater percentage of tar was precipitated (Menares *et al.*, 2020). Active pyrolysis occurred during this process. Also, the highest weight loss was recorded for sugarcane bagasse at about 60 wt% (180- 470°C), while bamboo possessed the lowest weight loss of 27 wt% (180-480°C). These losses in weight were attributed to the degradation of light volatile compounds below 100°C. The last phase, known as the carbonization stage, begins at the end of the second stage up to an asymptotic value of thermogravimetry (TG) shows no significant weight loss was recorded during this stage due to secondary reactions such as cracking and repolymerization, leading to

slow decomposition (conservative minor devolatilization) of the lignin contents at a temperature of about 470-850°C (Merdun and Laouge, 2021). Hence, this leads to the formation of solid residues (Biochar). During this process, the passive pyrolysis process occurred. The overall weight losses are ANB (25 wt%), ANC (38 wt%), ANG (98 wt%), ANM (60 wt%), ANP (95 wt%), ANW (80 wt%). These results are supported by the works done by Baffour-Awuah *et al.* (2021); Okokpujie *et al.* (2019) and Isah *et al.* (2020). Sugarcane bagasse (ANG) possessed the highest weight loss after undergoing exothermic thermal decomposition at different pyrolysis temperatures, closely followed by Palm kernel shell. At the same time, bamboo had the least weight loss percentage. Hence, Sugarcane bagasse is more suitable for the pyrolysis process among the samples examined next to palm kernel shell, shea butter wood, and lemon grass, respectively, as the rate of weight loss, is proportional to the energy released (Balogun *et al.*, 2021).

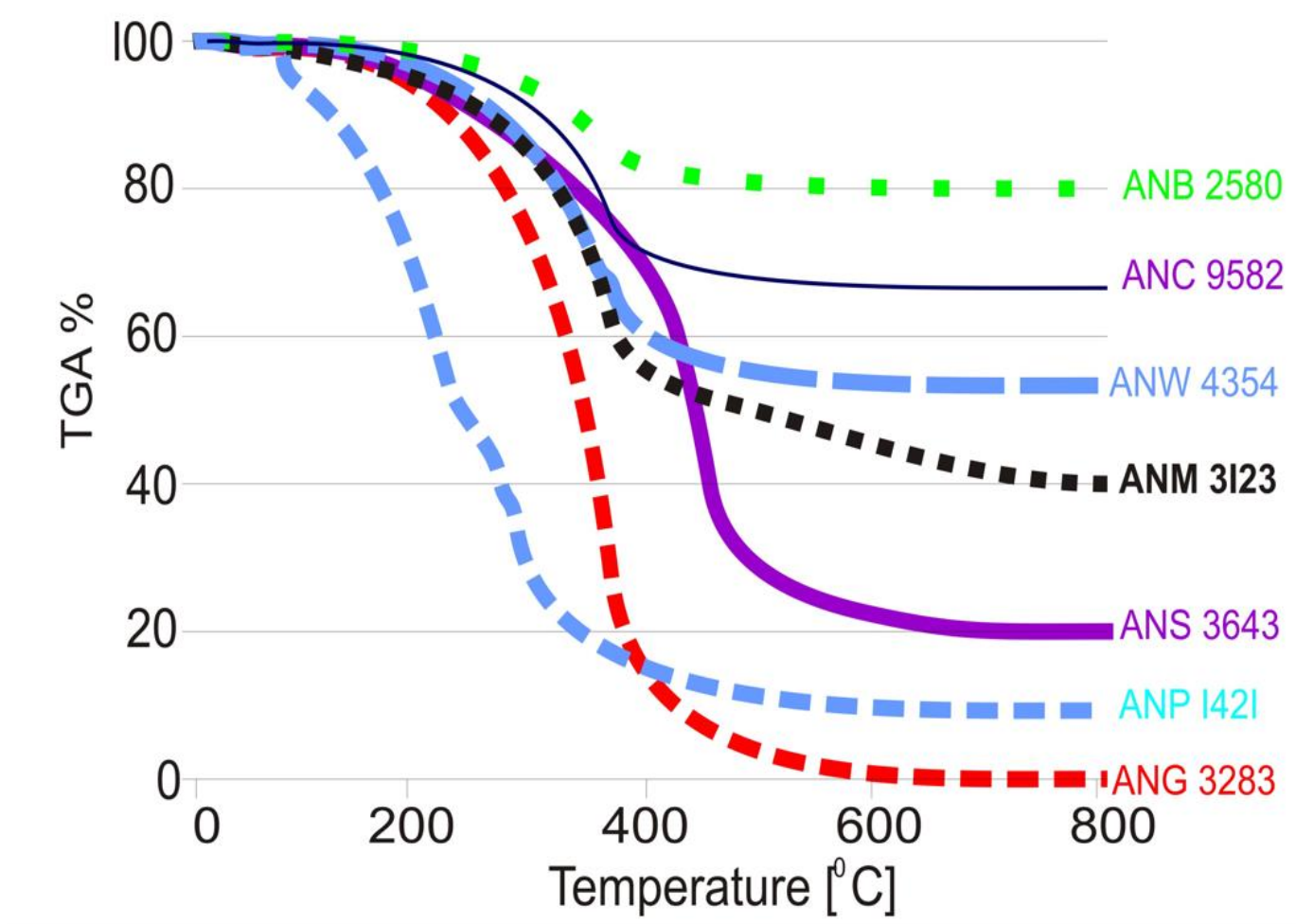


**Figure 4.1. TGA of weight loss at a heating rate 10⁰C/min for Bamboo (ANB 2580);
 Corncobs (ANC 9582); Lemon grass (ANW 4354); Obeche wood (ANM 3123);
 Shea butter wood (ANS 3643); Palm kernel shell (ANP 1421); Sugarcane bagasse (ANG 3283)**

4.6 Ignitability Index

The ignitability index (I_i) is essential in rating a biomass's quality. It helps to evaluate the tendency of the biomass to burn or ignite during the pyrolysis process. Biomass with high I_i enhances rapid decomposition of the biomass in the pyrolysis plants. The error bar indicates the variation of the data obtained from repeated number of experimental runs, and the average ignitability values ranged from 0.26 for corn cob to 0.33 for palm kernel (Figure 4.2). Palm kernel shell possessed the highest ignitability index, closely followed by sugarcane bagasse, while corn cob had the lowest ignitability index. The increase in ignitability index recorded for palm kernel shell, sugarcane bagasse, Siam weed and shea butter was due to their high HHV and low moisture content. Hence, palm kernel shea, shea butter wood, and sugarcane bagasse are more suitable for pyrolysis.

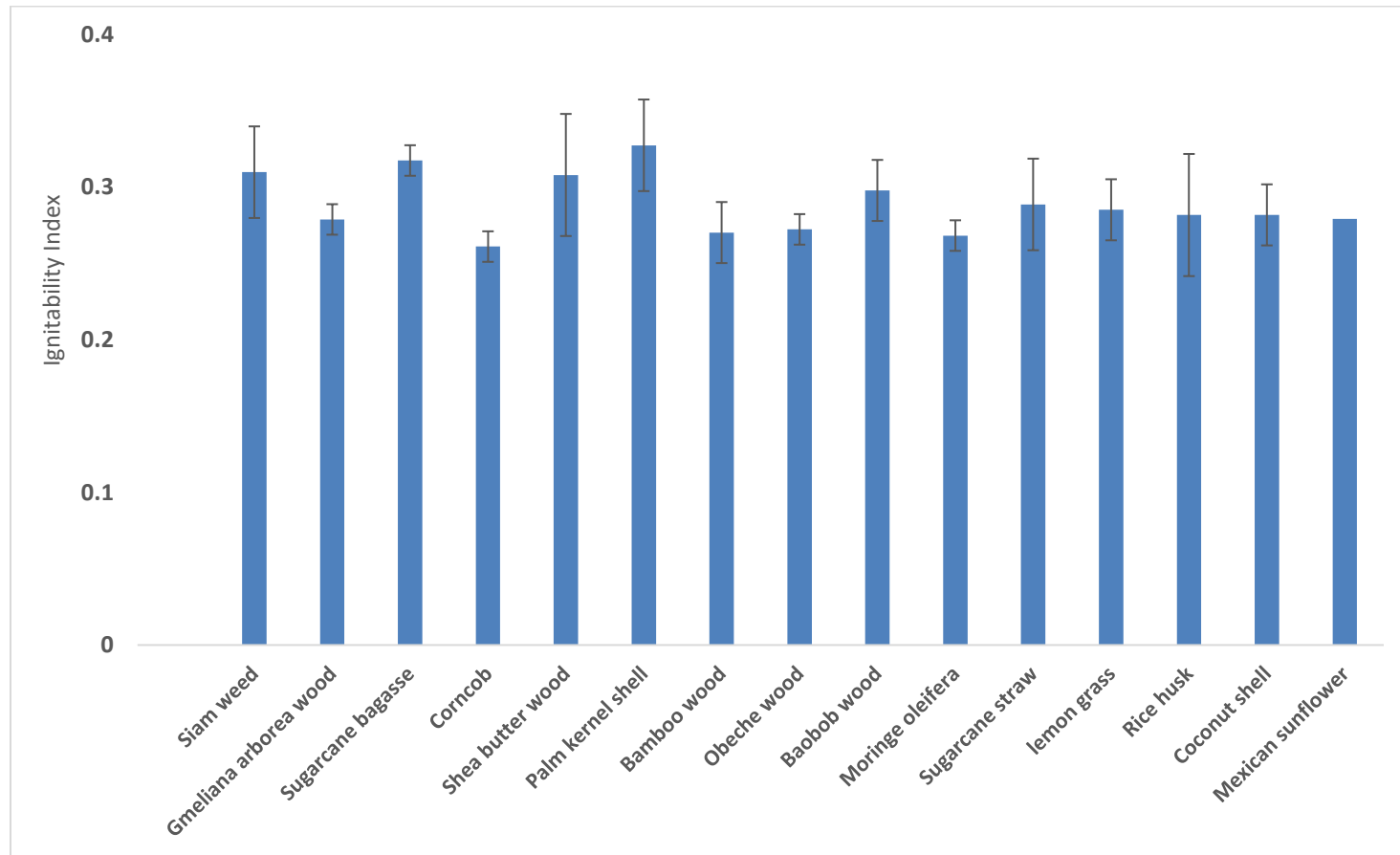


Figure 4.2: Ignitability index

4.7 Statistical Design format for Bio-oil, Biochar, and NCG yields

Tables 4.5- 4.7 present the products of pyrolysis based on the combination of pyrolysis operating parameters such as temperature, reaction time, heating rate, nitrogen flow rate, and particle sizes each at five (5) levels provided to the Design Expert Version 13.0. Fifty (50) experimental runs were suggested by the Design-Expert Software. The experiments were performed by utilizing the same operating parameters proposed by the software and the complete set of the experiments via the combination of operating parameters and the results of the pyrolysis products' yields which served as input parameters to the software for further analysis and prediction.

The optimum bio-oil yield (46.5 wt%) for PKS (Table 4.5) was attained at the temperature (T) of 520°C, reaction time (R) of 15 min, heating rate (H) of 17.5°C/min, nitrogen flow rate (N) of 125 cm³/min, and particle size (P) of 0.5 mm. In the case of SCB, the optimum bio-oil yield (47.1 wt%) was recorded at T, R, H, N, P of 520°C, 15 min, 22.5 °C/min, 175 cm³/min and 0.7 mm respectively. Considering SBW, optimum bio-oil yield (47.9 wt%) obtained at T of 520 °C, R of 15 min, H of 22.5°C/min, N of 175 °C/min and P of 0.7 mm. SBW is more suitable for bio-oil yield closely followed by SCB due to their high quantity of bio-oil yield. The bio-oil yields increased as temperature increased from 320 to 520°C. Further increase in temperature above 520 °C decreased the bio-oil yield due to secondary cracking of the bio-oil leading to a high yield of NCG from 22.5 wt% to 34.7 wt% NCG (Varma and Mondal, 2020). Minimum bio-oil yield (36 wt%) for PKS was found at the T, R, H, N, and P of 320 °C, 5 min, 27.5 °C/min, 25 cm³/min, and 0.9 mm respectively. In the case of SCB, minimum bio-oil yield (40.1 wt%) was obtained at a T of 720°C, R of 25 min, H of 27.5°C/min, N of 225 cm³/min and P of 0.1 mm. Similarly, the minimum bio-oil yield (38.5 wt%) for SBW was attained at a T, R, H, N, and P of 720°C, 5 min, 7.5°C/min, 25 cm³/min, and 0.9 mm respectively. The results of the bio-oil yields for the biomass under investigation closely agreed with the report of Laouge *et al.* (2020), Gautam and Chaurasia (2019), Hossain *et al.* (2017), Varma and Mondal (2017), and Paenpong *et al.* (2016) who reported optimum bio-oil yields of 48.27 wt% at a T of 400°C, N of 200 mL/min of 1.5 mm for fast pyrolysis of Pearl Millet, 46.93 wt% at a T of 450°C fast pyrolysis of Bamboo, and 48.26 wt% at a T of 450°C, R of 1 mm, N of 200 cm³/min for fast pyrolysis of Oil palm fibre, 45.23 wt% at the T of 500°C, H of 300°C/min, N of 100 cm³/min, and P of 0.5 mm for fast pyrolysis

of Sugarcane bagasse and 45.9 wt% at the T of 550°C, P of 0.325 mm, and N of 7.75 L/min for fast pyrolysis of Cassava rhizome respectively. The optimum values are higher than 32.2 wt% at 400°C and 30.5 wt% at the T of 400°C, R of 5min, and P of 0.3mm reported by Sahoo *et al.* (2021) for slow pyrolysis of Pigeon pearl stalk and Ahmad *et al.* (2017) for co-pyrolysis of Lemongrass and residual cooking oil respectively, but slightly less than 50.5 wt% at 600°C, H of 50 °C/min, and N of 5 L/min reported by Mohammed *et al.* (2017) for intermediate pyrolysis of Napier grass.

The optimum values of biochar yields (41.1 wt%) for PKS was found at the T of 320°C, R of 5 min, H of 7.5°C/min, N of 25 cm³/min, and P of 0.9 mm. In the case of SCB, the optimum biochar yield (40 wt%) was attained at a T, R, H, N, and P of 320°C, 5 min, 7.5°C/min, 25 cm³/min, and 0.9 mm respectively. Likewise, for SBW, the optimum biochar yield (40.8 wt%) was obtained at a T of 320°C, R of 5 min, H of 7.5°C/min, N of 25 cm³/min, and P of 0.9 mm. These values (biochar yields) agreed well with Sahoo *et al.* (2021) and Mohammed *et al.* (2017) who reported optimum biochar yields (43.66 wt%) at the T of 750°C, N of 25 L/min, and H of 50 °C/min for slow pyrolysis of Bamboo and 46.41 wt% at the T of 450°C, N of 25 L/min, and H of 10°C/min for intermediate pyrolysis of Napier grass. This optimal value recorded is higher than 26.2 wt% at the T of 450°C reported by Guatam and Chaurasia, 2020 (2021) for fast pyrolysis of Bamboo. The biochar yield decreased with increasing temperature due to complete pyrolysis process caused by rapid emission of volatile matters and thermal decomposition of the biomass, thereby, enhancing the yields of aromatic compounds (Zhang *et al.*, 2017; Varma and Mondal, 2017; Guedes *et al.*, 2018; Guatam and Chaurasia, 2020, Sahoo *et al.*, 2021). The minimum biochar yields of 25.6 wt% and 24.1 wt% was obtained for PKS and SBW respectively at the T of 720°C, R of 25 min, H of 7.5°C/min, N of 225 cm³/min, and P of 0.1 mm, while in the case of SCB, minimum biochar yields (26.6 wt%) was recorded at a T, R, H, N, and P of 720°C, 25 min, 27.5°C/min, 225 cm³/min, and 0.1 mm respectively.

Table 4.5: Experimental Design Matrix and the Corresponding Pyrolysis Products Yields from Palm Kernel Shell

Std	Run	Factor A: Temperature(°C)	Factor B: Reaction time(min)	Factor C: Heating rate(°C/min)	Factor D: Nitrogen flow rate(cm ³ /min)	Factor E: Particle size(mm)	Response 1: Bio-oil(w%)	Response 2: Biochar(w%)	Response 3: Non-condensable gases(w%)
36	1	520	10	17.5	125	0.5	43.1	33.3	23.6
48	2	520	15	17.5	125	0.5	46.5	33.3	20.2
35	3	520	5	17.5	125	0.5	43.2	32.4	24.4
16	4	720	25	27.5	225	0.1	38.6	28.4	33
17	5	320	5	7.5	25	0.9	36.9	41.1	22
47	6	520	15	17.5	125	0.5	46.1	33.2	20.7
37	7	520	15	12.5	125	0.5	43.3	33.4	23.3
18	8	720	5	7.5	25	0.9	38.5	29.4	32.1
22	9	720	5	27.5	25	0.9	40	28.4	31.6
23	10	320	25	27.5	25	0.9	38.1	38.3	23.6
7	11	320	25	27.5	25	0.1	37.1	37.2	25.7
34	12	420	15	17.5	125	0.5	39.9	35.8	24.3
43	13	520	15	17.5	125	0.5	46.3	33.3	20.4
1	14	320	5	7.5	25	0.1	36.9	40.6	22.5
3	15	320	25	7.5	25	0.1	37.4	38.6	24
39	16	520	15	17.5	75	0.5	43.1	34.2	22.7
32	17	720	25	27.5	225	0.9	40.2	27.4	32.4
12	18	720	25	7.5	225	0.1	36.5	25.6	33.3
5	19	320	5	27.5	25	0.1	37.1	38.8	24.1
31	20	320	25	27.5	225	0.9	37.1	39.1	23.8
44	21	520	15	17.5	125	0.5	46.2	32.9	20.9
21	22	320	5	27.5	25	0.9	36	40.1	23.9
30	23	720	5	27.5	225	0.9	39.6	29.6	30.8
19	24	320	25	7.5	25	0.9	36.3	40.3	23.4
42	25	520	15	17.5	125	0.3	43.2	32.7	24.1
14	26	720	5	27.5	225	0.1	39.6	28.5	31.9
25	27	320	5	7.5	225	0.9	36.8	40	23.2
41	28	520	15	17.5	125	0.5	46.4	33.6	20
38	29	520	15	22.5	175	0.7	44.4	32.4	23.2
6	30	720	5	27.5	25	0.1	40	27.6	32.4
20	31	720	25	7.5	25	0.9	40.8	28.5	30.7
46	32	520	15	17.5	125	0.5	43.5	32.9	23.6
9	33	320	5	7.5	225	0.1	36.2	38.9	24.9
50	34	520	15	17.5	25	0.5	43.7	33.6	22.7
8	35	720	25	27.5	25	0.1	39.6	27.4	33
11	36	320	25	7.5	225	0.1	37.2	37.3	25.5
33	37	620	15	17.5	125	0.5	38.7	33.1	28.2
4	38	720	25	7.5	25	0.1	38.6	29.5	31.9
49	39	520	15	17.5	125	0.5	43.4	32.4	24.2
10	40	720	5	7.5	225	0.1	39.9	27.1	33
40	41	520	15	17.5	225	0.5	44.2	32.1	23.7
2	42	720	5	7.5	25	0.1	39.7	29.6	30.7
13	43	320	5	27.5	225	0.1	36.5	37.7	25.8
29	44	320	5	27.5	225	0.9	36.2	37.7	26.1
27	45	320	25	7.5	225	0.9	36.4	38.6	25
28	46	720	25	7.5	225	0.9	40.8	26.1	33.1
26	47	720	20	7.5	225	0.9	40.1	28.5	31.4
24	48	720	25	27.5	25	0.9	39.5	27.5	33
45	49	520	15	17.5	125	0.5	43.6	33.1	23.3
15	50	320	25	27.5	225	0.1	36.9	36.8	26.3

Table 4.6: Experimental Design Matrix and the Corresponding Pyrolysis Products Yields from Sugarcane bagasse

Run	Factor A: Temperature(°C)	Factor B: Reaction time(min)	Factor C: Heating rate(°C/min)	Factor D: Nitrogen flow rate(cm ³ /min)	Factor E: Particle size(mm)	Response 1: Bio-oil(w%)	Response 2: Biochar(w%)	Response 3: Non-condensable gases(w%)
1	520	10	17.5	125	0.5	45.1	34.5	20.4
2	520	15	17.5	125	0.5	46.8	33.9	19.3
3	520	5	17.5	125	0.5	45.6	33.4	21
4	720	25	27.5	225	0.1	42.1	26.6	31.3
5	320	5	7.5	25	0.9	41.1	40	18.9
6	520	15	17.5	125	0.5	46.7	33.5	19.8
7	520	15	12.5	125	0.5	45.2	33.8	21
8	720	5	7.5	25	0.9	40.5	29.3	30.2
9	720	5	27.5	25	0.9	42.8	28.4	28.8
10	320	25	27.5	25	0.9	42.7	39.6	17.7
11	320	25	27.5	25	0.1	42.3	39.6	18.1
12	420	15	17.5	125	0.5	43.9	38.5	17.6
13	520	15	17.5	125	0.5	46.6	33.5	19.9
14	320	5	7.5	25	0.1	41.5	39.1	19.4
15	320	25	7.5	25	0.1	42.4	39.4	18.2
16	520	15	17.5	75	0.5	45.9	34.2	19.9
17	720	25	27.5	225	0.9	41.8	26.8	31.4
18	720	25	7.5	225	0.1	40.5	26.9	32.6
19	320	5	27.5	25	0.1	42.1	39.8	18.1
20	320	25	27.5	225	0.9	42.1	39.7	18.2
21	520	15	17.5	125	0.5	46.9	33.9	19.2
22	320	5	27.5	25	0.9	41.6	40.3	18.1
23	720	5	27.5	225	0.9	40.9	27.6	31.5
24	320	25	7.5	25	0.9	41.8	40	18.2
25	520	15	17.5	125	0.3	47.1	32.8	20.1
26	720	5	27.5	225	0.1	41.5	26.9	31.6
27	320	5	7.5	225	0.9	42	40.4	17.6
28	520	15	17.5	125	0.5	45.8	34.4	19.8
29	520	15	22.5	175	0.7	47.2	32.8	20
30	720	5	27.5	25	0.1	41.7	27.8	30.5
31	720	25	7.5	25	0.9	40.7	28.5	30.8
32	520	15	17.5	125	0.5	46.7	33.3	20
33	320	5	7.5	225	0.1	41	39.3	19.7
34	520	15	17.5	25	0.5	46.9	33.2	19.9
35	720	25	27.5	25	0.1	41.6	26.7	35.9
36	320	25	7.5	225	0.1	42	39.9	18.1
37	620	15	17.5	125	0.5	42.2	30.5	27.3
38	720	25	7.5	25	0.1	40.2	27.1	32.7
39	520	15	17.5	125	0.5	46.6	33.8	19.6
40	720	5	7.5	225	0.1	40.7	27.4	31.9
41	520	15	17.5	225	0.5	47.1	33.2	19.7
42	720	5	7.5	25	0.1	40.1	28.2	31.7
43	320	5	27.5	225	0.1	41.7	39.7	18.6
44	320	5	27.5	225	0.9	41.5	38.5	20
45	320	25	7.5	225	0.9	41.7	35.7	22.6
46	720	25	7.5	225	0.9	40.5	27.8	31.7
47	720	20	7.5	225	0.9	40.5	28.5	31
48	720	25	27.5	25	0.9	40.6	28.3	31.1
49	520	15	17.5	125	0.5	46.8	34.2	19
50	320	25	27.5	225	0.1	41.9	39.5	18.6

Table 4.7: Experimental Design Matrix and the Corresponding Pyrolysis Products Yields from Shell Buter Wood

Std	Run	Factor A: Temperature(°C)	Factor B: Reaction time(min)	Factor C: Heating rate(°C/min)	Factor D: Nitrogen flow rate(cm ³ /min)	Factor E: Particle size(mm)	Response 1: Bio-oil(w%)	Response 2: Biochar(w%)	Response 3: Non-condensable gases(w%)
36	1	520	10	17.5	125	0.5	45.2	33	21.8
48	2	520	15	17.5	125	0.5	46.3	32.1	21.6
35	3	520	5	17.5	125	0.5	45.1	31	23.9
16	4	720	25	27.5	225	0.1	41.1	25	33.9
17	5	320	5	7.5	25	0.9	39.1	40.8	20.1
47	6	520	15	17.5	125	0.5	46.2	32	21.8
37	7	520	15	12.5	125	0.5	46	32.8	21.2
18	8	720	5	7.5	25	0.9	38.5	27	34.5
22	9	720	5	27.5	25	0.9	40.8	26.3	32.9
23	10	320	25	27.5	25	0.9	40.7	39.6	19.7
7	11	320	25	27.5	25	0.1	40.3	39.2	20.5
34	12	420	15	17.5	125	0.5	44.5	38	17.5
43	13	520	15	17.5	125	0.5	46.1	32.1	21.8
1	14	320	5	7.5	25	0.1	39.5	40.1	20.4
3	15	320	25	7.5	25	0.1	40.4	39.6	20
39	16	520	15	17.5	75	0.5	45.3	33	21.7
32	17	720	25	27.5	225	0.9	41.7	25.4	32.9
12	18	720	25	7.5	225	0.1	41.2	24.1	34.7
5	19	320	5	27.5	25	0.1	40.1	39.8	20.1
31	20	320	25	27.5	225	0.9	41	39.4	19.6
44	21	520	15	17.5	125	0.5	45.8	32.5	21.7
21	22	320	5	27.5	25	0.9	40	40.3	19.7
30	23	720	5	27.5	225	0.9	40.1	25.5	34.4
19	24	320	25	7.5	25	0.9	40.2	40.4	19.4
42	25	520	15	17.5	125	0.3	45	31.9	23.1
14	26	720	5	27.5	225	0.1	41.8	25.1	33.1
25	27	320	5	7.5	225	0.9	39.3	40.2	20.5
41	28	520	15	17.5	125	0.5	45.9	32.3	21.8
38	29	520	15	22.5	175	0.7	47.9	31.8	20.3
6	30	720	5	27.5	25	0.1	41.5	25.8	32.7
20	31	720	25	7.5	25	0.9	39.4	26.1	34.5
46	32	520	15	17.5	125	0.5	46.3	32.2	21.5
9	33	320	5	7.5	225	0.1	40.3	39.9	19.8
50	34	520	15	17.5	25	0.5	46	32.4	21.6
8	35	720	25	27.5	25	0.1	41.8	25.4	32.8
11	36	320	25	7.5	225	0.1	40.2	39.1	20.7
33	37	620	15	17.5	125	0.5	43	30	27
4	38	720	25	7.5	25	0.1	40	25.8	34.2
49	39	520	15	17.5	125	0.5	46.1	32.2	21.7
10	40	720	5	7.5	225	0.1	39.7	25.6	34.7
40	41	520	15	17.5	225	0.5	45.7	31.8	22.5
2	42	720	5	7.5	25	0.1	41	26.5	32.5
13	43	320	5	27.5	225	0.1	40.5	36.4	23.1
29	44	320	5	27.5	225	0.9	40.9	39.4	19.7
27	45	320	25	7.5	225	0.9	40.5	39.7	19.8
28	46	720	25	7.5	225	0.9	40	25.7	34.3
26	47	720	20	7.5	225	0.9	41.1	26.3	32.6
24	48	720	25	27.5	25	0.9	42	25.6	32.4
45	49	520	15	17.5	125	0.5	46.2	32.5	21.3
15	50	320	25	27.5	225	0.1	40.9	39	20.1

4.8 Statistical Model Development

The products of pyrolysis were investigated using analysis of variance (ANOVA) by considering the quadratic model in the CCD technique. The quadratic model was selected as it has been adjudged to be fit for the optimization technique (Hossain *et al.*, 2017; Laouge *et al.*, 2020).

4.8.1 Statistical models for bio-oil yield

Equations (4.1 - 4.3) present the mathematical model used to predict the bio-oil yield using PKS, SCB, and SBW respectively, while appendices 1 – 3 summarized the results obtained via ANOVA analysis for the response of bio-oil using PKS, SCB, and SBW.

$$Y_{BO(PKS)} = 44.034 + 1.302A - 0.103D + 0.165E - 12.02A^2 + 6.12C^2 + 0.266A \times E \quad (4.1)$$

$$Y_{BO(SCB)} = 46.099 - 0.417A + 0.387C - 8.89A^2 + 3.19C^2 + 1.032D^2 + 0.216A \times C \quad (4.2)$$

$$Y_{BO(SBW)} = 46.119 - 0.4238A + 0.1498B + 0.3720C - 10.32A^2 - 1.06C^2 + 0.884D^2 + 5.80E^2 + 0.2226A \times C \quad (4.3)$$

Where, $Y_{BO(PKS)}$, $Y_{BO(SUG)}$, $Y_{BO(SHEA)}$ are the responses of the bio-oil yield (wt%) for palm kernel shell, sugarcane bagasse, and shea butter wood respectively, A, B, C, D, E refers to the coded value of T (°C), R (min), H (°C/min), N (cm³/min) and P (mm) respectively. The positive (+) sign in the mathematical model represents a synergic effect and the negative (-) sign indicates antagonistic effects on bio-oil yield.

Fischer test (F-value) and probability value (p-value) were found to be accepted for an analysis of regression models (Arvindekar *et al.*, 2016; Kumar *et al.*, 2019). F-value indicates how the mean square value of a developed regression model is compared to the mean square value of residuals (i.e., error). The higher the F-value, the more responsive, reproductive, and reliable is the regression model. Also, the p-value should be low in order for the model to hold a higher significance (Nizamuddin *et al.*, 2016; Lee *et al.*, 2017).

The ANOVA analysis for bio-oil yield obtained via intermediate pyrolysis show a higher F-value of 31.43, 73.37, 88.01 for palm kernel shell, sugarcane bagasse, and shea butter wood, and a low p-value (less than 0.05) recorded for all the biomass under investigation showed that the developed regression model is significant. PKS is more significant closely followed by SCB, while SBW is the least significant based on the F-value and p-value recorded. There is only a small chance (0.01%) that a model F-value this large might take place due to noise (Hassain *et al.*, 2017, Hassan *et al.*, 2017). In the case of PKS, it can be observed that temperature (A), nitrogen flow rate (D), particle sizes (E), the interaction of temperatures (A^2), the interaction of heating rates (C^2), and interaction of temperature and particle sizes (AE) are significant model terms. Considering SCB, temperature (A), heating rate (C), the interaction of temperatures (A^2), the interaction of heating rates (C^2), interaction of nitrogen flow rate (D^2), and the interaction of temperatures and heating rates (AC) are significant model terms. In the case of SBW, it can be deduced that temperature (A), reaction time (B), heating rate (C), the interaction of temperatures (A^2), the interaction of heating rates (C^2), the interaction of nitrogen flow rate (D^2), the interaction of particle sizes (E^2), and the interaction between temperatures and heating rates (AC) are significant model terms. Hence, The study positively influenced bio-oil yields. The lack of fit of 0.818, 0.056, and 0.082 ($p > 0.05$) for bio-oil yield using PKS, SCB, and SBW means that the developed mathematical model can predict and reproduce the experimental data as opined by Mohammed *et al.* (2017) and Laouge *et al.* (2020).

The coefficient of variation (CV%) is the overall experimental error expressed as a percentage of the overall mean. It is a measure of the reliability of the experimental. Generally, a low CV% ($\approx 10\%$) is considered to be a good indicator of the reproducibility of the models. The R^2 value which is the coefficient of determination for the regression model should be close to 1 which satisfies the criteria for a good model (Hossain *et al.*, 2017; Hassan *et al.*, 2017). In this present study, the CV% for bio-oil yield using PKS, SCB, and SBW are found to be 5.04%, 5.29%, and 5.63% respectively which are relatively low. This indicates good reproducibility and reliability of the experiment and investigated model. Similarly, the R^2 value of bio-oil yields using PKS, SCB, and SBW are 0.9800, 0.9801, and 0.9862 respectively which are very close to 1. Hence, the mathematical model under investigation is good and can replicate the experimental data for bio-oil yield.

The adjusted R^2 specifies the amount of variation which can be described by the model, that is, the R^2 value after adjusting the number of terms in the regression model relative to the number of design points. The predicted R^2 shows the amount of variation in the new data explained by the model. The difference between the adjusted and predicted R^2 should be within approximately 0.20 to be in reasonable agreement (Hossain *et al.*, 2017; Lee *et al.*, 2017; Laouge *et al.*, 2020). Considering bio-oil yield using PKS, the difference between the adjusted R^2 (0.9842) and predicted R^2 (0.8487) is 0.136. Hence, the study is in reasonable agreement, thereby making the experimental data reproducible. For SCB, the predicted R^2 of 0.9651 is in reasonable agreement (difference of 0.16) with an adjusted R^2 of 0.8051. Similarly, for SBW, the difference between the adjusted R^2 (0.9744) and predicted R^2 (0.8263) is 0.148. The study is in reasonable agreement, which make the model responsive, reliable and can replicate the experimental data.

4.8.2 Statistical models for biochar yield

The mathematical model used to predict the biochar yield using PKS, SCB and SBW are presented in Eqns. 4.4, 4.5 and 4.6 respectively.

$$Y_{BC(PKS)} = 50.16 - 0.03474A - 0.0478B - 0.0320C - 0.00489D + 2.30E + 0.00009A^2 - 0.00268A \times E - 0.000007B \times D \quad (4.4)$$

$$Y_{BC(SCB)} = 58.56 - 0.09A - 0.0256B + 0.839C - 0.00317D - 1.565E + 0.000056A^2 - 0.0242C^2 + 0.00394A \times E \quad (4.5)$$

$$Y_{BC(SBW)} = 60.34 - 0.0806A + 0.416B - 0.0584C - 0.004143D + 0.834E + 0.000044A^2 - 0.01568B^2 + 0.00192B \times C \quad (4.6)$$

Where, $Y_{BC(PKS)}$, $Y_{BC(SCB)}$, $Y_{BC(SBW)}$ are the responses of the biochar yield (wt%) for PKS, SCB, and SBW respectively.

Th results show a higher F-value of 340.53, 877.64, 661.08 for PKS SCB and SBW respectively and a low p-value (less than 0.05) was recorded for all the biomass under investigation showing that the developed regression model is significant as opined by Hossain *et al.* (2017) and Lee *et al.* (2017). SBW is more significant closely followed by SCB, while PKS possessed the least significance based on the F-value and p-value recorded. There is only a small chance (0.01%) that a model F-value this large might take place due to noise (Hassain

et al., 2017). The results showed that temperature, reaction time, heating rate, nitrogen flow rate, particle size, the interaction of temperatures, the interaction between temperature and particle size, the interaction between reaction time and particle size are significant model terms for PKS. In the case of SCB, it was observed that temperature, reaction time, heating rate, nitrogen flow rate, particle size, the interaction of temperatures, and interaction of heating rates are significant model terms. Also, considering SBW, it was deduced that temperature, reaction time, heating rate, nitrogen flow rate, particle size, the interaction of temperatures, the interaction of reaction time, the interaction between reaction time and heating rate, the interaction between reaction time and nitrogen flow rate are significant model terms. Hence, the study positively influenced biochar yields. The lack of Fit of 0.051, 0.071 and 0.39 ($p > 0.05$) for biochar yield using PKS, SCB and SBW means that the developed mathematical model can predict and reproduce the experimental data.

In the study, the CV% for biochar yield using PKS, SCB, SBW is found to be 5.46%, 6.38%, and 5.37% respectively which are relatively low compared to what Kumar *et al.* (2019) reported. Hence, the investigated model can be reproduced. Likewise, the R^2 value of biochar yields using PKS, SCB, SBW is 0.9887, 0.9956, and 0.9901 respectively which are also very close to 1. Thus, the mathematical model under investigation is good and can replicate the experimental data for biochar yield. Considering biochar yield using PKS, the difference between the adjusted R^2 (0.9781) and the predicted R^2 (0.8518) is 0.13. Hence, the study are in reasonable agreement. Thereby making the predicted model responsive and reliable. For SCB, the predicted R^2 of 0.9899 is in reasonable agreement (difference of 0.10) with an adjusted R^2 of 0.8899. Similarly, for SBW, the difference between the adjusted R^2 (0.9868) and predicted R^2 (0.8656) is 0.12. Hence, The study are in reasonable agreement. Thereby making the experimental value data reproducible.

4.8.3 Statistical models for NCG yield

The results of the ANOVA analysis for NCG obtained from the intermediate pyrolysis of PKS, SCB, and SBW showed a higher F-value of 487.74, 418.66, 303.95 for PKS, SCB, and SBW respectively and a low p-value (less than 0.05) was recorded for all the biomass under investigation showed that the developed regression model is significant as postulated by Lee *et al.* (2017). PKS is more significant closely followed by SCB, while SBW is the least significant

based on the F-value and p-value recorded. There is only a small chance (0.01%) that a model F-value this large might take place due to noise (Hassain *et al.*, 2017). Considering PKS, it was observed that temperature, reaction time, heating rate, nitrogen flow rate, the interaction of temperatures, combined effects of temperature and heating rate, the interaction between temperature and nitrogen flow rate, and interaction between temperature and particle size are significant model terms. In the case of SCB, temperature, nitrogen flow rate, particle size, the interaction of temperatures, the interaction between temperature and reaction time are significant model terms. Likewise, for SBW, temperature, nitrogen flow rate, the interaction of reaction time, the interaction between temperature and heating rate, and interaction between temperature and particle size are significant model terms. Thus, the study positively influenced NCG yields.

Equations 4.7 - 4.9 depict the mathematical model used to predict the NCG yield using PKS, SCB, and SBW respectively

$$Y_{NCG(PKS)} = 22.782 + 3.88A + 0.243B + 0.335C + 0.455D + 5.493A^2 - 0.204A \times C - 0.258A \times D + 0.104A \times E \quad (4.7)$$

$$Y_{NCG(SCB)} = 20.02 + 6.429A + 0.215D - 0.301E + 5.133A^2 + 0.328A \times B \quad (4.8)$$

$$Y_{NCG(SBW)} = 21.795 + 6.844A + 0.333D + 5.057B^2 - 0.390A + 0.081D \times E \quad (4.9)$$

Where $Y_{NCG(PKS)}$, $Y_{NCG(SCB)}$, $Y_{NCG(SBW)}$ is the response of the biochar yield (wt%) for PKS, SCB, and SBW respectively.

Lack of Fit of 1.35, 0.06 and 0.09 ($p > 0.05$) for NCG yield using PKS, SCB and SBW means that the developed mathematical model can predict and reproduce the experimental data. The CV% for using NCG yield, PKS, SCB, SBW is found at 6.13%, 5.36%, and 5.42% respectively which are relatively low. Hence, the investigated model can be reproduced. Also, the R^2 value of NCG yields for PKS, SCB, SBW are 0.9921, 0.9905, and 0.9856 respectively, which are very close to 1. Therefore, the mathematical model under investigation is good and can replicate the experimental data for NCG yield. In the case of NCG yield using PKS, the difference between the adjusted R^2 (0.9880) and the predicted R^2 (0.8780) is 0.11. Hence, The study are in

reasonable agreement. For SCB, the predicted R^2 of 0.8660 is in reasonable agreement (difference of 0.12) with the adjusted R^2 of 0.9860. Similarly, for SBW, the difference between the adjusted R^2 (0.9723) and predicted R^2 (0.8323) is 0.14. Hence, they are in reasonable agreement and the predicted model can reproduce the experimental data accurately (Lee *et al.*, 2017).

4.9 Influence of Individual Parameters on the Products of Pyrolysis

4.9.1 Influence of temperature on the products of pyrolysis

The influence of variation in temperatures through the range 320°C, 420°C, 520°C, 620°C, 720°C on bio-oil, biochar, and NCG yields a constant reaction time, heating rate, nitrogen flow rate and particle size from PKS, SCB, and SBW respectively are shown in Figure 4.3. Temperature appears to be the most important parameter that influences products of pyrolysis as it provides the amount of heat needed to degrade the biomass bonds in the reactor from pyrolysis products (Guedes *et al.*, 2018).

At the initial stage (Figure 4.3a), the bio-oil yields (40.7 wt%) and NCG (23.2 wt%) from SBW, SCB, and PKS are low due to incomplete pyrolysis process (Varma and Mondal, 2017), thereby leading to a high yield of biochar of 41.0 wt%. Further increase in pyrolysis temperature from 420 to 520°C increased the bio-oil yield until it attained an optimum value of 47.7 wt% at 520°C. An increase in temperature above 520°C (between 520-720°C) reduced the yield of bio-oil from 47.7 to 41.1 wt%. This is attributed to secondary cracking of the bio-oil leading to a high yield of NCG from 22.5 to 34.7 wt% as well as secondary decomposition of the biochar to produce NCG. Hence, decrease in bio-oil yield. This study followed the same trend as the report of Tsai *et al.* (2006); Lazzari *et al.* (2016); Varma and Mondal (2017); Guedes *et al.* (2018); and Chukwuneke *et al.* (2019) who reported maximum value of bio-oil yield at a temperature of 450 – 525 °C. Hence, the experimental results are relatively accurate and reliable.

The SBW possessed the optimum bio-oil yield of 47.9 wt%, closely followed by SCB (47.1 wt%), while PKS (44.4 wt%) had the least value of bio-oil yield as shown in Figure 4.7b. Similarly, for biochar yield (Figure 4.3c), the optimum value of 39.2, 40.9 and 40.5 wt% were recorded for PKS, SBW, and SCB respectively. In the case of NCG (Figure 4.3d), it was observed that PKS (37.9 wt%), closely followed by SBW (34.7 wt%), and SCB (32.6 wt%)

recorded the peak, medium, and least values. SCB is more suitable for bio-oil production, closely followed by SBW at varied temperatures (320-720°C) due to the quantity of bio-oil yield when compared with other biomass samples at constant reaction time, heating rate, nitrogen flow rate, and particle size are kept constant. In the case of biochar yield, SCB is more preferable for biochar yield, closely followed by SBW under the same operating parameters. Similarly, PKS is more preferable for NCG yields next to SBW. The suitability of biomass for bio-oil, biochar and NCG is attributed to the high quantity of pyrolysis' yields relative to the biomass when subjected to the same operating conditions.

The optimum values obtained at varied operating parameters correlated with the findings of Guatam and Chaurasia (2020), Varma and Mondal (2017), and Kumar *et al* (2019) who reported the maximum value of bio-oil yield as 46.93, 45.23, and 46.00 wt% respectively

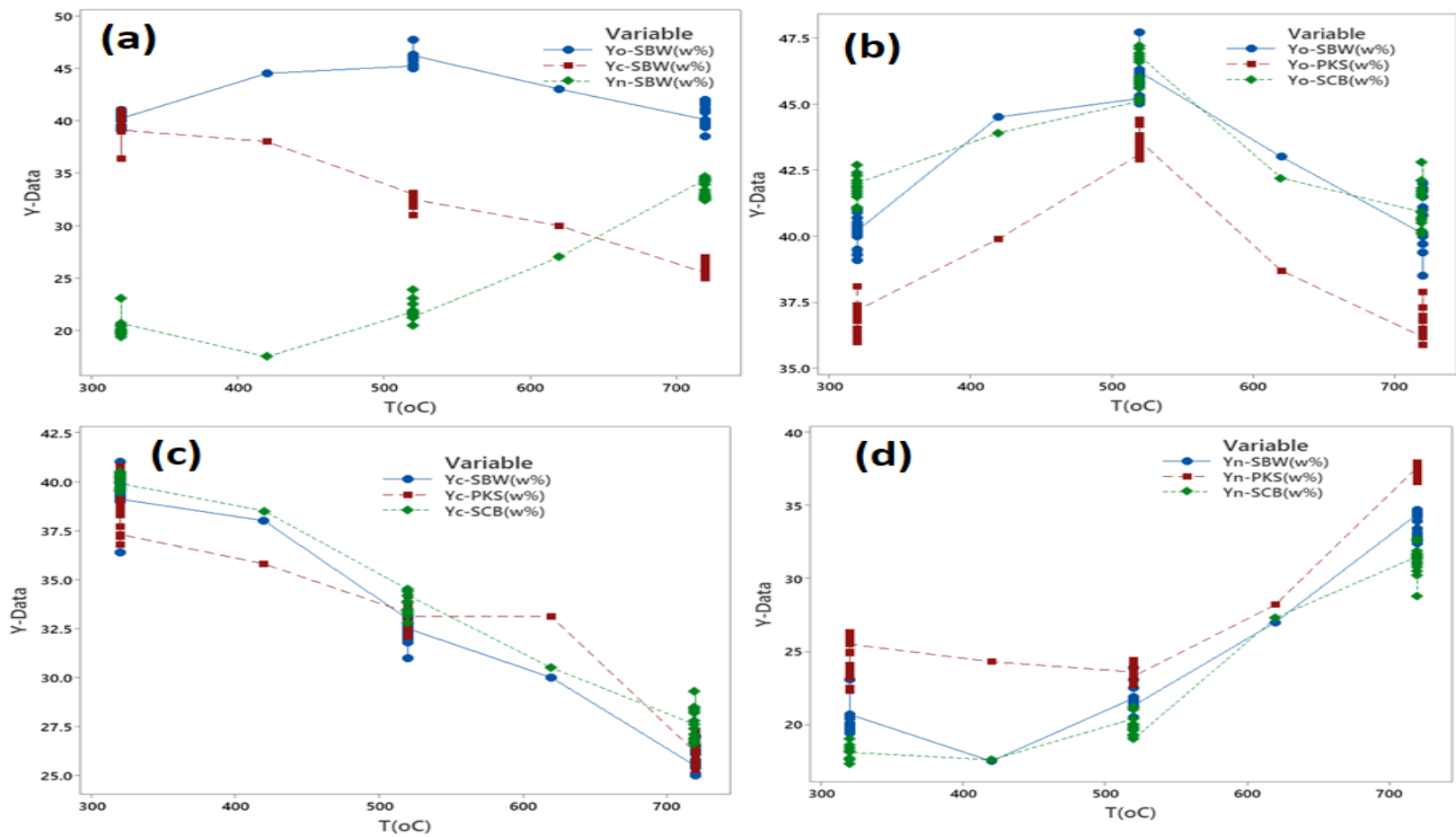


Figure 4.3: Influence of temperature on (a) products of pyrolysis from SBW (b) Bio-oil yield from PKS, SCB, SBW (c) Biochar yield from PKS, SCB, SBW (d) NCG yield from PKS, SCB, SBW

4.9.2 Influence of particle size on the products of pyrolysis

Figure (4.4) depicts the influence of the variation of particle sizes on products of pyrolysis at a constant temperature, heating rate, reaction time and nitrogen flow rate. An increase in the particle size from 0.4 to 0.6 mm showed no major influence on the bio-oil yield as the variation for bio-oil yields was approximately 3 wt% which is 42.3 to 45.4 wt%. An increase in particle size, increased the temperature gradient inside the biomass particle, thereby increasing the distance between the biomass particle surfaces to its center. This resulted in an incomplete pyrolysis process due to the low heat transfer between the hot and cold material as well as a decrease in volatile matter formation (Guedes *et al.*, 2018; Varma and Mondal, 2017). Hence, this led to high biochar from 32.5 to 40.5 wt% (Figure 4.4c) and lower yields of bio-oil from 45.4 to 39.3 wt%. At a low particle size of less than 0.4-0.6 mm, uniform heat transfer was achieved which increased bio-oil yield (Figure 4.4b). Hence, a low particle size of less than 0.5 mm will be suitable for bio-oil yield as it ensures faster and uniform heat transfer as well as high volatile matter production. These findings are in consonant with the reports of Stefanidis *et al.* (2014); Bartoli *et al.* (2016); Madhu *et al.* (2018) and Varma and Mondal (2017) who postulated that low particle size results in high bio-oil and low biochar yields.

The optimum, medium and least values of bio-oil yields were 46.5, 45.6, and 43.2 wt% (Figure 4.4b) as recorded for SCB, SBW, and PKS respectively. In the case of biochar yields (Figure 4.4c), SBW possessed the peak value (40.9 wt%), next to PKS (39.3 wt%) while SCB (37.6 wt%) had the lowest value. Furthermore, the PKS (25.6 wt%) recorded the peak value NCG yield (Figure 4.8c), while SBW (22.4 wt%) and SCB (20.1 wt%) recorded the medium and lowest values respectively. Hence SCB, SBW, and PKS are more suitable for bio-oil, biochar and NCG yields at varied particle sizes (0-1 mm) with constant temperature, reaction time, heating rate and nitrogen flow rate

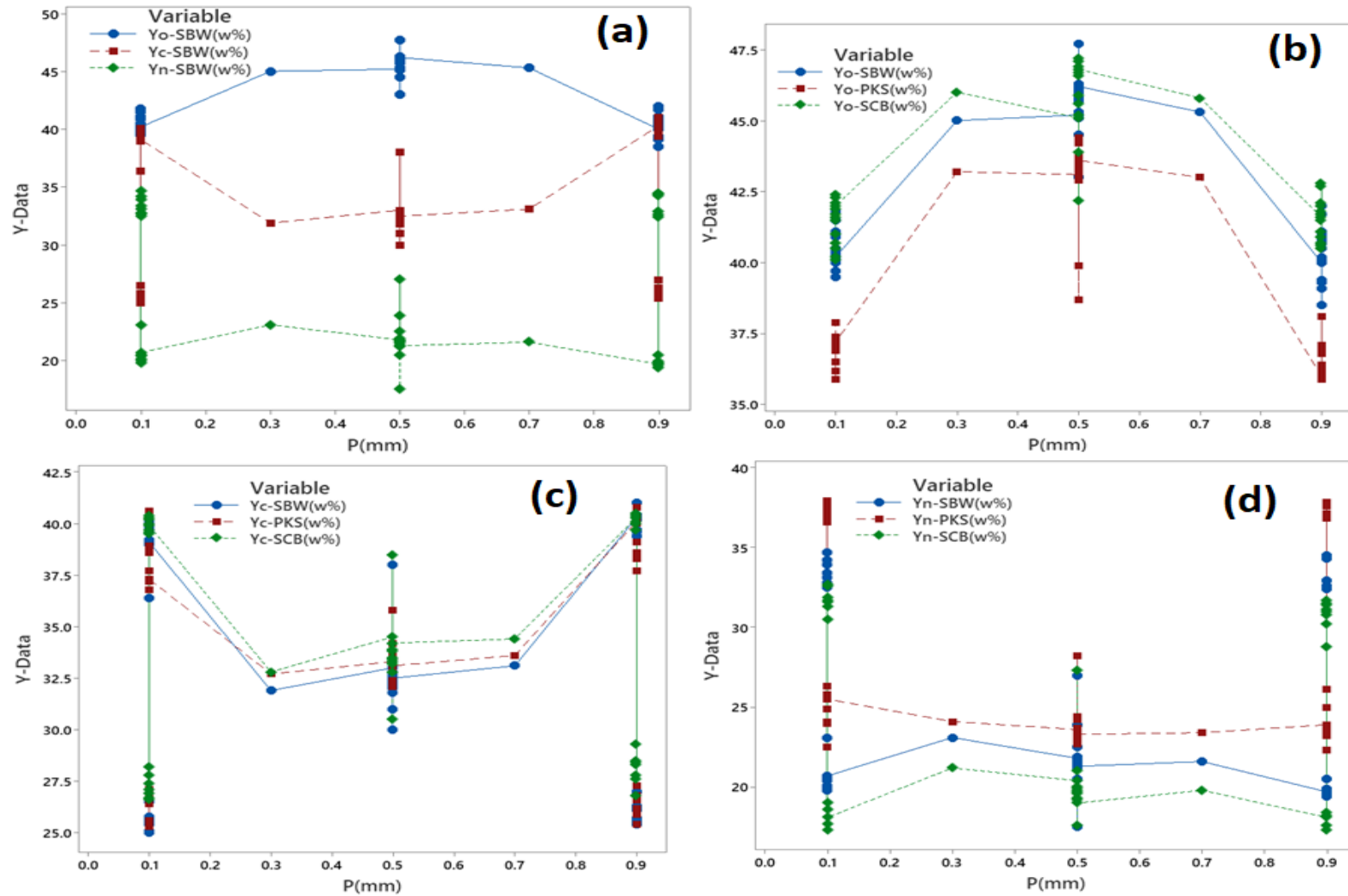


Figure 4.4: Influence of particle size on (a) products of pyrolysis from SBW (b) Bio-oil yield from PKS, SCB, SBW (c) Biochar yield from PKS, SCB, SBW (d) NCG yield from PKS, SCB, SBW

4.9.3 Influence of heating rate on the products of pyrolysis

The heating rate is paramount in an intermediate pyrolysis process as it enhances the thermal decomposition of the biomass in the reactor, leading to an increase in bio-oil yields. The utilization of suitable biomass particle size for the pyrolysis process helps to reduce the bottleneck of poor heat transfer because biomass is a poor conductor of heat (Guedes *et al.*, 2018). Figure (4.5) depicts the influence of variation in heating rate on the yield of pyrolysis' products at a constant temperature, reaction time, nitrogen flow rate and particle size. An increase in the heating rate increased bio-oil yield from 38.4 to 47.1 wt% (Figure 4.5a) due to rapid devolatilization of the biomass in the reactor resulting in complete pyrolysis process (Guedes *et al.*, 2018). The NCG yield (Figure 4.9a) decreased initially from 35.3 to 22.5 wt% at a heating rate of 5 to 17.5°C/min and then increased continuously from 22.4 to 34.0 wt% as the heating rate increased. The biochar yield increased due to low heating rate at the beginning of pyrolysis process from 25.3 to 33.4 wt% leading to incomplete pyrolysis process and then decreased continuously from 33.4 to 25.6 wt% as the heating rate increased leading to an increase in bio-oil yields at a high heating rate. These findings agreed with the reports of Guedes *et al.* (2018), who reported maximum bio-oil yield with an increase in heating rate.

The optimum bio-oil yield of 47.4 wt% was obtained from SBW, closely followed by 47.1wt% recorded for SCB while PKS had the least bio-oil yield of 43.8 wt% at a varying heating rate of 5 to 17.5°C/min while other operating parameters were kept constant (Figure 4.9b). Considering biochar, the peak, medium, and minimum values were recorded for SCB, (33.4 wt%), PKS (32.5 wt%), and SBW (31.8 wt%) respectively, while PKS, SBW, and SCB have peak, medium, and least values of 37.4, 34.7 and 33.1 wt% respectively. Hence, SBW is preferable for bio-oil yield, while SCB and PKS are more suitable for biochar and NCG yields respectively at a varied heating rate (7.5-27.5°C/min) with constant temperature, reaction time, nitrogen flow rate, and particle size.

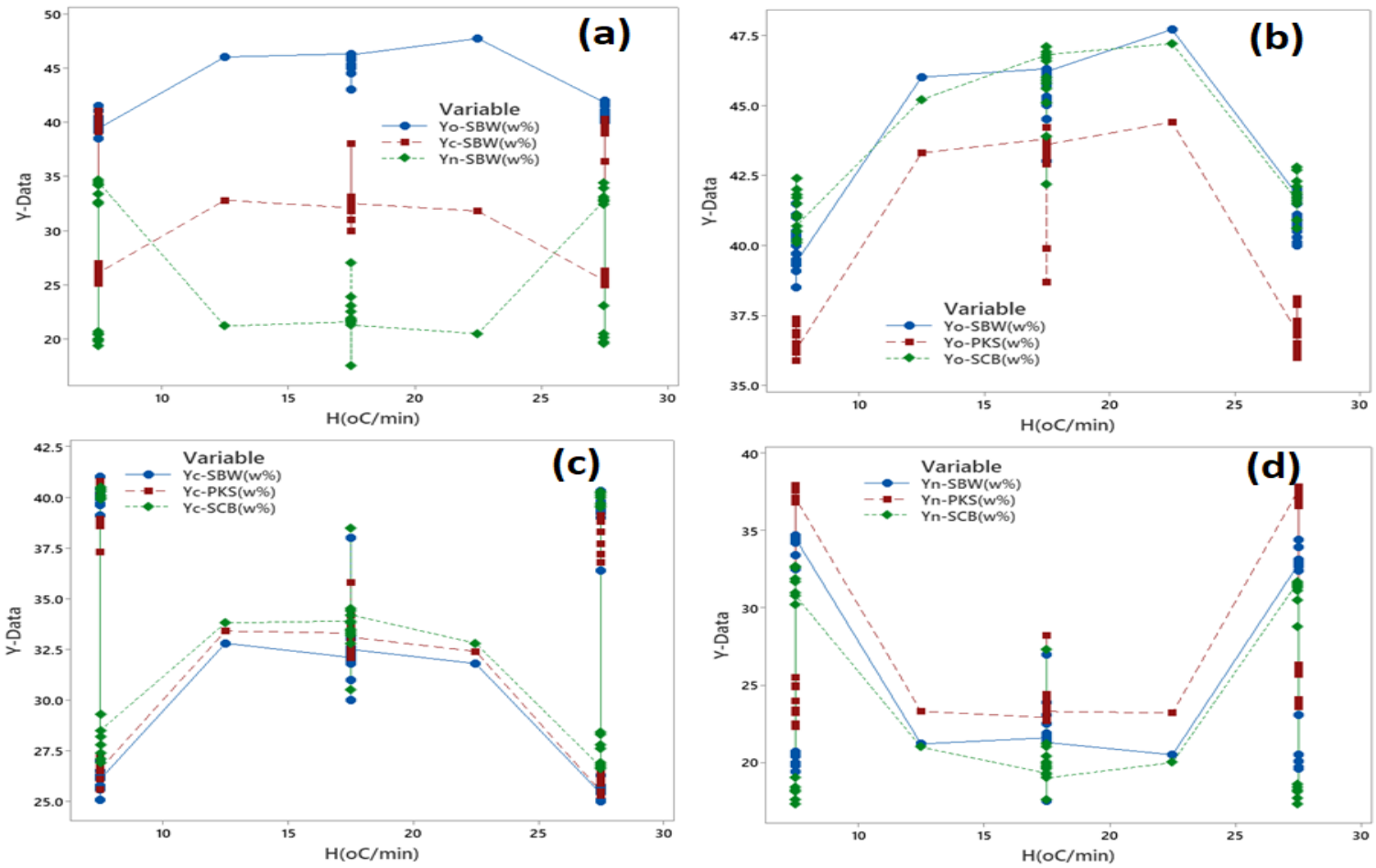


Figure 4.5: Influence of heating rate on (a) products of pyrolysis from SBW (b) Bio-oil yield from PKS, SCB, SBW (c) Biochar yield from PKS, SCB, SBW (d) NCG yield from PKS, SCB, SBW

4.9.4 Influence of Reaction Rate on the Products of Pyrolysis

Reaction time is the amount of time that the biomass sample is sustained in the reactor at a particular temperature. The influence of varying the reaction time on the yield of bio-oil, biochar, and NCG at a constant temperature of 520 °C, a heating rate of 17.5°C/min, nitrogen flow rate of 125 cm³/min, and particle size of 0.4-0.6 mm are shown in Figure 4.6. An increase in the reaction time from 5 to 15 min increased the bio-oil yield from 40.3 to 46.1 wt% (Figure 4.6a). However, a further increase in reaction time above 15 min resulted in a decrease in bio-oil yield from 46.1 to 40.9 wt%. The NCG increased (20 to 24 wt%) as the reaction time increased from 5 to 20 mins due to secondary reaction of the vapours which reduced the yield of bio-oil and then decreased slightly with further increase in reaction time. The biochar yield decreased from 32.1 to 20.5 wt% as the reaction time increased from 5 to 20 mins and then increased slightly as the reaction time increased further due to carbonization and re-polymerization. A constant value of bio-oil (45.2 wt%) and biochar (31.4 wt%) yields were recorded at a reaction time of 10 to 20 min indicating that the pyrolysis process was complete even at 10 min reaction time. These trends agreed well with the report of Bartoli *et al.* (2016); Hassan *et al.* (2017) and Oyebanji *et al.* (2021).

The lowest, medium and maximum values of bio-oil yield are 43.1, 45.8, and 46.7 wt% recorded for PKS, SBW, and SCB respectively. In the case of biochar yield, SBW, recorded the maximum value (40.0 wt%), closely followed by SBW (39.6 wt%), while PKS (38.2 wt%) has the least value. Furthermore, the PKS (25.0 wt%) recorded the maximum value for NCG yield, while SBW (23.6 wt%) and SCB (19.4 wt%) recorded the medium and least value of NCG yield at a reaction time of 5 to 25 min.

Hence SCB, SBW, and PKS are more suitable for bio-oil, biochar, and NCG yields respectively at varied reaction time (5-25 min), while other parameters are kept constant.

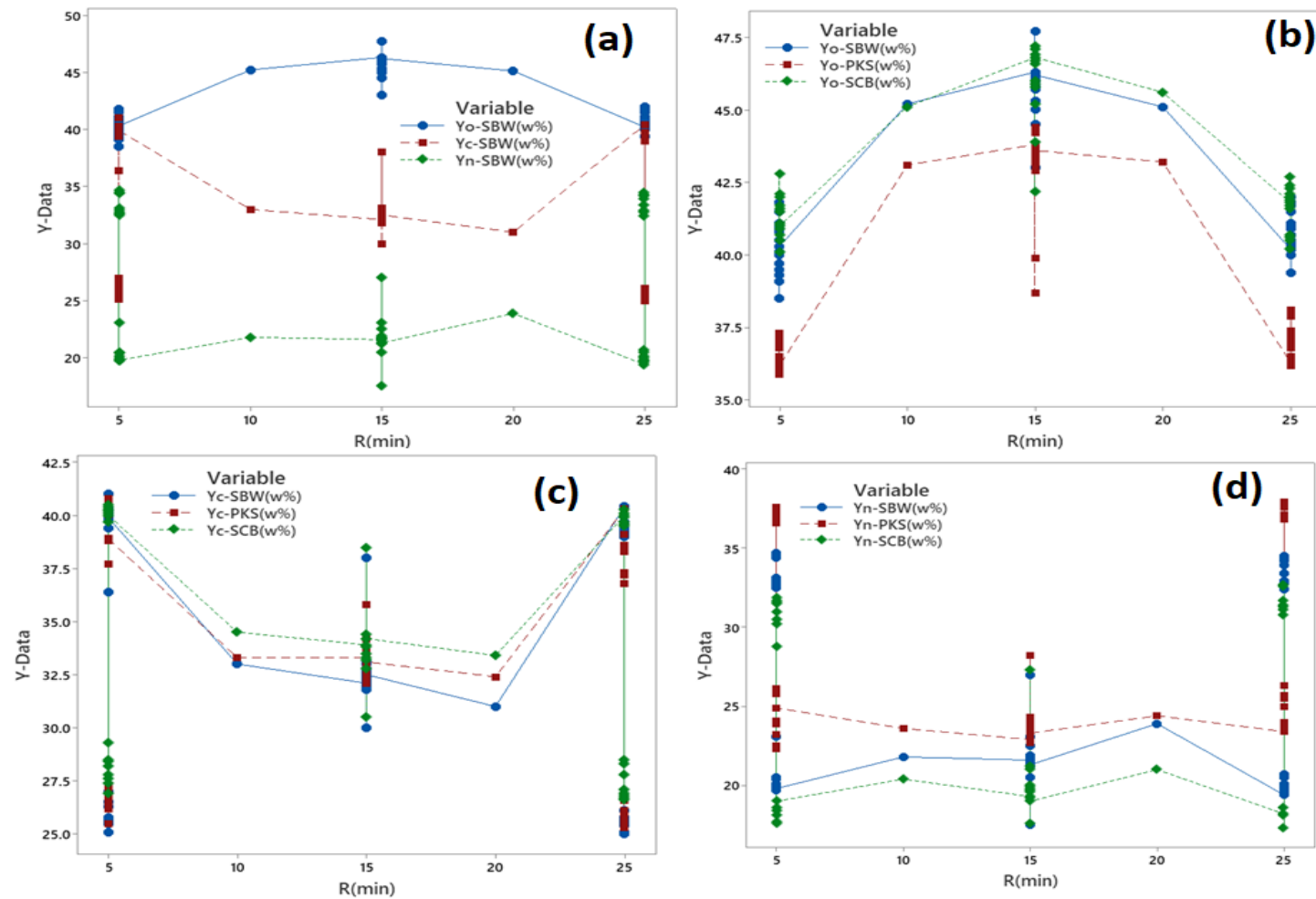


Figure 4.6: Influence of reaction time on (a) products of pyrolysis from SBW (b) Bio-oil yield from PKS, SCB, SBW (c) Biochar yield from PKS, SCB, SBW (d) NCG yield from PKS, SCB, SBW

4.9.5 Influence of nitrogen flow rate on the products of pyrolysis

Nitrogen gas is a crucial parameter in the pyrolysis process because it helps to purge the vapours produced during the pyrolysis (Tripathi *et al.*, 2020). The influence of the variation of nitrogen flow rate on bio-oil, biochar, and NCG yields at a constant temperature of 520°C, a heating rate of 17.5 °C/min, a reaction time of 15min, and particle size of 0.4-0.6 mm are shown in Figure (4.7).

An increase in nitrogen flow rate from 25 to 125 cm³/min shortened the vapour residence time which reduced secondary reactions such as thermal cracking, re-polymerization, and re-condensation of vapour, enhancing heat transfer and causing the volatile vapour removal from the hot pyrolysis zone to become volatile (Guedes *et al.*, 2018; Varma and Mondal, 2017). Hence, increased bio-oil yield from 42.9 to 46.1 wt%, while the NCG decreased continuously (Figure 4.7a). Further increase in nitrogen flow rate above 125 cm³/min resulted in bio-oil yield decrease from 46.1 to 43.8 wt% as biochar yield increased (Figure 4.7a). This may be attributed to incomplete condensation which caused more volatile components emitting from the reactor as part of NCG due to the short residence time in the condenser (Mohammed *et al.*, 2017; Morali and Sensoz, 2015).

SCB recorded the optimum bio-oil yield (46.2 wt%) closely followed by SBW (45.0 wt%), while PKS had the lowest bio-oil yield (43.3 wt%) as shown in Figure 4.11b. In the case of biochar yield, the lowest, medium, and maximum values of biochar yields were 39.9, 39.7, and 39.2 wt% recorded for SBW, SCB, and PKS respectively. SBW, recorded the maximum value (40.0 wt%), closely followed by SBW (39.6 wt%), while PKS (38.2 wt%) has the least value as shown in Figure 4. 11c. Furthermore, the PKS (37.5 wt%) recorded the maximum value for NCG yield, while SBW (32.7 wt%) and SCB (31.4 wt%) recorded the medium and least values of NCG yields (Figure 4.7d). Hence SCB, SBW, and PKS are more suitable for bio-oil, biochar, and NCG yields respectively at a varied nitrogen flow rate (25-225 cm³/min), while other parameters are kept constant.

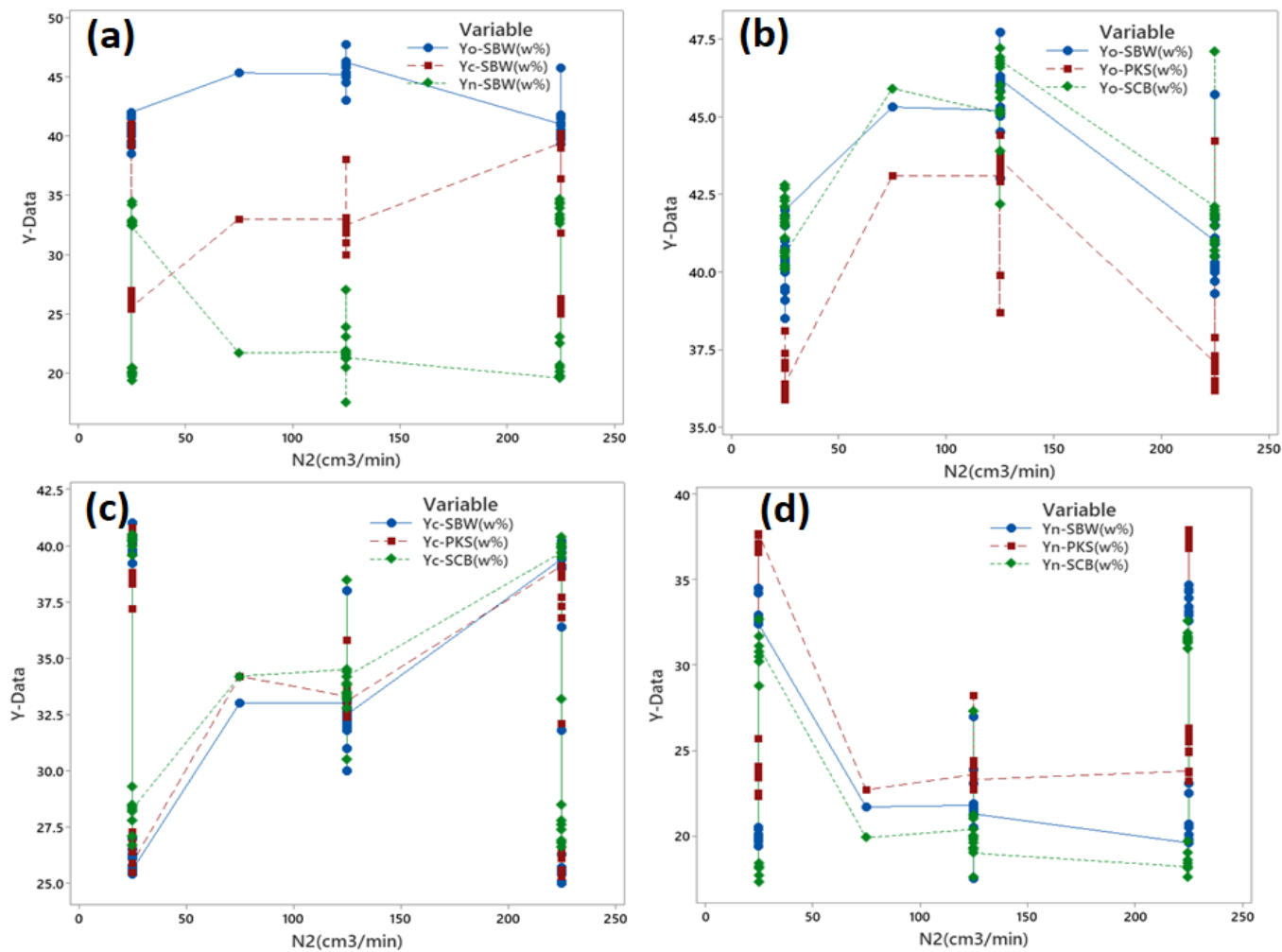


Figure 4.7: Influence of nitrogen flow rate on (a) products of pyrolysis from SBW (b) Bio-oil yield from PKS, SCB, SBW (c) Biochar yield from PKS, SCB, SBW (d) NCG yield from PKS, SCB, SBW

4.10 Influence of Two Most Significant Parameters on the Products of Pyrolysis

Figures (4.8a-4.8d) present a three-dimensional (3D) response surface graph of the combined effects of the two most important parameters that are significant for the optimum yield of bio-oil when other parameters are kept constant. Figure 4.8a shows the interaction between the temperature and heating rate on bio-oil conversion when R (15min), N (125 cm³/min), and P (0.5 mm) are kept constant. The bio-oil yield increased continuously with an increase in T (320-520°C) and H (7.5-12.5°C/min) due to complete pyrolysis during the thermochemical conversion process (Singh *et al.*, 2020; Kumar *et al.*, 2019). A decrease in bio-oil yield was noticed at a T (520-720°C) and H (22.5-27.5°C/min) due to secondary cracking that might enhance the yield of NCG and biochar (Guatam and Chaurasia, 2020; Varma and Mondal, 2017). The maximum bio-oil yield was of 46.6 wt% was obtained at constants R (15 min), N (125 cm³/min), and P (0.5 mm). Similar trend was obtained using sugarcane bagasse biomass sample. These findings are supported by Laouge *et al.* (2020), and Kumar *et al.* (2019) who obtained an optimum bio-oil yield of 47.6 and 46.1 wt% respectively. Figure 4.8b depicts the combined effects of nitrogen flow rate and reaction time on bio-oil conversion in 3D response surface by keeping T (520°C), H (17.5°C/min), and P (0.5 mm) constant. It can be deduced that an increase in N (25 to 175 cm³/min) and R (5-15 min) caused the bio-oil yield to increase from 43.4 to 44.4 wt% due to non-proliferation of secondary reactions such as thermal cracking, re-polymerization, and re-condensation of vapour that enhanced heat transfer and rapid devolatilization of the biomass in the reactor (Dhanavath *et al.*, 2019). The yield for bio-oil decreased from 44.5 to 33 wt% at a N (175-225 cm³/min) and R (15-25 min) due to incomplete condensation leading to the emission of some uncondensed volatile components from the reactor with nitrogen stream (Morali and Sensoz, 2015; Varma and Mondal, 2017; Mohammed *et al.*, 2017). The optimum bio-oil yield of 44.5 wt% was obtained at constant T (520°C), H (17.5°C/min), and P (0.5 mm). These findings and trends correlate very well with the report of Laouge *et al.* (2020), Kumar *et al.* (2019), and Varma and Mondal (2017) who obtained an optimum bio-oil yield of 48.27, 46.0, and 42 wt% respectively from various lignocellulose biomass via pyrolysis process at a T (400-550°C), R (60 min), and N (200 ml/min). The bio-oil increased with an increase in T (320 – 520°C) and nitrogen flow rate (25 to 125 cm³/min) due

to complete pyrolysis process (Figure 4.8c). Further increase in temperature and nitrogen flow rate decreased the bio-oil yield due to an increase in secondary reactions such as thermal cracking, re-polymerization, and re-condensation of vapour (Laouge *et al.*, 2020). Figure 4.8d depicts the 3D response surface showing the two most important parameters (interaction of temperature and particle size) at constant N (min), H (°C/min) and N (cm³/min). At a temperature of 520°C, where the optimum bio-oil yield was recorded, it was found that the yield decreased with the increase in particle size due to incomplete pyrolysis process caused by low rate of heat transfer (Laouge *et al.* 2020; Varma and Mondal, 2017).

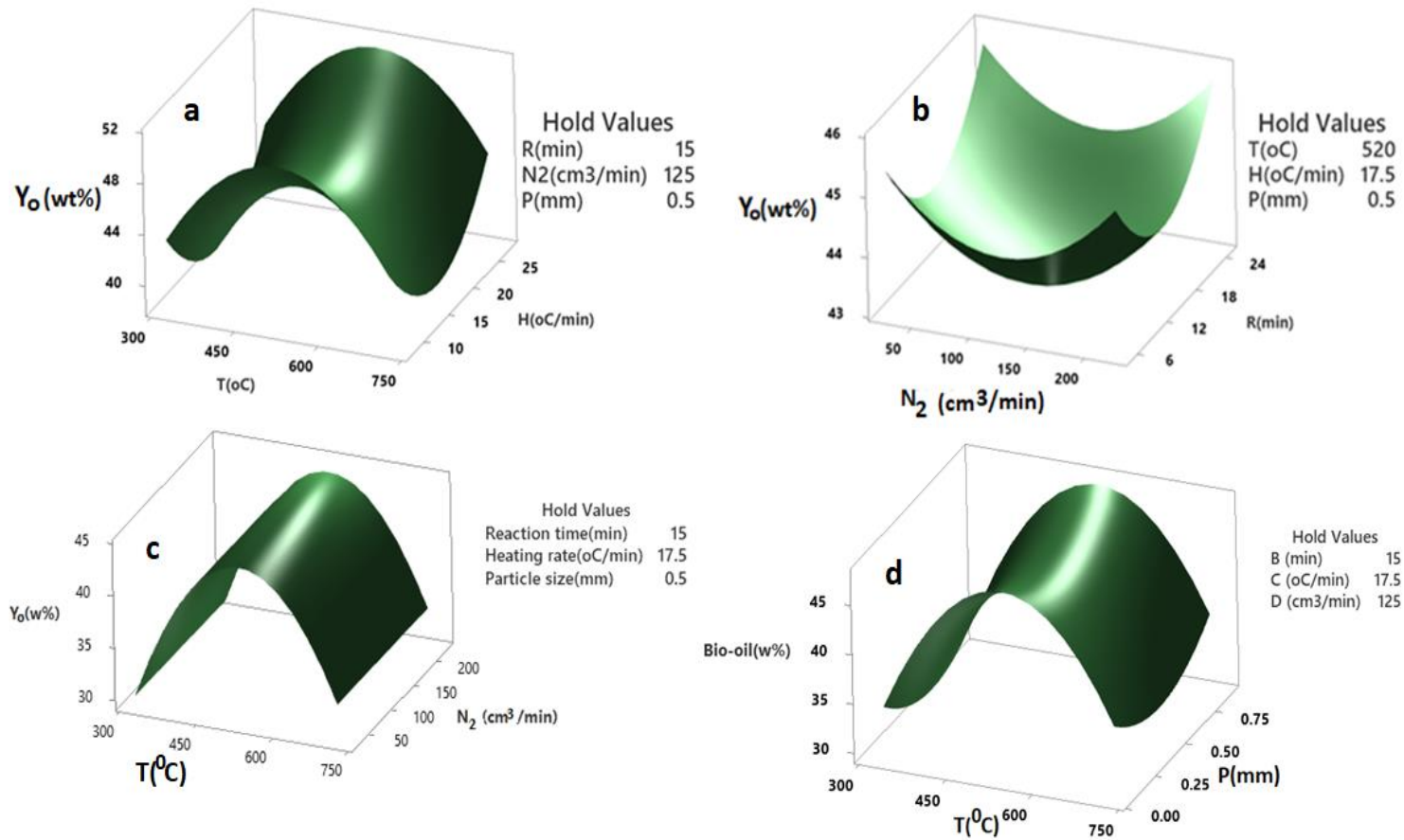


Figure 4.8: Surface Plot of Bio-oil (wt%) against (a) Temperature (°C), Heating rate (°C/min) for SBW (b) Nitrogen flow rate (cm³/min), Reaction time (min) for SBW (c) Temperature (°C), Nitrogen flow rate (cm³/min) for SBW (d) Temperature (°C), Particle sizes (mm) for PKS

The combined effects of the two most important operating parameters that are significant to biochar conversion based on the results obtained via ANOVA are shown in Figure 4.9. At the initial stage, optimum biochar yield (32.1 wt%) was obtained (Figure 4.9a) with constant T (520°C), H (17.5°C/min), and P (0.5 mm). This increase was due to an incomplete pyrolysis process. The biochar conversion declined from 32.2 to 29 wt% with a continuous increase in the R (5 to 25 min) and N (25 to 225 cm³/min) due to the existence of secondary cracking reactions of the biomass samples leading to degradation of the biochar residues or large primary decomposition of the biomass samples (Varma and Mondal, 2017). The combined effect of temperature and particle size on biochar yield are presented in Figure (4.13b). An increase in particle size coupled with a decrease in temperature favoured biochar yield due to the incomplete pyrolysis process, lower thermal cracking, and low heat transfer caused by a wider temperature gradient in the biomass (Chukwuneke *et al.*, 2019). An optimum biochar conversion (41.3 wt%) was recorded when the R (15 min), heating rate (17.5°C/min), and N (125 cm³/min) are kept constant. This study is in consonant with the finding of Gautam and Chaurasia (2020); Chukwuneke *et al.*, (2019), and Hassain *et al.* (2017) who reported optimum biochar yield of 46.93, 38, and 48.26 wt% respectively for lignocellulose biomass samples at a T (350-450°C), N (200 cm³/min) and R (7 min).

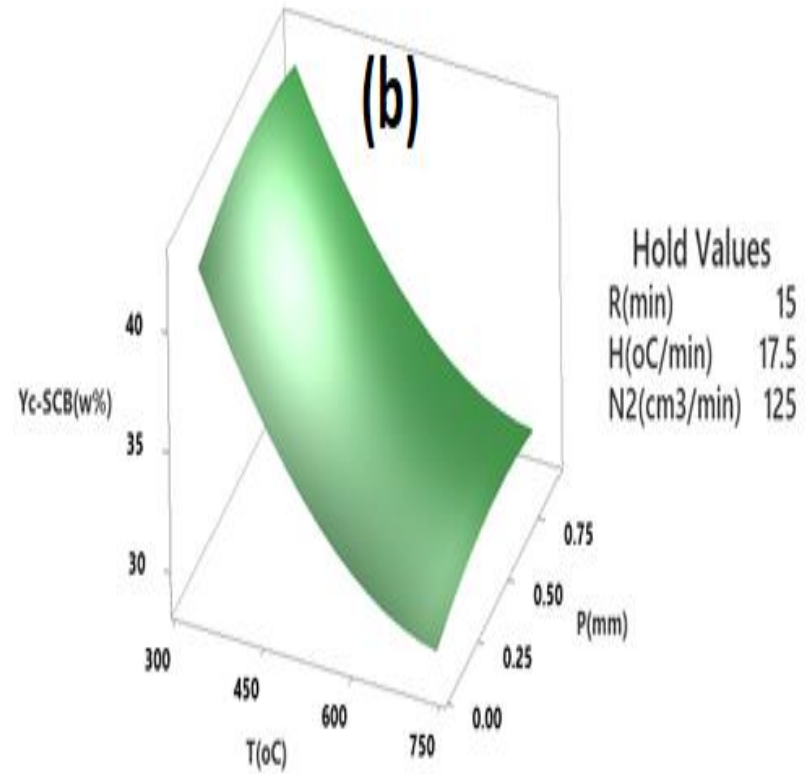
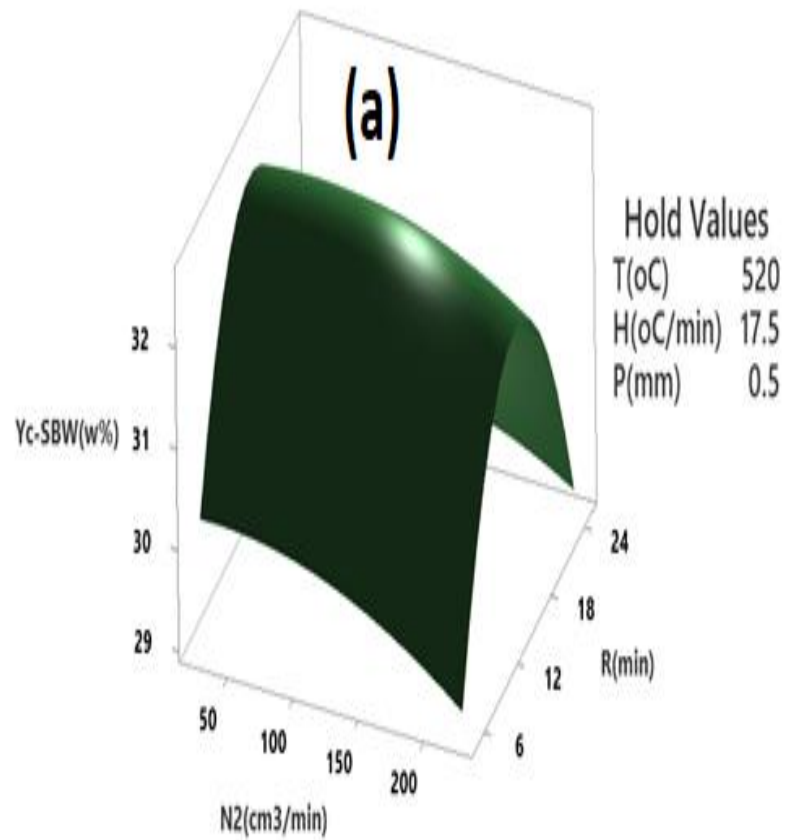


Figure 4.9: Surface Plot of Biochar (wt%) against (a) Reaction time (min), Nitrogen flowrate (cm³/min) using Shea butter wood (b) Temperature (°C), Particle size (mm) using Sugarcane Bagasse

The response surface of the combined effects of operating parameters based on their significant to NCG conversion are shown in Figure 4.10. It can be observed that the NCG yield increased as the N_2 increased from 25 – 75 cm^3/min with a decrease in P from 45.5 to 43.6 wt%. The increase in the NCG may be attributed to thermal cracking, repolymerization, and recondensation of vapour, enhance heat transfer leading to volatile vapour removal from hot pyrolysis zone (Gautam and Chaurasia., 2020; Varma and Mondal, 2017). An optimum NCG conversion (34.8 wt%) was obtained at a constant T (520°C), R (15 min), H (17.5°C/min). Figure 4.10b depicts the two most important two parameters (T and H) on the NCG conversion at a constant R (15 min), P (0.5 mm), and N (125 cm^3/min) are kept constant. The NCG yield increased continuously with the simultaneous increase in temperature and heating rate. The increase in the NCG conversion was due to secondary cracking as well as secondary decomposition of the biochar at a high temperature and heating rate (Guatam and Chaurasia, 2020; Varma and Mondal (2017). An optimum NCG yield (33.8 wt%) was attained at a constant R (15 min), P (0.5 mm), and N (125 cm^3/min). Similarly, the NCG conversion increased continuously with a simultaneous increase in temperature and N (Figure 4.10c) due to incomplete condensation at a high temperature and nitrogen flow rate causing some amount of volatile components to be emitted from the reactor with nitrogen stream (Morali and Sensoz, 2015). An optimum NCG conversion (33.1 wt%) was obtained at a constant R (15 min), P (0.5mm), and H (17.5°C/min). At a temperature of 620°C, where the optimum NCG yield (35.7 wt%) was attained, it was deduced that the NCG yield decreased with an increase in P (0.9 mm) due to incomplete condensation, incomplete pyrolysis process, and repolymerization leading to a high yield of biochar at a low nitrogen and heating rate as shown in Figure 4.10d. This trend closely agreed with the report of Gautam and Chaurasia (2020) and Varma and Mondal (2017) was recorded optimum NCG conversion of 27.6 and 39 wt% respectively at a temperature of 650°C

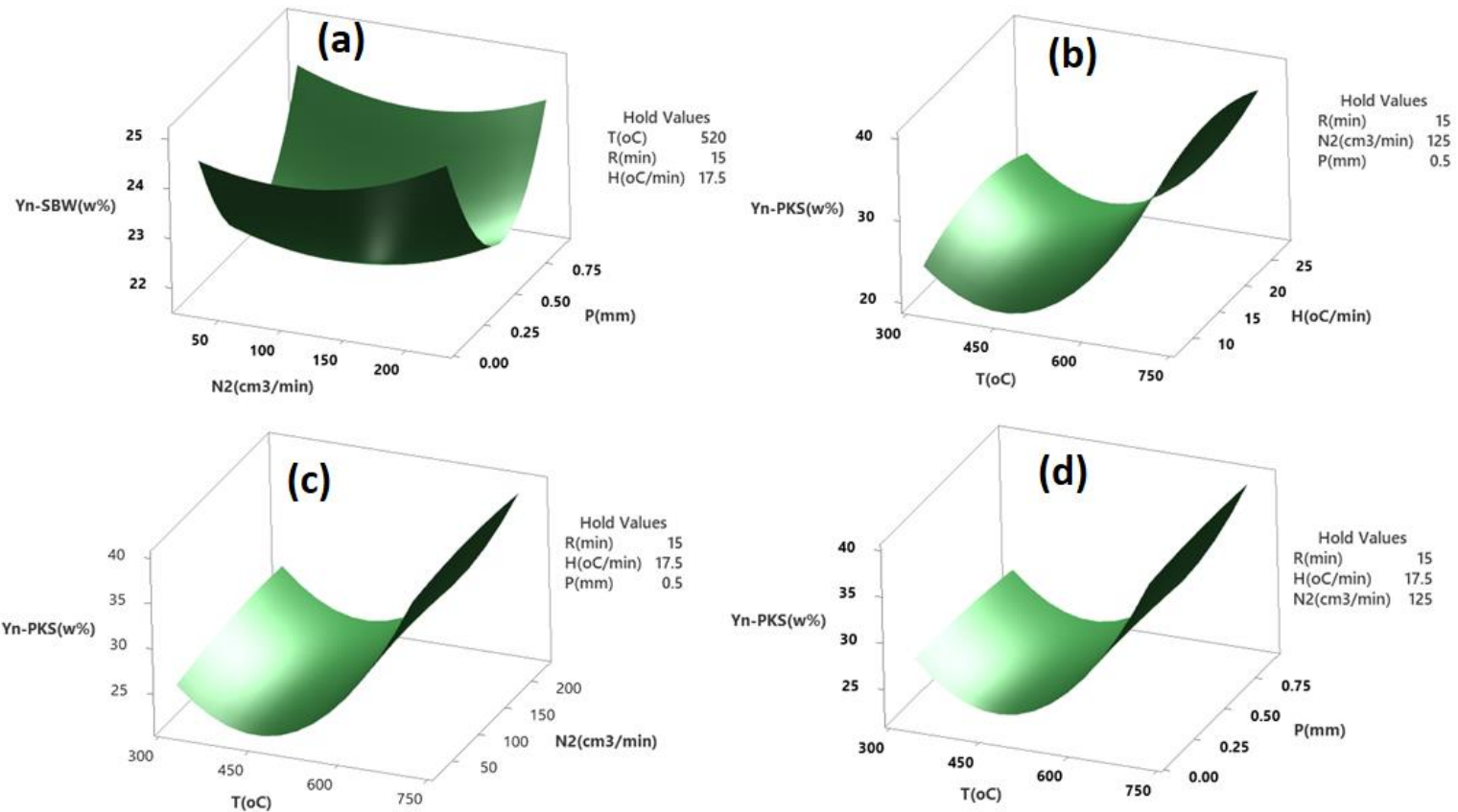


Figure 4.10: Surface Plot of NCG (wt%) against (a) Nitrogen flow rate (cm^3/min), Particle size (mm) using Shea butter wood (b) Temperature ($^{\circ}\text{C}$), Heating rate ($^{\circ}\text{C}/\text{min}$) using Palm kernel shell (c) Temperature ($^{\circ}\text{C}$), Nitrogen flow rate(cm^3/min) using Palm kernel shell (d) Temperature ($^{\circ}\text{C}$), Particle size (mm) using Palm kernel shell

4.11 Optimized Value of Pyrolysis Operating Parameters for Bio-Oil, Biochar and NCG Yields

The optimization plot obtained from the response surface model (Figures. 4.11-4.13) determines the values of the operating parameters (T, R, H, N, P) required for an optimal yield of bio-oil, biochar, and non-condensable gases. The plots generate the maximum, minimum, and optimal production of products of pyrolysis via the interaction of all the parameters. Results showed that varying the T, R, H, N, and P had a great effect on products of pyrolysis. It can be deduced that for optimum bio-oil yield using PKS (46.80 wt%), the optimal values of the operating parameters must be set simultaneously at a T, R, H, N, and P of 493.7 °C, 15.5 min, 24.5 °C/min, 225 cm³/min, and 0.1 mm (Figure 4.11a). In the case SCB, the optimum bio-oil yield (47.5 wt%) was recorded at optimal values are 487.5 °C, 15.7 min, 24.7°C/min, 25.0 cm³/min, and 0.1 mm as shown in Figure (4.11b). Likewise, for SBW, the optimum bio-oil yield (48.4 wt%) was attained at optimal values are 517.4 °C, 14.3 min, 24.7 °C/min, 119.5 cm³/min, and 0.7 mm (Figure 4.11c), any values below and above these values would reduce the yield of bio-oil as an increase in T above 520°C resulted to secondary cracking leading to a reduction in bio-oil yield. The bio-oil yield for SBW was more when compared with PKS and SCB due to their high volatile matter, cellulose and hemicellulose contents (Mohammed *et al.*, 2017). The quantity of bio-oil yields correlated very well with the findings of Gautam and Chaurasia (2020), Laouge *et al.* (2020), Kumar *et al.* (2019), Varma and Mondal (2017) and Muhammed *et al.* (2017), who reported optimum bio-oil yield of 42 wt% for the pyrolysis of rice husk at T of 450°C; 48.27 wt% for fast pyrolysis of pear millet at T of 400°C, P of 1.5 mm and N of 200 mL/min; 46 wt% for pyrolysis of sacbiocharum munja at T of 525°C and R of 60 min; 45.5 wt% for fast pyrolysis of sugarcane bagasse at T of 500°C and H of 50°C/min and 50.27 wt% for intermediate pyrolysis of Napier grass at T of 600°C, N of 50°C/min and 5 L/min respectively.

For an optimum yield of biochar using PKS (40.7 wt%), the optimal values of T, R, H, N and P are 330°C, 6.5 min, 7.5°C/min, 25 cm³/min, and 0.9 mm (Figure 4.12a). Considering biochar yield for SCB (40.5 wt%), the optimal values are 357°C, 6.5 min, 12.8°C/min, 25 cm³/min, and 0.9 mm (Figure 4.12b), while in the case of SBW (40.5 wt%), the optimal values are 346.4°C, 8.9 min, 7.5°C/min, 25 cm³/min, and 0.9 mm for T, R, H, N and P respectively (Figure 4.12c). The biochar yield decreased with increasing temperature due to complete pyrolysis process

caused by rapid emission of volatile matters and thermal decomposition of the biomass from 320 to 720°C, thereby enhancing the yields of aromatic compounds (Sahoo *et al.*, 2021). The optimum value of biochar yield for PKS was higher when compared to SCB and SBW due to their low volatile matter and higher mass fraction of lignin. The results presented in this study closely agreed with the report of Gautam and Chaurasia (2020) with an optimum biochar (46.2 wt%) for the pyrolysis of rice husk at T of 450°C, Guedes *et al.* (2018) with an optimum biochar yield (46 wt%) for the pyrolysis of cassava rhizome at T of 450°C and N of 7.75 L/min, Hossain *et al.* (2017) with an optimum biochar yield (48.26 wt%) for slow pyrolysis of oil palm fibre at T of 450°C, N of 200 cm³/min and microwave power of 400 Watts.

Furthermore, to attain optimum NCG yield using PKS (33.32 wt%), the optimal values must be set at a T, R, H, N, and P respectively are 720°C, 25 min, 7.5 °C/min, 138.1 cm³/min, and 0.1 mm (Figure 4.13a). In the case of SCB (35.5 wt%), the optimal values are 700°C, 24 min, 25.9°C/min, 25 cm³/min, and 0.1 mm (Figure 4.13b). Likewise, the NCG for SBW (34.2 wt%), was obtained at optimal values are 720°C, 20 min, 7.5 °C/min, 225 cm³/min, and 0.1 mm T, R, H, N, and P (Figure 4.13c). Any values below and above this range will reduce the yield of bio-oil, biochar, and NCG. An increase in T from 320 to 720°C caused the volatile matters to decomposed slowly to form more aromatic compounds. Hence, an increase in NCG. These values are similar to the findings of Gautam and Chaurasia (2020), Mohammed *et al.* (2017) and Varma and Mondal (2017) who reported an optimum NCG yields of 27.6 wt% at T of 650°C for the pyrolysis of rice husk, 31.5 wt% for intermediate pyrolysis of Napier grass at T of 600°C, N of 5 L/min and H of 50°C/min and 31 wt% fast pyrolysis of sugarcane bagasse at T of 650°C.

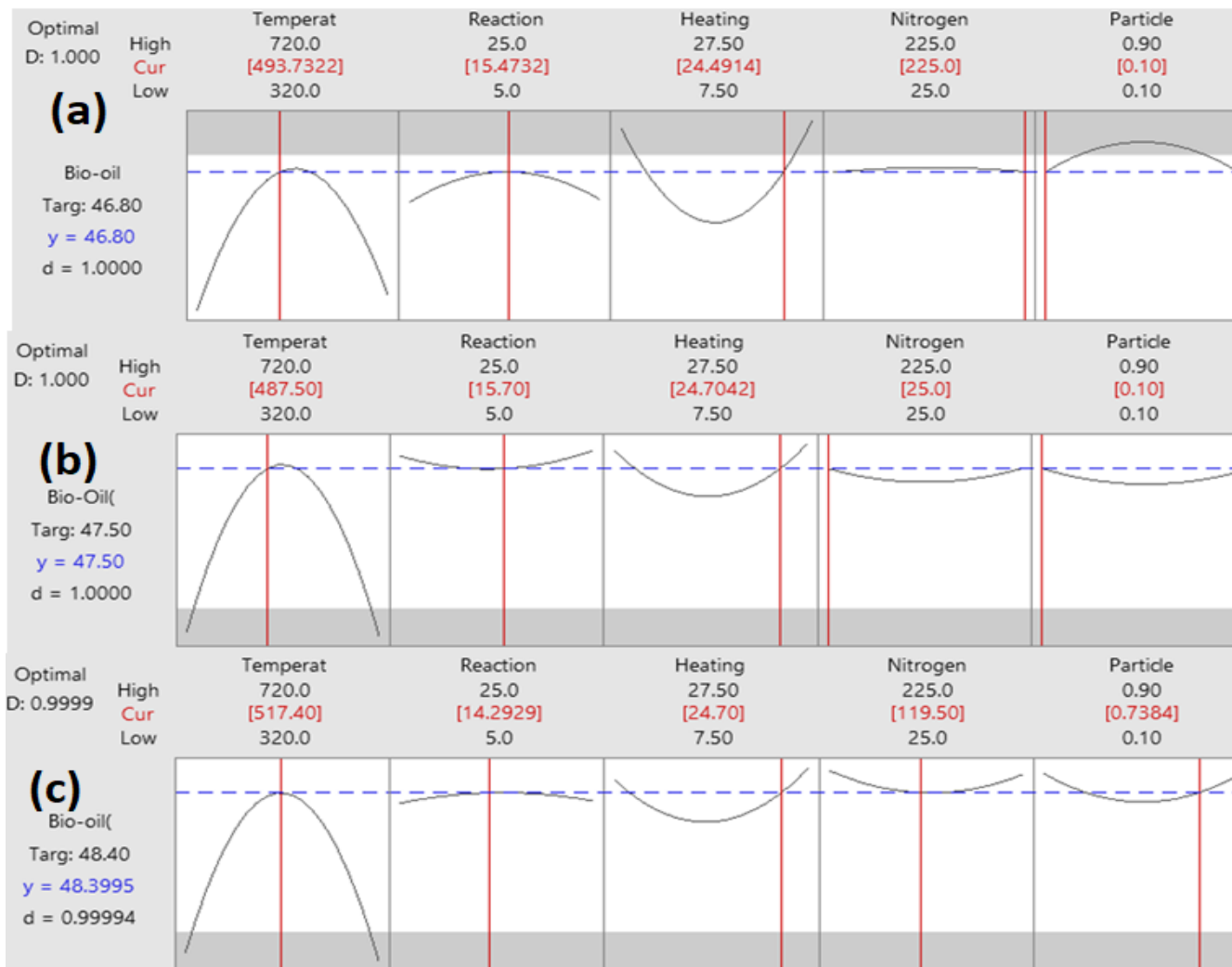


Figure 4.11: Response Optimization for (a) Bio-oil using PKS (b) Bio-oil using SCB (c) Bio-oil using SBW

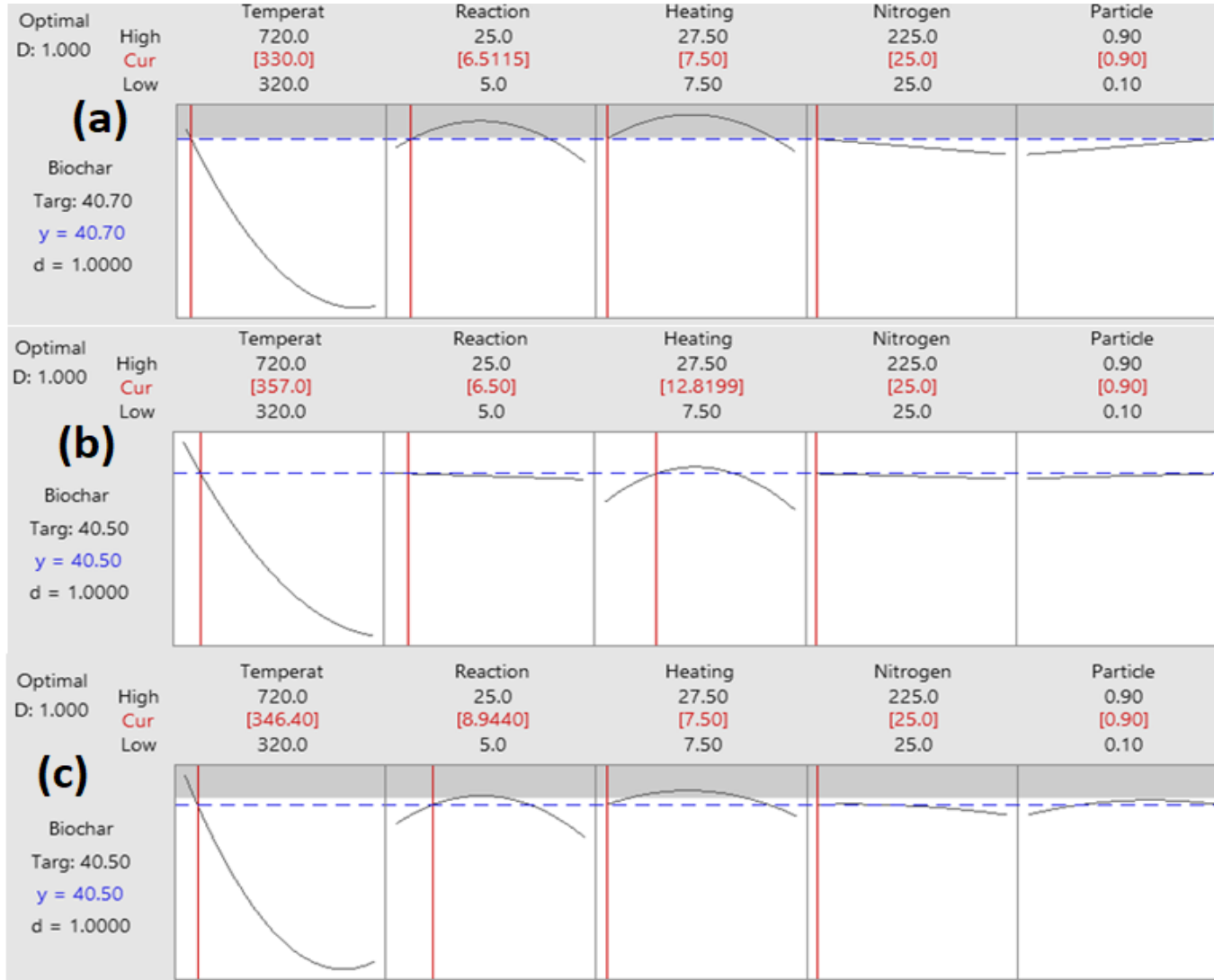


Figure 4.12: Response Optimization for (a) Biochar using PKS (b) Biochar using SCB (c) Biochar using SBW

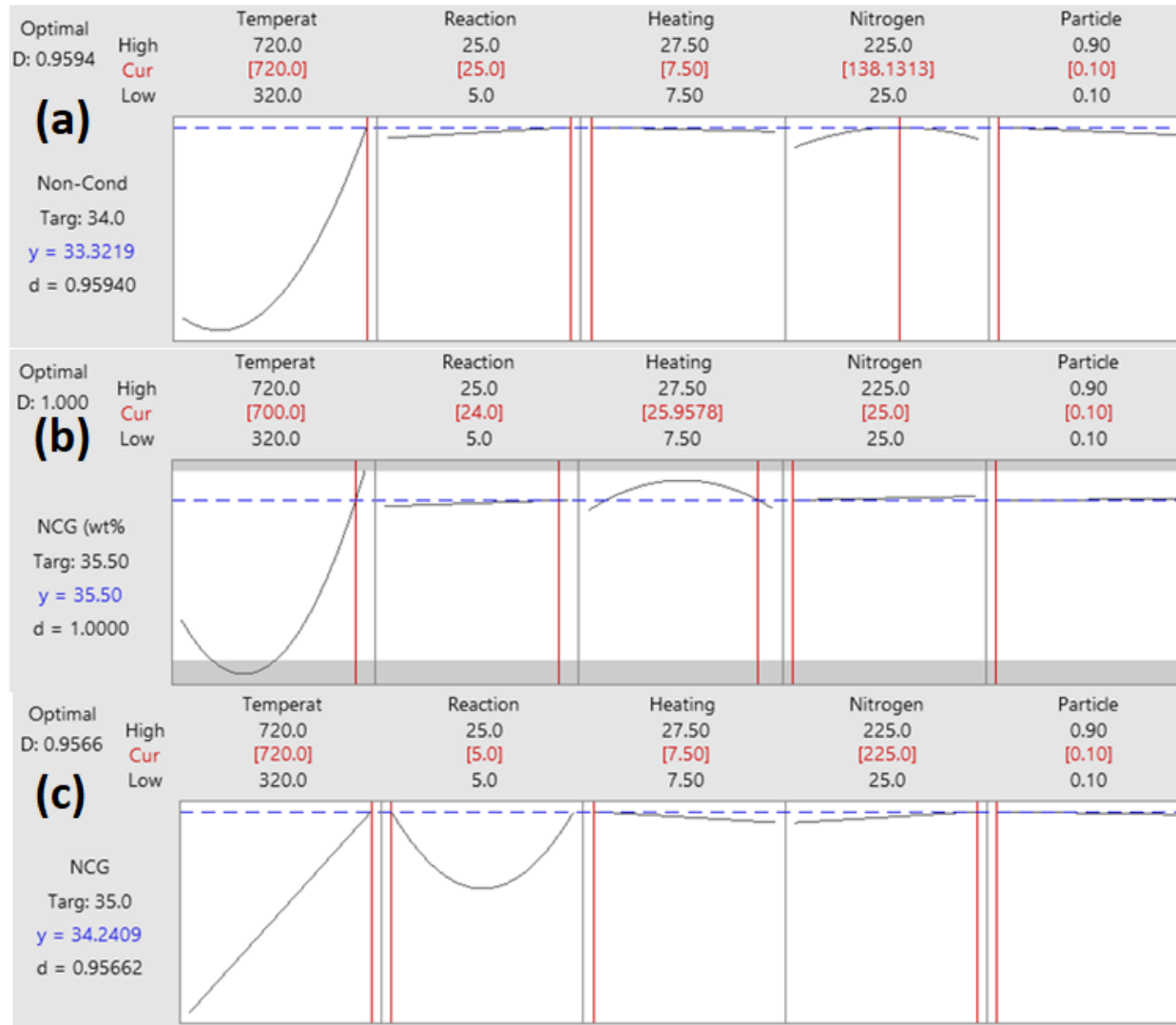


Figure 4.13: Response Optimization for NCG (wt%) using (a) PKS (b) SCB (c) SBW

Table 4.8 depicts the optimized value of pyrolysis operating parameters as well the actual and predicted optimum pyrolysis yields. The optimum yields for bio-oil are 46.80, 47.50, and 48.4 wt% for PKS, SCB, and SBW respectively. In the case of biochar yield, the optimum yields are 40.7, 40.5, and 40.5 wt% for PKS, SCB, and SBW. Lastly, PKS, SCB, and SBW recorded an optimum yield for NCG as 33.3, 35.5, and 34.2 wt% respectively. These values closely correlate with the experimental data as shown in Table 4.8. Hence, the mathematical model was able to predict the optimum yields of bio-oil, biochar and NCG accurately.

Table 4.8: Summary of optimization of operating parameters for bio-oil, biochar, and NCG yields

<i>Biomass Yields</i>	<i>T</i>	<i>R</i>	<i>H</i>	<i>N</i>	<i>P</i>	<i>Y_{experiment}</i>	<i>Y_{optimized}</i>
$Y_{BO(PKS)}$	487.5	15.7	24.7	25	0.1	46.5	46.8
$Y_{BC(PKS)}$	330	6.5	7.5	25	0.9	41.1	40.7
$Y_{N(PKS)}$	700	24	25.9	25	0.1	33.3	33.3
$Y_{BO(SCB)}$	517.4	14.3	24.7	119.5	0.7	47.2	47.5
$Y_{BC(SCB)}$	357	6.5	12.8	25	0.9	40	40.5
$Y_{N(SCB)}$	720	25	75	138.1	0.1	35.9	35.5
$Y_{BO(SBW)}$	493.7	15.5	24.5	225	0.1	47.9	48.4
$Y_{BC(SBW)}$	346.4	8.9	7.5	25	0.9	40.8	40.5
$Y_{N(SBW)}$	720	20	75	225	0.1	34.7	34.2

It can be seen (Figure 4.14) that the predicted values are closely packed around the regression line similar to the report of Hossain *et al.* (2017). The predicted values for the bio-oil, biochar, and NCG yields (Figure 4.14a-4.14c) are in tandem with their experimental values. The selected quadratic response surface model for the products of pyrolysis appropriately describes the experimental data within the selected operating conditions. The regression model showed a strong correlation between the model prediction and its actual results for bio-oil, biochar, and NCG yields. Hence, the developed regression model is dependable and usable to predict products of pyrolysis from lignocellulose biomass samples.

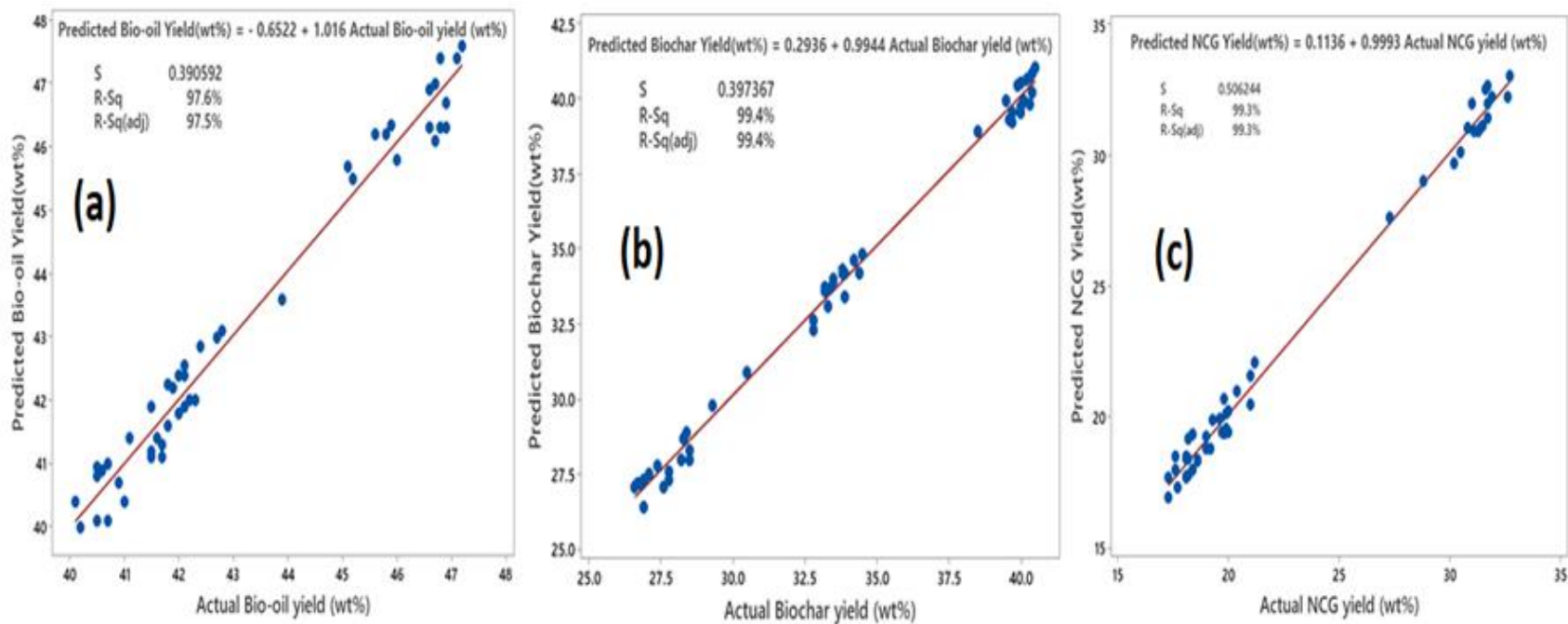


Figure 4.14: Actual and predicted (a) Bio-oil yield (b) Biochar yield (c) NCG yield

Table 4.9 shows the results obtained from the statistical analysis between the values of pyrolysis yields obtained at the optimal condition and previous studies. The results showed no significant difference between the two values at $p > 0.05$, making the optimum parameters responsive, accurate, reliable, and validated. Also, the operating parameters gave pyrolysis yields that are better and significantly different from what is obtainable in all the literature at my disposal.

Table 4.9: Optimum values of pyrolysis products obtained from this study and previous works.

Biomass	Bio-oil						Biochar						Non-Condensable Gases					
	Y^1_o	Y^2_o	Y^3_o	$Y^4_{O(Ave)}$	$Y_{O(Opt)}$	$\% \Delta_o$	Y^1_c	Y^2_c	Y^3_c	$Y^4_{C(Ave)}$	$Y_{c(Opt)}$	$\% \Delta_c$	Y^1_N	Y^2_N	Y^3_N	$Y^4_{N(Ave)}$	$Y_{N(Opt)}$	$\% \Delta_N$
PKS	46.2 ^(a)	38.4 ^(b)	47.4 ^(c)	44	46.8	6%	34.8 ^(j)	38 ^(k)	39 ^(l)	37.3	40.7	9%	20.5 ^(r)	15.2 ⁽ⁱ⁾	25 ^(l)	20.23	33.32	65%
SCB	45.2 ^(d)	45 ^(e)	39.2 ^(f)	43.1	47.5	10%	33.3 ^(m)	36 ^(e)	39.7 ⁽ⁿ⁾	36.3	40.5	11%	31.4 ^(d)	37 ^(e)	27.5 ^(f)	31.97	35.5	11%
SBW	50 ^(g)	46.8 ^(h)	40 ⁽ⁱ⁾	45.6	48.4	6%	38 ^(o)	38.9 ^(p)	38.6 ^(q)	38.6	40.5	5%	33.3 ^(p)	21 ^(s)	36.5 ^(q)	30.27	35.3	17%

(a) Abnisa *et al.* (2011); (b) Ahmad *et al.* (2017); (c) Sukiran *et al.* (2016); (d) Varma and Mondal (2017); (e) Saif *et al.* (2020); (f) Gautam and Chaurasia (2020); (g) Oyebanji *et al.* (2021); (h) Kumagai *et al.* (2015); (i) Lyu *et al.* (2015); (j) Haung *et al.* (2020) (k) Zainal *et al.* (2016); (l) Waluyo *et al.* (2018); (m) Gautam and Chaurasia (2020); (n) Guida and Hannioui (2017); (o) Mazlan *et al.* (2015); (p) Chukwuneke *et al.* (2019); (q) Alvarez-Biocharez (2019); (r) Ihoharudin *et al.* (2020); (j) Huang *et al.* (2020); (l) Waluyo *et al.* (2018); (s) Gao *et al.* (2019); $Y^1_o = Y^2_o = Y^3_o =$ Bio-oil Yields from Literatures; $Y^1_c = Y^2_c = Y^3_c =$ Biochar Yields from Literatures; $Y^1_N = Y^2_N = Y^3_N =$ NCG Yields from Literatures; $Y_{o(Ave)} = Y_{c(Ave)} = Y_{N(Ave)} =$ Average Bio-oil, Biochar and NCG Yields from Literatures; $\% \Delta_o = \% \Delta_c = \% \Delta_N =$ Percentage change between the optimum yields from this study and that of literatures.

Table 4.10: Statistical Analysis of optimum values of pyrolysis products obtained from this study and previous works.

Bio-Oil Yields

Anova: Single

Parameter

SUMMARY

<i>Groups</i>	<i>Count</i>	<i>Sum</i>	<i>Average</i>	<i>Variance</i>
Column 1	3	142.7	47.56667	0.643333
Column 2	3	141.4	47.13333	6.413333
Column 3	3	130.2	43.4	19.56
Column 4	3	126.6	42.2	20.44

ANOVA

<i>Source of Variation</i>	<i>SS</i>	<i>df</i>	<i>MS</i>	<i>F</i>	<i>P-value</i>	<i>F crit</i>
Between Groups	64.54917	3	21.51639	1.828977	0.219965	4.066181
Within Groups	94.11333	8	11.76417			
Total	158.6625	11				

Biochar Yields

Anova: Single

Parameter

SUMMARY

<i>Groups</i>	<i>Count</i>	<i>Sum</i>	<i>Average</i>	<i>Variance</i>
Column 1	3	121.7	40.56667	0.013333
Column 2	3	108.8	36.26667	2.613333
Column 3	3	110.5	36.83333	9.723333
Column 4	3	117.31	39.10333	0.305033

ANOVA

<i>Source of Variation</i>	<i>SS</i>	<i>df</i>	<i>MS</i>	<i>F</i>	<i>P-value</i>	<i>F crit</i>
Between Groups	36.06736	3	12.02245	3.800054	0.058182	4.066181
Within Groups	25.31007	8	3.163758			
Total	61.37743	11				

NCG Yields

Anova: Single

Parameter

SUMMARY

<i>Groups</i>	<i>Count</i>	<i>Sum</i>	<i>Average</i>	<i>Variance</i>
33.32	2	70.8	35.4	0.02
20.5	2	64.7	32.35	1.805
15.2	2	58	29	128
25	2	64.04	32.02	40.5

ANOVA

<i>Source of Variation</i>	<i>SS</i>	<i>df</i>	<i>MS</i>	<i>F</i>	<i>P-value</i>	<i>F crit</i>
Between Groups	41.06935	3	13.68978	8.321498	0.0310874	6.591382
Within Groups	170.325	4	42.58125			
Total	211.39435	7				

4.12 Design of Experiment (DOE) for Energy, Exergy Efficiency and Exergy Destruction of Bio-oil, Biochar, and NCG yields

The results obtained from experimental runs were used to calculate the energy and exergy efficiency of bio-oil, biochar and NCG yields and their exergy destruction shown in Tables 4.11-4.13. The exergy of pyrolysis products was influenced by two thermodynamic properties known as enthalpy and entropy controlled directly by temperature.

An increasing the temperature from 320 to 520°C increased the energy and exergy efficiency of bio-oil yield from 28.9 to 52.8 % and 25.7 to 47.8 % respectively. The energy and exergy efficiency of bio-oil yield decreased from 52.8 to 31.6 % and 40.7 to 28.5 % respectively (Table 4.11), with increasing particle size from 0.1 to 0.9 mm due to low heat transfer and incomplete pyrolysis process (Ramesh and Murugavelh, 2020). Hence, increasing the energy and exergy efficiency of biochar yield from 9.3 to 33.5 % and 4.7 to 30.3 % respectively. Also, nitrogen flow rate from 125 to 225 cm³/min reduced the energy and exergy efficiency of bio-oil yield due to large energy and exergy escaping from the non-condensed volatile components with the NCG caused by short residence time in the condensation (Youcai and Tao, 2021; Etika *et al.*, 2019). Hence, leading to an increase in energy and exergy efficiency of NCG yield from 3.5 to 10.1 % and 1.6 to 8.9 % respectively. Continuous increase in the operating parameters for pyrolysis operating results in high volatile emission, unstrained expansion and spontaneous chemical reaction leading to energy and exergy destruction within the pyrolysis plant from 3.1 to 7.9 % (Singh *et al.*, 2020; Wang *et al.*, 2016). Similar trends for the energy and exergy efficiency of bio-oil, biochar and NCG yields occurred in Table 4.12-4.13.

Optimum energy (46.9 %) and exergy (44.6 %) efficiency of bio-oil yield for PKS were attained at T of 520°C, R of 15 min, H of 17.5°C/min, N of 125 cm³/min and P of 0.5 mm (Table 4.11). In the case of SCB, optimum energy (51.3 %) and exergy (46.3 %) efficiency of bio-oil yield was found at T, R, H, N and P of 520°C, 10 min, 17.5 °C/min, 125 cm³/min and 0.5 mm respectively (Table 4.12). Similarly, the optimum energy and exergy efficiency of bio-oil yields from SBW was 52.8 and 47.8 % respectively. This optimal value was obtained at T of 520°C, R of 15 min, H of 22.5 °C/min, N of 175 cm³/min and P of 0.7 mm (Table 4.13). Considering the energy and exergy efficiency of biochar yields, PKS attained an optimal value of 33.5 and 30.6 % at T, R, H, N, P of 320°C, 5 min, 7.5 °C/min, 25 cm³/min and 0.9 mm respectively

(Table 4.11). SCB recorded an optimal yield of 29.5 and 25.7% at T of 320°C, R of 5 min, H of 7.5°C/min, N of 225 cm³/min and P of 0.9 mm (Table 4.12), while SBW possessed an optimal yield of 28.4 and 22.5% at T of 320°C, R of 5 min, H of 7.5°C/min, N of 225 cm³/min and P of 0.9 mm (Table 4.13). In the case of energy (15.6 %) and exergy (13.8 %) efficiency of NCG yields, PKS was found at T, R, H, N, P of 720°C, 25 min, 7.5 °C/min, 225 cm³/min and 0.1 mm respectively (Table 4.11). SCB recorded an optimal yield of 15.7 and 11.5 % respectively at 720°C, 25 min, 27.5°C/min, 25 cm³/min and 0.1 mm (Table 4.12) Likewise, for SBW, the optimal yield of 14.6 and 10.3 was recorded at T, R, H, N, P of 720°C, 25 min, 27.5°C/min, 25 cm³/min and 0.1 mm respectively (Table 4.13). SBW possessed the highest energy and exergy efficiency of bi-oil yield closely followed by SCB, while PKS had the least energy and exergy efficiency of bio-oil yields. Also, PKS is more suitable for bio-oil yields due to its high energy and exergy efficiency, next to SCW, while SBW had the least energy and exergy efficiency. These trends correlate very well with the report of Wang *et al.* (2016); Ramesh and Murugavelh (2020); Singh *et al.* (2020), and Zhang *et al.* (2020).

PKS recorded an optimum exergy destruction for Bio-oil (7.9%), biochar (6.1 %) and NCG (6.3 %) (Table 4.11). The optimal value was SCB 6.4 % for bio-oil, 8.3% for biochar and 6.8 % for NCG yields ((Table 4.11). In the case of SBW, the optimal exergy destruction for bio-oil, biochar and NCG was 9.9, 7.3 and 5.7% respectively (Table 4.11).

Table 4.11: Experimental design matrix and the corresponding response results for palm kernel shell

Std	Run	Factor A: Temperature(°C)	Factor B: Reaction time(min)	Factor C: Heating rate(°C/min)	Factor D: Nitrogen flow rate(cm ³ /min)	Factor E: Particle size(mm)	En _o (%)	Ex _o (%)	En _c (%)	Ex _c (%)	En _n (%)	Ex _n (%)	Ed _o (%)	Ed _c (%)	Ed _n (%)
36	1	520	10	17.5	125	0.5	43.6	39.6	20.6	16.4	7.5	4.5	4	4.2	3
48	2	520	15	17.5	125	0.5	47.4	44.6	22.5	17.5	5.3	4.2	2.8	5	1.1
35	3	520	5	17.5	125	0.5	44.6	40.5	19.5	12.5	4.6	3.6	4.1	7	1
16	4	720	25	27.5	225	0.1	39.7	35.7	13.5	10.5	10.6	6.4	4	3	4.2
17	5	320	5	7.5	25	0.9	32.7	28.5	33.5	30.2	1.3	0.7	4.2	3.3	0.6
47	6	520	15	17.5	125	0.5	46.1	44.2	22.9	17.4	5.6	2.5	1.9	5.5	3.1
37	7	520	15	12.5	125	0.5	46.1	40.6	21.5	15.7	5.3	2.5	5.5	5.8	2.8
18	8	720	5	7.5	25	0.1	38.6	34.6	9.5	5.3	13.4	10.6	4	4.2	2.8
22	9	720	5	27.5	25	0.9	35.7	30.6	7.6	4.7	10.5	5.7	5.1	2.9	4.8
23	10	320	25	27.5	25	0.9	29.6	25.4	24.7	20.5	3.5	2.6	4.2	4.2	0.9
7	11	320	25	27.5	25	0.1	28.9	25.7	29.5	21.5	2.6	1.5	3.2	8	1.1
34	12	420	15	17.5	125	0.5	40	34.6	28.9	23.5	6.4	4.3	5.4	5.4	2.1
43	13	520	15	17.5	125	0.5	46.3	44.5	22.7	17.1	5.3	1.5	1.8	5.6	3.8
1	14	320	5	7.5	25	0.1	30.6	26.4	30.5	24.6	4.3	2.5	4.2	5.9	1.8
3	15	320	25	7.5	25	0.1	32.6	26.5	29.6	24.6	3.5	1.6	6.1	5	1.9
39	16	520	15	17.5	75	0.5	44.6	37.5	22.4	17.4	6.6	3.6	7.1	5	3
32	17	720	25	27.5	225	0.9	35.7	31.5	10.4	5.3	13.6	10	4.2	5.1	3.6
12	18	720	25	7.5	225	0.1	36.5	30.6	9.4	5.3	13.8	10.1	5.9	4.1	3.7
5	19	320	5	27.5	25	0.1	30.2	24.6	29.6	21.6	4.3	3.5	5.6	8	0.8
31	20	320	25	27.5	225	0.9	33.6	29.5	27.4	23.6	4.1	2.5	4.1	3.8	1.6
44	21	520	15	17.5	125	0.5	46.3	44.1	22.9	17.3	5.4	4.2	2.2	5.6	1.2
21	22	320	5	27.5	25	0.9	30.6	27.4	32.5	27.5	3.8	1.5	3.2	5	2.3
30	23	720	5	27.5	225	0.9	37.4	32.6	9.6	4.7	11.4	8.4	4.8	4.9	3
19	24	320	25	7.5	25	0.9	29.7	23.5	28.4	22.5	2.5	0.3	6.2	5.9	2.2
42	25	520	15	17.5	125	0.3	44.7	38.6	25.3	20.5	5.4	3.4	6.1	4.8	2
14	26	720	5	27.5	225	0.1	39.5	33.4	13.5	11.4	13.5	8.4	6.1	2.1	5.1
25	27	320	5	7.5	225	0.9	30.7	25.7	28.5	21.5	3.6	2.5	5	7	1.1
41	28	520	15	17.5	125	0.5	45.3	44.5	22.7	17.9	5.6	2.1	0.8	4.8	3.5
38	29	520	15	22.5	175	0.7	43.7	36.8	18.4	16.4	12.7	6.4	6.9	2	6.3
6	30	720	5	27.5	25	0.1	38.6	33.6	10.6	6.3	10.7	8.4	5	4.3	2.3
20	31	720	25	7.5	25	0.9	41.6	37.5	5.7	2.6	9.6	5.3	4.1	3.1	4.3
46	32	520	15	17.5	125	0.5	46.1	44.1	22.4	17.5	5.3	2.7	2	4.9	2.6
9	33	320	5	7.5	225	0.1	28.5	22.5	28.6	22.5	3.7	2.5	6	6.1	1.2
50	34	520	15	17.5	25	0.5	43.7	39.6	17.4	12.6	7.4	4.3	4.1	4.8	3.1
8	35	720	25	27.5	25	0.1	39.7	35.7	10.4	6.3	12.5	9.4	4	4.1	3.1
11	36	320	25	7.5	225	0.1	32.6	28.5	26.7	20.6	3.6	1.5	4.1	6.1	2.1
33	37	620	15	17.5	125	0.5	45.3	42.6	14.7	11.5	6.5	4.6	2.7	3.2	1.9
4	38	720	25	7.5	25	0.1	41.4	37.5	11.6	8.4	12.4	8.5	3.9	3.2	3.9
49	39	520	15	17.5	125	0.5	46.2	44.3	22.6	17.5	5.6	2.7	1.9	5.1	2.9
10	40	720	5	7.5	225	0.1	41.5	37.5	10.6	7.4	12.6	10.2	4	3.2	2.4
40	41	520	15	17.5	225	0.5	46.2	41.6	18.4	12.9	8.4	4.6	4.6	5.5	3.8
2	42	720	5	7.5	25	0.1	40.7	36.5	14.3	10.8	10.8	8.4	4.2	3.5	2.4
13	43	320	5	27.5	225	0.1	31.7	27.4	28.6	23.6	3.6	2.5	4.3	5	1.1
29	44	320	5	27.5	225	0.9	33.6	25.7	30.4	25.6	1.4	0.4	7.9	4.8	1
27	45	320	25	7.5	225	0.9	35.2	30.6	33	30.5	2.8	1.7	4.6	2.5	1.1
28	46	720	25	7.5	225	0.9	40.6	33.7	13.2	7.4	9.6	6.3	6.9	5.8	3.3
26	47	720	20	7.5	225	0.9	41.3	35.9	15.3	10.7	9.4	6.8	5.4	4.6	2.6
24	48	720	25	27.5	25	0.9	42.5	36.4	8.5	5.3	12.7	9.5	6.1	3.2	3.2
45	49	520	15	17.5	125	0.5	46.3	44	22.5	17.4	5.5	2.6	2.3	5.1	2.9
15	50	320	25	27.5	225	0.1	34.5	30.6	27.4	24.2	4.5	3.2	3.9	3.2	1.3

En_o = Energy efficiency of Bio-oil yields; **En_c** = Energy efficiency of Biochar yields; **En_n** = Energy efficiency of NCG yields; **Ex_o** = Exergy efficiency of Bio-oil yields; **Ex_c** = Exergy efficiency of Biochar yields; **Ex_n** = Exergy efficiency of NCG yields; **Ed_o** = Exergy destruction of Bio-oil yields; **Ed_c** = Exergy destruction of Biochar yields; **Ed_n** = Exergy destruction of NCG yields

Table 4.12: Experimental design matrix and the corresponding response results for Sugarcane bagasse

Std	Run	Factor A: Temperature(°C)	Factor B: Reaction time(min)	Factor C: Heating rate(°C/min)	Factor D: Nitrogen flow rate(cm ³ /min)	Factor E: Particle size(mm)	Response 1: En ₁ (%)	Response 2: En ₂ (%)	Response 3: En ₃ (%)	Response 4: Ex ₄ (%)	Response 5: En ₅ (%)	Response 6: Ex ₆ (%)	Response 7: Ed ₇ (%)	Response 8: Ed ₈ (%)	Response 9: Ed ₉ (%)
36	1	520	10	17.5	125	0.5	51.3	46.4	17.5	14.7	5.7	3.5	4.9	2.8	2.2
48	2	520	15	17.5	125	0.5	50.2	45.7	18.5	15.3	6.3	3.7	4.5	3.2	2.6
35	3	520	5	17.5	125	0.5	49.5	43.6	18.9	13.6	5.3	2.6	5.9	5.3	2.7
16	4	720	25	27.5	225	0.1	45.7	41.6	10.4	6.8	14.6	10.5	4.1	3.6	4.1
17	5	320	5	7.5	25	0.9	39.6	33.6	27.3	22.7	1.5	0.3	6	4.6	1.2
47	6	520	15	17.5	125	0.5	50.7	45.9	18.3	15.8	6.3	3.7	4.8	2.5	2.6
37	7	520	15	12.5	125	0.5	50.3	45.3	20.5	17.4	8.4	5.3	5	3.1	3.1
18	8	720	5	7.5	25	0.1	45.3	39.5	11.3	5.3	15.3	11.5	5.8	6	3.8
22	9	720	5	27.5	25	0.9	45.8	38.5	10.6	6.8	12.4	9.4	7.3	3.8	3
23	10	320	25	27.5	25	0.9	35.7	30.5	26.7	23.2	4.6	1.6	5.2	3.5	3
7	11	320	25	27.5	25	0.1	36.4	31.5	27.4	21.4	1.3	0.6	4.9	6	0.7
34	12	420	15	17.5	125	0.5	40.7	36.7	24.7	17.9	4.8	1.3	4	6.8	3.5
43	13	520	15	17.5	125	0.5	50.3	47.5	18.6	15.8	6.5	3.6	2.8	2.8	2.9
1	14	320	5	7.5	25	0.1	37.5	31.5	28.5	22.4	2.5	0.5	6	6.1	2
3	15	320	25	7.5	25	0.1	37.1	33.5	27.4	21.5	4.1	2.7	3.6	5.9	1.4
39	16	520	15	17.5	75	0.5	48.5	42.5	20.5	16.3	8.3	5.3	6	4.2	3
32	17	720	25	27.5	225	0.9	43.6	38.9	12.7	7.3	11.4	9.4	4.7	5.4	2
12	18	720	25	7.5	225	0.1	41.3	37.5	11.5	8.4	12.5	8.6	3.8	3.1	3.9
5	19	320	5	27.5	25	0.1	40.6	34.2	27.4	22.5	3.1	1.5	6.4	4.9	1.6
31	20	320	25	27.5	225	0.9	37.6	31.5	25.7	21.5	4.6	1.9	6.1	4.2	2.7
44	21	520	15	17.5	125	0.5	50.8	45.9	18.3	15.6	6.1	3.4	4.9	2.7	2.7
21	22	320	5	27.5	25	0.9	37.4	32.7	29.4	22.5	1.1	0.2	4.7	6.9	0.9
30	23	720	5	27.5	225	0.9	43.7	39.7	8.5	6.3	13.2	6.4	4	2.2	6.8
19	24	320	25	7.5	25	0.9	38.4	33.1	26.4	25.7	4.2	2.6	5.3	0.7	1.6
42	25	520	15	17.5	125	0.3	50	47	23.6	15.3	8.4	4.2	3	8.3	4.2
14	26	720	5	27.5	225	0.1	45.7	40.2	11.6	8.4	12.4	7.4	5.5	3.2	5
25	27	320	5	7.5	225	0.9	40.1	34.6	29.5	24.6	2.4	1	5.5	4.9	1.4
41	28	520	15	17.5	125	0.5	50.6	45.4	18.4	11.4	6.3	3.7	5.2	7	2.6
38	29	520	15	22.5	175	0.7	48.5	43.7	17.3	13.5	11.7	8.4	4.8	3.8	3.3
6	30	720	5	27.5	25	0.1	45.3	40.7	12.6	8.5	15.2	11.5	4.6	4.1	3.7
20	31	720	25	7.5	25	0.9	46.5	40.3	8.9	6.7	10.3	6.7	6.2	2.2	3.6
46	32	520	15	17.5	125	0.5	50.5	45.8	18.3	15.3	6.7	3.5	4.7	3	3.2
9	33	320	5	7.5	225	0.1	38.5	33.6	27.8	25.7	2.6	1.4	4.9	2.1	1.2
50	34	520	15	17.5	25	0.5	49.6	43.6	18.5	15.3	6.3	3.8	6	3.2	2.5
8	35	720	25	27.5	25	0.1	45.8	40.2	9.6	6.7	15.7	11.4	5.6	2.9	4.3
11	36	320	25	7.5	225	0.1	33.8	29.4	28.4	25.3	2.4	1	4.4	3.1	1.4
33	37	620	15	17.5	125	0.5	50	45.2	16.4	10.6	10.5	7.3	4.8	5.8	3.2
4	38	720	25	7.5	25	0.1	44.6	39.6	10.2	7.6	14.6	10.4	5	2.6	4.2
49	39	520	15	17.5	125	0.5	50.7	45.3	18.6	15.7	6.4	3.6	5.4	2.9	2.8
10	40	720	5	7.5	225	0.1	48.4	42.7	12.4	5.7	14.2	9.4	5.7	6.7	4.8
40	41	520	15	17.5	225	0.5	48.4	40.7	20.6	15.7	5.3	2.5	7.7	4.9	2.8
2	42	720	5	7.5	25	0.1	45.7	41.4	12.5	7.4	12.4	9.7	4.3	5.1	2.7
13	43	320	5	27.5	225	0.1	36.4	33.6	26.3	20.6	2.4	0.7	2.8	5.7	1.7
29	44	320	5	27.5	225	0.9	35.1	30.6	26.7	23.5	1.7	1	4.5	3.2	0.7
27	45	320	25	7.5	225	0.9	38.6	34.6	25.7	20.6	0.8	0.2	4	5.1	0.6
28	46	720	25	7.5	225	0.9	46.5	42.4	11.4	4.7	12.6	6.4	4.1	6.7	6.2
26	47	720	20	7.5	225	0.9	47.4	42.6	12.7	7.4	13.5	6.8	4.8	5.3	6.7
24	48	720	25	27.5	25	0.9	48.5	43.7	10.7	7.4	11.6	7.3	4.8	3.3	4.3
45	49	520	15	17.5	125	0.5	50.7	43.7	18.4	15.7	6.8	3.7	7	2.7	3.1
15	50	320	25	27.5	225	0.1	37.7	32.7	25.7	20.5	2.6	1	5	5.2	1.6

Table 4.13: Experimental design matrix and the corresponding response results for SBW

Std	Run	Factor A: Temperature(°C)	Factor B: Reaction time(min)	Factor C: Heating rate(°C/min)	Factor D: Nitrogen flow rate(cm ³ /min)	Factor E: Particle size(mm)	En ₀ (%)	Ex ₀ (%)	En _c (%)	Ex _c (%)	En _N (%)	Ex _N (%)	Ed ₀ (%)	Ed _c (%)	Ed _N (%)
36	1	520	10	17.5	125	0.5	46.6	44.5	20.6	18.1	7.5	5	2.1	2.5	2.5
48	2	520	15	17.5	125	0.5	47.6	44.8	19.2	15.3	7.9	4.5	2.8	3.9	3.4
35	3	520	5	17.5	125	0.5	47.4	44.9	19.1	14.2	8	5	2.5	4.9	3
16	4	720	25	27.5	225	0.1	43.2	41	10	5.7	13.6	9.6	2.2	4.3	4
17	5	320	5	7.5	25	0.9	40.1	35.1	28.9	23.3	2.5	0.6	5	5.6	1.9
47	6	520	15	17.5	125	0.5	47.4	45	19.5	15.8	7.5	4.3	2.4	3.7	3.2
37	7	520	15	12.5	125	0.5	47.9	44.2	19.8	14.8	7.3	4.2	3.7	5	3.1
18	8	720	5	7.5	25	0.1	41.4	41.5	10.6	6.3	13.7	10.6	0.1	4.3	3.1
22	9	720	5	27.5	25	0.9	45.5	41.8	11.5	5.7	13.1	11.3	3.7	5.8	1.8
23	10	320	25	27.5	25	0.9	40.7	36.2	25.8	22.5	3	1.1	4.5	3.3	1.9
7	11	320	25	27.5	25	0.1	40.8	35.8	26.8	23.6	2.8	0.7	5	3.2	2.1
34	12	420	15	17.5	125	0.5	44	39.7	23	15.3	4.9	2.1	4.3	7.7	2.8
43	13	520	15	17.5	125	0.5	47.9	44.6	19.6	15.4	7.8	4.6	3.3	4.2	3.2
1	14	320	5	7.5	25	0.1	41.4	35.1	27.4	22.4	2.9	1	6.3	5	1.9
3	15	320	25	7.5	25	0.1	41.8	35.8	28	24.7	3	1.4	6	3.3	1.6
39	16	520	15	17.5	75	0.5	46.5	44.6	19.4	15.6	7.8	4.6	1.9	3.8	3.2
32	17	720	25	27.5	225	0.9	45.7	42.8	11.3	6.3	12.4	10.6	2.9	5	1.8
12	18	720	25	7.5	225	0.1	45.8	43	10.8	6.6	14.9	10.7	2.8	4.2	4.2
5	19	320	5	27.5	25	0.1	41.2	38	28.3	21.7	2.5	0.5	3.2	6.6	2
31	20	320	25	27.5	225	0.9	42	36.2	27.5	25.8	2.3	0.9	5.8	1.7	1.4
44	21	520	15	17.5	125	0.5	47.5	44.9	19.3	15.6	7.8	4.1	2.6	3.7	3.7
21	22	320	5	27.5	25	0.9	41	34.7	27.5	24.4	2.1	1	6.3	3.1	1.1
30	23	720	5	27.5	225	0.9	45.3	45.1	10.5	5.1	11.7	9.5	0.2	5.4	2.2
19	24	320	25	7.5	25	0.9	40	36.8	28.5	23.5	3	1.7	3.2	5	1.3
42	25	520	15	17.5	125	0.3	47.3	44.6	21	14.6	7	5	2.7	6.4	2
14	26	720	5	27.5	225	0.1	45.3	41.5	12	6.8	12.5	8.9	3.8	5.2	3.6
25	27	320	5	7.5	225	0.9	42.7	36.1	27.8	21.1	3	1.6	6.6	6.7	5.7
41	28	520	15	17.5	125	0.5	47.9	44.6	19.7	14.1	7.9	4.5	3.3	5.6	3.4
38	29	520	15	22.5	175	0.7	52.8	47.8	20.6	16.3	11.5	9.3	5	4.3	2.2
6	30	720	5	27.5	25	0.1	45.1	43.5	10.8	6	13.6	9.6	1.6	4.8	4
20	31	720	25	7.5	25	0.9	45.6	43.8	10.3	5.3	14	10.4	1.8	5	3.6
46	32	520	15	17.5	125	0.5	47.5	44.8	19.3	14.3	7.5	4.6	2.7	5	2.9
9	33	320	5	7.5	225	0.1	40.8	34.8	28.4	22.4	3	0.8	6	6	2.2
50	34	520	15	17.5	25	0.5	47.4	44.1	18.5	17.4	7.4	4.7	3.3	1.1	2.7
8	35	720	25	27.5	25	0.1	45.6	41.6	10.6	5.6	14.3	10.3	4	5	4
11	36	320	25	7.5	225	0.1	40.6	33.1	28	23.5	1.6	0.2	7.5	4.5	1.4
33	37	620	15	17.5	125	0.5	50.5	42.7	14.6	11.4	9.4	5.8	9.9	3.2	3.6
4	38	720	25	7.5	25	0.1	45.7	40.7	10.7	5.4	13.6	9.7	5	5.3	3.9
49	39	520	15	17.5	125	0.5	47.6	44.8	19.5	15.7	7.3	4.3	2.8	3.8	3
10	40	720	5	7.5	225	0.1	45.6	40.9	11.5	6.4	12.5	10.5	4.7	5.1	2
40	41	520	15	17.5	225	0.5	46.9	41.4	19.2	14.8	6.8	4.3	5.5	4.4	2.5
2	42	720	5	7.5	25	0.1	45.7	41.5	12	5.1	13.6	10.1	4.2	7.3	3.5
13	43	320	5	27.5	225	0.1	41.3	34.8	27.5	24	3	1	6.5	3.5	2
29	44	320	5	27.5	225	0.9	40.3	35.2	28.4	22.5	2.3	0.1	5.1	5.9	2.2
27	45	320	25	7.5	225	0.9	41.8	38.5	28.2	23.6	2.6	1.5	3.3	4.6	1.1
28	46	720	25	7.5	225	0.9	45.6	45.2	10.4	5.2	11.7	9.4	0.4	5.2	2.3
26	47	720	20	7.5	225	0.9	45.8	45.5	11.6	6	12.7	10.3	6.4	5.6	2.4
24	48	720	25	27.5	25	0.9	45.1	41.3	12	6.5	14	10.5	3.8	5.5	3.5
45	49	520	15	17.5	125	0.5	47.5	37.7	19.6	15.6	7.6	4.5	9.8	4	3.1
15	50	320	25	27.5	225	0.1	40.7	35.9	28.3	23.7	1.7	0.8	4.8	4.6	0.9

4.13 Statistical Modelling for Energy Efficiency of Products of Pyrolysis

The data obtained from the experimental runs was utilized to calculate the energy and exergy efficiency of the bio-oil, biochar and NCG. The mathematical model of the energy and exergy analysis of the products of pyrolysis were investigated using analysis of variance (ANOVA) by considering the quadratic model in the CCD technique. Quadratic model was selected as it has been adjudged to be fit for the optimization technique similar to the method adopted in obtaining the mathematical model and optimization of pyrolysis yields as shown in Figure 3.2.

Equations 4.10, 4.11, and 4.12 present the mathematical model used to predict the energy efficiency for bio-oil, biochar and NCG respectively.

$$En_{BO} = 45.476 + 3.948A - 0.443C + 0.048E - 0.931A^2 - 0.67D^2 - 0.421AC - 0.323AE - 0.019BC \quad (4.10)$$

$$En_{BC} = 21.563 - 9.314A - 0.402B - 0.467C - 0.309E - 1.488A^2 - 0.703AE + 0.734BD \quad (4.11)$$

$$En_{NCG} = 3.515 + 3.121A + 0.208C - 0.384E + 1.599A^2 + 0.145BE + 0.063DE \quad (4.12)$$

Where En_{BO} , En_{BC} , En_{NCG} is the response of the energy efficiency bio-oil, biochar and NCG yield (wt%).

The results show a higher F-value 167.49, 45.15, 16.32 for energy efficiency of the bio-oil, biochar and NCG yields respectively and a low p-value (less than 0.05) was recorded for all the biomass under investigation showed that the developed regression model is significant. There is only a small chance (0.01%) that a model F-value this large might take place due to noise (Hassain *et al.*, 2017; Laouge *et al.*, 2020). The energy efficiency for bio-oil yield showed that, temperature, heating rate, particle size, interaction of temperatures, interaction of nitrogen flow rate, interaction of temperatures and heating rate, interaction of temperature and particle size, and interaction of reaction time and particle size positively are significant model terms. In the case of energy efficiency for biochar yield, temperature, reaction time, heating rate, nitrogen flow rate, particle size, interaction of temperatures, interaction of temperature and particle size, interaction of reaction time and nitrogen flow rate, interaction of nitrogen flow rate and particle

size. Also, for energy efficiency of NCG yield, temperature, reaction time, heating rate, nitrogen flow rate, particle size, interaction between temperatures, interaction between reaction time and particle size, and interaction between nitrogen flow rate and particle size are significant model terms. The significant parameters positively influence the energy efficiency of bio-oil, biochar and NCG yields. These findings are similar to the report of Wang *et al.* (2016); Ramesh and Murugavelh (2020), and Singh *et al.* (2020).

The lack of fit of 0.085 and 0.08 ($p < 0.05$) for energy efficiency for bio-oil and NCG yield means that the developed mathematical model can predict and reproduce the experimental data. Also, in the study, the CV% for energy efficiency of bio-oil, biochar and NCG yields are 6.29, 3.12, and 3.76 % respectively which are relatively low. Hence, the investigated model can be reproduced. Likewise, the R^2 value of energy efficiency of bio-oil, biochar, and NCG yields are 0.9922, 0.9863, and 0.9892 respectively which are very close to 1. Hence, the mathematical model under investigation is good and can replicate the experimental data for energy efficiency of bio-oil, biochar and NCG yields. For energy efficiency of bio-oil yield the difference between the adjusted R^2 (0.9786) and predicted R^2 (0.8756) is 0.1. Hence, The study are in reasonable agreement. For biochar yield, the predicted R^2 of 0.8415 is in reasonable agreement (difference of 0.13) with adjusted R^2 of 0.9711 Similarly, for NCG yields the difference between the adjusted R^2 (0.9621) and predicted R^2 (0.8521) is 0.11. Hence, they are in reasonable agreement.

4.14 Statistical Modelling for Exergy Efficiency of Products of Pyrolysis

The mathematical model utilized to predict the exergy efficiency of bio-oil, biochar and NCG yields are presented in Eqns. 4.13, 4.14 and 4.15 respectively.

$$Ex_{BO} = 41.863 + 3.937A - 9.63A^2 - 1.59B^2 - 0.219AB - 0.019BE \quad (4.13)$$

$$Ex_{BC} = 31.97 - 0.0161A - 0.000026A^2 \quad (4.14)$$

$$Ex_{NCG} = 6.330 + 4.149A + 1.199A^2 - 0.013AE - 0.169DE \quad (4.15)$$

Where Ex_{BO} , Ex_{BC} , Ex_{NCG} is the response to the exergy efficiency bio-oil, biochar, and NCG yield (wt%).

A higher F-value of 45.55, 21.72, 15.06 for exergy efficiency of bio-oil, biochar, and NCG yields respectively, and a low p-value (less than 0.05) was recorded for all the biomass under

investigation showed that the developed regression model is significant. There is only a small chance (0.01%) that a model F-value this large might take place due to noise (Hassain *et al.*, 2017; Laouge *et al.*, 2020).

The exergy efficiency for bio-oil yield showed that temperature, the interaction of temperatures, interaction between reaction time, interaction of temperatures and reaction time, interaction of reaction time and nitrogen flow rate, and interaction of reaction time and particle size positively are significant model terms. In the case of exergy efficiency for biochar yield, temperature, the interaction of temperature, and reaction time are significant model terms. Also, for the exergy efficiency of NCG yield, temperature, the interaction between temperatures, the interaction between reaction time and particle size, and the interaction between nitrogen flow rate and particle size are significant model terms. Lack of Fit of 0.117 and 0.08 ($p < 0.05$) for exergy efficiency of NCG yield means the developed mathematical model can predict and reproduce the experimental data. Also, the CV% for exergy efficiency of bio-oil, biochar, and NCG yields (Appendix 3.5a-3.5c) are 2.45, 1.56, and 4.56% respectively which are relatively low. Hence, the investigated model can be reproduced. Likewise, the R^2 value of exergy efficiency of bio-oil, biochar, and NCG yields are 0.9890, 0.9834, and 0.9818 respectively which are very close to 1. Hence, the mathematical model under investigation is good and can replicate the experimental data for energy efficiency of bio-oil, biochar, and NCG yields. For energy efficiency of bio-oil yield the difference between the adjusted R^2 (0.9641) and predicted R^2 (0.8441) is 0.12. Hence, they are in reasonable agreement. For biochar yield, the predicted R^2 of 0.8115 is in reasonable agreement (difference of 0.15) with the adjusted R^2 of 0.9615. Similarly, NCG yields the difference between the adjusted R^2 (0.9601) and predicted R^2 (0.8001) is 0.12. Hence, they are in reasonable agreement.

4.15 Influence of Operating Parameters on Energy and Exergy Efficiency of Products of Pyrolysis

It can be deduced (Figure 4.15a) that the exergy efficiency of individual gases such as CO, CH₄, CO₂, H₂ increased as temperature increased due to rapid devolatilization of the biomass samples to NCG at high temperature. CH₄ recorded the highest exergy efficiency closely followed by CO gas. Also, a rapid change increase in exergy efficiency was observed in CH₄

and H₂ gases because the bio-oil decomposes to CH₄ and H₂ gas at high temperatures (Wang *et al.*, 2016), while that of CO₂ was constant with temperature increase as observed in Figure 4.19a. This trend is similar to what Singh *et al.* (2020) and Wang *et al.* (2016) reported for energy and exergy analysis for torrefaction of pigeon pea stalk and pyrolysis of rice husk respectively. Figure 4.15b embodies the energy and exergy of pyrolysis yields and irreversibility against varying temperatures. The energy and exergy efficiency of bio-oil ranged from 40.6 to 53.6 and 34.2 to 47.9% respectively. For biochar yield, the energy and exergy efficiency ranged from 9.3-28.7 and 5.3-24.2% respectively. In the case of NCG yield, the energy and exergy efficiency ranged from 1.5-15.5 and 0.3-12% respectively. An increase in temperature (320-520°C), increased the energy and exergy efficiency of bio-oil and NCG, while the energy and exergy efficiency of the biochar yield decreased due to an increase in the total energy and exergy input needed to decompose the biomass sample to condensable and non-condensable gases. An increase in temperature above 520°C results in a moderate decrease in energy and exergy efficiency of bio-oil and a sharp drop in the energy and exergy efficiency of biochar due to secondary reactions of uncondensed volatile components that favour NCG yield. Also, an increase in temperature above 520°C results in thermal cracking of the bio-oil yield to NCG. Hence, favour the energy and exergy of NCG. Irreversibilities in the pyrolysis plant increased from 32.4 to about 42.7% due to entropy such as spontaneous chemical reaction, high volatile emission, a mixture of the biochar and vapour, and unrestrained expansion (Peters *et al.*, 2015a; Ramesh and Murugavelh, 2020; Singh *et al.*, 2020; The energy and exergy of biochar dropped as temperature increased due to the complete pyrolysis process and non-attainment of secondary reactions such as thermal cracking, repolymerization, and recondensation which supports the report of Wang *et al.* (2016); Dincer and Rosen (2021), and Singh *et al.* (2020). The energy efficiency is relatively higher than the exergy efficiency due to loss of inertia thermal effect, low heat transfer in the pyrolysis plant, large exergy of the escaping vapour from the pyrolysis plant, and additional thermal degradation of the pyrolysis plants (Dincer *et al.*, 2013; Peters *et al.*, 2015b).

An increase in temperature from 320 to 720°C (Figure 4.15c) increased the total exergy at the inlet sharply from 13800 – 18500 kJ/kg, due to the increase in the input electric exergy by the pyrolysis plant. The total exergy outlet initially increased from 11200 to 12600 kJ/kg at a temperature range of 320 to 420°C, but later decreased due to a severe pyrolysis process at a

temperature above 420°C. This is due to irreversibilities built up in the pyrolysis plant caused by high volatile emission, spontaneous chemical reactions, a mixture of the biochar and vapour, and unrestrained expansion (Wang *et al.* 2016; Ramesh and Murugarelh, 2020). Hence, the severe pyrolysis process is not suitable until the exergy lost can be recycled for biomass preheating as also reported by Boateng *et al.* (2012); Granados *et al.* (2014) and Singh *et al.* (2020). The irreversibilities in the plant can be minimized by reducing heat loss in the plant, better reactor design, and recirculation of the heat lost via pyrolysis products yields to reduce the energy and exergy input required to power the plant.

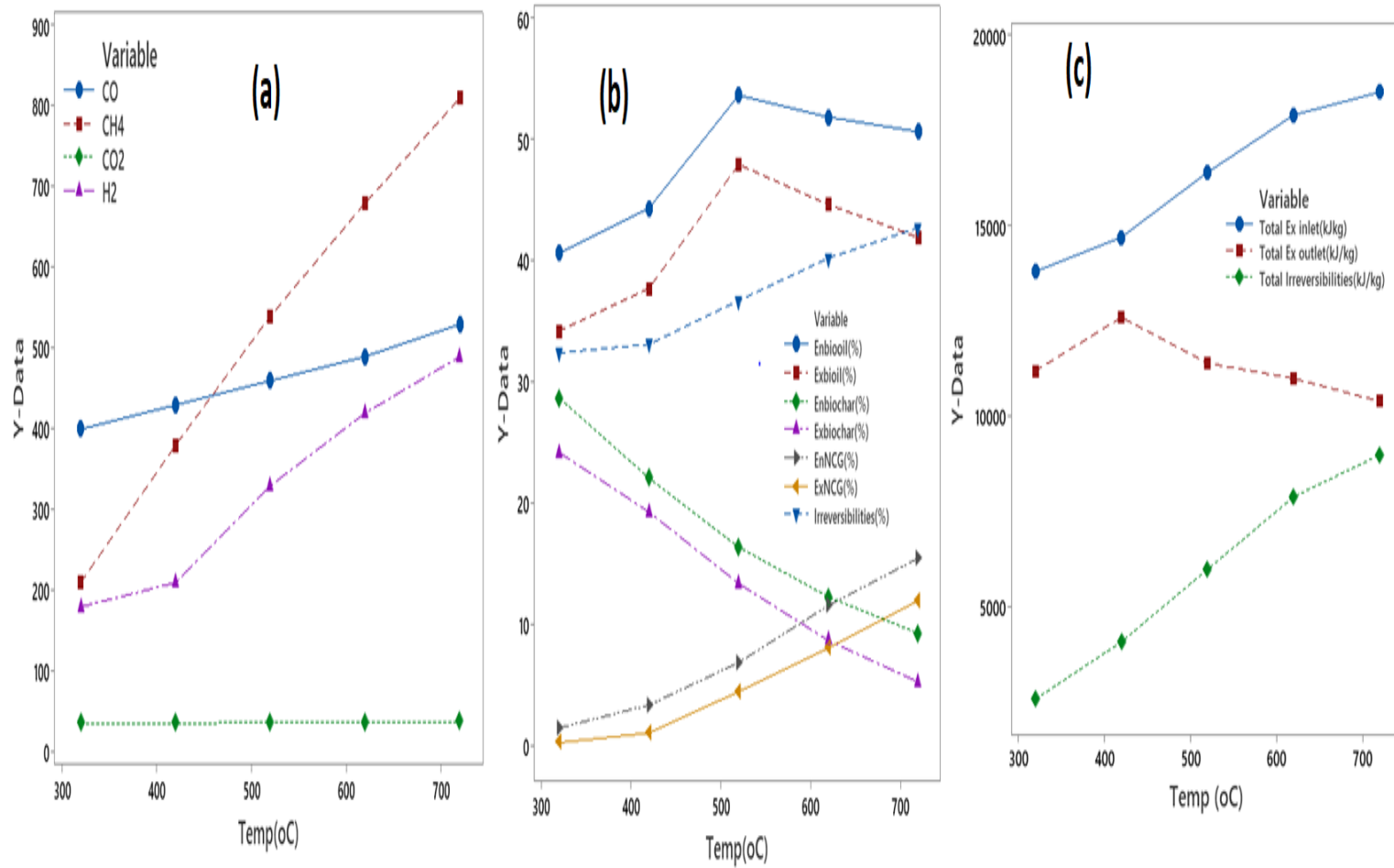


Figure 4.15: (a) Exergy efficiency of individual gases (b) Energy and exergy efficiency of pyrolysis products and irreversibilities against temperature (c) Exergy and irreversibilities against temperature

The energy efficiency increased (Figures. 4.16a-4.16c) at a temperature of 320°C and particle size of 0.1 mm. The efficiency of the bio-oil slightly reduced as the particle size and heating rate increased (Figures. 4.16a-4.16b) despite the continuous increase in temperature. Hence, an increase in energy efficiency occurred with an increase in temperature, but lesser particle size. The decrease in efficiency with a continuous increase in temperature and particle size is attributed to an increase in particle size above 0.5 mm (Figure 4.16a) which leads to incomplete heat transfer and low volatile component formation (Ramesh and Murugavelh, 2020), as well as a secondary reaction caused by a rapid increase in heating rate (Sensoz and Angin, 2008; Youcai and Tao, 2021) An increase in reaction time (5 to 15 min), heating rate (7.5 to 12.5°C/min), and particle size (0.1 to 0.3 mm) increased the energy and exergy efficiency of bio-oil yield (Figures. 4.16c-4.16d) due to faster and uniform heat transfer as well as large volatile formation, and complete pyrolysis process. Thereby leading to an increase in the energy efficiency of bio-oil yield (Peters *et al.*, 2015a; Wang *et al.*, 2020; Ramesh and Murugavelh, 202). Further increase in these operating parameters leads to a sharp decrease in energy and exergy efficiency of bio-oil yield due to thermal resistance built up in the biomass at high particle size, which widens the temperature gradient inside the biomass and reduces heat transfer between the hot and cold material (Guedes *et al.*, 2018; Etika *et al.*, 2019). The exergy efficiency of the bio-oil increased at the beginning with a low reaction time and temperature (Figure 4.16e). The efficiency dropped with an increase in reaction time and temperature due to large vapour escaping from the reactor (Singh *et al.*, 2020).

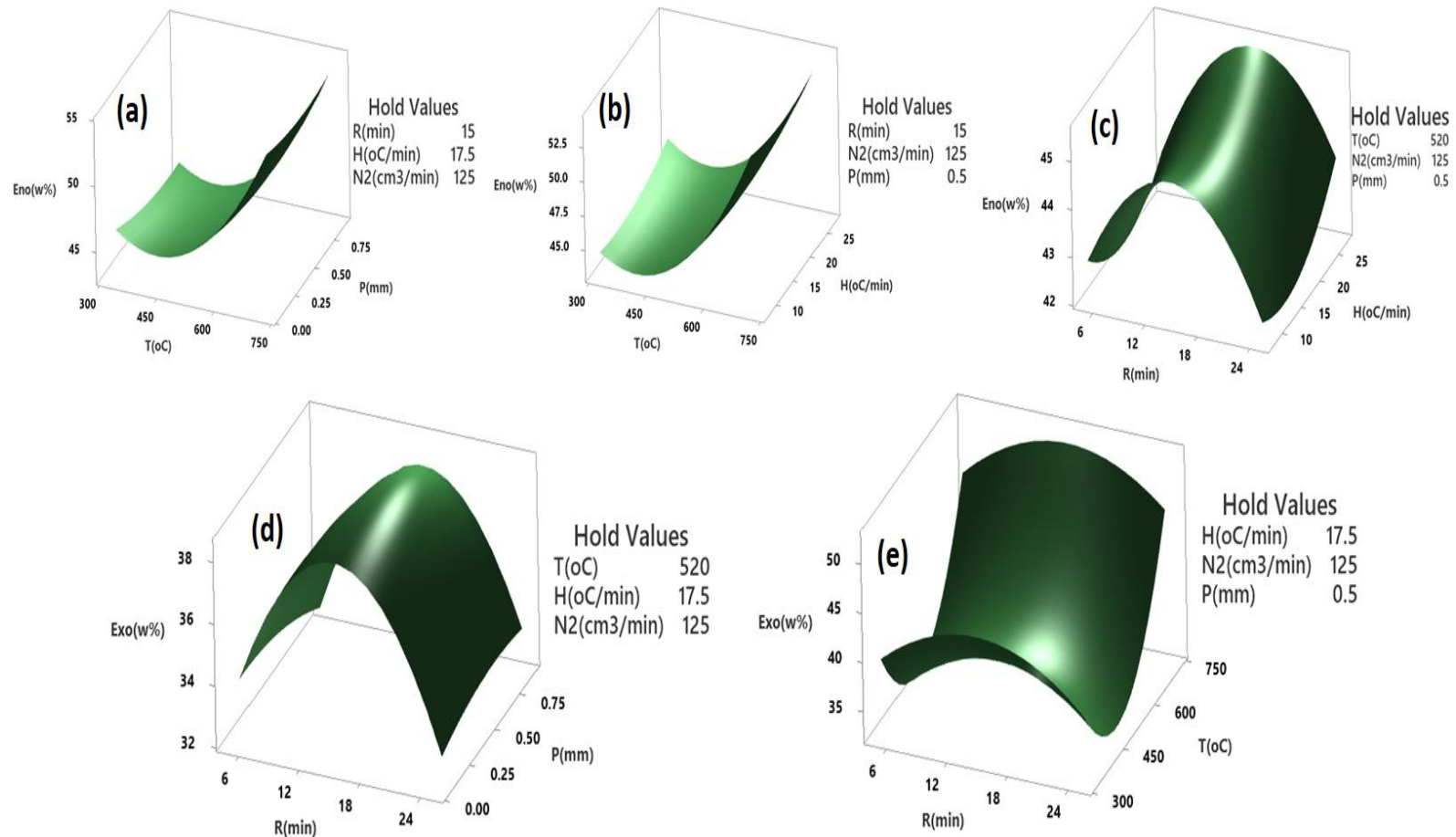


Figure 4.16: Influence of (a) temperature and particle size on the energy efficiency of bio-oil yield (b) temperature and heating rate on the energy efficiency of bio-oil yield (c) reaction time and heating rate on the energy efficiency of bio-oil yield (d) reaction time and particle size on exergy efficiency of bio-oil yield (e) reaction time and temperature on exergy efficiency of bio-oil yield.

An increase in reaction time (5-20 min) and a slight decrease in nitrogen flow rate positively influence the energy efficiency of biochar yield from 32.8- 34 % (Figure 4.17a) due to secondary reaction that resulted in repolymerization and recondensation of the vapour. In Figure 4.17b, a decrease in particle size ($> 0.3\text{mm}$) coupled with an increase in nitrogen flow rate (25 - 125 cm^3/min), enhanced the energy efficiency of biochar yield (33 - 34.8%). This increase was due to the high heat transfer and complete reaction during the pyrolysis process caused by lower particle size (Youcai and Tao, 2021). A decrease in particle size and increase in reaction time and nitrogen flow rate increased the energy and exergy efficiency of NCG yields. An increase in particle size caused the energy and exergy efficiency to decrease due to incomplete pyrolysis and low devolatilization (Dincer *et al.*, 2021). Likewise, the interaction of nitrogen flow rate and particle size (Figures. 4.17c-4.17f).

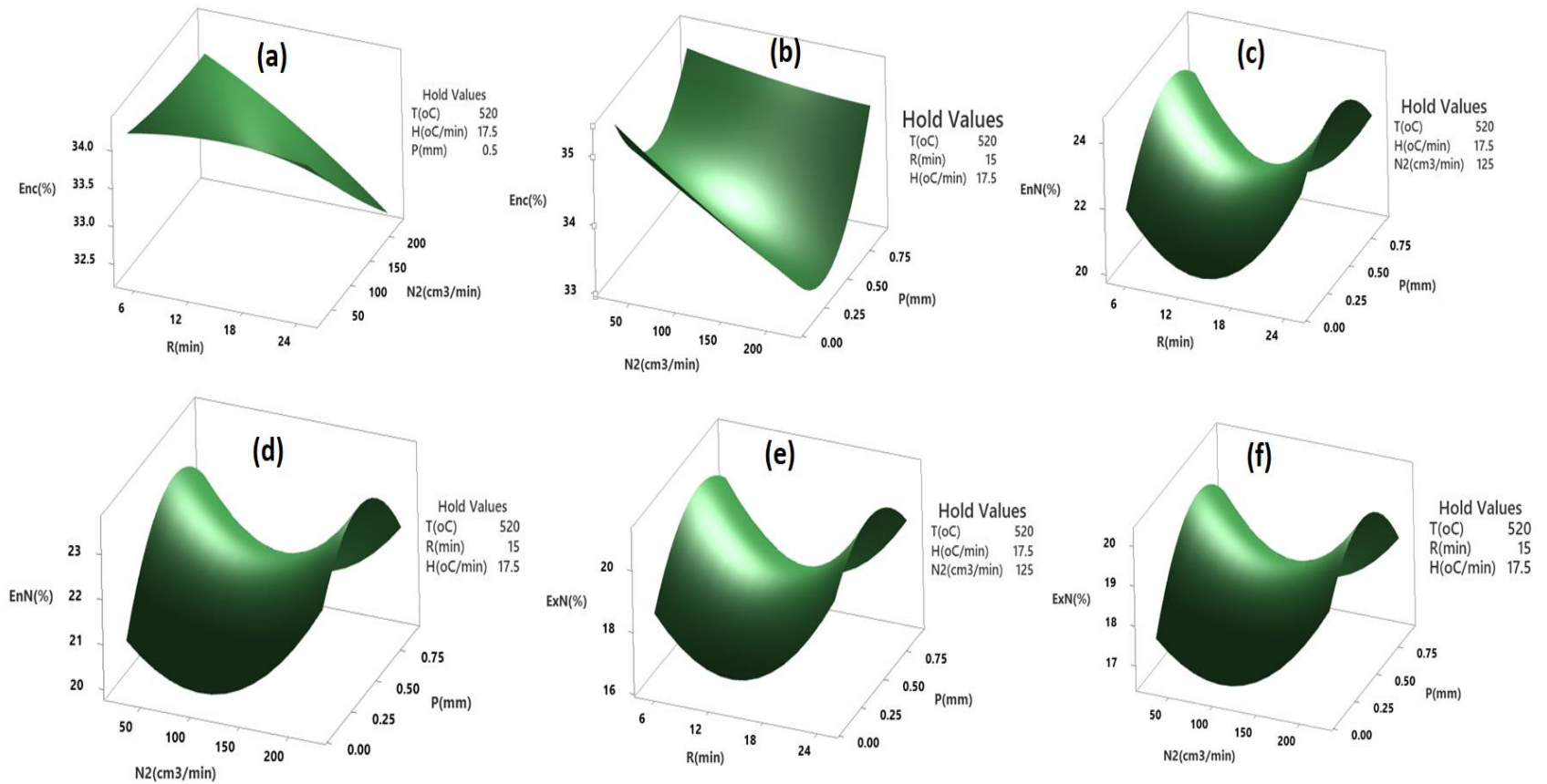


Figure 4.17: Influence of (a) reaction time and nitrogen flow rate on the energy efficiency of biochar yield (b) nitrogen flow rate and particle size on the energy efficiency of biochar yield (c) reaction time and nitrogen flow rate on the energy efficiency of NCG yield (d) nitrogen flow rate and particle size on the energy efficiency of NCG yield (e) reaction time and particle size on exergy efficiency of NCG yield (f) nitrogen flow rate and particle size on exergy efficiency of NCG yield.

4.16 Optimization of operating parameters on energy and exergy efficiency of products of pyrolysis

Figures 4.18-4.20 present the results of the optimization of the pyrolysis operating parameters for bio-oil, biochar and NCG yields. The optimum value of energy and exergy efficiency of bio-oil yields are 46.9 and 44.2 % at temperature, reaction time, heating rate, nitrogen flow rate, and particle size of 623.0°C, 15 min, 10.7 °C/min, 117.9 cm³/min, and 0.5 mm respectively (Figure 4.18). In the case of energy and exergy efficiency of biochar yield, the optimum is 33.34 and 30.56 % at a temperature, reaction time, heating rate, nitrogen flow rate, and particle size of 320°C, 20.4 min, 24.9°C/min, 25 cm³/min and 0.9 mm respectively (Figure 4.19), while that of NCG yield are 13.4 and 9.5% at a temperature, reaction time, heating rate, nitrogen flow rate and particle size of 691.7°C, 5 min, 7.5 °C/min, 225 cm³/min and 0.1 mm respectively (Figure 4.20). Table 4.10 depicts the summary of the optimized value of the operating parameters as well the pyrolysis yields obtained from experimental runs and design expert software (RSM). The optimized value obtained from the response surface methodology (RSM) closely correlates with the experimental data (Table 4.14). Hence, the mathematical model can be utilized to predict the energy and exergy efficiency of pyrolysis yields accurately.

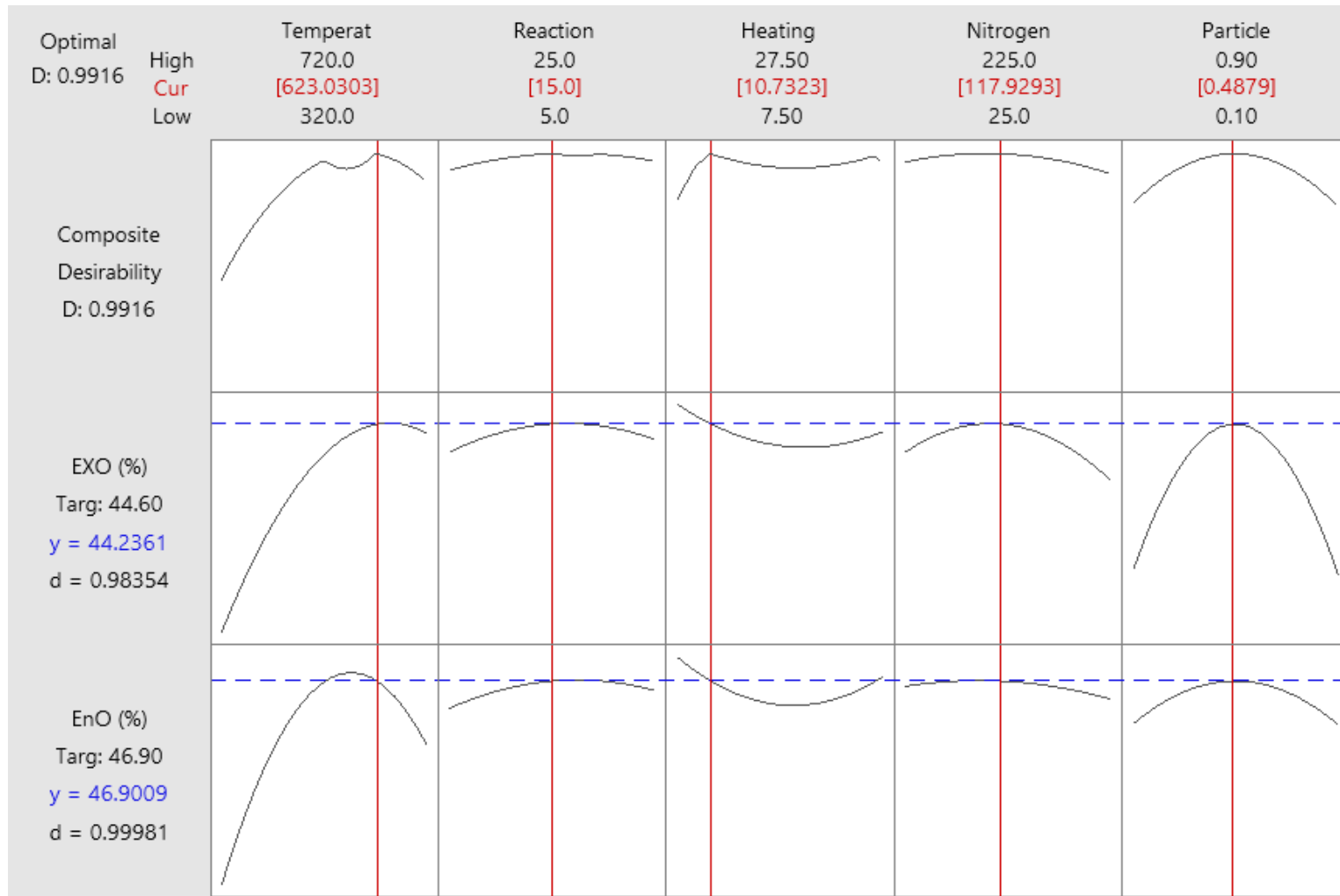


Figure 4.18: Optimization of energy and exergy efficiency of bio-oil yield

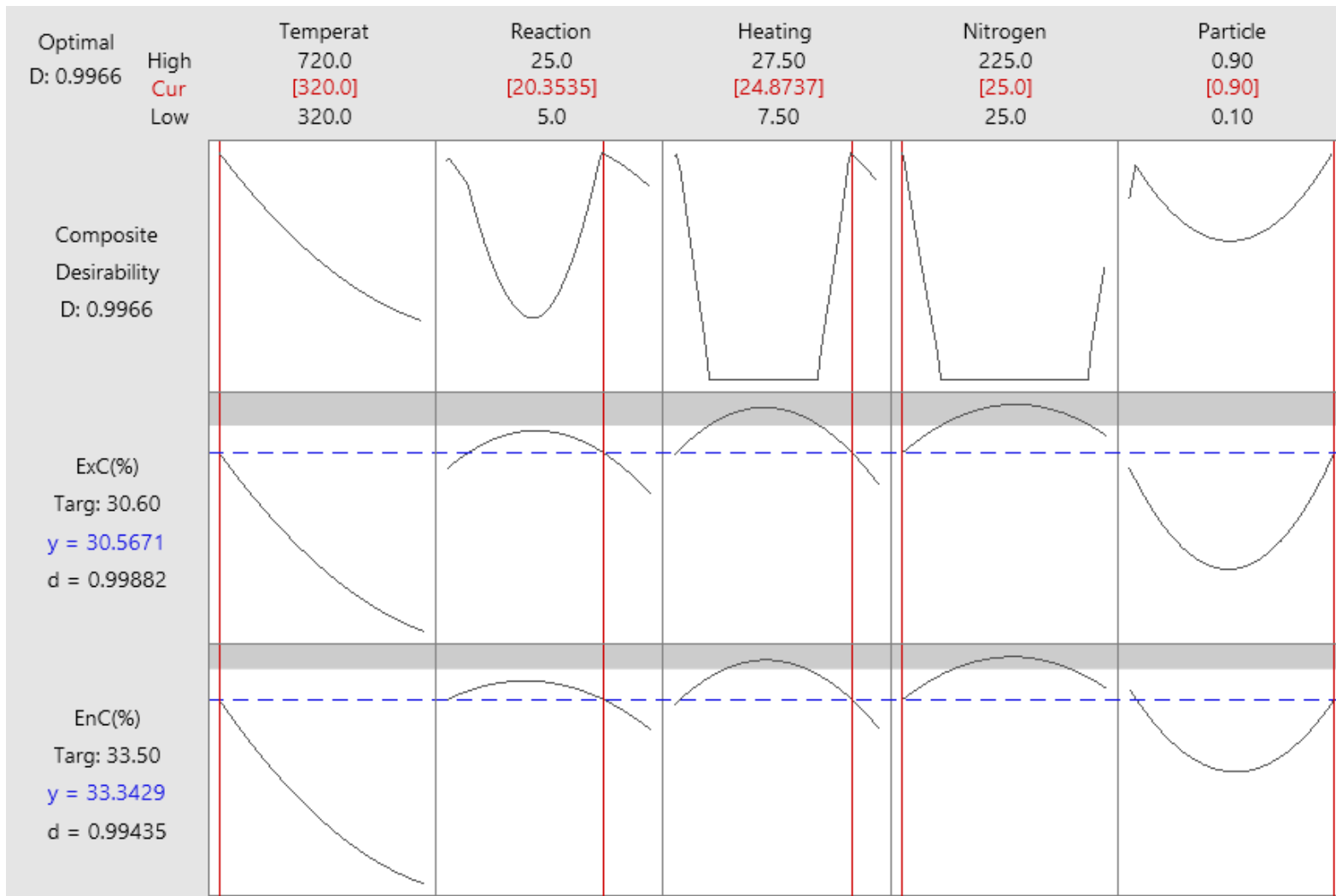


Figure 4.19: Optimization of energy and exergy efficiency of biochar yield

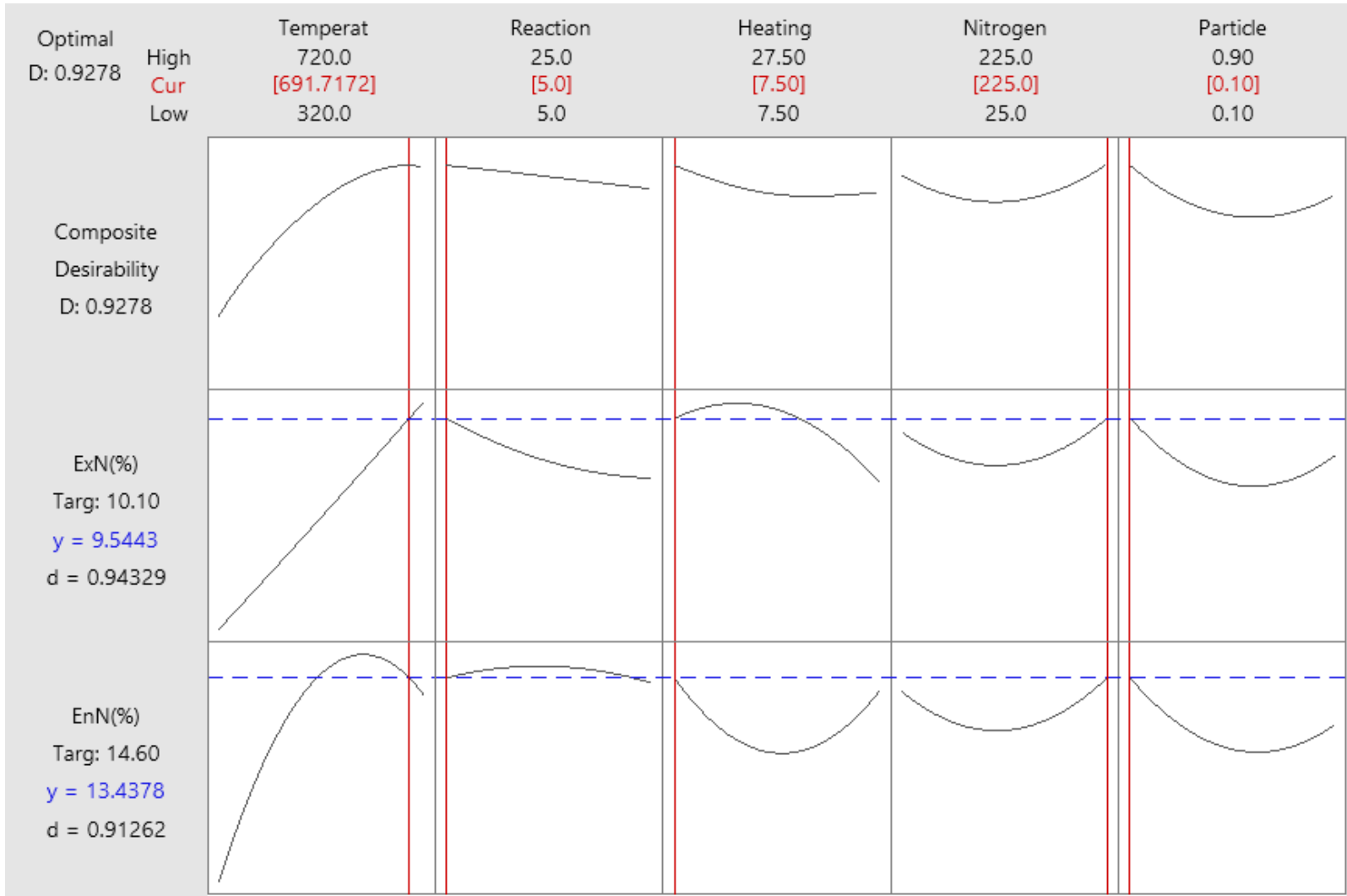


Figure 4.20: Optimization of energy and exergy efficiency of non-condensable gases yield

Table 4.14: Summary of optimization of operating parameters for energy and exergy efficiency of product of pyrolysis

Efficiency (%)	T(°C)	R(min)	H(°C/min)	N(cm³/min)	P (mm)	Yield_{experimental}	Yield_{optimization}
E _{nBO}	623.1	15	10.7	117.9	0.5	47.4	46.9
E _{xBO}	720	5	7.5	126	0.1	44.6	44.2
E _{nBc}	631.1	25	27.5	225	0.3	33.5	33.3
E _{xBc}	631.1	25	27.5	225	0.3	30.2	30.6
E _{nNCG}	320	9.2	21	111.1	0.9	13.8	13.4
E _{xNCG}	320	9.2	21	111.1	0.9	10.1	9.5

4.17 Physicochemical Properties of the Bio-oil Samples

Table 4.15 depicts the physicochemical properties of the bio-oil produced from PKS, SCB and SBW at optimum operating conditions. The HHV for PKS was 21.23 MJ/kg which is slightly close to 19.11 and 16.21 MJ/kg reported by Asadullah *et al.* (2013) and Abnisa *et al.* (2011). In the case of SCB, the HHV (29.99 MJ/kg) agreed well with 27.84 MJ/kg reported Varma and Mondal *et al.* (2017). Similarly, the HHV of 30.02 MJ/kg recorded for SBW in this study is in consonant with 29.52 and 29.60 MJ/kg reported by Chukwuneke *et al.* (2019) and Oyebanji *et al.* (2020) for fast pyrolysis of Mahogany and Ironwood. The HHV obtained in this study is lesser than the HHV of diesel (42-44 MJ/kg) and gasoline (44-46 MJ/kg) due to the increase in moisture contents in the bio-oil samples (Mohammed *et al.*, 2017; Chukwuneke *et al.*, 2019). This high moisture content was attributed to saponification and hydrolysis in the bio-oil yield (Joseph *et al.*, 2014). SBW possessed the peak HHV, next to SCB, while PKS has the least HHV due to their low carbon content (41.2 wt%) and high oxygen content (49.83 wt%). The density of the bio-oil at 40°C for PKS, SCB and SBW are 1.04, 0.915 and 0.96 g/cm³ respectively. These values correlate very well with the density specification of fuel oil (0.91 g/cm³), furnace oil (0.92 g/cm³) and heavy fuel oil (0.99 g/cm³) as reported by Oyebanji *et al.* (2018). The density of the bio-oil obtained from PKS is higher than that of SBW, while SCB has the least density. Hence, bio-oil yields from PKS and SBW are heavy crude oil for transformers due to their high density greater than 0.92 g/cm³, while SCB are furnace and fuel oil for automobile vehicles, ships, compressors, turbines, boilers, and machines, etc. The pH level of PKS (2.6), SCB (3.52) and SBW (5.93). The bio-oil is acidic due to the presence of free fatty acids such as phenolic, oleic, carboxylic, octadecanoic acids, etc., in the bio-oil (Varma and Mondal, 2017; Chukwuneke *et al.*, 2019; Laouge *et al.*, 2020). It is advisable to neutralize the bio-oil with alkaline via esterification or saponification process prior to their usage for automobile parts, fuel tanks and fuel for vehicle engines and boilers in order to prevent corrosion and other reactions of the bio-oil (Asadullah *et al.*, 2007; Onal *et al.*, 2017; Gautam and Chaurasia *et al.* (2020). Furthermore, the bio-oil obtained from SBW is a better fuel compared to SCB and PKS because of the low acidic value. The viscosity of the bio-oil @ 40°C are 2.6, 7.7 and 5.4 for PKS, SCB and SBW. The moderate viscosity of the bio-oil helps to prevent poor atomization, partial ignition of the oil, contamination of the lubricating oil with an unbiocharred deposit during their utilization of fuel for vehicle engine and formation of extreme carbon

residue on the injection nozzles and ignition chamber (Sensoz and Angin, *et al.*, 2008; Oyebanji *et al.*, 2022). The flash and pour points are 78 and -8 for PKS, 67 and -10 for SCB and 72 and +7 for SBW. The values recorded for PKS and SBW are close to diesel engines whose flash and pour points are 72 and -4 respectively. Similarly, the flash and pour points for SCB agreed very well with furnace oil whose values are 68 and +6. The lower the flash points the more flammable and bio-oil is the bio-oil samples (Oyebanji *et al.*, 2021). Hence, SCB is more flammable and volatile, followed by SWB, while PKS is least flammable and volatile.

Table 4.15: Physico-chemical Properties of the bio-oil produced from PKS, SCB and SBW at Optimum Operating Condition

Properties	PKS	SCB	SBW
Appearance	Dark brown	Dark brown	Pale brown
pH	2.6	3.52	5.93
Water content (wt%)	45	37	24.5
Density (g/cm ³)	1.04	0.915	0.96
Iodine value (mgKOH/mg)	98.80	118.3	136.5
Viscosity @ 40 ⁰ C (cst)	2.6	7.7	5.4
Carbon (wt%)	41.2	66.8	52.63
Hydrogen (wt%)	8.61	6.44	6.51
Nitrogen (wt%)	0.3	0.54	0.38
Sulphur (wt%)	0.06	0.06	0.08
Oxygen (wt%)	49.83	26.16	40.48
HHV (MJ/kg)	21.32	29.64	29.19
Flash point	78	68	72
Pour point	-8	+7	-4
Cetane index	34.1	35.8	37.7
Conradson carbon residue (%)	2.41	4.64	4.06

4.18 Fourier Transform Infrared Spectroscopy (FTIR) of Bio-oil Yields

Figure 4.21 depicts the spectra of Fourier Transform Infrared Spectroscopy (FTIR) of bio-oil yields from intermediate pyrolysis of PKS, SCB, and SBW at optimum operating condition over a wavenumber range between 500-4000 cm^{-1} in the spectrum analysis, while Table 4.16 present the functional group, molecular weight, transmittance and appearance extracted from Figure 4.21 through the aid of FT-IR biochar. FT-IR is a chemical analysis technique that detect the different functional group and chemical bonds presence in the samples via the use of infrared rays (Gautam and Chaurasia, 2020). The FTIR comprises different peaks with strong, medium and weak intensity corresponding to various bonds levels in the bio-oil samples. The strong broad peak in the range of wavelength 2900-3700 cm^{-1} is attributed to O-H stretching of Alcohol. The strong bond peak between 2050 and 2150 is ascribed N=C=S stretching indicating the presence of Isothiocyanate, while the peak at 831.2 cm^{-1} is attributed to C-Cl stretching due to the presence of Halo compound. The medium peak at 1416.4 is assigned to O-H stretching vibration of hydroxyl group due to the presence of carboxylic acid and water impurities (Kumar *et al.*, 2019). The weak broad peak at 1636.3 indicates the presence of C-H bending containing aromatic compound. The peak at 1274.7 cm^{-1} is due to C-O bending of aromatic ester. The peak at 1017.6 cm^{-1} is due to C-F stretching of fluoro compound. The functional groups presence is similar to what Abnisa *et al.* (2011) reported. The function group presence in the bio-oil makes it useful as fuel in automobile vehicle, furnace and marine equipment. It can also be utilized as catalyst for the production of drugs and plastic.

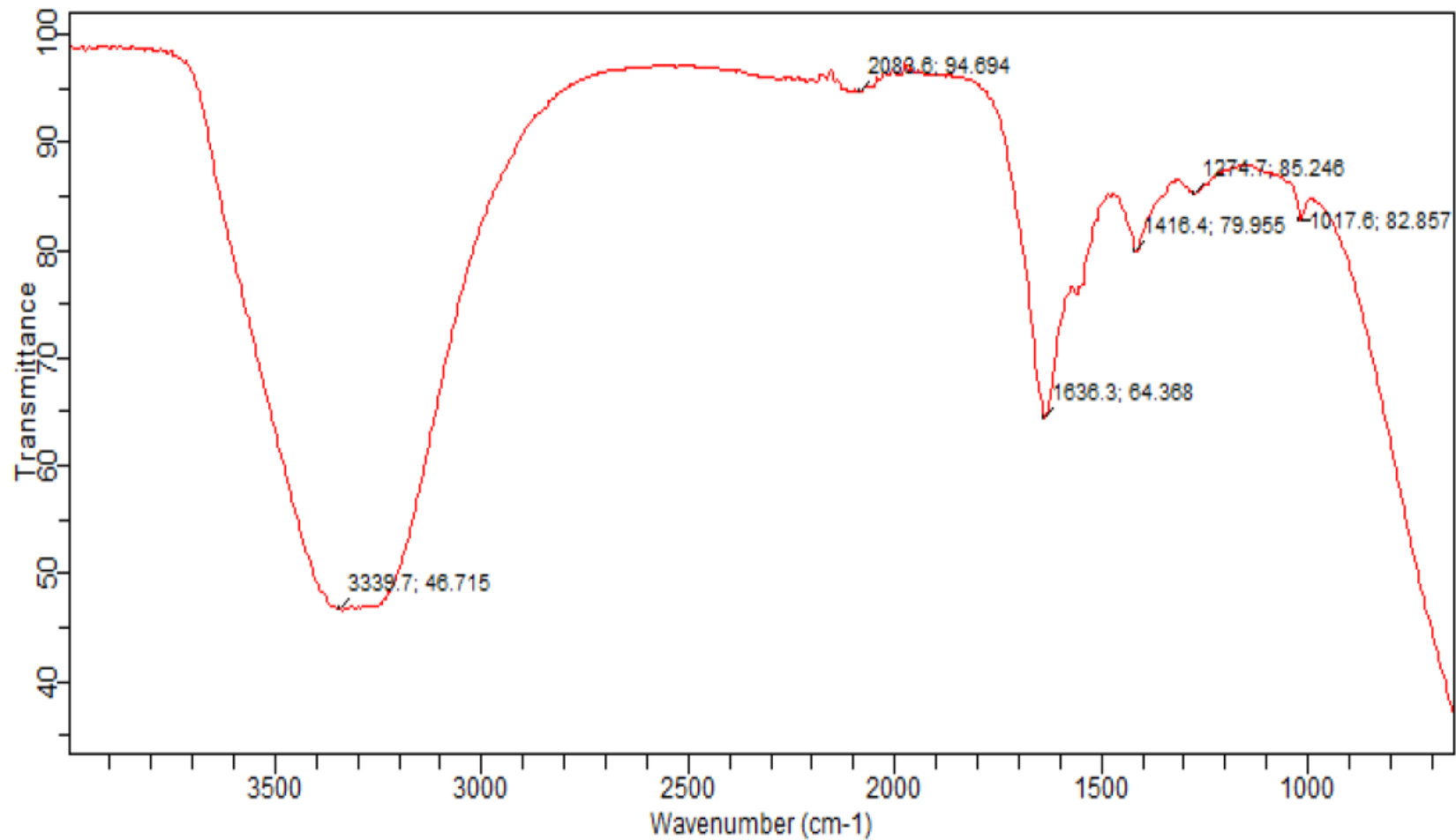


Figure 4.21: FT-IR spectrum of bio-oil yield from pyrolysis of PKS

Table 4.16: Functional group composition of bio-oil yield from pyrolysis of PKS

Functional Group	Wavelength (cm ⁻¹)		Molecular Motion	% Transmittance	Appearance
	Range	Actual			
Alcohols	2900-3700	3339.7	O-H stretch	48.715	Strong broad
Isothiocyanate	2050-2150	2083.6	N=C=S stretch	94.694	Strong broad
Aromatic compounds	1590-1730	1636.3	C-H bend	64.368	Weak broad
Carboxylic acids	1350-1450	1416.4	O-H bend	79.955	Medium broad
Aromatic Ester	1220-1320	1274.7	C-O stretch	85.246	Strong broad
Fluoro compound	980-1060	1017.6	C-F stretch	82.857	Strong broad

The FT-IR spectra of bio-oil yield obtained from intermediate pyrolysis of SCB indicates the amount of peaks with low, medium and high intensity as shown in Figure 4.22, this represents the complex nature of bio-biochar produced from PKS over a wavelength of 500 – 4000 cm^{-1} , while Table 4.17 presents the functional group, molecular weight, transmittance and appearance extracted from Figure 4.22 through the via FT-IR chart. The presence of oxygen-containing functional groups of the O-H bending bond, such as alcohol and carboxylic acid was confirmed by the broad peaks at 45.997 and 32.10 cm^{-1} respectively. The strong broad peak at 1274.7 cm^{-1} indicates the presence of C-O stretching and it is attributed to aromatic ester. The medium broad peak at 63.620 cm^{-1} indicates C=C of Alkene. These results are in consonance with the report of Varma and Mondal *et al* (2017); Guatam and Chaurasis *et al.* (2020). The presence of alkene, alcohol and ester are applicable for energy generation to power heavy equipment, ships, compressor and boilers, while the aromatic ester can be used as sweeteners and in production of perfumes.

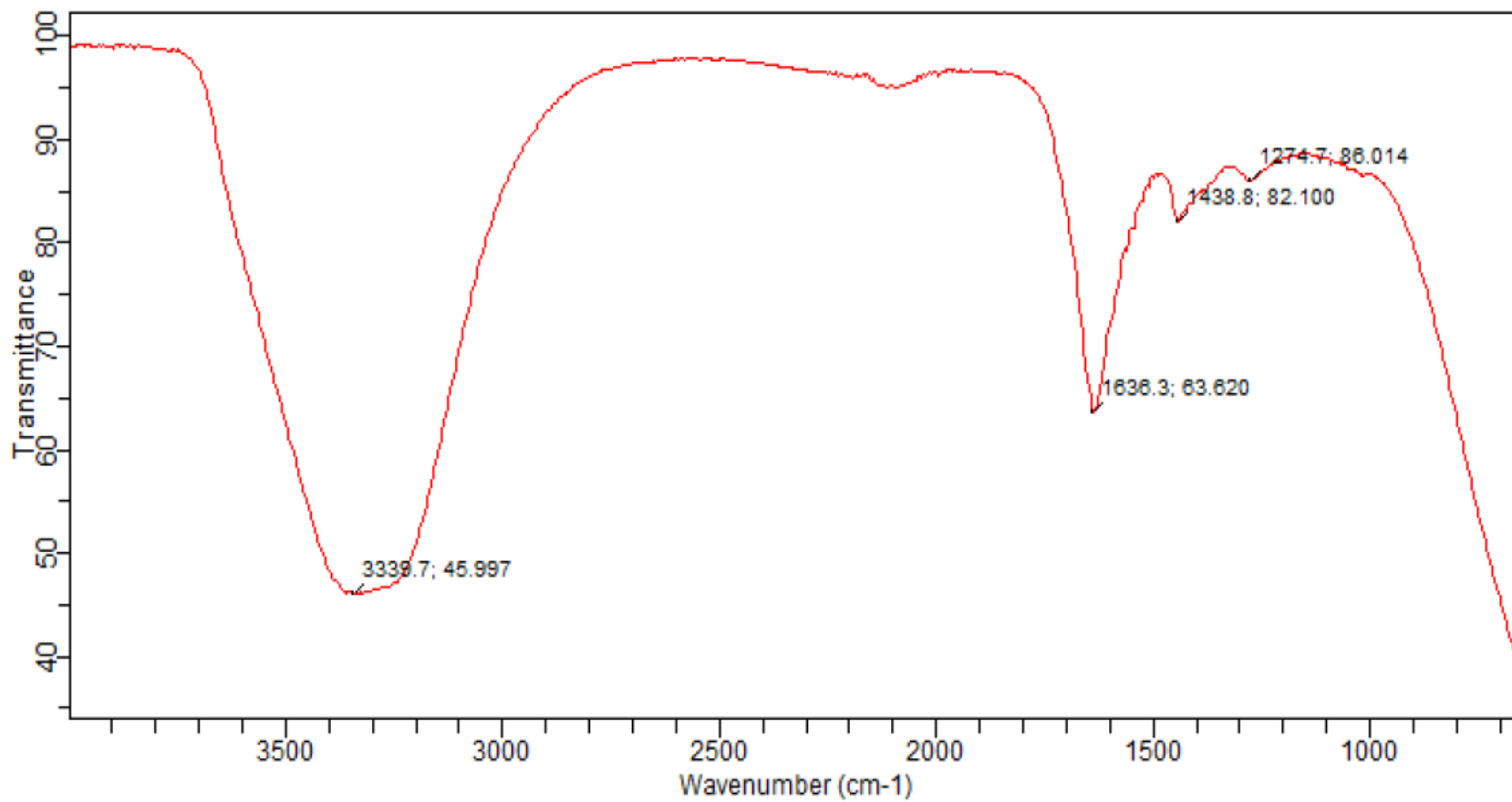


Figure 4.22: FT-IR spectrum of bio-oil yield from pyrolysis of SCB

Table 4.17: Functional group composition of bio-oil yield from pyrolysis of SCB

Functional Group	Wavelength (cm⁻¹)		Molecular Motion	% Transmittance	Appearance
	Range	Actual			
Alcohols	2800-3700	3339.7	O-H stretching	45.997	Strong broad
Alkene	1500-1730	1636.3	C=C stretching	63.620	Medium broad
Carboxylic acid	1350-1450	1438.8	O-H bending	32.10	Medium broad
Aromatic Ester	1250-1300	1274.7	C-O stretching	86.01	Strong broad

Figure 4.23 shows the FT-IR spectrum chart, while Table 4.18 depicts the functional group compositions present in the bio-oil obtained from intermediate pyrolysis of SBW. The C-O stretching of strong absorbance range between 1080-1150 cm^{-1} indicates the presence of secondary alcohol. The peak at 1639.8 is ascribed to N-H bending due to the presence of amine. Isothiocyanate is present when strong broad peaks in the range of 2050–2150 cm^{-1} are caused by C-H=S stretching vibration. A strong peak at 3389.2 cm^{-1} and 1349.3 cm^{-1} with a O-H symmetry was seen, suggesting the presence of Alcohol and phenol respectively, whereas wave number 2400.4 cm^{-1} with a O=C=O stretching was discovered, indicating the presence of carbon (iv) oxide. Aromatic compound C-H is attributed to a very low intensity peak between 1750–1790 cm^{-1} , while a halo compound with C-Cl bending vibrations was found with a wavenumber of 831.2 cm^{-1} . The functional group present in the bio-oil agreed well with the report Chukwunke *et al.* (2019) and Oyebanji *et al.* (2022) reported for woody biomass, sugarcane bagasse and Palm kernel shell. The presence of alcohols in the bio-oil samples is due to thermal degradation of cellulose and hemicellulose content of the biomass samples, while the presence of alkene, phenol and aromatic compound are attributed to the decomposition of lignin content of the biomass samples (Sun *et al.*, 2011; Yorgun and Yildiz, 2015). The presence of alcohol, phenol and Esters present in the constituents are used for the production of biodiesel and raw materials for petrochemical industries, while the carbon (iv) is used for food preservation (Varma and Mondal, 2017).

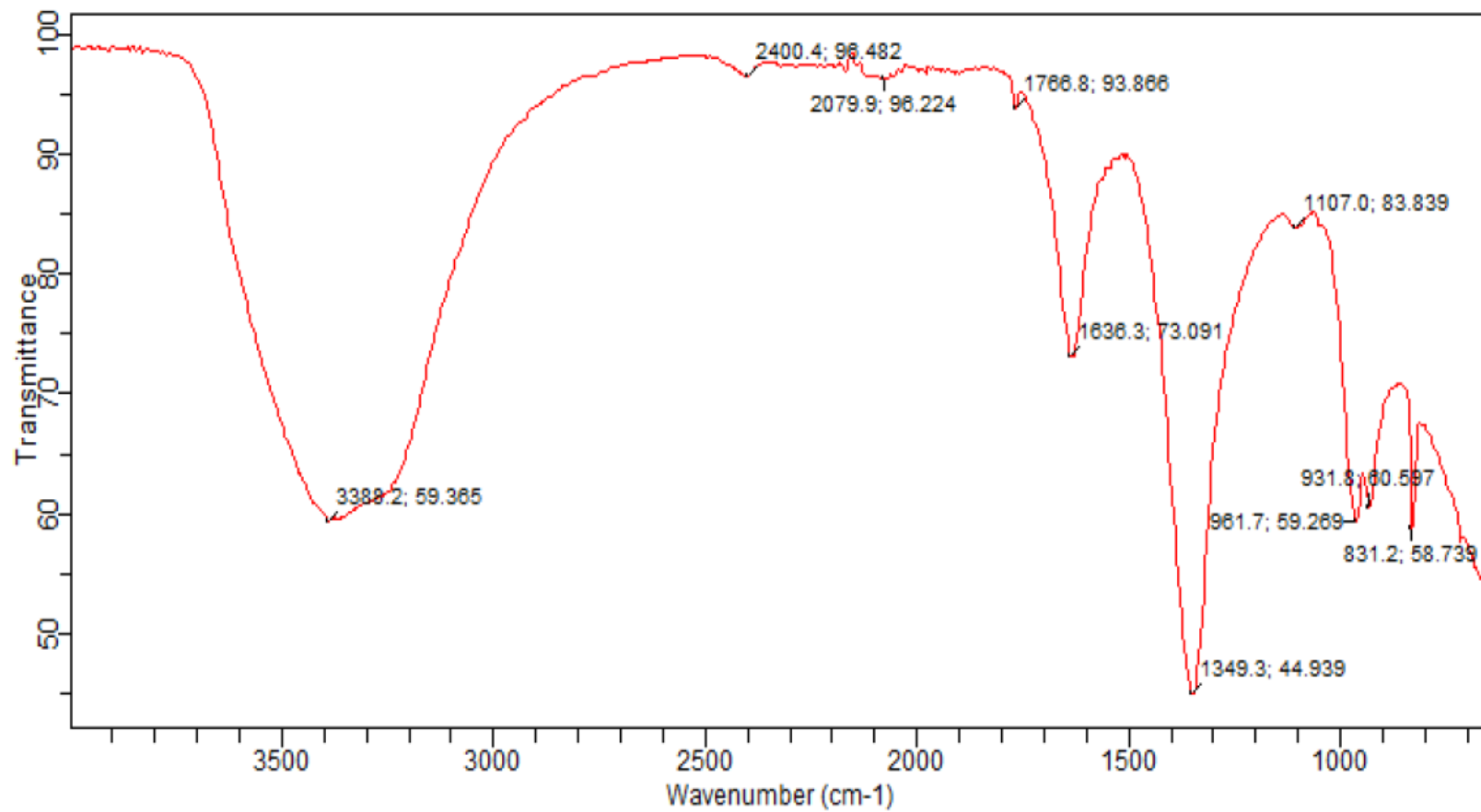


Figure 4.23: FT-IR spectrum of bio-oil yield from pyrolysis of SBW

Table 4.18: Functional group composition of bio-oil yield from pyrolysis of SBW

Functional Group	Wavenumber (cm ⁻¹)		Molecular Motion	% Transmittance	Appearance
	Range	Actual			
Alcohol	2900-3700	3389.2	O-H stretching	59.385	Strong broad
Carbon dioxide	2350-2450	2400.4	O=C=O stretching	98.482	Strong broad
Isothiocyanate	2050-2150	2079.9	N=C=S stretching	98.224	Strong broad
Aromatic compound	1750-1790	1766.8	C-H bending	93.866	Weak broad
Amine	1550-1750	1638.8	N-H bending	73.091	Medium broad
Phenol	1150-1570	1349.3	O-H bending	44.939	Medium broad
Secondary Alcohol	1080-1150	1107.0	C-O stretching	83.839	Strong broad
Alkene	950-1060	961.7	C=C bending	59.289	Strong broad
Alkene	900-950	931.8	C=C bending	60.597	Strong broad
Halo compound	800-850	831.2	C-Cl stretching	58.739	Strong broad

4.19 Fourier Transform Infrared Spectroscopy (FTIR) Spectrum Analysis for Biochar Yields

The various functional groups and chemical bonds present in the biochar samples were determined using Fourier transform infrared spectroscopy (FTIR). The FTIR analytical technique was used to determine infrared spectrum of absorption, emission, and photoconductivity of the biochar samples (Sun *et al.*, 2017). This helps to detect the functional group and chemical bond such as organic, polymeric and inorganic materials, etc. presence in the biochar samples (Mohammed *et al.*, 2017; Gautam and Chaurasia, 2020).

FTIR spectra of bio-biochar, as shown in Figure 4.24, displays the number of peaks with low, medium and high intensity, which indicate the complex nature of bio-biochar produced from PKS over a wavelength of $500 - 4000\text{cm}^{-1}$, while Table 4.19 depicts the functional group, molecular weight, transmittance and appearance extracted from Figure 4. 24, through the aid of FT-IR chart. The most prominent peaks at 3906.3 , 3809.3 , 3749.7 , 3649.7 , 3678.9 and 3600.6 cm^{-1} are originated due to O-H stretching vibrations confirm the presence of alcohol (Yang *et al.*, 2007; Mohammed *et al.*, 2017; Varma and Mondal, 2017). Alcohol can be used as fuels for engine and boilers (Gautam and Chaurasia, 2020). The low intensity peaks in the range of $2740-2750\text{ cm}^{-1}$ arise due to C-H stretching vibration indicate the presence of aldehyde (Saikia *et al.*, 2015). High intensity peak at 2113.4 and 1990.4 cm^{-1} attributes to C=C stretching vibration, which signifies the presence of alkynes and alkenes in bio-biochar, while the medium intensity peak at 1703.4 and 1871.1 cm^{-1} are originated from the aliphatic ketones and aromatic due to C=O and C-H functional groups (Moralı and Sensöz, 2015). Low intensity peaks between 1520 and 1320 cm^{-1} confirm the presence of oxygen containing functional groups of O-H bending bond indicate the presence of carbon dioxide, carboxylic acid, phenol, ester (Saikia *et al.*, 2015). The medium and strong peak at 1025 and 1524.5 cm^{-1} indicates C-N and N-O due to the presence of amines and nitro compound. The very low intensity peaks between 770 and 870 cm^{-1} are ascribed to alkene C=C and halo compound with C-Cl bending vibrations. Phenols are used in nylon and synthetic fiber, plywood, adhesives as well as automobile appliance industries (Ficci, 2012; Lazzari *et al.*, 2016). The presence of alcohol such as methanol, ethanol, propanol and butanol present in the biochar make them useful as oxygenated fuel additives in fossil-based fuels for diesel engines as alternative energy source (Sun *et al.*, 2017; Chen *et al.*, 2019). The biochar

sample can be applied in petrochemical industry and liquid transportation fuel due to the present of alkene, alkyne, carboxylic acids and aliphatic hydrocarbons (Moralı and Sensöz, 2015; Guatam and Chaurasia, 2020). Also, the alkene is utilized in the synthesis of fuels (gasoline, diesel and kerosene), butadiene, detergent, plastic and alcohol (Stauffer *et al.*, 2008).

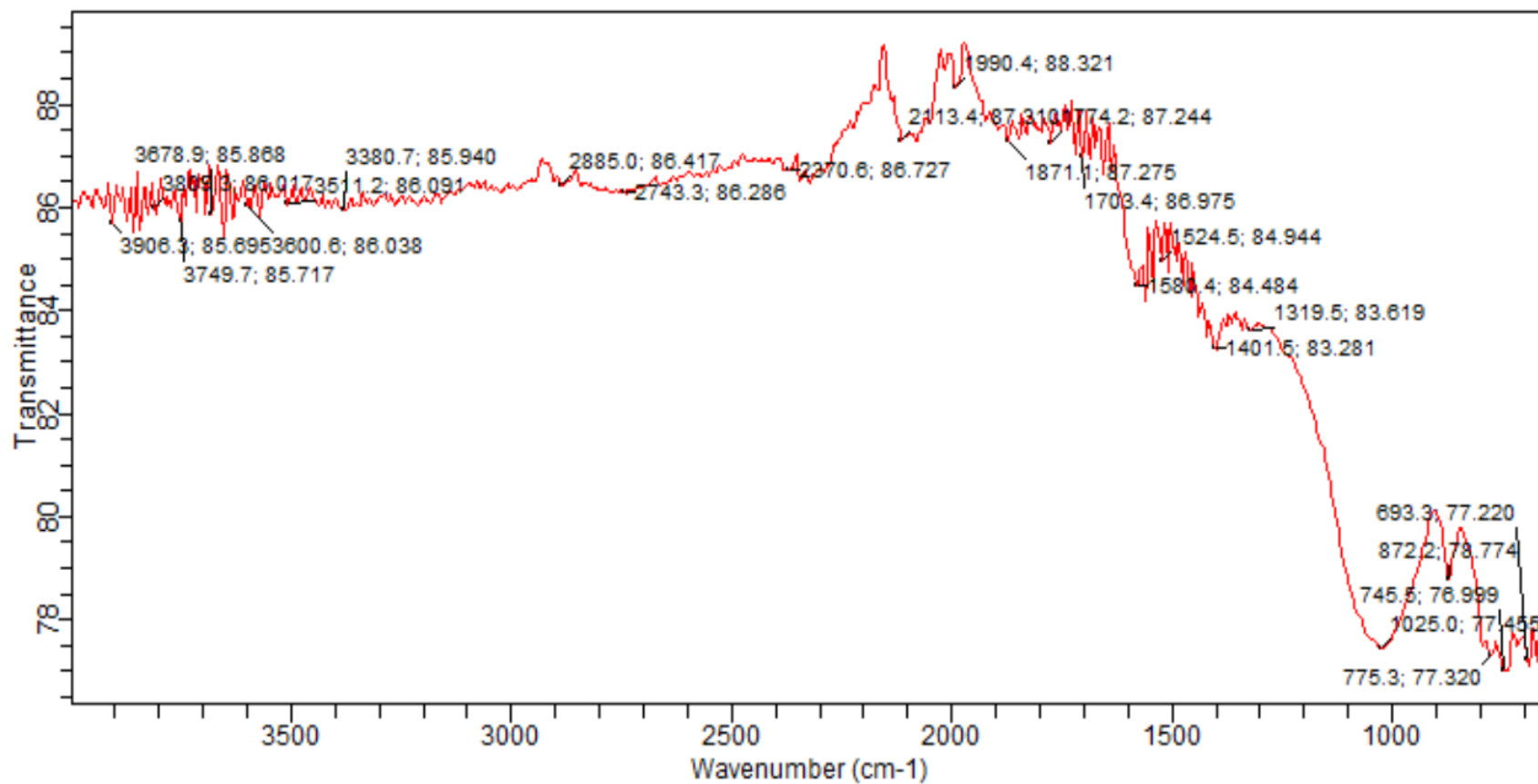


Figure 4.24: FT-IR spectrum of biochar yield from pyrolysis of PKS

Table 4.19: Functional group composition of biochar yield from pyrolysis of PKS

Functional Group	Wave Length (cm ⁻¹)		Molecular Motion	% Transmittance	Appearance
	Range	Actual			
Alcohol	3900-3920	3906.3	O-H stretch	85.695	Medium Sharp
Alcohol	3800-3820	3809.3	O-H stretch	86.017	Medium Sharp
Alcohol	3750-3780	3749.7	O-H stretch	85.717	Medium Sharp
Alcohol	3670-3710	3678.9	O-H stretch	85.868	Medium Sharp
Alcohol	3595-3610	3600.6	O-H stretch	86.038	Medium Sharp
Aliphatic Primary Amine	3350-3400	3380.7	N-H stretch	85.94	Medium
Carboxylic Acid	2880-2900	2885	O-H stretch	86.417	Strong Broad
Aldehyde	2740-2750	2743.3	C-H stretch	86.288	Medium
Carbon dioxide	2365-2380	2370.6	O=C=O stretch	86.727	Strong
Alkyne	2110-2120	2113.4	C≡C stretch	87.31	Weak
Alkene	1990-2000	1990.4	C=C stretch	88.321	Medium
Aromatic Compound	1865-1875	1871.1	C-H bending	87.275	Weak
Vinyl/phenyl Ester	1770-1785	1774.2	C=O stretch	87.244	Strong
Aliphatic Ketone	1695-1710	1703.4	C=O stretch	86.975	Strong

Cyclic Alkene	1575-1585	1580.4	C=C stretch	84.484	Medium
Nitro Compound	1520-1535	1524.5	N-O stretch	84.944	Strong
Carboxylic Acid	1390-1410	1401.5	O-H bending	83.281	Medium
Phenol	1315-1320	1319.5	O-H bending	83.619	Strong
Amine	1020-1027	1025	C-N stretch	77.455	Medium
Alkene	870-875	872.2	C=C bending	78.774	Strong
Alkene	770-779	775.3	C=C bending	77.32	Strong
Halo Compound	740-749	745.5	C-Cl stretch	78.999	Strong
1,4- disubstituted	690-695	693.3	C-H bending	77.22	Strong

Figure 4.25 and Table 4.20 showed the FTIR spectra of functional group in the biochar samples. The medium broad peak at 1341.8, 2996.8, and between 3680 and 3910 cm^{-1} indicates that the biochar contained a chemical compound with a hydroxyl group (O-H), such as phenol, carboxylic acids, and alcohol, which are used as fuels and by-products for industrial applications (Laougé, *et al.*, 2020). The peak at 3600.6 cm^{-1} suggests the existence of N-H stretch containing compounds as aliphatic primary amine are applied in petrochemical industry (Morali and Sensöz, 2015). The peak range from 2365 to 2320 cm^{-1} is ascribed to the O=C=O functional group, while the peak at a frequency in 3168.2 cm^{-1} is due to C-H stretching vibration, which also exist at peak level 2773.1 cm^{-1} showing the existence of aldehyde and alkene (Guo *et al.*, 2015; Bordoloi *et al.*, 2015). The alkynes presence in the biochar is ascribed to the C=C vibration at 2190.7 cm^{-1} , which exists in an organic phase. The presence of a broadband corresponding to 1994.1 cm^{-1} was assigned to N=C=S stretching. The vibration around 1893.5 cm^{-1} present in the organic phase is ascribed C-H bending indicating the presence of aromatic compounds while the peak between 790 and 800 cm^{-1} indicates the presence of 1,2,3-trisubstituted in both cases is due to C-H bending vibrations (Mohammad *et al.*, 2017; Pan *et al.*, 2012). The strong band around 1848.8, 1796.6, 1751.8, 1703.4 cm^{-1} are due to C=O vibration indicating the presence of anhydride, acid halides, esters and aliphatic ketones. Vibration observed around 1561.8 cm^{-1} and 872.2 cm^{-1} in both phases is attributed to C=C stretching and it indicates the presence of cyclic alkenes and alkenes while the peak value at 745.4 cm^{-1} was assigned to C-C bending also indicate the presence of alkenes. The fingerprint between 1400 and 1450 cm^{-1} are ascribed to fluoro compound C-F stretching vibrations while 1215.1 cm^{-1} with C-N stretching indicate the presence of amines. The various chemical compounds in the biochar such as alkenes, alkynes, alcohol, Cyclic Alkene, phenol, ether, ketones and aliphatic can be used in pharmaceutical industries and as fuel for engine, furnaces, turbines, compressors and boilers. Also, the ester content is used to determine oil conversion into biodiesel (Kim *et al.*, 2011; Varma and Modal, 2017).

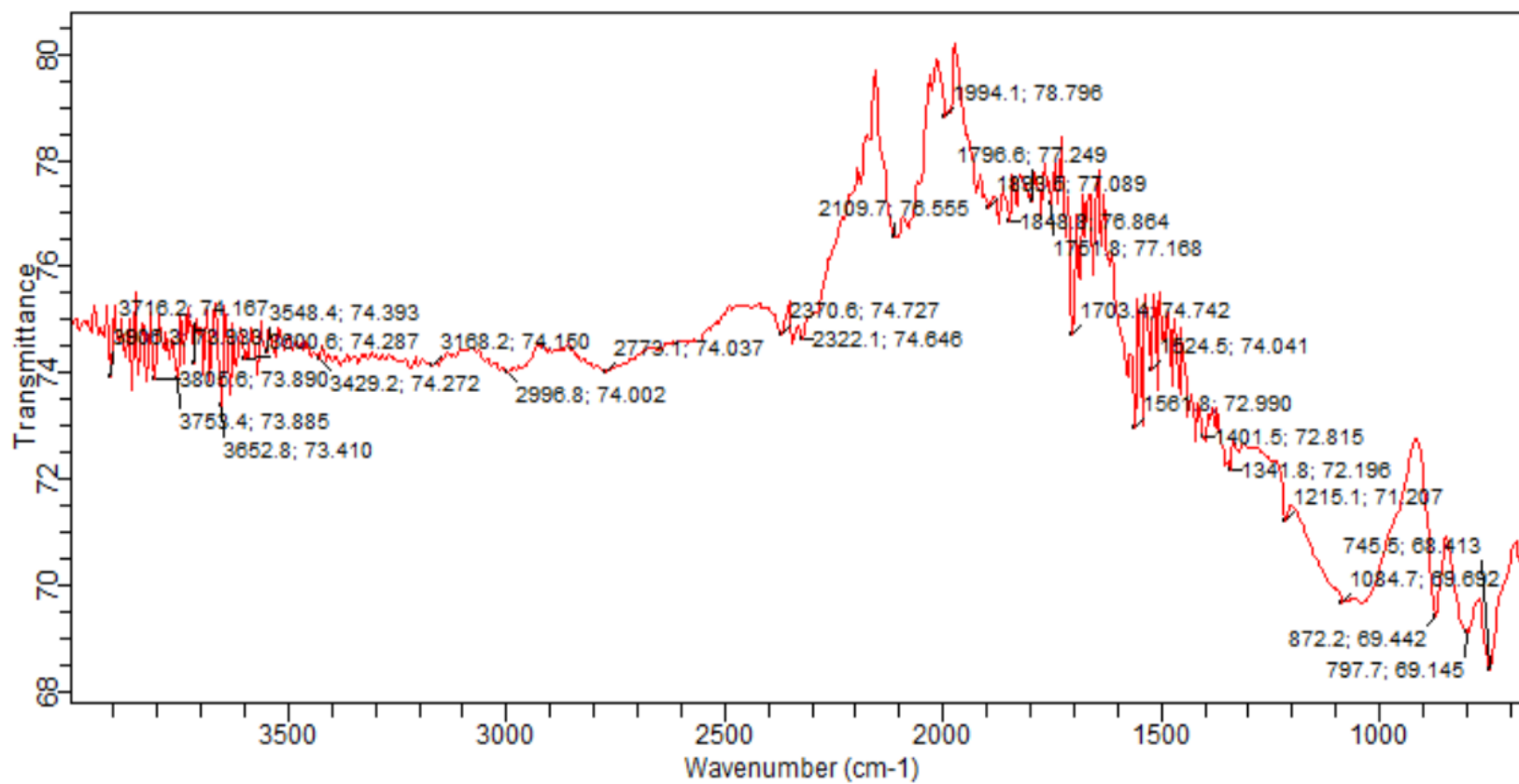


Figure 4.25: FT-IR spectrum of biochar yield from pyrolysis of SCB

Table 4.20: Functional group composition of biochar yield from pyrolysis of SCB

Functional Group	Wave Length (cm ⁻¹)		Molecular Motion	% Transmittance	Appearance
	Range	Actual			
					Medium
Alcohol	3900-3910	3906.3	O-H stretch	73.933	Sharp
					Medium
Alcohol	3800-3810	3805.6	O-H stretch	73.89	Sharp
					Medium
Alcohol	3750-3760	3753.4	O-H stretch	73.885	Sharp
					Medium
Alcohol	3715-3720	3716.2	O-H stretch	74.167	Sharp
					Medium
Alcohol	3680-3660	3652.8	O-H stretch	74.167	Sharp
Aliphatic Primary Amine	3600-3615	3600.6	N-H stretch	74.281	Medium Sharp
					Strong
Alcohol	3425-3430	3429.2	O-H stretch	74,272	Broad
					Medium
Alkene	3165-3170	3168.2	C-H stretch	74.15	Broad
					Strong
Carboxylic Acid	2995-3010	2996.8	O-H stretch	74.002	Broad
Aldehyde	2760-2775	2773.1	C-H stretch	74.037	Medium
			O=C=O		
Carbon dioxide	2365-2375	2370.6	stretch	74.727	Strong

			O=C=O		
Carbon dioxide	2320-2330	2322.1	stretch	74.646	Strong
Alkyne	2100-2115	2109.7	C=C stretch	76.555	Weak
			N=C=S		
Isotriocyanate	1990-1995	1994.1	stretch	78.796	Strong
Aromatic			C-H		
Compound	1890-1895	1893.5	bending	77.089	Weak
Anhydride	1840-1850	1848.8	C=O stretch	76.864	Strong
Acid Halide	1790-1800	1796.6	C=O stretch	77.249	Strong
Esters	1750-1765	1751.8	C=O stretch	77.168	Strong
Aliphatic					
Ketone	1700-1710	1703.4	C=O stretch	74.742	Strong
Cyclic Alkene	1560-1575	1561.8	C=C stretch	72.99	Medium
Fluro					
Compound	1400-1415	1401.5	C-F stretch	72.815	Strong
			O-H		
Phenol	1340-1355	1341.8	bending	72.196	Medium
Amine	1210-1220	1215.1	C-N stretch	71.207	Strong
Aliphatic Ether	1020-1085	1084.7	C-O stretch	69.692	Strong
Alkene	865-880	872.2	C=C stretch	69.442	Strong
1,2,3-			C-H		
trisubstituted	790-800	797.7	bending	69.145	Strong
Alkene	740-755	745.5	C-C bending	68.143	Strong

The functional group compositions present in the bio-biochar from SBW were identified at the wavelength range between 500– 4000 cm^{-1} in the FT-IR Spectrum analysis as shown in Figure 4.26. The possible functional group compositions and possible compounds are tabulated in Table 4.21. The presence of a broadband corresponding to 3842.9 cm^{-1} was assigned to O–H stretching. A broad absorption band observed between 3840-3590 cm^{-1} is credited to the O–H stretching vibrations of alcohol and a strong broad with the range of 2870-2890 cm^{-1} which indicate the presence of carboxylic acid. The peak value between 3150 and the 2970 cm^{-1} region is assigned as stretching of C–H saturated bonds suggesting the presence of alkanes and alkenes. The band absorbance at 2762 cm^{-1} could be caused by C-H stretching groups probably from aldehydes. The band in the region from 2370-2390 cm^{-1} shows the presence of carbon dioxide in the O=C=O stretching group. The peak at 2113.4 cm^{-1} indicates the presence of alkyne with a C=C stretch. The peak at 1990.4 cm^{-1} indicates the presence of isotriocyanate with N=C=S stretch. The observed peak at 1871.1 cm^{-1} shows the presence of C-H bending vibration form of aromatic compounds, while the deformation vibration at 745.5 cm^{-1} indicates the presence of 1,2-disubstituted. The band in the region from 1780-1705 cm^{-1} shows the possible presence of conjugated acid halide, esters and conjugated aldehyde in the C=O stretching group. The peak at 1561.8 cm^{-1} indicates the presence of N-O stretch containing compounds as Nitro compound while the peak at 1401.5 cm^{-1} indicates the presence of C-F stretch containing compound as Fluro Compound and the peak at 1341.8 cm^{-1} indicates the presence of C–N stretch (alkyl) containing compounds as compound amines. The bands in the region from 1200-1090 cm^{-1} shows the possible presence of vinyl ether, aliphatic ether, esters and in the C-O stretching group are used in dye industries (Kim *et al.*, 2011). The absorbance peak at 1036.2 cm^{-1} could be assigned to the Sulfoxide S=O stretching, while the peak at 872.2 cm^{-1} corresponds to the stretching of alkenes C=O. The band between 670-810 cm^{-1} indicates the presence of halo compounds with the C–Cl stretch and C-Br stretch group which is a substitute for one or one hydrogen atom in the hydrocarbon are application in automobile and petrochemical industries such as dry-cleaning solvents and coolants in refrigerators and air conditioners (Guatam and Chaurasis, 2020). The functional groups reported in this study have been detected by (Ogunsanwo *et al.*, 2014; Pinto *et al.*, 2018; Chukwuneke *et al.*, 2019; Oyebanji *et al.*, 2022) for woody biomass samples.

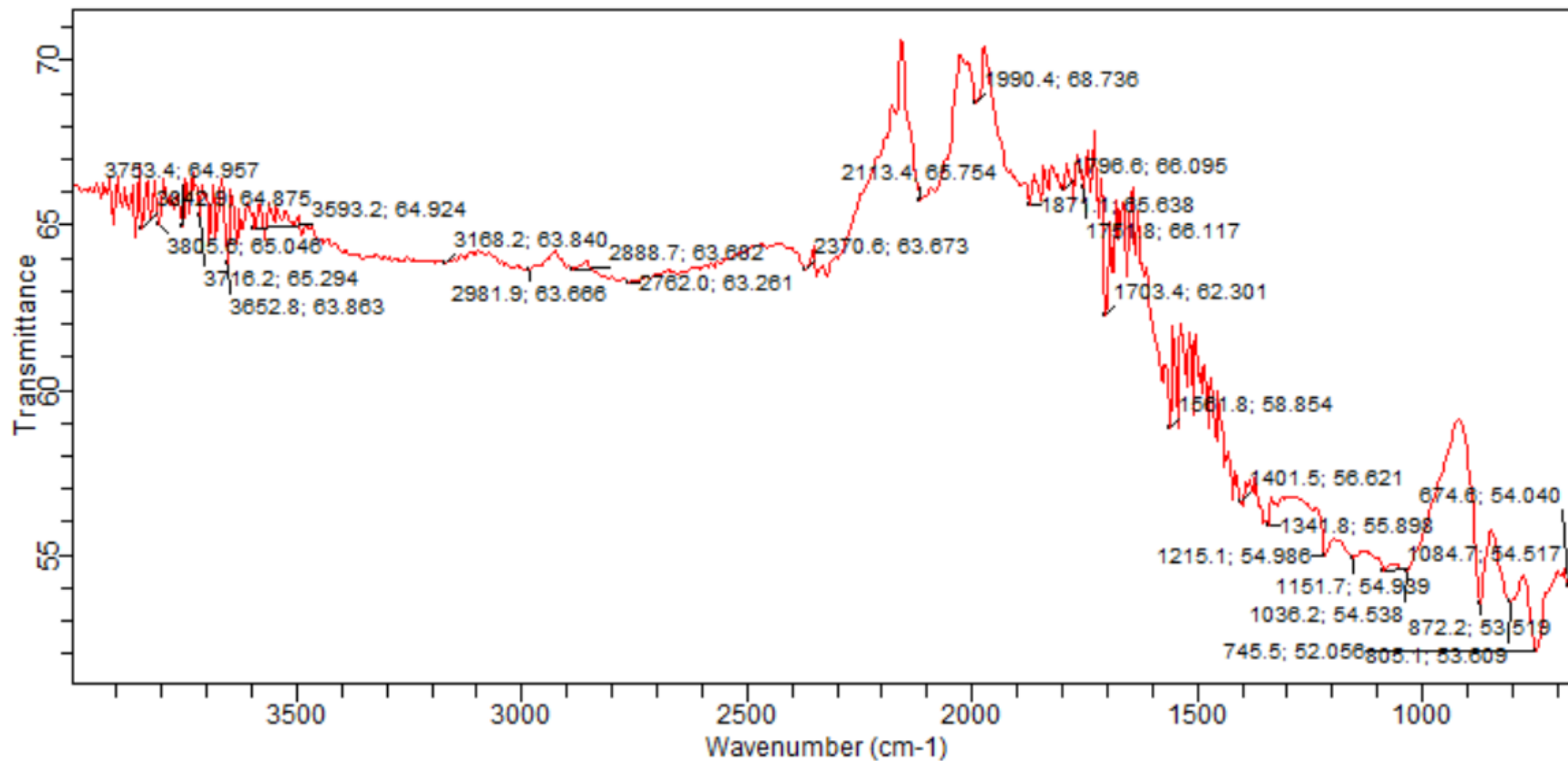


Figure 4.26: FT-IR spectrum of biochar yield from pyrolysis of SBW

Table 4.21: Functional group composition of biochar yield from pyrolysis of SBW

Functional Group	Wave Length (cm^{-1})		Molecular Motion	% Transmittance	Appearance
	Range	Actual			
Alcohol	3840-3850	3842.9	O-H stretch	64.875	Medium Sharp
Alcohol	3775-3810	3805.6	O-H stretch	64.046	Medium Sharp
Alcohol	3750-3760	3753.4	O-H stretch	69.957	Medium Sharp
Alcohol	3715-3725	3716.2	O-H stretch	69.4	Medium Sharp
Alcohol	3650-3665	3652.8	O-H stretch	63.883	Medium Sharp
Alcohol	3590-3600	3593.2	O-H stretch	64.924	Strong Broad
Alkene	3150-3170	3168.2	C-H stretch	63.84	Medium
Alkane	2970-2990	2981.9	C-H stretch	63.666	Medium
Carboxylic Acid	2870-2890	2888.7	O-H stretch	63.682	Strong Broad
Aldehyde	2755-2770	2762	C-H stretch	63.261	Medium
Carbon dioxide	2370-2390	2370.6	O=C=O stretch	63.673	Strong
Alkyne	2110-2115	2113.4	C=C stretch	65.754	Weak
Isothiocyanate	1990-2000	1990.4	N=C=S stretch	68.736	Strong

Aromatic			C-H		
Compound	1870-1890	1871.1	bending	65.638	Weak
Conjugated					
Acid Halide	1780-1800	1796.6	C=O stretch	66.095	Strong
Esters	1750-1760	1751.8	C=O stretch	66.117	Strong
Conjugated					
Aldehyde	1665-1705	1703.4	C=O stretch	62.301	Strong
Nitro					
Compound	1550-1565	1561.8	N-O stretch	58.854	Strong
Fluro					
Compound	1395-1410	1401.5	C-F stretch	56.621	Strong
Aromatic					
Amine	1340-1350	1341.8	C-N stretch	55.898	Strong
Vinyl Ether	1200-1220	1215.1	C-O stretch	54.986	Strong
Haliphatic					
Ether	1150-1155	1151.7	C-O stretch	54.934	Strong
Ester	1050-1090	1084.7	C-O stretch	54.517	Strong
Sulfoxide	1030-1045	1036.2	S=O stretch	54.538	Strong
Alkene	850-890	872.2	C=O stretch	53.518	Strong
Halo					
Compound	800-810	805.1	C-Cl stretch	53.609	Strong
			C-H		
1,2 dis tribute	740-755	745.5	bending	52.056	Strong
Halo					
Compound	670-680	674.6	C-Br stretch	54.04	Strong

4.20 Gas Chromatography and Mass Spectrometry (GC-MS) Analysis for Bio-oil Yields

The chemical composition of the bio-oil obtained from PKS, SCB and SBW was evaluated using GC-MS at Multi-user Science Research laboratory. The GC-MS spectrum of the bio-oil from OBW, SCB and PKS is presented in Figures 4.27-4.29. Bio-oil consists of over 300 compounds (Lok *et al.*, 2019; Laouge *et al.*, 2020). In this study, over 200 different compounds were detected during the GC-MC analysis which is in consonant with what Laouge *et al.* (2020) reported, while the list of components presence in the bio-oil samples that possessed a percentage area peak greater than 0.5 %, with their retention time was tabulated in Table 4.22-4.24, those with lesser percentage peak area were not examined. The bio-oils consists of phenol, oleic acid, 9,17-octadecadienal, undecanoic acid, octadecadienoic acid, methyl esters, butenal and ketones. The most important element present in the bio-oil samples are phenol, oleic acids, 9, 17 – octadecadienoyl, (2), 9, 12 - octadecadienoyl chloride, 9-oxabicyclo (6, 1, 0) nonane with their relative percentage area of 23.82, 32.22, 25.72, 7.09, 27.46, 28.84% respectively. The phenol presence in the bio-oil is also visible during the FTIR analysis. Alkanes and esters compounds are very useful sources of energy which can be used to improve the quality of fuel to power turbines. Furthermore, the present of by-products such as oleic acids, methyl ester, 9,17-octadecdienal, 9-12- octadecadienoyl chloride in the sample makes it useful as fuel for high-speed diesel engines, powering heavy machines, vehicles locomotion, marine equipment, mining types of machinery and manufacturing industries etc. (Mohammed *et al.*, 2017) due to physicochemical properties of the bio-oil presented in section 4.17. The organic phase consisted of phenols and oleic acids which are vital in human health, The study act as defense response such as anti-aging, anti-inflammatory and antioxidant. Also, the derivative of phenol such as bisphenol-A, phenolic resins and caprolactam are utilized in plywood adhesives, nylon, synthetic fiber and automobile appliance industries (Varma and Mondal, 2017). Other compounds like the oleic acids, 7-octanoic acids, cyclopentane undecanoic acids and Octanoid acids possessed some impurities which might corrode and attack automobile engine components. These acids can further be upgraded to other chemicals via esterification and saponification methods etc. to enhance their usefulness for petrochemical and pharmaceutical industries to prevent heart disease, reducing cholesterol, antibacterial and antifungal agent to treat bacterial infections, candidiasis, ringworm, athlete's foot. Also, the oleic acid and tetradecanoic acid can be used in pharmaceutical and dyes industries Hydrocarbons found in the chromatography such as Butenal

are used in manufacture of rubber accelerators, synthetic resins, solvents and plasticizers. The methyl esters present are widely used to replace mineral spirits in the textile screen ink industry and graphics arts industries. Ketones are one of the compounds found in the composition of PKS, this compound are used in the medicine, textile, plastics and nail removers' industries. The presence of hydrocarbons fatty acids, alcohol, esters, phenolic and ketone compounds represents that it can be effectively used as biodiesel (Chukwunke *et al.*, 2019). The phenol, pentaethylene glycol monododecyl ether and methy ester are obtained from the decomposition of lignin in the biomass sample. An innovative replacement for the phenols made from fossil fuels that can be utilized to make adhesives, fire-resistance foams, and resins. The results agreed very well with the report of Varma and Mondal (2017); Laouge *et al.* (2020); and Oyebanji *et al.* (2022).

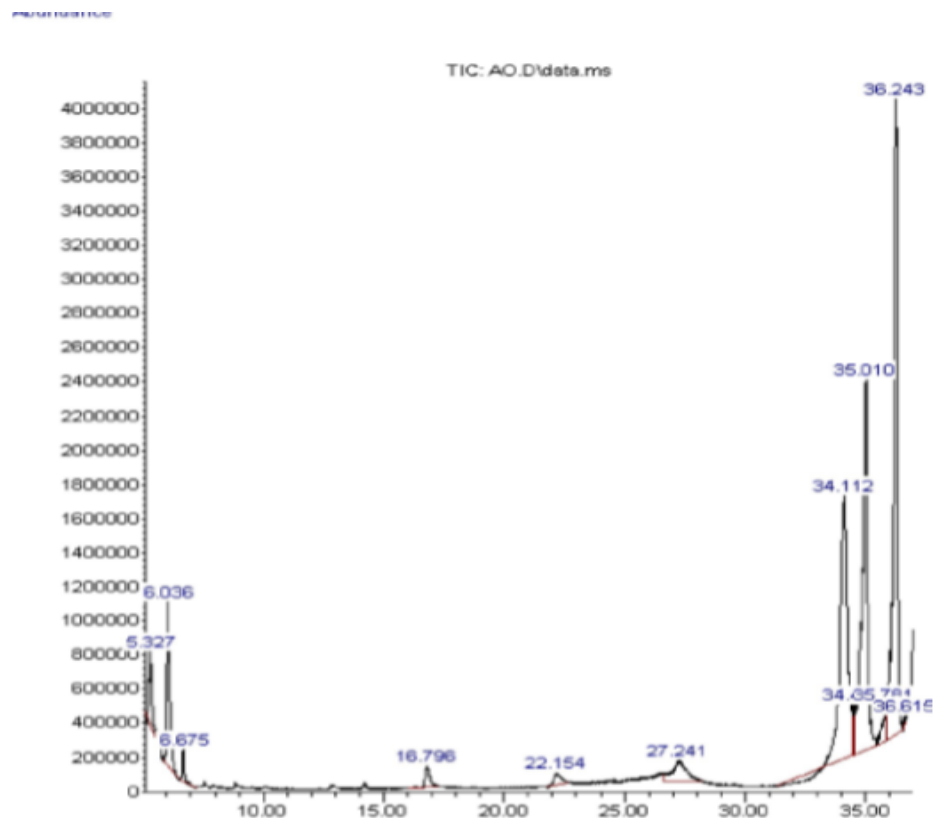


Figure 4.27: GC-MS of bio-oil compound produced from pyrolysis of PKS

Table 4.22: Chemical composition of bio-oil yield from PKS using GC-MS analysis

S/N	Retention Time	Compound Name	Molecular Formula	Molecular Weight	Area %
1	5.327	2-cyclopenten-1-one, 2-methyl	C ₆ H ₈ O	96.0	2.67
2	6.036	Phenol	C ₆ H ₆ O	94.0	6.04
3	6.675	Phenol, 2-methoxy-	C ₁₀ H ₁₂ O ₂	124.0	0.75
4	16.796	11-Octadecenoic acid, methyl ester	C ₁₉ H ₃₆ O ₂	264.0	1.26
5	22.154	15-crown-5	C ₁₀ H ₂₀ O ₅	133.0	1.15
6	27.241	Pentaethylene glycol monododecyl ether	C ₂₂ H ₄₆ O ₆	363.0	3.97
7	34.112	Oleic acid	C ₁₈ H ₃₄ O ₂	264.0	23.97
8	34.489	Oleic acid	C ₁₈ H ₃₄ O ₂	264.0	0.71
9	35.010	9,17-Octadecdienal, (Z)	C ₁₈ H ₃₂ O	235.0	25.72
10	35.781	9,12-Octadecadienoyl chloride, (Z, Z)	C ₁₈ H ₃₁ ClO	264.0	1.44
11	36.243	Oleic acid	C ₁₈ H ₃₄ O ₂	264.0	32.22

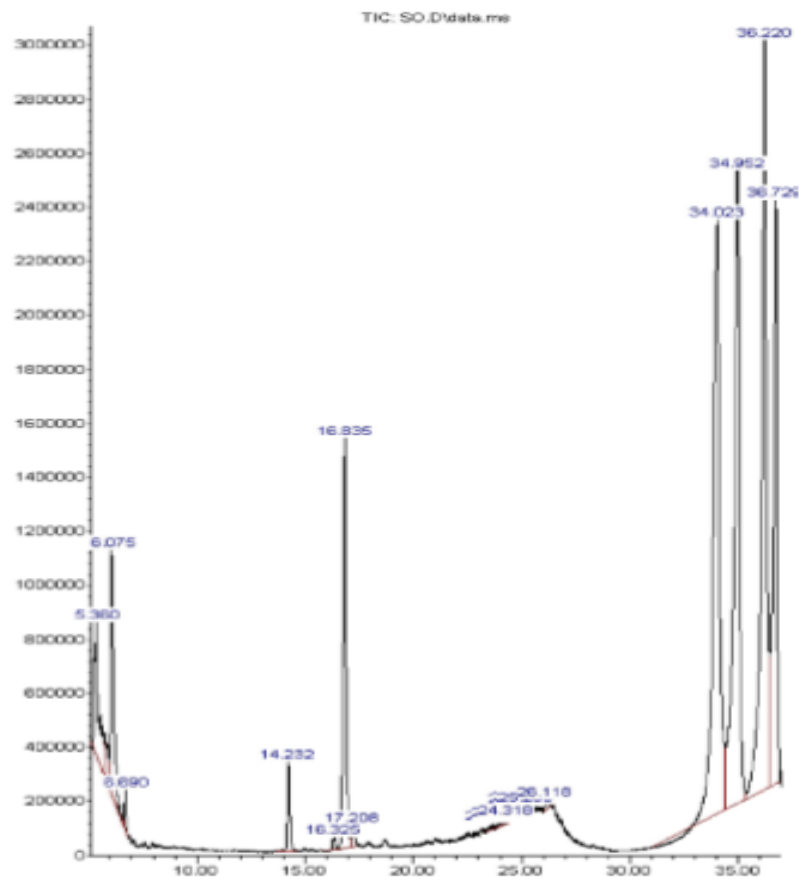


Figure 4.28: GC-MS of bio-oil compound produced from pyrolysis of SCB

Table 4.23: Chemical composition of bio-oil yield from SCB using GC-MS analysis

S/N	Retention Time	Compound Name	Molecular Formula	Molecular Weight	Area %
1	5.360	2-Butenal,2-ethenyl	C ₆ H ₈ O	96.0	3.41
2	6.075	Phenol	C ₆ H ₆ O	94.0	4.54
3	14.232	Hexadecanoic acid, methyl ester	C ₁₇ H ₃₄ O	227.0	1.26
4	16.835	9,12-Octadecadienal	C ₁₈ H ₃₂ O	147.0	7.09
5	34.023	Oleic Acid	C ₁₈ H ₃₄ O ₂ (CH ₃ (CH ₂) ₇ CH-CH(CH ₂) ₇ COOH)	264.0	23.82
6	34.952	Oleic Acid	C ₁₈ H ₃₄ O ₂ (CH ₃ (CH ₂) ₇ CH-CH(CH ₂) ₇ COOH)	264.0	21.58
7	36.220	Oleic Acid	C ₁₈ H ₃₄ O ₂ (CH ₃ (CH ₂) ₇ CH-CH(CH ₂) ₇ COOH)	264.0	22.79
8	36.729	9,12-Octadecadienoyl chloride	C ₁₈ H ₃₁ ClO	264.0	13.30

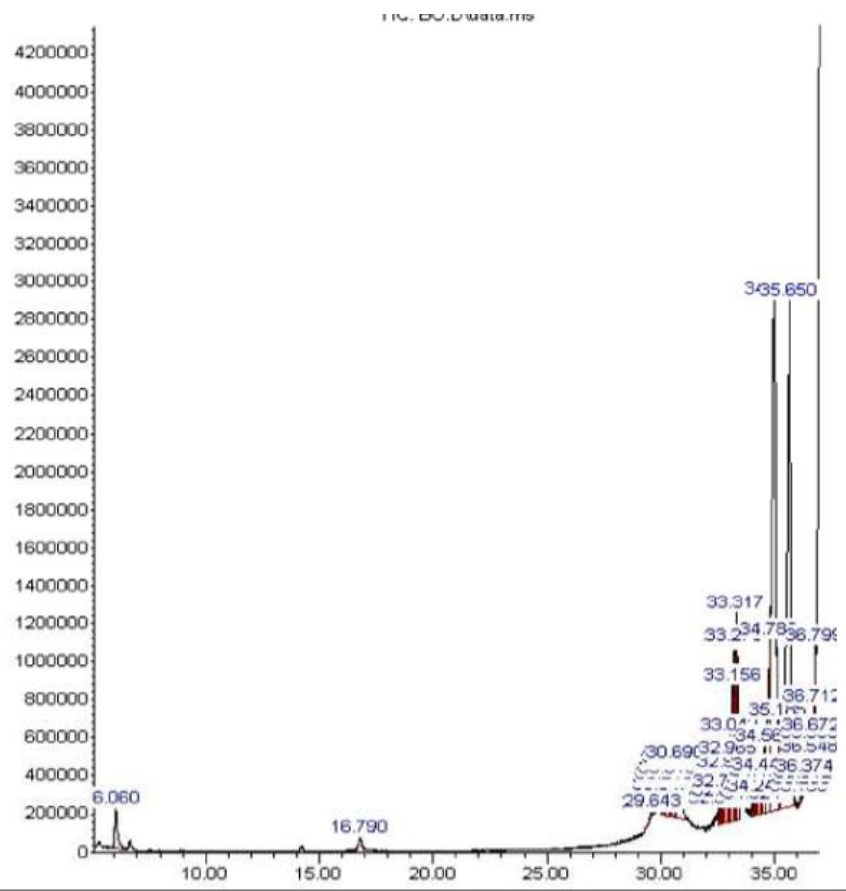


Figure4.29: GC-MS of bio-oil compound produced from pyrolysis of SBW

Table 4.24: Chemical composition of bio-oil yield from SBW using GC-MS analysis

S/N	Retention time (min)	Compound Name	Formula	Molecular Weight	Area %
1	6.060	Phenol	C ₆ H ₆ O	94.0	6.060
2	30.142	Oleic acid	C ₁₈ H ₃₄ O ₂	264.0	0.62
3	30.315	11 (2-Cyclopenten-1-yl) undecanoic acid	C ₁₆ H ₂₈ O ₂	147.0	0.83
4	30.378	Cyclopentaneundecanoic acid	C ₁₆ H ₃₀ O ₂	211.0	1.11
5	30.474	7-Octanoic acid	C ₈ H ₁₆ O ₃	142.0	0.80
6	30.589	Cyclopentaneundecanoic acid	C ₁₆ H ₃₀ O ₂	211.0	1.74
7	30.626	Cyclopentaneundecanoic acid	C ₁₆ H ₃₀ O ₂	211.0	0.89
8	30.690	Oleic acid	C ₁₈ H ₃₄ O ₂	264.0	2.76
9	32.748	Oleic acid	C ₁₈ H ₃₄ O ₂	264.0	0.65
10	32.875	Oleic acid	C ₁₈ H ₃₄ O ₂	264.0	1.14
11	33.042	9-Octadecenal	C ₁₈ H ₃₄ O	248.0	1.49
12	33.156	Cyclopentaneundecanoic acid	C ₁₆ H ₃₀ O ₂	211.0	3.22
13	33.217	Oleic acid	C ₁₈ H ₃₄ O ₂	264.0	2.66
14	33.251	Oleic acid	C ₁₈ H ₃₄ O ₂	264.0	0.91
15	33.270	Oleic acid	C ₁₈ H ₃₄ O ₂	264.0	1.46
16	33.317	Oleic acid	C ₁₈ H ₃₄ O ₂	264.0	6.05
17	34.334	9,12-octadecadienoyl chloride	C ₁₈ H ₃₁ ClO	264.0	0.63
18	34.408	Oleic acid	C ₁₈ H ₃₄ O ₂	264.0	0.61
19	34.560	Oleic acid	C ₁₈ H ₃₄ O ₂	264.0	1.77
20	34.789	Oleic acid	C ₁₈ H ₃₄ O ₂	264.0	6.01
21	34.957	9-Oxabicyclo (6,1,0) nonane	C ₈ H ₁₄ O	126.0	28.84
22	35.185	9,12-octadecadienoyl chloride	C ₁₈ H ₃₁ ClO	264.0	2.02
23	35.650	9,12-octadecadienoyl chloride	C ₁₈ H ₃₁ ClO	264.0	27.46

4.21 SEM Analysis for Biochar Yields

Figures 4.30, 4.31 and 4.32 depicts the surface morphology of PKS (300x, 500x, 1000x, 1500x), SCB (300x, 500x, 1000x, 1500x) and SBW (300x, 500x, 1000x, 1500x) obtained at optimized conditions each possessing three colorations. The SEM analysis helps to determine the product quality, high resolution, and potential failure analysis during their usage as fuel as listed in objective four (4) in this study. The whitish deposits on the surfaces of the biochars was attributed to the inorganic materials such as potassium that were volatilized during the pyrolysis process (Mary *et al.*, 2016; Lee *et al.*, 2017). The biochar samples were observed to exhibited a better microstructure and good morphology. However, biochar obtained from PKS (Figure 4.30) possessed some cleaves, which could be attributed to recondensation and repolymerization during pyrolysis process (Hossain *et al.*, 2017). The cloudy and cloggy formation was noticed in bio-biochar micrographs and rapid efflorescence was noticed during the pyrolysis process which the rapid transfer of heat within the biochars pore (Varma and Mondal, 2017). A heterogeneous porosity and rough texture were noticed in all the biochars due to the emission of volatile matters caused by temperature at 520°C (Pradhan *et al.*, 2016; Varma and Mondal, 2017; Hossain *et al.*, 2017). The present of pores with difference sizes and shape within the biochar surfaces is attributed to the emission of volatile matter during pyrolysis process. Hence, the biochars are applicable as catalyst for energy generation such as dry methane reforming to produce clean fuels e.g., syngas and hydrogen (Foong *et al.*, 2020). Also, the pore in the biochar indicates that the pyrolysis temperature did not lead to total collapse or destruction of the cell walls of the biochars. The high porosity indicates an increase in surface area at adsorptive capacity of the biochar. Thereby, increasing the space for water, pollutant and nutrient retention as reported by Hossain *et al.* (2016) and Varma and Mondal (2017).

The biochar surface exhibited a structural deformation and a change of cell structure was noticed due to the influence of temperature, nitrogen flow rate and reaction time. This finding confirms with what Hossain *et al.*, (2017) reported on microwave pyrolysis of oil palm fiber (OPF). The biochar obtained from SCB, SBW and PKS possess a high, medium and least surface morphology respectively. Hence, SCB is more suitable for energy generation when compared with SBW and PKS due to high surface area and morphology.

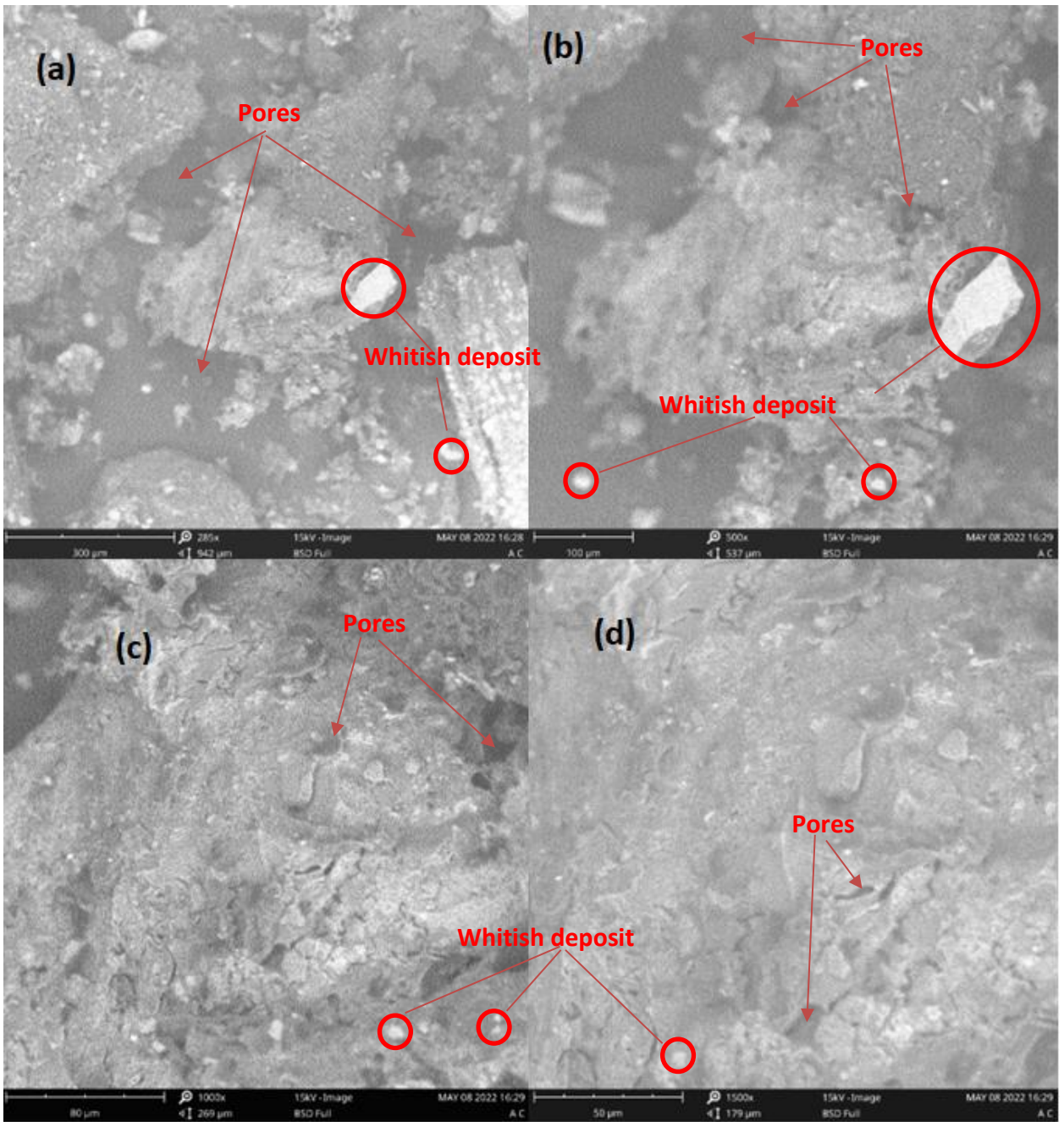


Figure 4.30: SEM Analysis of PKS (a) 300x (b) 500x (c) 1000x (d)1500x

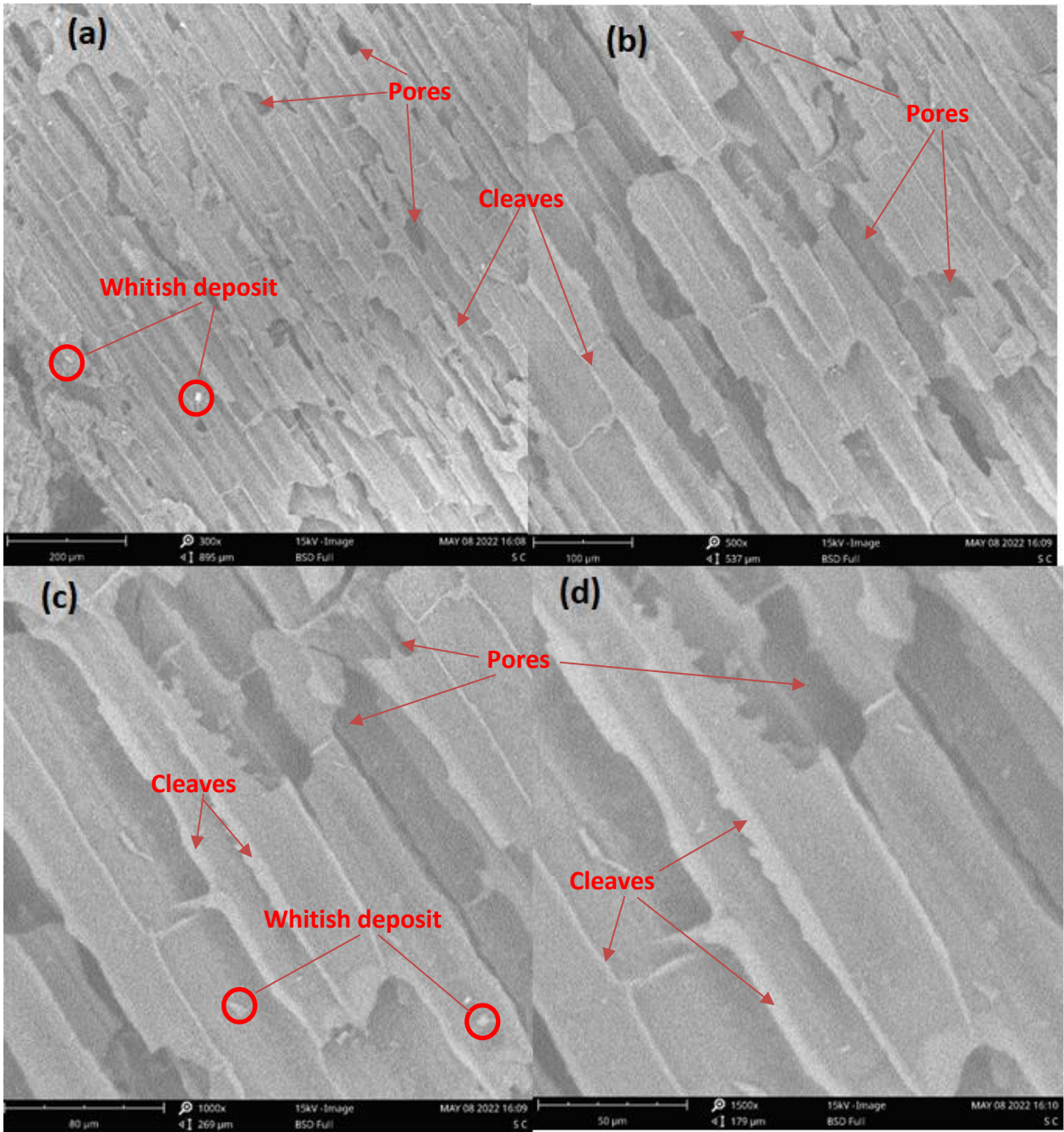


Figure 4.31: SEM Analysis of SCB (a) 300x (b) 500x (c) 1000x (d)1500x

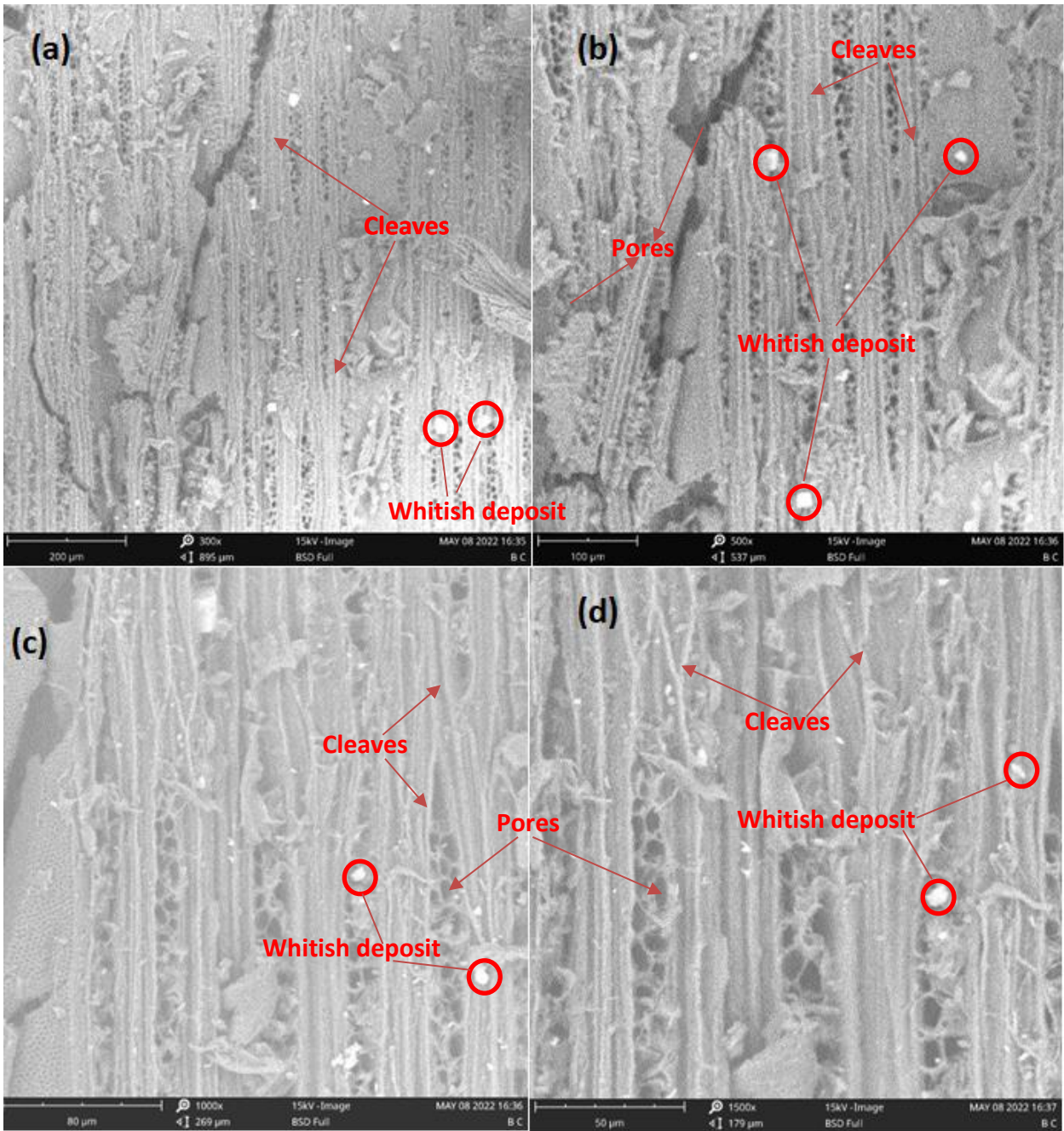
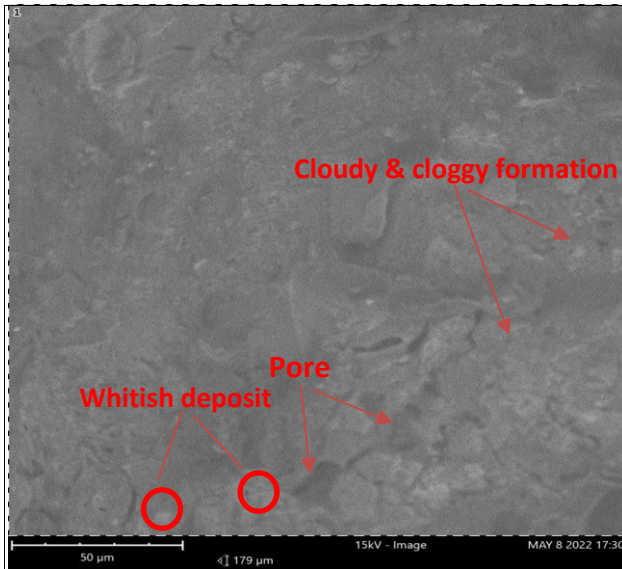


Figure 4.32: SEM Analysis of SBW (a) 300x (b) 500x (c) 1000x (d)1500x

4.22 SEM/EDX Analysis for Biochar Yields

The SEM/EDX images of palm kernel shell (PKS), shea butter wood (SBW) and sugarcane bagasse (SCB) are depicted in Figures. 4.33, Figure 4.34 and Figure 4.35 respectively. The SEM/EDX helps to determine the quality, image morphology, and qualitative and quantitative chemical composition, distribution, crystalline structure and crystal orientations in SEM/EDX analysis in the biochar yield to ascertain their usage as fuel and industrial application.

The SEM image indicated that the sample possessed a unique morphology, good surface texture, and better microstructure (Figures 4.33-4.35). The refined microstructure of the biochar samples was attributed to their high energy potential for use as solid fuel (Tripathi *et al.*, 2020; Foong *et al.*, 2020). The biochar samples possessed two well-defined phases. The whitish and dark grey for PKS sample (Figure 4.33) was noticed to be oval and circular shaped, while those of SBW and SCB samples were in form of stripes or lines along the samples. The samples possessed an abundant pore on the surface with distinct grain size and grain boundaries, indicating their suitability to be utilized as catalysts support for energy application and also as absorbent for use in adsorption-related process such as dye and heavy metal removal in water treatment or nutrient retention in crops cultivation (Foong *et al.*, 2020). The EDS image of the samples further showed the presence of elements such as carbon, calcium, oxygen, silicon, cobalt, nickel, copper, zinc, potassium, aluminum, magnesium, chromium, manganese titanium, sodium, gallium, copper, iron, scandium, phosphorus, titanium. The presence of the sodium, copper, carbon, oxygen, manganese and cobalt present in the biochar would be utilized for energy generation such as fuel cells, electric cables, super capacitors and batteries and for agricultural purposes (Beguin *et al.*, 2009; Xiong *et al.*, 2016; Haggstrom *et al.*, 2018; Kumar *et al.*, 2020b; Adekiya *et al.*, 2020; Sahoo *et al.*, 2021). The EDS image of the biochar obtained from SCB (Figure 4.34) possessed high energy content for potential use as solid fuel relative to PKS (Figure 4.33) and SBW (Figure 4.35) due to its high percentage weight of carbon. Also, the biochar obtained from SCB would exhibit a better mechanical property such as hardness, toughness, tensile strength when compared to PKS and SBW due to their high carbon contents. Hence, it can burn easily without irregular deformation (Foong *et al.*, 2020).



Element Number	Element Symbol	Element Name	Atomic Conc.	Weight Conc.
52	Te	Tellurium	6.55	32.87
6	C	Carbon	57.70	27.25
20	Ca	Calcium	11.99	18.89
8	O	Oxygen	15.65	9.85
14	Si	Silicon	3.72	4.11
27	Co	Cobalt	1.05	2.44
19	K	Potassium	0.89	1.37
13	Al	Aluminium	0.89	0.94
12	Mg	Magnesium	0.87	0.83
24	Cr	Chromium	0.37	0.77
25	Mn	Manganese	0.32	0.69

FOV: 179 μm, Mode: 15kV - Image, Detector: BSD Full, Time: MAY 8 2022 17:30

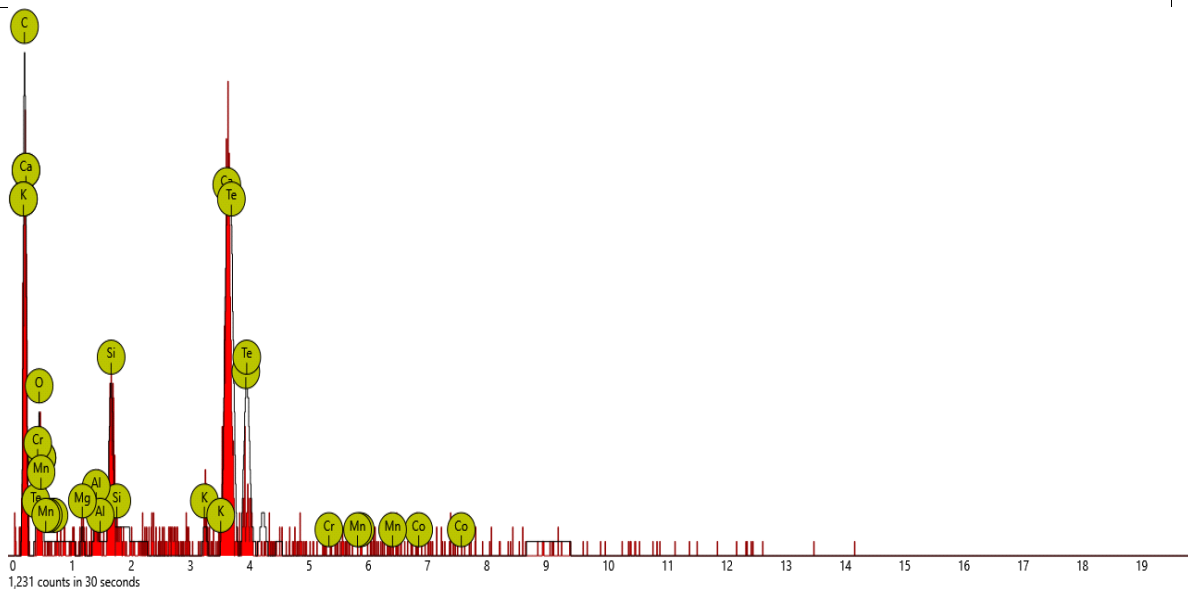


Figure 4.33: SEM/EDX Analysis of PKS.

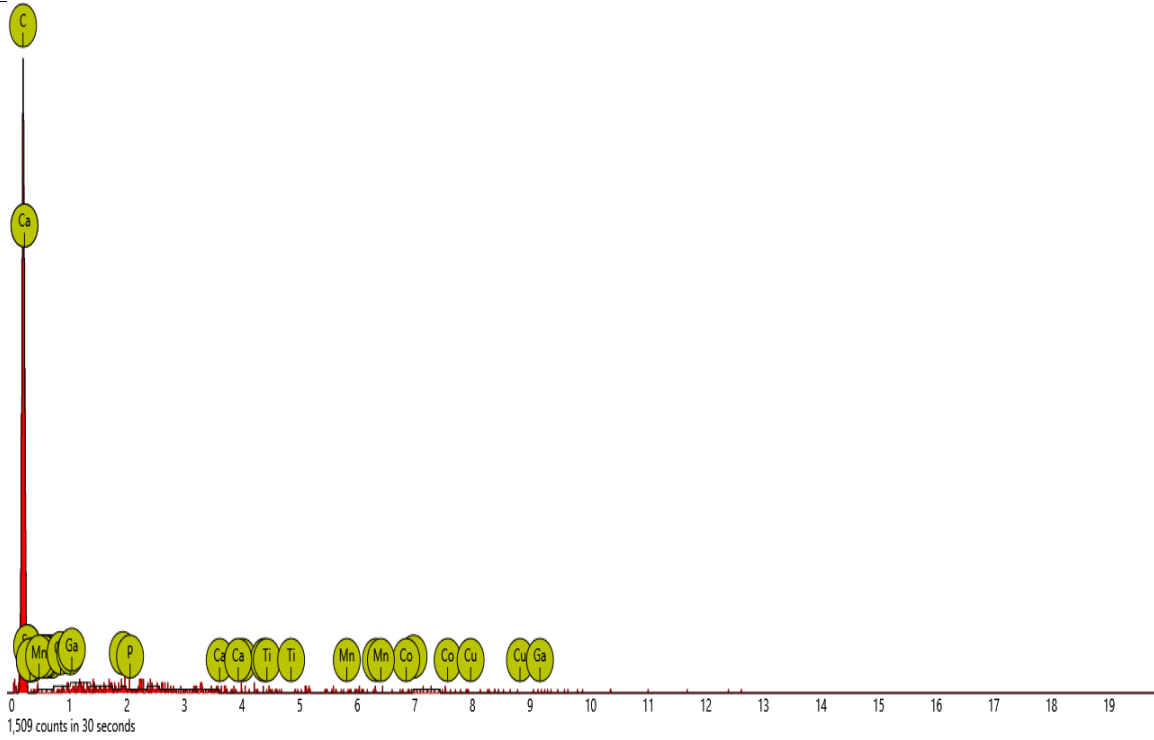
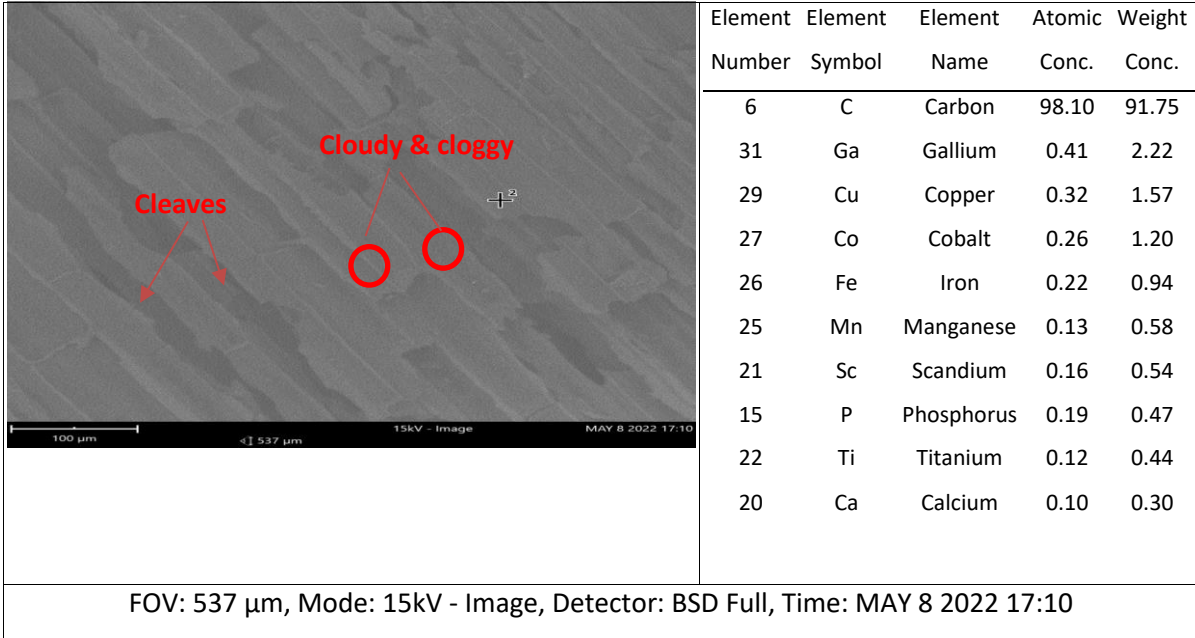
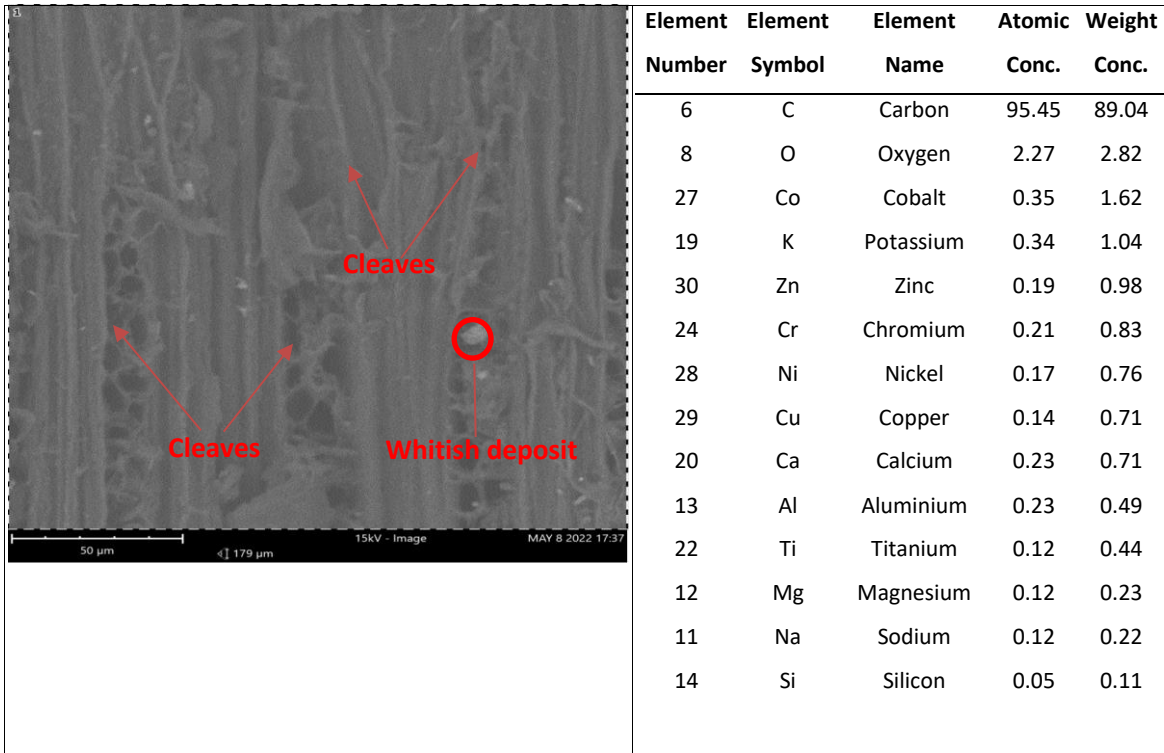


Figure 4.34: SEM/EDS Analysis of SCB.



FOV: 179 μm, Mode: 15kV - Image, Detector: BSD Full, Time: MAY 8 2022 17:37

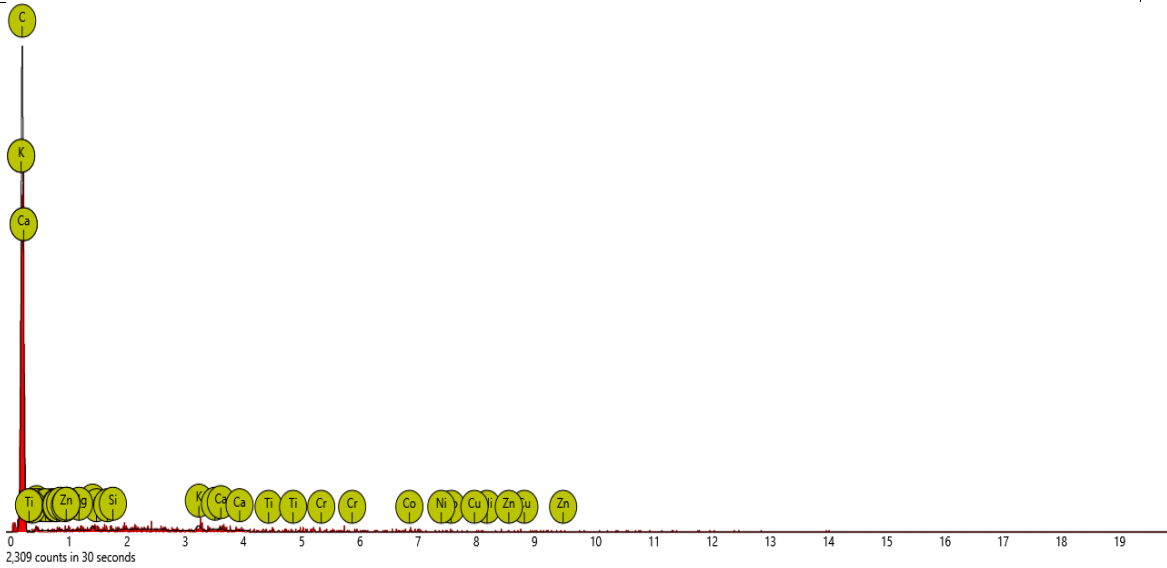


Figure 4.35: SEM/EDS of SBW sample

Table 4.25: Products of Pyrolysis and their Applications

Pyrolysis Products	Areas of Application	Reasons	References
Bio-oil	1. Energy generation to power vehicles, ships, transformers, compressors, furnaces, marine equipment, and heavy machine	Due to the presence of phenol, alcohol, alkane, ester, carboxylic acid, oleic acid, aromatic, etc.	Mohammed <i>et al.</i> (2017); Varma and Mondal, (2017); Chukwuneke <i>et al.</i> (2019); Laouge <i>et al.</i> (2020); Oyebanji <i>et al.</i> (2022)
	2. Oxygenated fuel additive in fossil fuel-based fuel for diesel engine.	Due to the presence of alcohol, phenol, and aromatic compound.	Sun <i>et al.</i> (2017); Chen <i>et al.</i> (2019)
	3. An additive in the petrochemical industry for the production of detergent, plastic, perfumes, dry-cleaning, solvent, and coolant in air conditioning and refrigerator.	Due to the presence of amine, halo-compound, alcohol, phenol, ester, primary amine, Carbon (iv) oxide, aldehyde, etc.	Stauffer <i>et al.</i> (2008); Ficci (2012); Lazzari <i>et al.</i> (2016); Morah and Sensoz (2015); Gautam and Chaurasis (2020)
	4. Pharmaceutical industry for drug production.	Ketone, Isothiocyanate phenol, alcohol (Methanol, ethanol, propanol, butanol, etc.	Kim <i>et al.</i> (2017)
Biochar	1. Catalysts for energy generation such as dry methane reforming to	Due to the presence of heterogeneous pore, cleaves, and rapid	Hossain <i>et al.</i> (2017); Varma and Mndal

<p>produce clean fuels e.g., syngas and hydrogen, Solid fuel for cooking and heating, fuel cell, supercapacitor, electric cables, and batteries.</p>	<p>effervescence as well as a chemical compound such as phenol, alcohol, alkynes, alkene, aromatic ester, acids halides, nitro compound, ester, etc.</p>	<p>(2017); Haggstrom <i>et al.</i> (2018)</p>
<p>2. Industrial sectors for water treatment for dye and heavy metal removal and agricultural sectors for nutrients retention in crops cultivation.</p>	<p>Due to their adsorption related process (pores with different shapes and sizes)</p>	<p>Foong <i>et al.</i> (2020); Sahoo <i>et al.</i> (2021)</p>

CHAPTER FIVE

SUMMARY, CONCLUSION AND RECOMMENDATIONS

5.1 Summary

The efficient conversion of biomass via the pyrolysis process to bio-oil, biochar, and NCG had been a major concern to many researchers due to improper selection of biomass prior to experimentation as a result of paucity of information on the geographical location, the intrinsic composition of the biomass, soil type, and climatic conditions where the biomass samples are sourced and cultivated. Also, inability to attain the right operating conditions and optimization of the desired product quality and quantity.

This study determined the physicochemical, structural, and thermal properties of fifteen lignocellulosic biomass samples to aid the appropriate selection of three biomass that possessed the highest energy potential to be used as fuel for pyrolysis operation and to reduce environmental pollution during the pyrolysis process. After that, mathematical models and optimization of biomass operating parameters (temperature, reaction time, heating rate, nitrogen flow rate, and particle sizes) were performed using a RSM based on the outcome of experimental runs to enhance the quantity of pyrolysis yields. The study also optimized the pyrolysis' yields and the outcomes were used to calculate the energy and exergy efficiency of the pyrolysis process to determine the useful energy and detect the energy losses.

The type of experimental design used was the CCD and a RSM was utilized to generate a design matrix. Thereafter, experimental runs were performed to obtain the quantity of bio-oil, biochar, and NCG yield, as well as the energy and exergy efficiency of the pyrolysis products were determined. The results obtained from the experimental runs served as input parameters in the modelling and optimization of pyrolysis' operating parameters to improve the quantity of the products of pyrolysis as well as the energy and exergy efficiency of bio-oil, biochar, and non-condensable gases (NCG). Also, the influence of individual parameters in addition to the two most important combined effects (interaction) of the operating parameters on the quantity of products of pyrolysis as well as the energy and exergy efficiency were investigated.

The results obtained during a preliminary investigation of biomass samples such as physicochemical, structural composition, and thermal properties to aid the appropriate selection

of biomass for pyrolysis operation showed that shea butter wood was best suited for biofuel generation, closely followed by sugarcane bagasse and palm kernel shell due to their high energy potential. At the same time, moringa oleifera possessed the least properties for the pyrolysis process. The high percentage of VM, carbon, hydrogen, HHV, ignitability index, cellulose, and hemicellulose content recorded in the selected biomass enhanced devolatilization reactivity, ignitability, and burn gases in the reactor, as well as a good production of hydrocarbons content during the pyrolysis process. Also, the low ash content prevented harmful chemical deposits in the reactor during the pyrolysis process.

It was observed that all the operating parameters and their interaction influenced, to an extent, pyrolysis yields. Reduce particle size of biomass (< 0.5 mm) was be suitable for bio-oil yield as it ensures faster and uniform heat transfer as well as high volatile matter production leading to a high yield of bio-oil and NCG.

An increase in the nitrogen dosage regime (25 to 175 cm^3/min) and reaction time (5-15min) caused the bio-oil yield to increase due to the non-proliferation of secondary reactions such as thermal cracking, re-polymerization, and re-condensation of vapour that enhanced heat transfer and rapid de-volatilization of the biomass in the reactor. An increase in temperature from 320 to 720°C enhanced pyrolysis yields and the total exergy at the inlet sharply from 13800 – 18500 kJ/kg. This increase was attributed to an increase in input electric exergy in the pyrolysis plant. The energy and exergy of biochar dropped as temperature increased due to the complete pyrolysis process and non-attainment of secondary reactions such as thermal cracking. It can be deduced that the exergy efficiency of individual gases such as CO, CH₄, CO₂, H₂ increased as temperature increased due to the rapid devolatilization of the biomass samples to NCG at high temperatures. Also, irreversibilities in the pyrolysis plant were caused by high volatile emission, spontaneous chemical reactions, a mixture of the biochar and vapour, and unrestrained expansion. The predicted values obtained from the developed mathematical model was similar to the actual values going by the manner of the dots pattern cluster around the regression line. The regression models also showed a strong similarity between the predicted model and the experimental results. Statistical analysis (ANOVA) showed that the model was significant (low P-value < 0.0001 and high F-value). This implies that the mathematical model is responsive, accurate, and reliable in predicting the quantity of pyrolysis yields and the energy and exergy of the products of pyrolysis.

The optimum bio-oil yields recorded for PKS is 46.8 wt% at (T: 493.7°C, R: 15.5 min, H: 24.5°C/min, P N: 255 cm³/min, P: 0.1 mm), SCB was 47.5 wt% at (T: 487.5°C, R: 15.7 min, H: 24.7°C/min, P N: 25 cm³/min, P: 0.1 mm), while that of SBW was 48.4 wt% at (T: 517.4°C, R: 14.3 min, H: 24.7°C/min, N: 119.5 cm³/min, P: 0.1 mm). Considering biochar yields, the optimum values for PKS (40.7 wt%) was attained at T (330°C), R (6.5 min), H (7.5°C/min), N (25 cm³/min) and P (0.9 mm). In the case of SCB, the optimum value was 40.5 wt% at T, R, H, N, P of 357°C, 6.5 min, 12.8°C/min, 25 cm³/min and 0.9 mm respectively. Likewise, for SBW, the optimum value of 40.5 wt% was obtained at T (346.4°C), R (8.9 min), H (7.5°C/min), N (25 cm³/min) and P (0.9 mm). The optimum yields of NCG for PKS was 33.32 wt% at (T: 720°C, R: 25 min, H: 7.5 °C/min, N: 138.1 cm³/min, P: 0.1 mm), SCB was 35.5 wt% (T: 720°C, R: 24 min, H: 25.9 °C/min, N: 25 cm³/min, P: 0.1 mm), and SBW was 34.2 wt% at (T: 720 °C, R: 20 min, H: 7.5 °C/min, N: 255 cm³/min, P: 0.1 mm). Hence, SBW, PKS and SCB are more suitable for bio-oil, biochar and NCG yields respectively.

The optimum value of energy and exergy efficiency of bio-oil yields are 46.9 and 44.2% at a temperature, reaction time, heating rate, nitrogen flow rate, and particle size of 623.0 °C, 15 min, 10.7°C/min, 117.9 cm³/min, and 0.5 mm respectively. In the case of energy and exergy efficiency of biochar yield, the optimum is 33.34 and 30.56 % at a temperature, reaction time, heating rate, nitrogen flow rate, and particle size of 320°C, 20.4 min, 24.9°C/min, 25 cm³/min and 0.9 mm respectively, while that of NCG yield are 13.4 and 9.5 % at a temperature, reaction time, heating rate, nitrogen flow rate and particle size of 691.7°C, 5 min, 7.5 °C/min, 225 cm³/min and 0.1 mm respectively.

The bio-oil yields from PKS and SCB are heavy crude oil due to their high density greater than 0.92 g/cm³, while SCB are furnace and fuel oil for transformer, and ship etc. The pH level is PKS (2.6), SCB (3.52) and SBW (5.93). Hence, the bio-oil is acidic in nature due to the presence of organic acids, phenolic and aldehyde in the bio-oil. The bio-oil obtained from SBW is a better fuel compared to SCB and PKS because the low acidic value. It is advisable to neutralize prior to their usage for automobile parts, fuel tanks and fuel for vehicle engines and boilers in order to prevent corrosion and other reactions of the bio-oil. The viscosity of the bio-oil @ 40°C are 2.6, 7.7 and 5.4 cst for PKS, SCB and SBW. The low viscosity of the bio-oil helps to prevent poor atomization, partial ignition of the oil, contamination of the lubricating oil with an uncharred deposit during their utilization of fuel for vehicle engine and formation of

extreme carbon residue on the injection nozzles and ignition chamber. SCB is more flammable and volatile due to their low flash point, followed by SWB, while PKS is least flammable and volatile.

The results obtained from FTIR and GCMS showed the presence of alcohols in the bio-oil samples is due to thermal degradation of cellulose and hemicellulose content of the biomass samples, while the presence of phenol and aromatic compound are attributed to the decomposition of lignin content of the biomass samples. The presence of Alkene, Alcohol, Alkynes, Aromatic compounds, Phenol, Halo compound and Esters present in the bio-oil and biochar samples make them useful as fuel for vehicles, ships, aircraft etc., furnace, turbine, compressor, boiler, Aliphatic primary amine, production of biodiesel, and raw materials for petrochemical industries.

The SEM image depicts the presence of pores with difference sizes and shape within the biochar surfaces is attributed to the emission of volatile matter during pyrolysis process. Hence, the biochars are applicable as catalyst for energy generation such as dry methane reforming to produce clean fuels e.g., syngas and hydrogen as well as absorbent for use in adsorption-related process such as dye and heavy metal removal in water treatment or nutrient retention in crops cultivation.

The EDX image of the biochar obtained from SCB possessed high energy content for potential use as solid fuel relative to PKS and SBW due to its high percentage weight of carbon. Also, the biochar obtained from SCB would exhibit a better mechanical property such as hardness, toughness, tensile strength when compared to PKS and SBW due to their high carbon contents. Hence, it can burn easily without irregular deformation.

5.2 Conclusion

This study modelled and optimized the pyrolysis' operating parameters using RSM to enhance the quantity, quality, energy, and exergy efficiency of pyrolysis yields. The results showed that the operating parameters under investigation as well as their interaction greatly influenced pyrolysis yields. Also, an increase in temperature increases the energy and exergy efficiency of bio-oil and NCG, but decreases the energy and exergy for biochar yield. The ANOVA analysis indicated that there is no significant difference between the experimental and predicted results as $P\text{-value} < 0.001$ and a high $F\text{-value}$. Hence, the model is dependable and

usable to predict products of bio-oil, biochar, and NCG yields as well as energy and exergy efficiency of pyrolysis yields from lignocellulose biomass samples.

The optimum bio-oil (46.5 wt%), biochar (40.7 wt%), and NCG (33.3 wt%) yields were recorded using PKS. In the case of SCB, 47.1, 40.0, and 35.9 wt% were obtained for bio-oil, biochar, and NCG yields respectively. Considering SBW, the bio-oil, biochar, and NCG yields were 47.9, 40.8, and 34.6 wt% respectively. Hence, SBW, PKS, and SCB are more suitable for bio-oil, biochar, and NCG yields.

SBW possessed the peak HHV (30.02 MJ/kg), next to SCB whose HHV is 29.99 MJ/kg, while PKS has the least HHV (21.23 MJ/kg) due to their low carbon content (41.2%) and high oxygen content (49.23%). The presence of fuel properties in the bio-oil and biochar samples such as phenolic compounds, alcohol, oleic acids, aromatic hydrocarbons, ketone, furfural and nitrogen-containing compounds make the pyrolysis products useful as fuel for internal combustion engines, ships, furnace, compressor, boilers, raw material for the production of biodiesel, chemical additive and pharmaceutical industries.

This study has been able to achieved the set objectives such as physicochemical, structural and thermal properties of the biomass, modelling and optimization of pyrolysis operating parameters, energy and exergy analysis as well as characterization of the pyrolysis yields to investigate their quality.

This study has successfully demonstrated the application of RSM based on CCD to model and optimize pyrolysis yields as well as the energy and exergy the efficiency of bio-oil, biochar, and NCG.

5.3 Recommendations

The results obtained from the characterization of the biomass samples showed that SBW, SCB, and PKS are recommended for pyrolysis process due to their high energy potential. The EDS spectra of the biochar obtained from SCB possessed high energy content for potential use as solid fuel relative to PKS and SBW due to its high percentage weight of carbon. Also, the biochar obtained from SCB would exhibit a better mechanical property such as hardness, toughness, tensile strength when compared to PKS and SBW due to their high carbon contents. Hence, it can burn easily without irregular deformation.

An upgrade of the fuel is necessary to enhance their quality for renewable energy applications. It is advisable to neutralize acidity and further converts the bio-oil prior to their usage for automobile parts, fuel tanks and fuel for vehicle engines and boilers in other to prevent corrosion and other reactions of the bio-oil. Also, the optimum yield of co-pyrolysis of the different biomass samples used in this study should be performed, and the results should be compared with the single pyrolysis process.

5.4 Contribution to Knowledge

In this study, five operating parameters were utilized to generate fifteen (15) models to predict the products of pyrolysis and the energy, and exergy efficiency of bio-oil, biochar and NCG using PKS, SBW, and SCB. The models were found reliable to predict experimental data required to optimize the products of pyrolysis as well as their energy and exergy efficiency which probably, is the first of its kind. Also, the predicted models and the optimized values of the operating parameters can be utilized for the present and future pyrolysis process. Furthermore, the optimized operating parameters that gave a yield that are better and significantly different from what is obtainable in all the literatures at my disposal.

This study was able to carry out complete characterization of the pyrolysis yields and it was established that SCB, SBW, and PKS are more suitable for optimum yield of bio-oil, biochar, and NCG yields discretely. It deduced from this study that SBW is a better fuel compared to SCB and PKS because the low acidic value. Also, the bio-oil obtained from SCB was more flammable and volatile followed by SWB, while PKS is least flammable and volatile. It is also established that the optimum values of the operating parameters predicted will ensure reduction in the cost, materials, time and bottleneck involved when performing the experiments to investigate the pyrolysis yield.

Four (4) journal articles have been published while three (3) journal articles have been accepted for publication in *Mathematical Modelling of Engineering Problems*, *portugaliae electrochimica acta* and *Revue des Composites et des Materiaux Avances-Journal of Composite and Advanced Materials*. Also, six (6) manuscripts are at present under review.

REFERENCES

- Abnisa, F., Daud, W.M.A. and Sahu, J.N. (2011). Optimization and characterization studies on bio-oil production from palm shell by pyrolysis using response surface methodology. *Biomass and Bioenergy*, 35 (2011), 3604-3616. doi: 10.1016/j.biombioe.2011.05.011.
- Abomohra, A. E., Sheikh, H. M. A., El-Naggar, A. H. and Wang, Q. (2021). Microwave vacuum co-pyrolysis of waste plastic and seaweeds for enhanced crude bio-oil recovery: Experimental and feasibility study towards industrialization. *Renewable and Sustainable Energy Review*, 149 (2021). <https://doi.org/10.1016/j.rser.2021.111335>.
- Acevedo, J. C., Solano, S. P., Durán, J. M., Posso, F. R., Arenas, E. (2019). Estimation of potential hydrogen production from palm kernel shell in Norte de Santander, Colombia. *Journal of Physics: Conference Series 1386* (2019). doi:10.1088/1742-6596/1386/1/0120931
- Adegoke, O. A., Fuwape, J. A., Fabiyi, J. S. (2014). Combustion Properties of Some Tropical Wood Species and Their Pyrolytic Products Characterization. *Energy and Power*, 4(3), 54-57. doi:10.5923/j.ep.20140403.02. n
- Adekiya, A. O., Agbede, T. M., Olayanju, A., Wutem, S. E., Aboyeji, C. M., Dunsin, O., Aremu, C. O., Owolabi, A. O., Ajiboye, B. O., Okunlola, O. F. and Adesola, O. O (2020). Biochar, poultry manure and NPK fertilizer: sole and combine application effects on soil properties and ginger (*Zingiber officinale* Roscoe) performance in a tropical Alfisol. *Open Agriculture*, 5(1). <https://doi.org/10.1515/opag-2020-0004>
- Adeleke, A. A., Odusote, J. K., Ikubanni, P. P., Agboola, O. O., Balogun, A. O. and Lasode, O. A. (2021). Tumbling strength and reactivity characterization of hybrid fuel briquette of coal and biomass wastes blends. *Alexandra Engineering Journal*, 60 (5), 4619-4625. <https://doi.org/10.1016/j.aej.2021.03.069>
- Adeleke, A.A., Odusote, J.K., Ikubanni, P.P., Lasode, O.A., Malathi, M. and Paswan, D. (2020). The ignitability, fuel ratio and ash fusion temperatures of torrefied woody biomass. *Heliyon*, 6(3). doi: 10.1016/j.heliyon. 2020.e03582.
- Adeniyi, A., Ighalo, J. (2020). ASPEN Plus predictive simulation of soft and hard wood pyrolysis for bio-energy recovery. *International Journal of Environment and Waste Management.*, 26. 234. 10.1504/IJEW.2020.10028695.

- Aghbashloa, A., Tabatabaeib, M., Nadiane, M. H., Davoodniae, V. and Soltanianc, S. (2019). Prognostication of lignocellulosic biomass pyrolysis behavior using ANFIS model tuned by PSO algorithm. *Fuel*, 253 (2019), 189–198. <https://doi.org/10.1016/j.fuel.2019.04.169>.
- Aguiar, A., Milessi, T. S., Mulinari, D. R., Lopes, M. S., de Costa, S. M. and Candido, R. G. (2021). Sugarcane straw as a potential second-generation feedstock for biorefinery and white biotechnology applications. *Biomass and Bioenergy*, 144 (2021). <https://doi.org/10.1016/j.biombioe.2020.105896>.
- Ahmad, M.S., Mehmood, M. A., Ayed, A. S., Ye, G., Luo, H., Ibrahim, M., Rashid, U., Nehdi, A. I. and Qadir, G. (2017). Kinetic analyses and pyrolytic behavior of para grass (*Urochloa mutica*) for its bioenergy potential. *Bioresources Technology*, 224 (2017), 708-713 <https://doi.org/10.1016/j.biortech.2016.10.090>.
- Ahmed, A., Baker, M.S.A., Azad, A. K., Sukri, R. S. and Phusunti, N. (2018). Intermediate species for bio-oil and biochar production. *Energy Conversion and Management*, 176 (15), 393-408. <http://dx.doi.org/10.1016/j.enconman.2018.09.041>.
- Akinola, A. O. and Fapetu, O. P. (2015). Characteristics Study of Wood Wastes from Sawmills. *British Journal of Applied Science and Technology*, 6(6), 606-612. BJAST.2015.115
- Akogun, O. A., Waheed, M. A., Ismail, S. O., Dairo, O. U. (2022). Physical and Combustion Indices of Thermally Treated Cornhusk and Sawdust Briquettes for Heating Applications in Nigeria. *Journal of Natural Fibers*. doi:10.1080/15440478.2020.1764445.
- Aladin, A., Alwi, R. S. and Syarif, T. (2017). *Design of pyrolysis reactor for production of bio-oil and biochar simultaneously*. AIP Conference Proceedings, 1840 (1). Doi:10.1063/1.4982340.
- Alfa, M. I., Owamah, H. I., Onokwai, A. O., Gopikumar, S., Oyebisi, S. O., Kumar, S. S., Bajar, S., Samuel, O. D. and Ilabor, S. C. (2021). Evaluation of biogas yield and kinetics from the anaerobic co-digestion of cow dung and horse dung: a strategy for sustainable management of livestock manure. *Energy, Ecology and Environment*, 6 (5), 425-434. <http://doi.org/10.1007/s40974-020-00203-0>.
- Alatzas, S., Moustakas, K., Malamis, D. and Vakalis, S. (2019). Biomass Potential from Agricultural Waste for Energetic Utilization in Greece. *Energies*, 12 (2019), 1095-2015. <http://dx.doi.org/10.3390/en12061095>.

- Alipanahpour, D. E., Ghaedi, M., Ghezelbash, G.R., Asfaram, A. and Purkait, M.K. (2017). Highly efficient simultaneous biosorption of Hg²⁺, Pb²⁺ and Cu²⁺ by Live yeast *Yarrowia lipolytica* 70562 following response surface methodology optimization: Kinetic and isotherm study. *J. Ind. Eng. Chem.*, 48 (2017), 162–172. <https://doi.org/10.1016/j.jiec.2016.12.035>.
- Aliyu, S. J., Kucha, E. L., and Ibrahim, S. J. (2021). Modelling and simulation of a Single Cyclone for Optimal Efficiency for a Batch-Type Fixed-Bed Down-Draft Gasifier using CFD. IOP Conf. Ser.: Mater. Sci. Eng. <https://iopscience.iop.org/article/10.1088/1757-899X/1107/1/012038/meta>
- Al-Weshahi, M.A., Anderson, A. and Tian, G. (2013). Exergy efficiency enhancement of MSF desalination by heat recovery from hot distillate water stages. *Appl Therm Eng*, 53 (2015):226-33.
- American Society for Testing and Materials, ASTM D1102-84. -*Standard Test Method for Ash in Wood*, 2007.
- American Society for Testing and Materials, ASTM E872-82 *Standard Test Method for Volatile Matter in the Analysis of Particulate Wood Fuels*. West Conshohocken, PA: ASTM International, 2006
- American Society for Testing and Materials, E 1358 – 97: *Standard Test Method for Determination of Moisture Content of Particulate Wood Fuels Using a Microwave Oven*. West Conshohocken, PA: ASTM International, 2006
- American Society for Testing and Materials, ASTM D2015-00: *Standard Test Method for Gross Calorific Value of Coal and Coke by Adiabatic Bomb Calorimeter*. West Conshohocken, 2000, 9pp.
- American Society for Testing and Materials, ASTM D4239-11: *Standard test method for sulphur in sample of coal and coke using high temperature tube furnace combustion*. West Conshohocken, PA: ASTM International, 2011.
- American Society for Testing and Materials, ASTM D5373-21. *Standard test methods for determination of carbon, hydrogen and nitrogen in analysis samples of coal and carbon in analysis samples of coal and coke*. West Conshohocken, PA: ASTM International, 2016.
- Arni, S. A. (2018). Comparison of slow and fast pyrolysis for converting biomass into fuel. *Renewable energy*, 124 (2018), 197-201. <https://doi.org/10.1016/j.renene.2017.04.060>
- Arvindekar, A.U. and Laddha, K.S. (2016). An efficient microwave-assisted extraction of anthraquinones from *Rheum emodi*: optimisation using RSM, UV and HPLC analysis and

- antioxidant studies. *Ind Crops Prod*, 83(2016), 587–595.
<https://doi.org/10.1016/j.indcrop.2015.12.066>
- Asadullah, M., Rahman, M.A., Ali, M.M., Rahman, M.S., Motin, M.A., Sultan, M.B. and Alam, M.R. (2007). Production of bio-oil from fixed bed pyrolysis of bagasse. *Fuel*, 86, 2514–2520.
<https://doi.org/10.1016/j.fuel.2007.02.007>
- Asibor, J. O., Akhator, E. P. and Obanor, A. I. (2019). Energy Potential Study of Some Tropical Wood Species from Nigeria. *CJAST*, 37(4), 1-10.
- Augustine, O. A., Opeyemi, A. A., Oyinlola, M. O. and Temitayo, E. O. (2015). Compositional analysis of lignocellulosic materials: Evaluation of an economically viable method suitable for woody and non-woody biomass. *American Journal of Engineering Research (AJER)*, 4, 14-19.
- Ayeni, A. O., Adeeyo, O. A., Oresegun, O. M., Oladimeji, T. E. (2015). Compositional analysis of lignocellulosic materials: Evaluation of an economically viable method suitable for woody and non-woody biomass. *American Journal of Engineering Research (AJER)*, 4 (4), 14-19.
- Ayeni, A. O., Daramola, M. O., Awoyomi, A., Elehinafe, F. B., Ogunbiyi, A., Sekoai, P. T. and Folayan, J. A. (2018). Morphological modification of *Chromolaena odorata* cellulosic biomass using alkaline peroxide oxidation pretreatment methodology and its enzymatic conversion to biobased products. *Cogent Engineering*, 5 (1), DOI: [10.1080/23311916.2018.1509663](https://doi.org/10.1080/23311916.2018.1509663).
- Aziz, M. A., Rahman, M. A. and Molla, H. (2018). Design, fabrication and performance test of a fixed bed batch type pyrolysis plant with scrap tire in Bangladesh. *Journal of Radiation Research and Applied Science*, 11 (4), 113-116. <https://doi.org/10.1016/j.jrras.2018.05.001>.
- Baffour-Awuah, E., Akinlabi, S. A., Jen, T. C., Hassan, S., Okokpujie, I. P. and Ishola, F. (2021). Characteristics of Palm Kernel Shell and Palm Kernel Shell-Polymer Composites: A Review. *IOP Conference Series: Materials Science and Engineering*, 1107(1), [https://doi:10.1088/1757-899X/1107/1/012090](https://doi.org/10.1088/1757-899X/1107/1/012090).
- Balogun, A. O., Sotoudehniakarani, F. and McDonald, A. G. (2017). Thermo-kinetic, spectroscopic study of brewer's spent grains and characterization of their pyrolysis products. *Journal of Analytical and Applied Pyrolysis*, 127 (2017), 8-16.
[HTTPS://DOI.ORG/10.1016/J.JAAP.2017.09.009](https://doi.org/10.1016/j.jaap.2017.09.009)
- Balogun, A.O., Lasode, O.A. and McDonald, A.G. (2018). Thermo-physical, Chemical and Structural Modifications in Torrefied Biomass Residues. *Waste Biomass Valor.*, 9 (2018), 131–138.
<https://doi.org/10.1007/s12649-016-9787-7>

- Balogun, A. O., Lasode, O. A., Onokwai, A. O., Ezugwu, C. A., Olayanju, T. M. A. and Osueke, C. O. (2019). Elemental analysis and combustion characteristics evaluation of Nigeria biomass resources. *International Journal of Mechanical Engineering and Technology*, 10(2), 1522-1527. <http://www.iaeme.com/ijmet/issues.asp?JType=IJMETandVType=10andIType=02>
- Balogun, A. O., Adeleke, A. A., Ikunbanni, P. P., Adegoke, S. O., Alayat, A. M. and McDonald, A. G. (2021). Physico-chemical characterization, thermal decomposition and kinetic modeling of *Digitaria sanguinalis* under nitrogen and air environments. *Case Studies in Thermal Engineering*, 26 (2021). <https://doi.org/10.1016/j.csite.2021.101138>
- Bardazzi, R. and Paziienza, M. G. (2020). When I was your age: Generational effects on long-run residential energy consumption in Italy. *Energy Research and Social Science*, 70 (2020). <https://doi.org/10.1016/j.erss.2020.101611>.
- Bartoli, M., Rosi, L., Giovannelli, A., Frediani, P. and Frediani, M. (2016). Production of bio-oils and bio-char from *Arundo donax* through microwave assisted pyrolysis in a multimode batch reactor. *J. Anal. Appl. Pyrolysis*, 122 (2016), 479–489. <https://doi.org/10.1016/j.jaap.2016.10.016>.
- Baruah B, Tiwari P, Thakur P. and Katak R. (2018). TGA-FTIR analysis of upper assam oil shale, optimization of lab-scale pyrolysis process parameters using RSM, *Journal of Analytical and Applied Pyrolysis* (2018). <https://doi.org/10.1016/j.jaap.2018.08.005>
- Beguin, F., Raymundo-Pineiro, E. and Frackowiak, E. (2019). *Electrical double-layer capacitors and pseudocapacitors*. *Carbons for Electrochemical Energy Storage and Conversion Systems*. CFC Press, 329-375.
- Bello, O. S., Adegoke, K. S. and Akinyunni, O. O (2017). Preparation and characterization of a novel adsorbent from *Moringa oleifera* leaf. *Appl Water Sci.*, 7(2017), 1295–1305. DOI 10.1007/s13201-015-0345-4.
- Bertero, M. and Sedran, U. (2015). Coprocessing of bio-oil in fluid catalytic cracking. *Recent Advances in Thermo-Chemical Conversion of Biomass*, 2015. <https://doi.org/10.1016/B978-0-444-63289-0.00013-2>
- Biswas, B., Kumar, A., Fernandes, A.C., Saini, K., Negi, S., Muraleedharan, U.D. and Bhaskar, T. (2020). Solid base catalytic hydrothermal liquefaction of macroalgae: effects of process parameter on product yield and characterization. *Bioresour. Technol.* 307 (2020). <https://doi.org/10.1016/j.biortech.2020.123232>.

- Boateng, A.A., Mullen, C.A., Osgood-Jacobs, L., Carlson, P. and Macken, N. (2012). Mass balance, energy, and exergy analysis of bio-oil production by fast pyrolysis. *J Energy Resour Technol*, 2012, 134. <https://doi.org/10.1115/1.4007659>.
- Bonfim, W. B. and De-Paula, H. M. (2021). Characterization of different biomass ashes as supplementary cementitious material to produce coating mortar. *Journal of Cleaner Production*, 291 (2021), 125869. <https://doi.org/10.1016/j.jclepro.2021.125869>.
- Bordoloi, N., Narzari, R., Chutia, R.S., Bhaskar, T. and Kataki, R. (2015). Pyrolysis of Mesua ferrea and Pongamia glabra seed cover: characterization of bio-oil and its subfractions. *Bioresour. Technol.*, 178, 83-89. <https://doi.org/10.1016/j.biortech.2014.10.079>
- Bridgwater, T., Meier, D. And Radlein, D. (1999). An Overview of Fast Pyrolysis of Biomass. *Organic Geochemistry*. 30, 1479-1493. 10.1016/S0146-6380(99)00120-5.
- Bridgwater, A. V. (2012). Review of Fast Pyrolysis of Biomass and Product Upgrading. *Biomass Bioenergy*, 38 (2012), 68-94. <https://doi.org/10.1016/j.biombioe.2011.01.048>.
- Campuzano, F., Brown, R. C. and Martinez, J. D. (2019). Auger reactors for pyrolysis of biomass and wastes. *Renewable and Sustainable Energy Review*, 102 (2019), 372409. <https://doi.org/10.1016/j.rser.2018.12.014>.
- Cantrell, K. B., Hunt, P. G., Uchimiya, M., Nova, J. M. and Rio, K. S. (2012). Impact of pyrolysis temperature and manure source on physicochemical characteristics of biochar. *Bioresour Technol.*, 107 (2012), 419-428. <https://doi.org/10.1016/j.biortech.2011.11.084>
- Cao, L., Yu, I. K. M., Liu, Y., Ruan, X., Tsang, D. C. W., Hunt, A. J., Ok, Y. S., Song, H. and Zhang, S. (2018). Lignin Valorization for the Production of Renewable Chemicals: State-of-the-art Review and Future Prospects. *Bioresour Technol.*, 269 (2018), 465-475. <https://doi.org/10.1016/j.fuel.2019.116531>.
- Carrasco, J. L., Gunukula, S., Boateng, A. A., Mullen, C. A. DeSisto, W. J and Wheeler, M. C. (2017). Pyrolysis of forest residues: An approach to techno-economics for bio-fuel production. *Fuel*, 193 (2017), 477–484. <https://doi.org/10.1016/j.fuel.2016.12.063>.
- Channiwala, S.A. and Parikh, P.P. (2002). A unified correlation for estimating HHV of solid, liquid and gaseous fuels. *Fuel*, 81(8), 1051–1063. [https://doi.org/10.1016/S0016-2361\(01\)00131-4](https://doi.org/10.1016/S0016-2361(01)00131-4)
- Chen, Z. L., Zhang, J. Q., Huang, L., Yuan, Z. H., Li, Z. J and Liu M. C. (2019) Removal of Cd and Pb with biochar made from dairy manure at low temperature. *J Integr Agric* 18(1), 201–210. [https://doi.org/10.1016/S2095-3119\(18\)61987-2](https://doi.org/10.1016/S2095-3119(18)61987-2).

- Chowdhury, Z. Z., Kaushik, P., Wageeh, A., Yehye, S. S., Syed, T. S., Ganiyu, A. A., Emy, M., Rahman F.R. and Rafie, B. J. (2017). Pyrolysis: A Sustainable Way to Generate Energy from Waste. *Dimensions*. <https://www.intechopen.com/books/pyrolysis/pyrolysis-a-sustainable-way-to-generate-energy-from-waste>
- Chukwunneke, J.L., Ewulonu, M.C., Chukwujike, I.C. and Okolie, P.C. (2019). Physico-chemical analysis of pyrolyzed bio-oil from swietenia macrophylla (mahogany) wood. *Heliyon*, 5 (6). <https://doi.org/10.1016/j.heliyon.2019.e01790>.
- Crespo, Y. A., Naranjo, R. A., Quitana, Y., G., Sanchez, C. G. and Sanchez, E. M. (2017). Optimization and characterization of bio-oil produced by Acacia mangium Willd wood pyrolysis. *Wood Sci Technol*. Springer-Verlag Berlin Heidelberg 2017. DOI 10.1007/s00226-017-0913-x
- Dahunsi, S. O., Osueke, C. O., Olayanju, T. M. A. and Lawal, A. I. (2019). Co-digestion of Theobroma cacao (Cocoa) pod husk and poultry manure for energy generation: Effects of pretreatment methods. *Bioresources Technology*, 283 (2019), 229-241. <https://doi.org/10.1016/j.biortech.2019.03.093>.
- Daiglou, V, Stehfest E, Wicke B, Faaij A and Vuuren D. (2016). Projections of the Availability and Cost of Residues from Agriculture and Forestry. *GCB Bioenergy*, 8(2016), 456–70. <https://doi.org/10.1111/gcbb.12285>.
- Daniela, B., Giovanni, B., Tobias, W., Matthias, S., Sara, B., Luca, G., Marco, B., Andrea, S., Silvia, S., Alberto, P. (2020). Effects of woody biochar on dry thermophilic anaerobic digestion of organic fraction of municipal solid waste. *Journal of Environmental Management*, 267 (2020). 10.1016/j.jenvman.2020.110633, 267, (110633).
- Dhanavath, K.N., Bankupalli, S., Sugali, C.S., Perupogu, V., Nandury, S.V. and Bhargava, S., *et al.* (2019). Optimization of process parameters for slow pyrolysis of neem press seed cake for liquid and char production. *J Environ Chem Eng*, 7 (1). <https://doi.org/10.1016/j.jece.2019.102905>
- Dideolu, J. D., Candice, R. E., Jacob, B., McKenna, B., Caroline, F., Michael, A. B., Cosmin, M., Sue, E. N., and Dorin, B. (2018). An evaluative comparison of lingo cellulosic pyrolysis products derived from various parts of Populus deltoides trees and Panicum virgatum grass in an inductively heated reactor. *Energy Conversion and Management*, 171 (2018), 710-720. <https://doi.org/10.1016/j.enconman.2018.06.026>.

- Dincer, I. and Rosen, M.A. (2013). Thermodynamic fundamentals. In: Dincer I, Rosen MA, editors. *Exergy, Energy, environment and sustainable development*. Amsterdam, The Netherlands: Elsevier Ltd, 2013, 1-20.
- Dincer, I. and Rosen, M.A. (2021). Exergy and energy analyses. *Exergy*, 23-35. <http://dx.doi.org/10.1016/B978-0-12-824372-5.00002-6>
- Ding, Y., Zhang, W., Yu, L. and Lu, K. (2019). The accuracy and efficiency of GA and PSO optimization schemes on estimating reaction kinetic parameters of biomass pyrolysis. *Energy*, 176 (2019), 582-588. <https://doi.org/10.1016/j.energy.2019.04.030>.
- Dusso, D., Tellz, J., Fuertes, V. C., Paoli, J. M. D. and Moyano, L. (2022). Vacuum pyrolysis of chia flour residues: An alternative way to obtain omega-3/omega-6 fatty acids and calcium-enriched biochars. *Journal of Analytical and Applied Pyrolysis*, 161 (2022). <https://doi.org/10.1016/j.jaap.2021.105379>.
- Dwivedi, K. K., Shrivastav, P., Karmakar, M. K., Pramanick, A. K. and Chatterjee, P. K. (2019). A comparative study on pyrolysis characteristics of bituminous coal and low-rank coal using thermogravimetric analysis (TGA). *International Journal of Coal Preparation and Utilization*, 42 (1), 1-11. DOI: 10.1080/19392699.2019.1566130
- Echeverria, C., Bazan, G., Sanchez-Gonzalez, J., Lescano, L., Pagador, S., Linares, G. (2018). Pre-treatment by Acidification and Freezing on Corn cob Polymers and its Enzymatic Hydrolysis. *Asian Journal of Scientific Research*, 11, 222-231. Doi:10.3923/ajsr.2018.222.231
- Efomah, A. N. and Gbabo, A. (2015). The Physical, Proximate and Ultimate Analysis of Rice Husk Briquettes Produced from a Vibratory Block Mould Briquetting Machine. *International Journal of Innovative Science, Engineering and Technology*, 2(5), 814-822.
- Eke, J., Onwudili, J. A. and Bridgmont, A. V. (2019). Influence of Moisture contents on the fast pyrolysis of Trommel Fines in a bubbling fluidized bed reactor. *Waste and biomass valorization*, 11 (2020), 3711-3722. <https://doi.org/10.1007/s12649-018-00560-2>
- Ethaib, Saleem., Omar, Rozita., Mustapa Kamal, Siti., Kamal, Mustapa., Radiah, Dayang., Biak, Awang and Zubaidi, Salah. (2020). Microwave-Assisted Pyrolysis of Biomass Waste: A Mini Review. *Processes*, 8 (9), 1190. 10.3390/pr8091190.
- Etika, T., Ginting, A. S., Setiawan, R. P., Joelianingsih and Tambunan, A. H. (2019). Exergy Analysis on Pyrolysis Process of Oil Palm Empty Fruit Bunch. IOP Conf. Series: *Materials Science and Engineering*, 557 (2019), doi:10.1088/1757-899X/557/1/012058.

- Esfandi, S., Baloochzadeh, S., Asayesh, M., Ehyaei, M. A., Ahmadi, A., Rabanian, A. A., Das, B. and Costa, V. A. F., Davarpanah, A. (2020). Energy, Exergy, Economic, and Exergoenvironmental Analyses of a Novel Hybrid System to Produce Electricity, Cooling, and Syngas. *Energies*, 2020, 13, 6453. doi:10.3390/en13236453
- Evangelou, M. W. H., Conesa, H. M., Robinson, B. H., Schulin, R. (2012). Biomass Production on Trace Element–Contaminated Land: A Review. *Environmental Engineering Science*, 29(9), 823-839. DOI:10.1089/ees.2011.0428
- Fahmy, T.Y.A., Fahmy, Y., Mobarak, F., El-Sakhawy, M and Abou-Zeid, R.E. (2020). Biomass pyrolysis: past, present, and future. *Environ Dev Sustain*, 22(2020), 17–32 <https://doi.org/10.1007/s10668-018-0200-5>.
- Ferreira, M.F.P., Oliveira, B.F.H., Pinheiro, W.B.S., Correa, N.F., França, L.F. and Ribeiro, N.F.P. (2020). Generation of biofuels by slow pyrolysis of palm empty fruit bunches: Optimization of process parameters and characterization of physical-chemical products. *Biomass and Bioenergy*, 140 (2020). 140. <https://doi.org/10.1016/j.biombioe.2020.105707>.
- Ficci (2012). *Indian chemical and petrochemical industry*. India Chem
- Fontes, C. P., Honorato, T. L., Rabelo, M. C. and Rodrigues, S. (2009). Kinetic study of mannitol production using cashew apple juice as substrate. *Bioprocess and Biosystems Engineering*, 32 (4), 493–499.
- Foong, S.Y., Liewc, R.K., Yanga, Y., Chengd, Y.W., Yeke, Y.N., Maharib, W.A., Leeb, X.Y., Hanb, C. X., Vof, D. N., Leg, Q. V., Aghbashloh, M., Tabatabaeii, M., Sonnek, C., Penga, W. and Lamb, S. S. (2020). Valorization of biomass waste to engineered activated biochar by microwave pyrolysis: Progress, challenges, and future directions. *Chemical Engineering Journal*, 389 (2020). <https://doi.org/10.1016/j.cej.2020.124401>.
- Gajeraa, Z. R., Vermaa, K., Tekadeb, S. P. and Sawarkara, A. N. (2020). Kinetics of co-gasification of rice husk biomass and high sulphur petroleum coke with oxygen as gasifying medium via TGA. *Bioresource Technology Reports*, 11 (2020), 100479. <https://doi.org/10.1016/j.biteb.2020.100479>.
- Gautam, N. and Chaurasia, A. (2020). Study on kinetics and bio-oil production from rice husk, rice straw, bamboo, sugarcane bagasse and neem bark in a fixed-bed pyrolysis process. *Energy*, 190 (2020). <https://doi.org/10.1016/j.energy.2019.116434>.

- Ge, S., Yek, P. N. Y., Cheng, Y. W., Xia, C., Mahari, W. D. W., Liew, R. K., Peng, W., Yuan, T., Tabatabaei, M., Aghbashlo, M., Sonne, C. and Lam, S. S. (2021). Progress in microwave pyrolysis conversion of agricultural waste to value-added biofuels: A batch to continuous approach. *Renewable and Sustainable Energy Review*, 135 (2021). <https://doi.org/10.1016/j.rser.2020.110148>.
- Gianluca, Greco., Christian, Di Stasi., Filipe, Rego., Belén, González, and Joan, J. Manyà. (2020). Effects of slow-pyrolysis conditions on the products yields and properties and on exergy efficiency: A comprehensive assessment for wheat straw, *Applied Energy*, 279 (2020). <https://doi.org/10.1016/j.apenergy.2020.115842>.
- Gonzalez-Quiroga, A., Reyniers, P. A., Kulkarni, S. R., Torrgrosa, M. M., Perreault, P., Heynderickx, G. J., Geem, K. M. V. and Marin, G. B. (2017). Design and cold flow testing of a Gas-Solid Vortex Reactor demonstration unit for biomass fast pyrolysis. *Chemical Engineering Journal*, 329 (2017), 198-210. <https://doi.org/10.1016/j.cej.2017.06.003>
- Gonzalez, A. M., Jaem, R. L. and Lora, E. (2019). Thermodynamic assessment of the integrated gasification-power plant operating in the sawmill industry: An energy and exergy analysis. *Renewable Energy*, 147 (2019). <http://dx.doi.org/10.1016/j.renene.2019.09.045>
- Goodman, B. A (2020). Utilization of waste straw and husks from rice production: A review. *Journal of Bioresources and Bioproducts*, 5 (3), 143–162. <https://doi.org/10.1016/j.jobab.2020.07.001>
- Gourmelon, S., Hetreuxa, R. and Floquet, P. (2015). A New Graphical Representation of the Exergy Balance. *Chemical Engineering Transactions*, 43, 2015.
- Goyal, H., Seal, D., Saxena, R. C. (2008). Bio-fuels from thermochemical conversion of renewable resources: A review. *Renewable and Sustainable Energy Reviews*, 12. 504-517. [10.1016/j.rser.2006.07.014](https://doi.org/10.1016/j.rser.2006.07.014).
- Granados, D.A., Velasquez, H.I. and Chejne, F. (2014). Energetic and exergetic evaluation of residual biomass in a torrefaction process. *Energy*, 74(2014), 181-9. <https://doi.org/10.1016/j.energy.2014.05.046>
- Gravalos, I., Xyradakis, P., Kateris, D., Gialamas, T., Bartzialis, D. and Giannoulis, K. (2016). An Experimental Determination of Gross Calorific Value of Different Agroforestry Species and Bio-Based Industry Residues. *Natural Resources*, 7 (2016), 57-68. doi: 10.4236/nr.2016.71006.

- Guedes, R. E., Lunaa, A. S. and Torres, A. R. (2018). Operating parameters for bio-oil production in biomass pyrolysis: A review. *Journal of Analytical and Applied Pyrolysis*, 129 (2018), 134–149. <https://doi.org/10.1016/j.jaap.2017.11.019>.
- Guo, Y., Song, Y., Lu, W., Ma, J., Xu, Q. and Wang, D. S. (2015). Hydrothermal liquefaction of Cyanophyta: evaluation of potential bio-crude oil production and component analysis. *Algal Res.* 11, 242-247. <https://doi.org/10.1016/j.algal.2015.06.025>.
- Gupta, G. K., Gupta, P. K. and Mondal, M. K. (2020). Experimental process parameters optimization and in-depth product characterizations for teak sawdust pyrolysis. *Waste Management*, 87 (2019), 499–511. <https://doi.org/10.1016/j.wasman.2019.02.035>.
- Haggstrom, F. and Delsing, J. (2018). IOT Energy Storage- A forecast. *Nergy Harvesting and Systems*, 5 (3-4), 43-51.
- Halder, P., Kundu, S., Patel S., Parthasarathy, R., Pramanik, B., Paz-Ferreiro, J. and Shah, K. (2019). TGA-FTIR study on the slow pyrolysis of lignin and cellulose-rich fractions derived from imidazolium-based ionic liquid pre-treatment of sugarcane straw. *Energy Conversion and Management*, 200 (2019). <https://doi.org/10.1016/j.enconman.2019.112067>.
- Hameed, S., Sharma, A., Pareek, V., Wu, H. and Yu, Y. (2019). A review on Biomass Pyrolysis Models: Kinetic, Network and Mechanistic Models. *Biomass and Bioenergy*, 123 (2019), 104-122. <https://doi.org/10.1016/j.biombioe.2019.02.008>.
- Hassan, S.N. A., Ishak, M. A. and Ismail, K. (2017). Optimizing the physical parameters to achieve maximum products from co-liquefaction using response surface methodology. *Fuel*, 207 (2017), 102–108. <https://doi.org/10.1016/j.fuel.2017.06.077>.
- Heidari, A., Khaki, E., Younesi, H. and Lu, H. R. (2019). Evaluation of Fast and Slow Pyrolysis Methods for Bio-Oil Activated Carbon Production from Eucalyptus Wadtes using aa Life Cycle Assessment Approach. *Journal of Cleaner Production*, 241 (2019). <https://doi.org/10.1016/j.jclepro.2019.118394>.
- Hejazi, B., Grace, J. R., Bi, X. and Mahecha-Botero, A. (2016). Coupled Reactor and Particle Model of Biomass Drying and Pyrolysis in a Bubbling Fluidized Bed Reactor. *Journal of Analytical and Applied Pyrolysis*, 121 (2016), 213-229. <https://doi.org/10.1016/j.jaap.2016.08.002>.
- Hossain, M. A., Ganesan, P., Jewaratnam, J. and Chinna, K. (2017). Optimization of process parameters for microwave pyrolysis of oil palm fiber (OPF) for hydrogen and biochar production. *Energy*

Conversion and Management, 133 (2017), 349–362.
<http://dx.doi.org/10.1016/j.enconman.2016.10.046>.

- IBM Micromedex (2019). Charcoal, Activated (Oral Route). *Mayo Clinic*. Retrieved 15 February 2019.
- Ibikunle, R. A., Titiladunyo, I. F., Akinnuli, B. O., Dahunsi, S. O. and Olayanju, T. M. A. (2019). Estimation of Power Generation from Municipal Solid Wastes: A case Study of Ilorin. *Energy Report*, 5 (2019), 126-135. <https://doi.org/10.1016/j.egy.2019.01.005>
- Ibikunle, R.A., Titiladunayo, I.F., Dahunsi, S.O., Akeju, E.A. and Osueke, C.O. (2021). Characterization and projection of dry season municipal solid waste for energy production in Ilorin metropolis, Nigeria. *Waste Management and Research*, 1-10. <https://doi.org/10.1177/0734242X2098>
- Ibikunle, R. A., Lukman, A. F., Titiladunayo, I. F., Haadi, A. (2022). Modeling energy content of municipal solid waste based on proximate analysis: R-k class estimator approach. *Cogent Engineering*, 9 (1). <https://doi.org/10.1080/23311916.2022.2046243>
- Inayat, A., Rocha-Meneses, L., Ghenai, C., Abdallah, M., Shanableh, A., Al-Ali, K., Alghfeli, A. and Alsuwaidi, R. (2022). Co-pyrolysis for bio-oil production via fixed bed reactor using date seeds and plastic waste as biomass. *Case Study in Thermal Engineering*, (2022). <https://doi.org/10.1016/j.csite.2022.101841>.
- Isabel, Q., Rodrigo, N, and Ramzy, K. (2017). Energy potential from rice husk through direct combustion and fast pyrolysis: A review. *Waste Management*, 59 (2017), 200-210. <https://doi.org/10.1016/j.wasman.2016.10.001.s>
- Isah, A. N., Eterigho, E. J., Olutoye, M. A., Garba, M. U., and Okokpujie, I. P. (2020). Development and Test Performance of Heterogeneous Catalysts on Steam Reforming of Bioethanol for Renewable Hydrogen Synthesis: A Review. *Journal of Advanced Research in Fluid Mechanics and Thermal Sciences*, 73 (1), 69-108. <https://doi.org/10.37934/arfmts.73.1.69108>
- Isitan, S. Ceylan, S., Topcu, Y., Hintz, C., Tefft, J., Chellappa, T., Guo, J. and Goldfarb, J. L. (2019). Product quality optimization in an integrated biorefinery: Conversion of pistachio nutshell biomass to biofuels and activated biochars via pyrolysis. *Energy Conversion and Management*, 127 (2019), 576–588.
- Jaffar, M.N., Nahil, M.A. and Williams, P.T. (2020). Pyrolysis-catalytic hydrogenation of cellulose-hemicellulose-lignin and biomass agricultural wastes for synthetic natural gas production.

- Journal of Analytical and Applied Pyrolysis*, 145 (2020).
<https://doi.org/10.1016/j.jaap.2019.104753>.
- Jafri, N., Wong, W. Y., Doshi, V., Yoon, L. W. and Cheah, K.H. (2018). A review on Production and Characterization of Biochars for Application in Direct Carbon Fuel Cells. *Process Safety and Environmental Protection*, 118 (2018), 152-166. <https://doi.org/10.1016/j.psep.2018.06.036>
- Jahirul, M. I., Rasul, M. G., Chowdhury, A. A. and Ashwath, N. (2012). Biofuels Production through Biomass Pyrolysis—A Technological Review. *Energies* 5 (2015), 4952-5001. doi:10.3390/en5124952.
- Jalalifar, S., Abbassi, R., Garaniya, V., Salehi, F., Papari, S., Hawboldt, K. and Strezov, V. (2020). CFD analysis of fast pyrolysis process in a pilot-scale auger reactor. *Fuel*, 273 (2020).
- Junna, S., Fuhong, H., Yinghua, P. and Zhenhua, Z. (2017). Effects of pyrolysis temperature and residence time on physicochemical properties of different biochar types. *Acta Agriculturae Scandinavica, Section B — Soil and Plant Science*, 67 (1), 12-22. <https://doi.org/10.1080/09064710.2016.1214745>.
- Kadlimatti, H.M., Raj Mohan, B. and Saidutta, M.B. (2019). Bio-oil from microwave assisted pyrolysis of food waste-optimization using response surface methodology. *Biomass and Bioenergy*, 123 (2019), 25-33. <https://doi.org/10.1016/j.biombioe.2019.01.014>.
- Kan, T., Strezov, V. and Evans, T. J. (2016). Pyrolysis: A Review of Products Properties and Effects of Pyrolysis Parameters. *Renewable and Sustainable Energy Review*, 57 (2015). DOI:[10.1016/j.rser.2015.12.185](https://doi.org/10.1016/j.rser.2015.12.185)
- Kartal, F. and Ozveren, U. (2021). An improved machine learning approach to estimate hemicellulose, cellulose, and lignin in biomass. *Carbohydrate Polymer Technologies and Applications*, 2 (2021). <https://doi.org/10.1016/j.carpta.2021.100148>
- Kazawadi, D., Ntalikwa, J. and Kombe, G. (2021). A review of intermediate pyrolysis as a technology of biomass conversion for coproduction of bio-oil and adsorption biochar. *Journal of Renewable Energy*, 2021. <https://doi.org/10.1155/2021/5533780>
- Khan, M. S., Benelmir, R. and Donnot, A. (2020). *Thermodynamic analysis of pyrolysis of olive mill wastewater sludge in fluidized bed reactor*. 2020 5th International Conference on Renewable Energies for Developing Countries (REDEC).4168.

- Khonde, R.D. and Chaurasia, A.S. (2016). Rice husk gasification in a two-stage fixed-bed gasifier: production of hydrogen rich syngas and kinetics. *Int J Hydrogen Energy*, 41 (21), 8793-8802. <https://doi.org/10.1016/j.ijhydene.2016.03.138>.
- Kiliç M, Pütün E, and Pütün A. E. (2014). Optimization of *Euphorbia rigida* fast pyrolysis conditions by using response surface methodology. *J Anal Appl Pyrol*, 110 (1), 163–71. <https://doi.org/10.1016/j.jaap.2014.08.018>
- Kim, P., Johnson, A., Edmunds, C.W., Radosevich, M., Vogt, F., Rials, T.G. and Labbé, N. (2011). Surface functionality and carbon structures in lignocellulosic-derived biochars produced by fast pyrolysis. *Energy Fuels*, 25, 4693–4703. <https://doi.org/10.1021/ef200915s>
- Kostas, E., Duran-Jimenez, G., Shepherd, B., Meredith, W., Stevens, L., Williams, S., Lye, G and Robinson, J. (2020). Microwave pyrolysis of olive pomace for bio-oil and bio-char production. *Chemical Engineering Journal*, 387 (2020). <https://doi.org/10.1016/j.cej.2019.123404>
- Kpalo, S. Y., Zainuddin, M. F., Manaf, L. A. and Roslan, A. M. (2021). Evaluation of hybrid briquettes from corncob and oil palm trunk bark in a domestic cooking application for rural communities in Nigeria. *Journal of Cleaner Production*, 284 (2021). <https://doi.org/10.1016/j.jclepro.2020.124745>
- Kshirsagar, M. P. and Kalamkar, V. R. (2020). Application of multi-response robust parameter design for performance optimization of a hybrid draft biomass cook stove. *Renewable Energy*, 153 (2020), 1127-1139. <https://doi.org/10.1016/j.renene.2020.02.049>
- Kuhe, A. and Aliyu, S. J. (2015). Gasification of loose groundnut shells in a throatless downdraft gasifier. *International Journal of Renewable Energy*, 4(2), 125-130. <https://doi.org/10.14710/ijred.4.2.125-130>.
- Kumar, M., Mishra, P.K. and Upadhyay, S.N. (2019). Pyrolysis of *Saccharum munja*: Optimization of process parameters using response surface methodology (RSM) and evaluation of kinetic parameters, *Bioresource Technology Reports* (2019). <https://doi.org/10.1016/j.biteb.2019.100332>.
- Kumar, A., Kumar, J. and Bhaskar, T. (2020a). Utilization of lignin: A sustainable and eco-friendly approach. *Journal of the Energy Institute*, 93 (1), 235-271. <https://doi.org/10.1016/j.joei.2019.03.005>.

- Kumar, A., Bhattacharya, T., Hasnain, M., Nayak, A. K. and Hasnain, S. (2020b). Applications of biomass-derived materials for energy production, conversion and storage. *Material Science for Energy Technologies*, 3 (2020), 905-920. <https://doi.org/10.1016/j.mset.2020.10.012>
- Kumar, R. Strezov, V., Weldekidan, H., He, J., Singh, S., Kan, T. and Dastjerdi, B. (2020c). Lignocellulose biomass pyrolysis for bio-oil production: A review of biomass pre-treatment methods for production of drop-in fuels. *Renewable and Sustainable Energy Reviews*, 123 (2020). <https://doi.org/10.1016/j.rser.2020.109763>.
- Kumar, D., Jeewan, S. and Tirkey, V. (2021). Modeling and multi-objective optimization of parameter air gasification performance parameters using Syzygium cumini biomass by integrating ASPEN Plus with Response surface methodology (RSM). *International Journal of Hydrogen Energy*, 46 (36), 18816-18831. <https://doi.org/10.1016/j.ijhydene.2021.03.054>.
- Laouge, Z. B., Çiğgin, A. S. and Merdun, H. (2020). Optimization and characterization of bio-oil from fast pyrolysis of Pearl Millet and Sida cordifolia L. by using response surface methodology. *Fuel*, 274. <https://doi.org/10.1016/j.fuel.2020.117842>.
- Lazzari, E., Schena, T., Primaz, C.T., da Silva, G.P, Machado, M.E., Cardoso, C.A.L., Jacques, R.A. and Caramão, E.B. (2016). Production and chromatographic characterization of bio-oil from the pyrolysis of mango seed waste. *Ind. Crops Prod.*, 83 (2016), 529–536. <https://doi.org/10.1016/j.indcrop.2015.12.073>.
- Lee, X. J., Lee, L.Y., Hiew, B. Y. Z., Gan, S., Thangalazhy-Gopakumar, S. and Ng, H. K. (2017). Multistage optimization of slow pyrolysis synthesis of biochar palm oil sludge for adsorption of lead. *Bioresources Technology*, 245 (2017), 944-953. doi: 10.1016/j.biortech.2017.08.175.
- Li, L., Rowbotham, J.S., Greenwell, H.C. and Dyer, P. W. (2016). New and Future Development in Catalysts: An introduction to pyrolysis and catalytic pyrolysis: versatile techniques for biomass conversion. *Biomass Conversion*, 2013, 173-208. <https://doi.org/10.2016/B978-0-444-53878-9.00009-6>.
- Liu, H., Ahmad, M. S., Alhumade, H., Elkamel, A., Sammak, S. and Shen, B. (2020). A hybrid kinetic and optimization approach for biomass pyrolysis: The hybrid scheme of the isoconversional methods, DAEM, and a parallel reaction mechanism. *Energy Conversion and Management*, 208 (2020). <https://doi.org/10.1016/j.enconman.2020.112531>

- Lok, C.M, Doorn, J.V. and Almansa, G.A. (2019). Promoted ZSM-5 catalysts for the production of bio-aromatics, a review. *Renew Sustain Energy Rev.*, (2019), 109-248. <https://doi.org/10.1016/j.rser.2019.109248>
- Madhu, P., Livingston, T. S. and Kanagasabapathy, H. (2018). Flash Pyrolysis of Lemon Grass (*Cymbopogon flexuosus*) for Bio-oil Production in an Electrically Heated Fluidized Bed Reactor. *Waste Biomass Valor.*, 9(2018), 1037–1046. <https://doi.org/10.1007/s12649-017-9872-6>.
- Magdziarza, A., Wilka, M. and Wądrzykb, M. (2020). Pyrolysis of hydrochar derived from biomass – Experimental investigation. *Fuel*, 267 (2020). <https://doi.org/10.1016/j.fuel.2020.117246>.
- Maliutina, K., Tahmasebi, A., Yu, J. and Saltykov, S. N. (2017). Comparative study on flash pyrolysis characteristics of microalgal and lignocellulosic biomass in entrained-flow reactor. *Energy Conversion and Management*, 151, 426–438. <https://doi.org/10.1016/j.enconman.2017.09.013>
- Mansor, A.M., Lim, J.S., Ani, F.N., Hashim, H., Ho, W.S. (2019). Characteristics of cellulose, hemicellulose and lignin of md2 pineapple biomass, *Chemical Engineering Transactions*, 72, p79-84. doi:10.3303/CET1972014
- Mary, G. S., Sugumaran, P., Niveditha, S., Ramalakshmi, B., Ravichandran, P. and Seshadri, S. (2016). Production, characterization and evaluation of biochar from pod (*Pisum sativum*), leaf (*Brassica oleracea*) and peel (*Citrus sinensis*) wastes. *Int J Recycl Org Waste Agricult*, 5 (2016), 43–53. <https://doi.org/10.1007/s40093-016-0116-8>
- Materazzi, M. and Lettieri, P. (2017). *Fluidized Beds for the Thermochemical Processing of Waste*. Reference Module in Chemistry, Molecular Sciences and Chemical Engineering, 2017. <https://doi.org/10.1016/B978-0-12-409547-2.12180-8>.
- Menares, T., Herrera, J., Romero, R., Osorio, P. and Arteaga-Pérez, L. E. (2020). Waste tires pyrolysis kinetics and reaction mechanisms explained by TGA and Py-GC/MS under kinetically-controlled regime. *Waste Management*, 102 (2020), 21–29. <https://doi.org/10.1016/j.wasman.2019.10.027>
- Menendez, J.A., Dominguez, A., Inguanzo, M. and Pis, J.J. (2004). Microwave pyrolysis of sewage sludge: Analysis of the gas fraction. *Journal of Analytical and Applied Pyrolysis*, 71 (2004), 657-667. <https://doi.org/10.1016/j.jaap.2003.09.003>
- Merdun, H. and Laouge, Z. B. (2020). Kinetic and thermodynamic analyses during co-pyrolysis of greenhouse wastes and coal by TGA. *Renewable Energy*, 163 (2021), 453-464. <https://doi.org/10.1016/j.renene.2020.08.120>

- Mishra, K. and Sinha, S. (2020). Development and assessment of Moringa oleifera (Sahajana) leaves filler/epoxy composites: Characterization, barrier properties and in situ determination of activation energy. *Polymer Composites*, 2020, 1–14. <https://doi.org/10.1002/pc.25771>
- Mohammed, I. Y., Abakr, Y. A., Yusup, S. and Kazi, F. K. (2017). Valorization of Napier grass via intermediate pyrolysis: Optimization using response surface methodology and pyrolysis products characterization. *Journal of Cleaner Production*, 142 (2017), 1848-1866. <https://doi.org/10.1016/j.jclepro.2016.11.099>
- Moralı, U. and Sensöz, S. (2015). Pyrolysis of hornbeam shell (*Carpinusbetulus*L.) in a fixed bed reactor: characterization of bio-oil and bio-char. *Fuel*, 150, 672–678. <https://doi.org/10.1016/j.fuel.2015.02.095>.
- Morgano, M.T., Bergfeldt, B., Leibold, H., Richter, F. and Stapf, D. (2018). Intermediate pyrolysis of agricultural waste: a decentral approach towards a circular economy. *Chemical Engineering Transactions*, 65(2018), 649-654. <http://dx.doi.org/10.3303/CET1865109>
- Mortari, D. A., Parondi, D., Rossi, G. B., Bonato, J. I., Godinho, M. and Pereira, F. M. (2021). The influence of water-soluble inorganic matter on combustion of grape pomace and its chars produced by slow and fast pyrolysis. *Fuel*, 284 (2020). <https://doi.org/10.1016/j.fuel.2020.118880>.
- Moshi, R., Jande, Y., Kivevele, T and Kim, W. (2020). *Simulation and performance analysis of municipal solid waste gasification in a novel hybrid fixed bed gasifier using Aspen plus*. *Energy Sources, Part A: Recovery, Utilization, and Environmental Effects*. 1-13. 10.1080/15567036.2020.1806404.
- Muller-Hagedorn, M. and Bockhorn, H. (2007). Pyrolytic behaviour of different biomasses (angiosperms) (maize plants, straws, and wood) in low temperature pyrolysis. *Journal of Analytical and Applied Pyrolysis*. 79 (2), 136–146. <https://doi.org/10.1016/j.jaap.2006.12.008>
- Munir, S., Daood, S.S., Nimmo, W., Cunliffe, A.M. and Gibbs, B.M. (2009). Thermal analysis and devolatilization kinetics of cotton stalk, sugar cane bagasse and shea meal under nitrogen and air atmospheres. *Bioresour Technol*, 100 (2009), 1413–8. <https://doi.org/10.1016/j.biortech.2008.07.065>
- Myers, R. H., Montgomery, D. C. (2000). *Response surface methodology: process and product optimization using designed experiments*. 2nd ed., John Wiley and Sons, USA.

- Nagarajan, J. and Prakash, L. (2021). Preparation and characterization of biomass briquettes using sugarcane bagasse, corncob and rice husk. *Materials Today: Proceedings*, 47 (2021), 4194–4198. <https://doi.org/10.1016/j.matpr.2021.04.457>
- Nam, J. Y., Lee, T. R., Park, S. J., Nam, H., Yoon, S. J., Mun, T., Yoon, S. M., Moon, J. H., Lee, J. G., Lee, D. H., Ra, H. W. and Seo, M. W. (2022). High temperature flash pyrolysis characteristics of waste plastics (SRF) in a bubbling fluidized bed: Effect of temperature and pelletizing. *Fuel*, 326 (2022). <https://doi.org/10.1016/j.fuel.2022.125022>.
- Narzari, R., Bordoloi, N., Sarma, B., Gogoi, L., Gogoi, N., Borkotoki, B. and Kataki, R. (2017). Fabrication of Biochars Obtained from Valorization of Biowaste and Evaluation of its Physicochemical Properties. *Bioresource Technology*, 242, 324-328. doi: 10.1016/j.biortech.2017.04.050.
- Nizamuddin, S., Mubarak, N., Tiripathi, M., Jayakumar, N. and Sahu, J. (2016). Ganesan P. Chemical, dielectric and structural characterization of optimized hydrochar produced from hydrothermal carbonization of palm shell. *Fuel*, 163(2016), 88–97. <https://doi.org/10.1016/j.fuel.2015.08.057>
- Nunes, L. J. R. (2022). Biomass gasification as an industrial process with effective proof-of-concept: A comprehensive review on technologies, processes and future developments. *Results in Engineering*, 14 (2022). <https://doi.org/10.1016/j.rineng.2022.100408>
- Nwosu, F. O. and Muzakir, M. M. (2015). Isolation and Physicochemical Characterization of Lignin from *Chromolaena Odorata* and *Tithonia Diversifolia*. *J. Appl. Sci. Environ. Management*, 19 (4) 787–792. <http://dx.doi.org/10.4314/jasem.v19i4.28>
- Nyazika, T., Jimenez, M., Samyn, F and Bourbigot, S. (2019). Pyrolysis modeling, sensitivity analysis, and optimization techniques for combustible materials: A review. *Journal of Fire Sciences*. 37. 073490411985274. 10.1177/0734904119852740.
- Obuka, N. S.P, Onyechi, P. C. and Okoli, N. C. (2019). Palm Oil Biomass Waste a Renewable Energy Resource for Power Generation. *Saudi Journal of Engineering and Technology (SJEAT)*, 679-691. DOI:10.21276/sjeat.2018.3.12.2.
- Ogunsanwo, O.Y., Adegoke, I.A. and Fuwape, J.A. (2014). Spectroscopic analysis of bio-oil produced from sawdust of three hard wood species in Nigeria. *J. Environ. Ext.* 11, 45–51.
- Ogunsola, O. E., Adeleke, O. and Aruna, A. T. (2018). Wood Fuel Analysis of Some Selected Wood Species within Ibadan. *IOP Conference Series: Earth and Environmental Science*, 173(2018), doi: 10.1088/1755-1315/173/1/012043.

- Okokpujie, I. P., Fayomi, O. S. I., and Oyedepo, S. O. (2019). The role of mechanical engineers in achieving sustainable development goals. *Procedia Manufacturing*, 35, 782-788. <https://doi.org/10.1016/j.promfg.2019.06.023>
- Okonkwo, U. C. Onokpите, E. and Onokwai, A. O. (2018). Comparative Study of the Optimal Ratio of Biogas Production from various Organic Wastes and Weeds for Digester/Restarted Digester. *Journal of King Saud University-Engineering Science*, 30 (2), 123-129. <https://doi.org/10.1016/j.jksues.2016.02.002>.
- Ojediran, J.O., Adeboye, K., Adewumi, A. D. and Okonkwo, C. E. (2020). Evaluation of briquettes produced from maize cob and stalk. *IOP Conf. Series: Earth and Environmental Science*, 445 (2020). Doi:10.1088/1755-1315/445/1/012052.
- Oladejo, O. S., Abiola, A. O., Olanipekun, A. A., and Ajayi, O. E. and Onokwai, A. O. (2020). Energy Potential of Solid Waste Generated in Landmark University, Omu-Aran, Kwara State, Nigeria. *LAUTECH Journal of Civil and Environmental Studies*, 5 (2020). [https://doi.org/10.36108/laujoces/0202/50\(0150\)](https://doi.org/10.36108/laujoces/0202/50(0150)).
- Olagbende, H.O., Aransiola, E. F., Ogunsina, B. S., Sanda, O. and Shonibare, O. O. (2016). Modification of a Fixed Bed Reactor System for Pyrolytic Conversion of Royal Poinciana Pods into Alternative Fuels. *International Journal of Renewable Energy Research*, 6 (4), 1349-1360.
- Onarheim, K., Hannula, I. and Solantausta, Y. (2020). Hydrogen enhanced biofuels for transport via fast pyrolysis of biomass: A conceptual assessment. *Energy*, 199 (2020). <https://doi.org/10.1016/j.energy.2020.117337>.
- Onokwai, A. O., Owamah, H. I., Ibiwoye, M. O., Ayuba, G. C., Olayemi, O. A. (2022). Application of Response Surface Methodology (RSM) for the optimization of energy generation from Jebba hydro-power plant, Nigeria. *ISH Journal of Hydraulic Engineering*, 28 (1), 1-9. <https://doi.org/10.1080/09715010.2020.1806120>.
- Owamah, H. I. Alfa, M. and Onokwai A. O. (2022). Preliminary evaluation of the effect of effect of chicken feather with no major pre-treatment on biogas production from horse dung. *Environmental Nanotechnology, Monitoring and Management*, 28 (1), 1-9. <http://doi.org/10.1016/j.enmm.2020.100347>.
- Oyebanji, J. A., Okekunle, P. O. and Lasode, A. O. (2018). Product yield distribution and characterization of bio-oil from west Africa cordia sawdust pyrolysis. *Nigeria Journal of Technological Research*. 13 (2), 25-30.

- Oyebanji, J.A., Okekunle, P. O., Oyedepo, S. O. and Fayomi, O. S. I. (2020). Physicochemical properties of wood sawdust: A preliminary study. *IOP Conf Series: Materials Science and Engineering*, 1107 (2021).
- Oyebanji, J. A., Okekunle, P. O., Oyedepo, S. O. and Fayomi, O. S. I. (2021). Characterization of Liquid and Solid Products from Pyrolysis of Terminalia ivorensis. *IOP Conf. Ser.: Mater. Sci. Eng.*, 1107 (1). <https://iopscience.iop.org/article/10.1088/1757-899X/1107/1/012127/meta>
- Oyebanji, J. A., Fayomi, O. S. I., Oyeniyi, O. I., Akor, P. G. and Ajayi, S. T. (2022). Physico-chemical analysis of pyrolyzed bio-oil from Lophira alata (Ironwood) wood. *Journal of Environmental Pollution and Management*, 4 (2022), 1-9.
- Oyejobi. D.O., Jameel, M., Sulong, N.H.R., Raji, S. A. and Ibrahim, H. A. (2020). Prediction of optimum compressive strength of light-weight concrete containing Nigerian palm kernel shells. *Journal of King Saud University – Engineering Sciences*, 32 (2020), 303–309. <http://dx.doi.org/10.1016/j.jksues.2019.04.001>
- Özsin, G. and Pütün, A. E. (2019). TGA/MS/FT-IR study for kinetic evaluation and evolved gas analysis of a biomass/PVC co-pyrolysis process. *Energy Conversion and Management*, 182 (2019), 143–153. <https://doi.org/10.1016/j.enconman.2018.12.060>
- Ozyuguran, A., Yaman, S. and Kucukbayrak, S. (2018). Prediction of calorific value of biomass based on elemental analysis. *International Advanced Researches and Engineering Journal*, 2(3), 254-260.
- Paenpong, C. and Pattiya, A. (2016). Effect of pyrolysis and moving-bed granular filter temperatures on the yield and properties of bio-oil from fast pyrolysis of biomass. *Journal of Analytical and Applied Pyrolysis*, 119 (2016), 40-51. <https://doi.org/10.1016/j.jaap.2016.03.019>
- Palumbo, A. W., Bartel, C. J., Sorli, J. C. and Weimer, A. W. (2019). Characterization of products derived from the high temperature flash pyrolysis of microalgae and rice hulls. *Chemical Engineering Science*, 196 (2019), 527-537. <https://doi.org/10.1016/j.ces.2018.11.029>.
- Pan, C., Chen, A., Liu, Z., Chen, P., Lou, H. and Zheng, X. (2012). Aqueous-phase reforming of the low-boiling fraction of rice husk pyrolyzed bio-oil in the presence of platinum catalyst for hydrogen production. *Bioresour. Technol.* 125, 335-339. <https://doi.org/10.1016/j.biortech.2012.09.014>

- Panneerselvam, R. and Sai, G. (2016). Computational Fluid Dynamics Modelling of Biomass Fast Pyrolysis in Fluidised Bed Reactors, Focusing Different Kinetic Schemes. *Bioresource Technology*, 213 (2016), 333-341. <https://doi.org/10.1016/j.biotech.2016.02.042>.
- Parvez, A.M., Mujtaba, I.M. and Wu, T. (2016). Energy, exergy and environmental analyses of conventional, steam and CO₂- enhanced rice straw gasification. *Energy*, 2016, 94(2016), 579-88. <https://doi.org/10.1016/j.energy.2015.11.022>
- Pattiya, A. (2018). Direct thermochemical liquefaction for energy applications. *Catalytic Pyrolysis*, 29-64. <https://doi.org/10.1016/B978-0-08-101029-7.00002-3>
- Paykani, A., Chehrmonavari, H., Tsolakis, A., Alger, T., Northrop, W. F., Reitz, R. D. (2022). Synthesis gas as a fuel for internal combustion engines in transportation. *Progress in Energy and Combustion Science*, 90 (2022). <https://doi.org/10.1016/j.pecs.2022.100995>
- Peters, J.F., Petrakopoulou, F. and Dufour, J. (2015b). Exergetic analysis of a fast pyrolysis process for bio-oil production. *Fuel Process Technol*, 119 (2014), 245-55.
- Peters, J.F., Petrakopoulou, F. and Dufour, F. (2015a). Exergy analysis of synthetic biofuel production via fast pyrolysis and hydrougrading. *Energy*, 79 (2015), 325-336.
- Piloto-Rodríguez, R., Tobío, I., Ortiz-Alvarez, M., Diaz, Y., Konradi, S. and Pohl, S. (2020). *An approach to the use of Jatropha curcas by-products as energy source in agroindustry*. *Energy Sources, Part A: Recovery, Utilization and Environmental Effects*. <https://doi.org/10.1080/15567036.2020.1749192>
- Pinto, O., Romero, R., Carrier, M., Appelt, J. and Segura, C. (2018). Fast pyrolysis of tannins from pine bark as a renewable source of catechols. *J. Anal. Appl. Pyrolysis*, 136, 69–76. <https://doi.org/10.1016/j.jaap.2018.10.022>
- Posom, J. and Sirisomboom, P. (2017). Evaluation of lower heating value and elemental composition of bamboo using near infrared spectroscopy. *Energy*, 121 (2017), 147-158. <https://doi.org/10.1016/j.energy.2017.01.020>
- Qian, Y., Zhan, J., Yu, Y., Xu, G. and Liu, X. (2019). CFD model of coal pyrolysis in fixed bed reactor. *Chemical Engineering Science*, 200 (8), 1-11. <https://doi.org/10.1016/j.ces.2018.12.064>
- Quan, C., Ma, Z., Gao, N. and He, C. (2018). Pyrolysis and combustion characteristics of corncob hydrolysis residue. *Journal of Analytical and Applied Pyrolysis*, 130 (2018), 72–78. <https://doi.org/10.1016/j.jaap.2018.01.025>

- Ramesh, N. and Murugavelh, S. (2020). A cleaner process for conversion of invasive weed (*Prosopis juliflora*) into energy-dense fuel: kinetics, energy, and exergy analysis of pyrolysis process. *Biomass Conversion and Biorefinery* (2020). <https://doi.org/10.1007/s13399-020-00747-5>.
- Rasool, T. and Kumar, S. (2020). Kinetic and Thermodynamic Evaluation of Pyrolysis of Plant Biomass using TGA. *Materials Today: Proceedings*, 21 (2020), 2087–2095. <https://doi.org/10.1016/j.matpr.2020.01.328>
- Roger, M. R., Roger P. and Mandla A. T. (2021). Cell Wall Chemistry from: Handbook of Wood Chemistry and Wood Composites CRC Press. <https://www.routledgehandbooks.com/doi/10.1201/b12487-5>
- Romuli, S., Karaj, S., Correa, C. R., Kruse, A. and Muller, J. (2019). Physico-mechanical properties and thermal decomposition characteristics of pellets from *Jatropha curcas* L. residues as affected by water addition. *Biofuels*, 12 (9), 1149-1156. 10.1080/17597269.2019.1594596.
- Ruiz, J. A., Juárez, M. C., Morales, M. P., Muñoz, P. and Mendivil, M. A. (2013). Biomass gasification for electricity generation: Review of current technology barriers. *Renewable and Sustainable Energy Reviews*, 18(0), 174-183. <https://doi.org/10.1016/j.rser.2012.10.021>
- Rupesh, S., Chandrasekharan, M. and Palatel, A. (2019). Energy and exergy analysis of syngas production from different biomasses through air-steam gasification. *Frontiers in Energy*, 14 (7), 1-13. <http://dx.doi.org/10.1007/s11708-016-0439-1>
- Sahoo, S. S., Vijay, V. K., Chandra, R. and Kumar, H. (2021). Production and characterization of biochar produced from slow pyrolysis of pigeon pea stalk and bamboo. *Cleaner Engineering and Technology*, 3 (2021). <https://doi.org/10.1016/j.clet.2021.100101>
- Saikia, R., Chutia, R.S., Katak, R. and Pant, K.K. (2015). Perennial grass (*Arundodonax* L.) as a feedstock for thermo-chemical conversion to energy and materials. *Bioresour. Technol.*, 188, 265–272. <https://doi.org/10.1016/j.biortech.2015.01.089>
- Saleh, A. R., Sudarmanta, B., Fansuri, H., and Muraza, O. (2019). Improve municipal solid waste gasification efficiency using a modified downdraft gasifier with variations of air input and preheated air temperature. *Energy Fuel*, 33 (2019), 11049-11056. <https://doi.org/10.1021/acs.energyfuels.9b02486>.
- Salina, F. H., Molina, F. B., Gallego, A. G. and Palacios-Bereche, R. (2021). Fast pyrolysis of sugarcane straw and its integration into the conventional ethanol production process through Pinch Analysis. *Energy*, 107 (2021), 2411-2502. <http://doi.org/10.1016/j.energy.2020.119066>

- Samuel, O. D., Waheed, M. A., Taheri-Garavand, A., Verma, T. N., Dairo, O. U., Bolaji, B. O., Afzal, A. (2021). Prandtl number of optimum biodiesels from food industrial waste oil and diesel fuel blend for diesel engine. *Fuel*, 285 (2021). <https://doi.org/10.1016/j.fuel.2020.119049>.
- Savasari, M., Emadi, M., Bahmanyar, M.A. and Biparva, P. (2015). Optimization of Cd (II) removal from aqueous solution by ascorbic acid-stabilized zero-valent iron nanoparticles using response surface methodology. *J. Ind. Eng. Chem.*, 21, 1403–1409. <https://doi.org/10.1016/j.jiec.2014.06.014>.
- Sawadogo, M., Kpai, N., Tankoano, I., Tanoh, S.T. and Sidib, S. (2018). Cleaner production in Burkina Faso: case study of fuel briquettes made from cashew industry waste. *J. Clean. Prod.* 195, 1047-1056. <https://doi.org/10.1016/j.jclepro.2018.05.261>
- Sekar, M., Ponnusamy, V. K., Pugazhendhi, A., Nizetic, S. and Praveenkumar, T. R. (2022). Production and utilization of pyrolysis oil from solidplastic wastes: A review on pyrolysis process and influence of reactors design. Production and utilization of pyrolysis oil from solidplastic wastes: A review on pyrolysis process and influence of reactors design. *Journal of Environmental Management*, 302 (15). <https://doi.org/10.1016/j.jenvman.2021.114046>
- Shaheed, R., Azhari, C. H., Ahsan, A. and Mohtar, W. H. M. W. (2015). Production and Characterization of Low-Tech Activated Carbon from Coconut Shell. *J. Hydrol. Environ. Res*, 3 (1), 6-14. <https://hdl.handle.net/10652/4505>
- Sharma, A., Shinde, Y., Pareek, V. and Zhang, D. (2015). Process Modelling of Biomass Conversion to Biofuels with Combined Heat and Power. *Bioresource Technology*, 198 (2015), 309-315. <https://doi.org/10.1016/j.biortech.2015.09.014>.
- Sharma, I., Rackermann, D., Ramirez, J., Cronin, D., Moghaddam, L., Beltramini, J. N., Teo, J., Li, K., Shi, C. and Doherty, W. O. S. (2022). Exploring the potential for biomethane production by the hybrid anaerobic digestion and hydrothermal gasification process: A review. *Journal of Cleaner Production*, 362 (15). <https://doi.org/10.1016/j.jclepro.2022.132507>
- Sensoz, S. and Angin, D. (2008). Pyrolysis of safflower (*Charthamus tinctorius* L.) seed press cake: Part 1. The effects of pyrolysis parameters on the product yields. *Bioresource Technology*, 99 (13), 5492-5497. <https://doi.org/10.1016/j.biortech.2007.10.046>
- Serov, A., Hrabovsky, M., Kopecký, V., Maslani, A., Hlina, M. and Hurba, O. (2019). Lignite Gasification in Thermal Steam Plasma. *Plasma Chemistry and Plasma Processing*, 39. 395–406. 10.1007/s11090-019-09957-w.

- Shi, X., Ronsse, F., Nachenius, R. and Pieters, J. G. (2019). 3D Eulerian-Eulerian modeling of a screw reactor for biomass thermochemical conversion. Part 2: Slow pyrolysis for char production. *Renewable Energy*, 143 (2019), 1477-1487. <https://doi.org/10.1016/j.renene.2019.05.088>
- Singh, R. K., Patil, T. and Sawarkar, A. N. (2020). Pyrolysis of garlic husk biomass: Physico-chemical characterization, thermodynamic and kinetic analyses. *Bioresource Technology Reports*, 12 (2020). <https://doi.org/10.1016/j.biteb.2020.100558>.
- Sinha, S., Jhalani, A., Ravi M R, and Ray, Anjan. (2000). Modeling of pyrolysis in wood: A review. *J. Solar Energy Society of India*. 10. 41-62.
- Snoussi, A., Chekir, N. and Ben B. A. (2020). Entropy generation in multi-stage flash desalination plants. *Int J Energy Environ Eng*, 11, 327–339, <https://doi.org/10.1007/s40095-020-00337-1>.
- Sobek, S and Werle, S. (2019). Solar pyrolysis of waste biomass: Part 1 reactor design. *Renewable Energy*, 143 (2019). <https://doi.org/10.1016/j.renene.2019.06.011>
- Soka, O, and Oyekola, O. (2020). A feasibility assessment of the production of char using the slow pyrolysis process. *Heliyon*. 6. e04346. 10.1016/j.heliyon. 2020.e04346.
- Stefanidis, S.D., Kalogiannis, K.G., Iliopoulou, E.F., Michailof, C.M., Pilavachi, P.A. and Lappas, A.A. (2014). A study of lignocellulosic biomass pyrolysis via the pyrolysis of cellulose, hemicellulose and lignin. *J. Anal. Appl. Pyrolysis*, 105 (2014), 105, 143–150. <https://doi.org/10.1016/j.jaap.2013.10.013>
- Stegen, S. and Kaparajua, P. (2020). Effect of temperature on oil quality obtained through pyrolysis of sugarcane Bagasse. *Fuel*, 276 (2020). <https://doi.org/10.1016/j.fuel.2020.118112>.
- Suárez, J.A., Luengo, C.A., Felfli, F.F., Bezzon, G. and Beatón, P.A. (2000). Thermochemical properties of Cuban biomass. *Energy Sources*, 22(2000), 851–7.
- Sun, P., Heng, M., Sun, S. and Chen, J. (2011). Analysis of liquid and solid products from liquefaction of paulownia in hot-compressed water. *Energy Convers. Manage.*, 52 (2011) 924–933. <https://doi.org/10.1016/j.enconman.2010.08.020>
- Sun, J., He, F., Pan, Y. and Zhang, Z. (2017). Effects of pyrolysis temperature and residence time on physicochemical properties of different biochar types. *Acta Agric. Scand. Sect. B Soil Plant Sci*. 67, 12–22. <https://doi.org/10.1080/09064710.2016.1214745>.
- Suriapparao, D. and Tejasvi, R. (2022). A review on role of process parameters on pyrolysis of biomass and plastics: Present scope and future opportunities in conventional and microwave-assisted

- pyrolysis technologies. *Process Safety and Environmental Protection*, 162 (2022), 435-462. <https://doi.org/10.1016/j.psep.2022.04.024>.
- Sustainable Development Report (SDR) (2020). dashboards.sdgindex.org. Retrieved 2020-09-23.
- Sustainable Development Goal (SDG) (2020). The government of Nigeria presents 2nd voluntary national review on sustainable development. Retrieved 2020-09-23.
- Tang, L and Huang, H. (2005). Plasma pyrolysis of biomass for production of syngas and carbon adsorbent. *Energy Fuels*, 19 (2005), 1174-1178. <https://doi.org/10.1021/ef049835b>
- Tang, Y., Dong, J., Chi, Y., Zhou, Z. and Ni, M. (2019). Energy and Exergy Analyses of Fluidized-Bed Municipal Solid Waste Air Gasification. *Energy and Fuels, American Chemical Society*, 30 (9), 7629-7637. Doi: 10.1021/acs.energyfuels.6b01418.
- Thengane, S. K., Gupta, A. and Mahajani, S. M. (2018). Co-gasification of high ash biomass and high ash coal in downdraft gasifier. *Bioresource Technology*, (2018), doi: <https://doi.org/10.1016/j.biortech.2018.11.007>
- Treedet, W. and Suntivarkorn, R. (2018). Design and operation of a low-cost bio-oil fast pyrolysis from sugarcane bagasse on circulating fluidized bed reactor in a pilot plant. *Fuel Processing Technology*, 179 (2018), 17-31. <https://doi.org/10.1016/j.fuproc.2018.06.006>
- Torsosa-Masia, A. A., Buhre, B. T. E., Gupta, R., Wall, T. F. (2007). Characterizing ash of biomass and waste. *Fuel Processing Technology*, 99 (11-12), 1071-1081. <http://dx.doi.org/10.1016/j.fuproc.2007.06.011>
- Tripathi, M., Bhatnagar, A., Mubarak, N. M., Sahu, J. N. and Ganesan, P. (2020). RSM optimization of microwave pyrolysis parameters to produce OPS char with high yield and large BET surface area. *Fuel*, 225. <https://doi.org/10.1016/j.fuel.2020.118184>.
- Tsai, W.T., Lee, M.K. and Chang, Y.M. (2006). Fast pyrolysis of rice straw, sugarcane bagasse and coconut shell in an induction-heating reactor. *J Anal Appl Pyrolysis*, 76 (2006), 230-7. <https://doi.org/10.1016/j.jaap.2005.11.007>
- Uddin, M. S., Joardder, M. U. H. and Islam, M. N. (2012). Design and Construction of Fixed Bed Pyrolysis System and Plum Seed Pyrolysis for Bio-Oil Production. *International Journal of Advance Renewable Energy Research*, 1(7), 405-409.
- Umar, H. A., Sulaiman, S. A., Said, M. A. B. and Ahmad, R. K. (2021). *Palm Kernel Shell as Potential Fuel for Syngas Production*. S. S. Emamian *et al.* (eds.), *Advances in Manufacturing*

Engineering, Lecture Notes in Mechanical Engineering, https://doi.org/10.1007/978-981-15-5753-8_25.

- Umar, H. A., Sulaiman, S. A., Ahmad, R. K., Tamili, S. N. (2020). Characterization of oil palm trunk and frond as fuel for biomass thermochemical. IOP Conf. Series: Material Science and Engineering, 863 (2020). Doi:10.1088/1757-899X/863/1/012011.
- Varma, A. K. and Mondal, P. (2017). Pyrolysis of sugarcane bagasse in semi-batch reactor: Effects of process parameters on product yields and characterization of products. *Industrial Crops and Products*, 95 (2017), 704–717. <https://doi.org/10.1016/j.indcrop.2016.11.039>.
- Vassilev, S. V., Baxter, D., Andersn, L. K. and Vassilev, C. G. (2010). An overview of the chemical composition of biomass. *Fuel*, 89 (2010), 913–933. <https://doi.org/10.1016/j.fuel.2009.10.022>
- Wan, K., Wang, Z., He, Y., Xia, J., Zhou, Z., Zhou, J. and Gen, K. (2015). Experimental and Modelling Study of Pyrolysis of Coal, Biomass and Blended Coal-Biomass Particles. *Fuel*, 139 (2015), 356-364. <https://doi.org/10.1016/j.fuel.2014.08.069>.
- Wang X, Lv W, Guo L, Zhai M, Dong P, Qi G. (2016). Energy and exergy analysis of rice husk high-temperature pyrolysis. *Int J Hydrogen Energy*, 41(46), 2112-21130. <https://doi.org/10.1016/j.ijhydene.2016.09.155>.
- Wang, Q., Sarkar, J. (2018). Pyrolysis Behaviors of Waste Coconut Shell and Husk Biomasses. *Int. J. of Energy Prod. and Mgmt.*, 3(1), 34–43.
- Wanga, X., Maa, D., Jina, Q., Denga, S., Stančinb, H., Tana, H. and Mikulčića, H. (2019). Synergistic effects of biomass and polyurethane co-pyrolysis on the yield, reactivity, and heating value of biochar at high temperatures. *Fuel Processing Technology*, 194 (2019). <https://doi.org/10.1016/j.fuproc.2019.106127>.
- Xing, J., Luo, K., Wang, H., Gao, Z., Fan, J. (2019). A comprehensive study on estimating higher heating value of biomass from proximate and ultimate analysis with machine learning approaches. *Energy*, 188 (2019). <https://doi.org/10.1016/j.energy.2019.116077>.
- Xiong, Q., Xu, F., Ramirez, E., Pannala, S. and Daw, C. S. (2016). Modeling the Impact of Bubbling Bed Hydrodynamics on Tar Yield and its Fluctuations during Biomass Fast Pyrolysis. *Fuel*, 164 (2016), 11-17. <https://doi.org/10.1016/j.fuel.2015.09.074>.
- Xueyong, R., Hongzhen, C., Hongshuang, D. and Jianmin, C. (2017). The preparation and characterization of pyrolysis bio-oil resorcinol-aldehyde resin cold-set adhesives for wood construction. *Polymers*, 9(232), 1-11. <https://doi.org/10.3390/polym9060232>

- Yan, L., Cao, Y. and He, B. (2019). Energy, exergy, and economic analysis of novel biomass-fueled power plant with carbon capture and sequestration. *Science of the Total Environment*, 690 (2019), 812-820. <https://doi.org/10.1016/j.scitotenv.2019.07.015>
- Yang, Y., Brammer, D. G., Wright, J.A., Scott, Serrano, C. and Bridgwater, A. V. (2017). Combined heat and power from the intermediate pyrolysis of biomass of materials: performance, economics and environmental impact. *Applied Energy*, 191, 639-652. <https://doi.org/10.1016/j.apenergy.2017.02.004>
- Yang, Y., Zhang, Y., Omairey, E., Cai, J., Gu, F. and Bridgwater, A.V. (2018). Intermediate pyrolysis of organic fraction of municipal solid waste and rheological study of the pyrolysis oil for potential use as bio-bitumen. *J. Clean. Prod.* 187 (2018), 390–399. doi: 10.1016/j.jclepro.2018.03.205.
- Yong, J., Kim, J., Oh, C. H. and Park, J. (2018). Production of bio-oil from fast pyrolysis of biomass using a pilot-scale circulating fluidized bed reactor and its characterization. *Journal of Environmental Management*, 234 (2018). <http://dx.doi.org/10.1016/j.jenvman.2018.12.104>.
- Yorgun, S. and Yildiz, D. (2015). Slow pyrolysis of paulownia wood: Effects of pyrolysis parameters on product yields and bio-oil characterization. *Journal of Analytical and Applied Pyrolysis*, 114 (2015), 68–78. <http://dx.doi.org/10.1016/j.jaap.2015.05.003>
- Yosoon, C., Chaeyoung, L., Jinyoung, S. (2017). Review of Renewable Energy Technologies Utilized in the Oil and Gas Industry. *International Journal of Renewable Energy Research*, 7 (2), 592-598.
- Youcai, Z. and Tao, Z. (2021). Biohydrogen production and hybrid process development: Pretreatment and aged refuse, dosage on biohydrogen production from food waste. *Energy and Resource Recovery from Food Waste*. 149-238. <https://doi.org/10.1016/B978-0-12-821728-3.00003-7>.
- Yueshi, W., Weihong, Y and Wlodzimierz, B. (2014). Energy and Exergy Analysis of High Temperature Agent Gasification of Biomass. *Energies*, 7(2014), 2107-2122. 10.3390/en7042107.
- Zhang, C., Ho, S.H., Chen, W.H., Xie, Y., Liu, Z. and Chang, J.S. (2018). Torrefaction performance and energy usage of biomass wastes and their correlations with torrefaction severity index. *Appl Energy*, 220 (2018), 598-604.
- Zhang, J. and Zhang, X. (2019). The thermochemical conversion of biomass into biofuels. *Biomass, Biopolymer-Based Materials, and Bioenergy*. 15(2019), 327-368. <https://doi.org/10.1016/B978-0-08-102426-3.00015-1>

- Zhang, Y., Ji, G., Ma, D., Chen, C., Wang, Y., Wang, W. and Li, A. (2020). Exergy and energy analysis of pyrolysis of plastic wastes in rotary kiln with heat carrier. *Process Safety and Environmental Protection* (2020), 142 (2020), 203-211. doi: <https://doi.org/10.1016/j.psep.2020.06.021>
- Zhong, S., Zhang, B., Liu, C., Aldeen, A. S., Mwenya, S. and Zhang, H. (2022). A minireview on catalytic fast co-pyrolysis of lignocellulosic biomass for bio-oil upgrading via enhancing monocyclic aromatics. *Journal of Analytical and Applied Pyrolysis*, 164 (2022). <https://doi.org/10.1016/j.jaap.2022.105544>

APPENDICES

Appendix 1a: Analysis of Variance (ANOVA) for the bio-oil yields using PKS

Source	Sum of Squares	Degree of freedom (df)	Mean Squares	F-value	P-value probability >F	Remark
Model	479.719	10	47.97	31.43	<0.0001	Significant
A-Temperature	53.751	1	53.751	36.05	<0.0001	Significant
B-Reaction time	0.327	1	0.327	0.22	0.642	Not Significant
C-Heating rate	0.487	1	0.487	0.33	0.571	Not Significant
D-N ₂ flow rate	8.42	1	8.42	5.24	0.022	Significant
E-Particle size	0.864	1	0.864	4.07	0.051	Significant
A ²	35.905	1	35.905	24.08	<0.0001	Significant
C ²	9.274	1	9.274	6.22	0.017	Significant
AB	0.992	1	0.992	0.67	0.42	Not Significant
AE	9.136	1	9.136	6.03	0.019	Significant
BE	3.034	1	3.034	2.03	0.162	Not Significant
Residual	58.154	39	1.491			
Lack of fit	43.334	32	1.354	0.64	0.818	Not Significant
Pure error	14.82	7	2.117			
Cor Total	537.873	49				

$R^2 = 98.00\%$; Adjusted $R^2 = 96.42\%$; Predicted $R^2 = 82.87\%$; CV% = 5.04

Appendix 1b: Analysis of Variance (ANOVA) for the bio-oil yields using SCB

Source	Sum of Squares	Degree of freedom (df)	Mean Squares	F-value	P-value probability >F	Remark
Model	269.927	10	26.993	73.37	<0.0001	Significant
A-Temperature	5.649	1	5.649	15.36	<0.0001	Significant
B-Reaction time	0.48	1	0.48	1.31	0.26	Not Significant
C-Heating rate	4.963	1	4.963	13.49	0.001	Significant
D-N ₂ flow rate	0.051	1	0.051	0.14	0.712	Not Significant
E-Particle size	0.011	1	0.011	0.03	0.863	Not Significant
A ²	20.294	1	20.294	55.17	<0.0001	Significant
C ²	2.617	1	2.617	7.11	0.011	Significant
D ²	1.724	1	1.724	4.69	0.037	Significant
AB	0.813	1	0.813	2.21	0.145	Not Significant
AC	1.488	1	1.488	4.04	0.049	Significant
Residual	4.347	39	0.368			
Lack of fit	14.247	32	0.445	3.96	0.056	Not Significant
Pure error	0.1	7	0.0143			
Cor Total	284.274	49				

$R^2 = 98.01\%$; Adjusted $R^2 = 96.51\%$; Predicted $R^2 = 80.51\%$; CV% = 5.29

Appendix 1c: Analysis of Variance (ANOVA) for the bio-oil yields using SB

Source	Sum of Squares	Degree of freedom (df)	Mean Squares	F-value	P-value probability >F	Remark
Model	291.151	11	27.627	88.01	<0.0001	Significant
A-Temperature	5.615	1	5.615	19.35	<0.0001	Significant
B-Reaction time	1.448	1	1.448	5.051	0.031	Significant
C-Heating rate	4.291	1	4.291	14.79	<0.0001	Significant
D-N ₂ flow rate	0.036	1	0.036	0.13	0.726	Not Significant
E-Particle size	0.008	1	0.008	0.03	0.871	Not Significant
A ²	23.201	1	23.201	79.97	<0.0001	Significant
C ²	1.451	1	1.451	5.01	<0.0001	Significant
D ²	1.444	1	1.444	4.98	0.032	Significant
E ²	3.622	1	3.622	12.49	0.001	Significant
AB	0.733	1	0.733	2.53	0.1	Not Significant
AC	1.476	1	1.476	5.09	0.03	Significant
Residual	11.024	38	0.29			
Lack of fit	10.195	31	0.329	2.78	0.082	Not Significant
Pure error	0.829	7	0.118			
Cor Total	302.175	49				

$R^2 = 98.62\%$; Adjusted $R^2 = 97.44\%$; Predicted $R^2 = 82.63\%$; CV% = 5.63

Appendix 2a: Analysis of Variance (ANOVA) for the biochar yield using PKS

Source	Sum of Squares	Degree of freedom (df)	Mean Squares	F-value	P-value probability >F	Remark
Model	1298.16	10	129.66	340.53	<0.0001	Significant
A-Temperature	1261.11	1	1261.11	3312.07	<0.0001	Significant
B-Reaction time	6.34	1	6.34	16.64	<0.0001	Significant
C-Heating rate	7.49	1	7.49	19.67	<0.0001	Significant
D-N ₂ flow rate	6.87	1	6.87	18.04	<0.0001	Significant
E-Particle size	4.39	1	4.39	11.54	0.002	Significant
A ²	2.94	1	2.94	7.72	0.0008	Significant
B ²	1.11	1	1.11	2.92	0.095	Not Significant
C ²	0.94	1	0.94	2.46	0.125	Not Significant
AE	1.32	1	1.32	3.47	0.07	Significant
BD	2	1	2	4.14	0.048	Significant
Residual	14.85	39	0.38			
Lack of fit	13.94	32	0.44	3.36	0.051	Not Significant
Pure error	0.91	7	0.13			
Cor Total	1313.01	49				

$R^2 = 98.87\%$; Adjusted $R^2 = 97.81\%$; Predicted $R^2 = 85.18\%$; CV% = 5.46

Appendix 2b: Analysis of Variance (ANOVA) for the biochar yield using SCB

Source	Sum of Squares	Degree of freedom (df)	Mean Squares	F-value	P-value probability >F	Remark
Model	1266.92	10	126.69	877.64	<0.0001	Significant
Temperature	1254.26	1	1254.26	8688.69	<0.0001	Significant
Reaction time	2.2	1	2.2	15.22	<0.0001	Significant
Heating rate	1.78	1	1.78	12.31	0.001	Significant
N ₂ flow rate	2.16	1	2.16	14.95	<0.0001	Significant
Particle size	3.02	1	3.02	20.89	<0.0001	Significant
A ²	1.5	1	1.5	10.41	0.003	Significant
C ²	1.36	1	1.36	9.44	0.004	Significant
AB	0.26	1	0.26	1.82	0.185	Not Significant
AD	0.48	1	0.48	3.29	0.077	Not Significant
AE	1.16	1	1.16	8.06	0.007	Significant
Residual	5.63	39	0.14			
Lack of fit	4.81	32	0.15	1.29	0.39	Not Significant
Pure error	0.82	7	0.12			
Cor Total	1272.55	49				

$R^2 = 99.56\%$; Adjusted $R^2 = 98.99\%$; Predicted $R^2 = 88.99\%$; CV% = 6.38

Appendix 2c: Analysis of Variance (ANOVA) for the biochar yield using shea butter wood

Source	Sum of Squares	Degree of freedom (df)	Mean Squares	F-value	P-value probability >F	Remark
Model	1576.26	9	175.14	661.08	<0.0001	Significant
A-Temperature	1556.31	1	1556.31	5874.38	<0.0001	Significant
B-Reaction time	1.14	1	1.14	4.32	0.044	Significant
C-Heating rate	4	1	4	15.09	<0.0001	Significant
D-N ₂ flow rate	4.79	1	4.79	18.09	<0.0001	Significant
E-Particle size	3.79	1	3.79	14.31	0.001	Significant
A ²	4.2	1	4.2	15.86	<0.0001	Significant
B ²	3.76	1	3.76	14.19	0.001	Significant
BC	0.81	1	0.81	3.07	0.088	Significant
BD	1.15	1	1.15	4.33	0.044	Not Significant
Residual	10.6	40	0.24			
Lack of fit	10.22	33	0.31	5.72	0.011	Significant
Pure error	0.38	7	0.05			
Cor Total	1586.86	49				

$R^2 = 99.01\%$; Adjusted $R^2 = 98.58\%$; Predicted $R^2 = 86.58\%$; CV% = 5.37

Appendix 3a: Analysis of Variance (ANOVA) for the NCG yield using PKS

Source	Sum of Squares	Degree of freedom (df)	Mean Squares	F-value	P-value probability >F	Remark
Model	1922.99	10	192.3	487.74	<0.0001	Significant
Temperature	1324.17	1	1324.17	3358.57	<0.0001	Significant
Reaction time	2.22	1	2.22	5.64	0.023	Significant
Heating rate	2.63	1	2.63	6.68	0.014	Significant
N ₂ flow rate	5.63	1	5.63	14.24	0.001	Significant
Particle size	1.36	1	1.36	3.45	0.071	Not Significant
A ²	23	1	23	58.34	<0.0001	Significant
C ²	1.41	1	1.41	3.57	0.066	Not Significant
AC	1.85	1	1.85	4.7	0.002	Significant
AD	2.59	1	2.59	6.56	0.036	Significant
AE	23.7	1	23.7	6	0.014	Significant
Residual	15.38	39	0.39			
Lack of fit	13.23	32	0.41	1.35	0.362	Not Significant
Pure error	2.15	7	0.31			
Cor Total	1938.37	49				

$R^2 = 99.21\%$; Adjusted $R^2 = 98.80\%$; Predicted $R^2 = 87.80\%$; CV% = 6.13

Appendix 3b: Analysis of Variance (ANOVA) for the NCG yield using SCB

Source	Sum of Squares	Degree of freedom (df)	Mean Squares	F-value	P-value probability >F	Remark
Model	1673.36	8	209.17	418.66	<0.0001	Significant
Temperature	1428.27	1	1428.27	2858.72	<0.0001	Significant
Reaction time	0.62	1	0.62	1.25	0.271	Not Significant
Heating rate	0.8	1	0.8	1.6	0.213	Not Significant
N ₂ flow rate	2.76	1	2.76	5.51	0.024	Significant
Particle size	2.66	1	2.66	5.33	0.026	Significant
A ²	36.58	1	36.58	73.21	<0.0001	Significant
D ²	1.43	1	1.43	2.86	0.099	Not Significant
AB	2	1	2	4.22	0.047	Significant
Residual	20.48	41	0.5			
Lack of fit	19.5	34	0.57	3.06	0.06	Not Significant
Pure error	0.99	7	0.14			
Cor Total	1693.04	49				

$R^2 = 99.05\%$; Adjusted $R^2 = 98.60\%$; Predicted $R^2 = 86.60\%$; CV% = 5.36

Appendix 3c: Analysis of Variance (ANOVA) for the NCG yield using SBW

Source	Sum of Squares	Degree of freedom (df)	Mean Squares	F-value	P-value probability >F	Remark
Model	1756.8	9	194.28	303.95	<0.0001	Significant
Temperature	1456.25	1	1456.25	2278.3	<0.0001	Significant
Reaction time	0.06	1	0.06	0.09	0.769	Not Significant
Heating rate	0.48	1	0.48	0.75	0.391	Not Significant
N ₂ flow rate	3.16	1	3.16	6.34	0.044	Significant
Particle size	1.09	1	1.09	1.7	0.199	Not Significant
B ²	285.42	1	285.42	446.54	<0.0001	Significant
AC	3.82	1	3.82	6.03	0.033	Significant
AE	1.8	1	1.8	2.84	0.101	Not Significant
DE	4.72	1	4.72	7.13	0.03	Significant
Residual	25.57	40	0.64			
Lack of fit	25.31	33	0.77	20.75	0.001	Significant
Pure error	0.26	7	0.04			
Cor Total	1761.39	49				
R ² =98.56%; Adjusted R ² =97.23%; Predicted R ² = 83.23%; CV% = 5.42						

Appendix 4a: Analysis of Variance (ANOVA) of energy efficiency of bio-oil yield

Source	Sum of Squares	Degree of freedom (df)	Mean Squares	F-value	P-value probability >F	Remark
Model	717.82	10	71.78	167.49	<0.0001	Significant
A-Temperature	644.25	1	644.25	1503.16	<0.0001	Significant
B-Reaction time	0.089	1	0.089	0.21	0.651	Not Significant
C-Heating rate	3.62	1	3.62	8.45	0.006	Significant
D-N ₂ flow rate	1.63	1	1.63	3.81	0.058	Not Significant
E-Particle size	10.19	1	10.19	23.78	<0.0001	Significant
A ²	15.13	1	15.13	35.3	<0.0001	Significant
D ²	3.19	1	3.19	7.44	0.01	Significant
AC	3.25	1	3.25	7.59	0.009	Significant
AE	2.53	1	2.53	5.91	0.02	Significant
BC	2.65	1	2.65	6.17	0.017	Significant
Residual	16.72	39	0.43			
Lack of fit	15.48	32	0.45	2.73	0.085	Not Significant
Pure error	1.24	7	0.19			
Cor Total	734.54	49				
R ² =99.22%; Adjusted R ² =97.86%; Predicted R ² = 87.86%; CV% = 6.29						

Appendix 4b: Analysis of Variance (ANOVA) of energy efficiency of biochar yield

Source	Sum of Squares	Degree of freedom (df)	Mean Squares	F-value	P-value probability >F	Remark
Model	565.06	9	62.78	45.15	<0.0001	Significant
A-Temperature	499.41	1	499.41	359.15	<0.0001	Significant
B-Reaction time	5.08	1	5.08	3.65	0.003	Significant
C-Heating rate	7.98	1	7.98	5.74	0.021	Significant
D-N ₂ flow rate	9.54	1	9.54	6.86	0.198	Not Significant
E-Particle size	2.38	1	2.38	1.71	<0.0001	Significant
A ²	22.43	1	22.43	16.31	0.011	Significant
AE	7.32	1	7.32	4.25	0.027	Significant
BD	5.69	1	5.69	5.26	0.05	Significant
DE	4.73	1	4.73	4.1	0.078	Not Significant
Residual	55.62	40	1.39	3.4		
Lack of fit	53.87	33	1.63	6.51	0.008	Significant
Pure error	1.76	7	0.25			
Cor Total	620.68	49				

$R^2 = 98.63\%$; Adjusted $R^2 = 97.11\%$; Predicted $R^2 = 84.11\%$; CV% = 3.12

Appendix 4c: Analysis of Variance (ANOVA) of energy efficiency of NCG yield

Source	Sum of Squares	Degree of freedom (df)	Mean Squares	F-value	P-value probability >F	Remark
Model	169.67	8	169.67	16.32	<0.0001	Significant
A-Temperature	9.21	1	9.21	7.08	0.011	Significant
B-Reaction time	3.83	1	3.83	2.94	0.094	Not Significant
C-Heating rate	0.85	1	0.85	0.65	0.424	Not Significant
D-N ₂ flow rate	4.19	1	4.19	3.22	0.08	Not Significant
E-Particle size	2.72	1	2.72	2.9	0.156	Not Significant
A ²	134.71	1	134.71	103.64	<0.0001	Significant
BE	6.39	1	6.39	4.92	0.032	Significant
DE	6.94	1	6.94	5.34	0.026	Significant
Residual	53.29	41	1.3			
Lack of fit	49.14	34	4.22	3.26	0.08	Not Significant
Pure error	4.16	7	0.59			
Cor Total	222.97	49				

$R^2 = 98.92\%$; Adjusted $R^2 = 96.21\%$; Predicted $R^2 = 85.21\%$; CV% = 3.76

Appendix 5a: Analysis of Variance (ANOVA) of exergy efficiency of Bio-oil yield

Source	Sum of Squares	Degree of freedom (df)	Mean Squares	F-value	P-value probability >F	Remark
Model	674.61	10	67.46	45.55	<0.0001	Significant
A-Temperature	514.42	1	514.42	347.32	<0.0001	Significant
B-Reaction time	0.09	1	0.09	0.06	0.808	Not Significant
C-Heating rate	0.008	1	0.008	0.01	0.943	Not Significant
D-N ₂ flow rate	1.72	1	1.72	1.16	0.29	Not Significant
E-Particle size	1.62	1	1.62	1.09	0.302	Not Significant
A ²	20.59	1	20.59	13.9	0.001	Significant
B ²	8.07	1	8.07	5.45	0.025	Significant
AB	8.1	1	8.1	5.47	0.025	Significant
BD	1.16	1	1.16	0.79	0.38	Not Significant
BE	6.57	1	6.57	4.44	0.042	Significant
Residual	57.76	39	1.48			
Lack of fit	55.51	32	1.74	5.4	0.03	Significant
Pure error	2.25	7	0.32			
Cor Total	732.37	49				

$R^2 = 98.90\%$; Adjusted $R^2 = 96.41\%$; Predicted $R^2 = 84.41\%$; CV% = 2.45

Appendix 5b: Analysis of Variance (ANOVA) of exergy efficiency of Biochar yield

Source	Sum of Squares	Degree of freedom (df)	Mean Squares	F-value	P-value probability >F	Remark
Model	505.58	9	56.17	21.72	<0.0001	Significant
A-Temperature	460.22	1	460.22	177.91	<0.0001	Significant
B-Reaction time	2.33	1	2.33	0.9	0.348	Not Significant
C-Heating rate	3.89	1	3.89	1.51	0.227	Not Significant
D-N ₂ flow rate	3.78	1	3.78	1.46	0.234	Not Significant
E-Particle size	2.02	1	2.02	0.78	0.382	Not Significant
A ²	18.48	1	18.48	7.14	0.011	Significant
AE	5.78	1	5.78	2.23	0.143	Not Significant
BE	3	1	3	1.16	0.288	Not Significant
DE	5.78	1	5.78	2.23	0.143	Not Significant
Residual	103.48	40	2.23			
Lack of fit	101.54	33	3	11.16	0.001	Significant
Pure error	1.94	7	0.28			
Cor Total	609.06	49				
R ² =98.34%; Adjusted R ² =96.05%; Predicted R ² = 81.15%; CV% = 1.56						

Appendix 5c: Analysis of Variance (ANOVA) of exergy efficiency of Biochar yield

Source	Sum of Squares	Degree of freedom (df)	Mean Squares	F-value	P-value probability >F	Remark
Model	172.15	9	19.13	15.06	<0.0001	Significant
A-Temperature	9.21	1	9.21	7.25	0.01	Significant
B-Reaction time	3.83	1	3.83	3.01	0.09	Not Significant
C-Heating rate	0.85	1	0.85	0.67	0.42	Significant
D-N ₂ flow rate	4.19	1	4.19	3.3	0.08	Not Significant
E-Particle size	2.72	1	2.72	2.14	0.15	Significant
A ²	134.71	1	134.71	106.03	<0.0001	Significant
BD	2.48	1	2.48	1.95	0.17	Not Significant
BE	6.38	1	6.38	5.03	0.031	Significant
DE	6.94	1	6.94	5.46	0.025	Significant
Residual	50.82	40	1.27			
Lack of fit	46.66	33	1.41	2.38	0.117	Significant
Pure error	4.16	7	0.59			
Cor Total	222.97	49				
R ² =99.12%; Adjusted R ² =97.01%; Predicted R ² = 85 .01%; CV% = 4.56						

Appendices 6: Budget Proposal of the Research

S/N	Activities	Quantities	AMOUNT(₦)	TOTAL(₦)
1	Collection and Preparation of Biomass Feedstock	Lump sum	80,000	80,000
2	Characterization of Feedstock and Pyro Products	Lump sum	550,000	650,000
3	Software for Data Analysis and Validation	Lump sum	100,000	100,000
4	Miscellaneous	Lump sum	150,000	150,000
Total				₦ 980,000
Grand Total				₦ 980,000


Journal Publications

The screenshot shows a ScienceDirect article page. The browser address bar displays the URL: [sciencedirect.com/science/article/pii/S2214785322036008](https://www.sciencedirect.com/science/article/pii/S2214785322036008). The page features the ScienceDirect logo and navigation options like 'Journals & Books', 'Corporate sign in', and 'Sign in / register'. The article title is 'Characterization of lignocellulose biomass based on proximate, ultimate, structural composition, and thermal analysis'. It is published in 'materialstoday: PROCEEDINGS', available online on 30 May 2022. The authors listed are A.O. Onokwai, E.S.A. Ajisegiri, I.P. Okokpujie, R.A. Ibikunle, M. Oki, and J.O. Dirisu. The page includes an outline, abstract, keywords, and a 'View PDF' button. On the right, there are sections for 'Recommended articles', 'Article Metrics' (showing 8 readers), and a 'FEEDBACK' button.

The screenshot shows an article page from the 'International Journal of Renewable Energy Development'. The journal's ISSN is 2252-4940. The article title is 'Characterization of Lignocellulosic Biomass Samples in Omu-Aran Metropolis, Kwara State, Nigeria, as Potential Fuel for Pyrolysis Yields'. The authors are Anthony O Onokwai, Imhade P Okokpujie, Emmanuel S Ajisegiri, Makanjuola Oki, Adeyinka O Adeoyeb, and Esther T Akinlabi. The article is categorized as 'Original Research Article' and is in Volume 11, No 4 (2022), published in November 2022. It has 208 views and 64 downloads. A line graph shows the number of views over time from 2017 to 2022, with a significant spike in 2022. The page also includes a 'Check for updates' button, a DOI link (<https://doi.org/10.14710/ijred.2022.45549>), and a Creative Commons Attribution-ShareAlike 4.0 International License notice.

ELEMENTAL ANALYSIS AND COMBUSTION CHARACTERISTICS EVALUATION OF NIGERIAN BIOMASS RESOURCES

Balogun, Kunle and Lasode, Muyiwa and Onokwai, A. O and Ezugwu, C. A and Olayanju, T.M.A. and Osueke, C.O. (2019) *ELEMENTAL ANALYSIS AND COMBUSTION CHARACTERISTICS EVALUATION OF NIGERIAN BIOMASS RESOURCES*. International Journal of Mechanical Engineering and Technology (IJMET), 10 (2). 1522 -1527. ISSN Print: 0976-6340 and ISSN Online: 0976-6359

 Text
ELEMENTAL_ANALYSIS_AND_COMBUSTION_CHARAC.pdf - Published Version
[Download \(480kB\)](#)

Official URL: <http://www.iaeme.com/ijmet/issues.asp?JType=IJMET&...>

Abstract

An investigative work was done to analyse the elemental composition and the combustion characteristics of some biomass resources that is, agricultural and forestry samples. The method of analysis was according to Association of Official Analytical Chemists (AOAC). The results shows that the higher heating value (HHV) for Sorghum husk, Araba (*Celbo pentandra*), were 17.2MJ/kg, and 18.0MJ/kg respectively. The analysis also reveals the presence of carbon, hydrogen, nitrogen, sulphur and oxygen in significant amount. These biomass wastes can be transformed in to valuable energy products in form of solid, liquid or gaseous fuels for either domestic or industrial applications.

Item Type: Article

Subjects: [S Agriculture > S Agriculture \(General\)](#)

Depositing User: [Mr.DIGITAL CONTENT CREATOR LMU](#)

Date Deposited: 09 Sep 2019 10:34

Last Modified: 09 Sep 2019 10:34

URI: <https://eprints.lmu.edu.ng/id/eprint/2195>

Comparative Calorific Evaluation of Biomass Fuel and Fossil Fuel

Osueke, C.O. and Olayanju, T.M.A. and Ezugwu, C. A and Onokwai, A. O and Ikpotokin, I. and Uguru-Okorie, D.C and Nnaji, F. C. (2018) *Comparative Calorific Evaluation of Biomass Fuel and Fossil Fuel*. International Journal Civil Engineering and Technology, 9 (13), pp. 1576-1590.

 Text
IJCIET_09_13_158.pdf - Published Version
[Download \(581kB\)](#)

Abstract

In recent years, fossil fuels have been preferably used both for domestic and industrial purposes. Fossil fuels are highly flammable and effective but are very hazardous to the human environment. It is also one of the causes of the ozone layer depletion which humanity is battling presently. Biomass fuels are majorly agricultural waste materials which have good properties that aid combustion, less hazardous and are effective for some domestic activities and in small-scale industries. This paper presents the calorific evaluation and analysis of fossil fuel and biomass fuel. It also highlights the effects of fossil fuels in terms of the dangers of increasing CO₂ concentration in the atmosphere. It presents biomass fuel as a potential substitute for fossil fuel as a renewable energy by comparing the calorific values of various combustible samples such as: rice husk, petrol, diesel, corn cob using a C200 bomb calorimeter at the Landmark University energy laboratory to determine the calorific values and to examine if biomass can be used as a suitable replacement for fossil fuels. Results show that corn cob has a higher calorific value than rice husk, but both corn cob and rice husk have sufficient energy to be used as substitutes for petrol and diesel and other fossil fuels to reduce the dangers of CO₂ concentration in the atmosphere and societies over-reliance on fossil fuel.

Item Type: Article

Subjects: [T Technology > T.J Mechanical engineering and machinery](#)



Download This Paper

Open PDF in Browser



Add Paper to My Library

Characterization of Adansonia Digitat (Baobab Wood) Bio-Oil and Bio-Char Produced Using a Fixed- Bed Tubular Reactor

18 Pages • Posted: 31 Jan 2022

[J.A. Oyebanji](#)

affiliation not provided to SSRN

[Anthony O. Onokwai](#)

Landmark University

[E.A Ajisegiri](#)

Landmark University